THESE POUR OBTENIR LE GRADE DE DOCTEUR DE

L'ECOLE NATIONALE SUPERIEURE DE CHIMIE DE MONTPELLIER

En Chimie et Physico-Chimie des Matériaux

École doctorale Science Chimique Balard-ED 459

Unité de recherche UMR 5253

Synthèse de nanoparticules de cuivre par dismutation de complexes de cuivre(I) et développement de nouvelles voies d'accès par stratégie organométallique.

Présentée par **Liyan OUYANG**

Le 14 Janvier 2022

Sous la direction des

Dr. Emmanuel VRANCKEN, Dr. Armelle OUALI et Pr. Alexa Courty

Devant le jury composé de

M. Jean-François POISSON, Professeur, Université Grenoble Alpes	Rapporteur
M. Simon TRICARD, Chargé de recherche CNRS/LPCNO Toulouse	Rapporteur
M. Benoît PICHON, Professeur, Université de Strasbourg	Président-Examinateur
M. Rodolphe JAZZAR, Directeur de recherche CNRS, University of California	Examinateur
Mme. Hélène GÉRARD, Professeure, Sorbonne Université	Examinatrice
Mme. Alexa COURTY, Professeure, Sorbonne Université	Co-Encadrante
Mme. Armelle OUALI, Chargée de recherche CNRS/ICG Montpellier	Co-Directrice
M. Emmanuel VRANCKEN, Maître de Conférences, ENSC Montpellier	Directeur

Acknowledgement

First, I would like to sincerely thank Pr. Jean-François POISSON, Dr. Simon TRICARD, Pr. Benoît PICHON, Dr. Rodolphe JAZZAR and Pr. Hélène GÉRARD for accepting to review my thesis and be part of my jury.

I appreciate Dr. Marc Taillefer and Dr. Eric Clot for allowing me to work in the ex-AM^{2}N (Architectures Moléculaires et Matériaux Nanostructurés) group/Département D1 Chimie & Matériaux Moléculaires (new) for these past three years. I would also like to thank Pr. Christophe Petit for welcoming me to MONARIS (MOlecule to NAno-objects: Reactivity, Interactions and Spectroscopies) during the first year of my thesis work.

I would like to thank Pr. Jean-Marc CAMPAGNE for welcoming me to be a part of CAMPAGNE team. Thanks a lot for your kindnesses, your humor, your support and your patience! You are the 'sunshine' for me during these 3 years of thesis life!

I want to thank my thesis director, Dr. Emmanuel VRANCKEN for your direction in performing this research and for all discussions that we had and helping me a lot during three years of my thesis work. I also appreciate your encouragement, unreserved help, patience and support through my whole PhD studies.

I would like to thank my co-supervisor Dr. Armelle OUALI for having supervised this thesis and helping me to finish the thesis. Thank you for your help, kindness, patience, support, and invaluable advice that you provided during these 3 years of thesis study, and also for always helping me to get better.

Also, I would like to thank my co-advisor Pr. Alexa COURTY in MONARIS for first leading me into the world of nanomaterial chemistry, giving me the first view of research in the nano-world. Thank you for all of your help, patience, kindness, encouragement, invaluable advice and all the discussion that we had and helping me during three years of study.

I must also express my deepest gratitude and sincere thanks to all people with whom I had the chance to collaborate during this thesis. I would therefore like to thank Pr. Hélène Gerard (LCT, Sorbonne Université), Dr. Rodolphe Jazzar (DR, CNRS/University of California, San Diego), Pr. Vincent Noël (ITODYS, Université de Paris).

I am very thankful to all people that I shared my 3 years of thesis life at the ex-AM^{2}N (actual D1) and MONARIS laboratories: Olivier, Renata, Eric, Pascale, Joris, Laure, Yvette, Joël, Cyril, David, Florian, Xavier, Anh-Tu (Tao), Mylène, Thierry, Nicolas and all the post-docs, doctoral students and interns: Chayma, Pierre, Sami, Rana, Catherine, Tiyati, Georg, Milton, Minh Loan, Eleonora, Armand, Lucas…, my special officemates in MONARIS Suyeon, Sonia, Arthur, Alter and Mario, and I would like to thank Jesse, Maya, Florent. Thank you all! I gratefully thank my family, 感谢爸爸, 妈妈, 平燕, 球球, 杰对我一直以来的支持, 我爱你们!

Abbreviations

BE	Binding energy
Bp	Boiling point
CuNPs	Copper nanoparticles
CAACs	Cyclic (Alkyl)(amino)carbenes
DDT	Dodecanethiol
DDA	Dodecylamine
eq	Equivalent
ESI-MS	Electrospray ionization mass spectrometry
EDX	Energy dispersive X-ray spectroscopy
fcc	Face-centered-cubic
HR-TEM	High resolution transmission electron microscopy
HMPT	Tris(dimethylamino)phosphine
HMPA	Hexamethylphosphoric acid triamide
FTIR	Fourier transform infrared spectroscopy
ICP-MS	Inductively coupled plasma mass spectrometry
LSPR	Localized surface plasmon resonance
MNPs	Metallic nanoparticles
MS	Mass spectrometry
NIR	Near infrared
NHC	N-heterocyclic carbene
NMR	Nuclear magnetic resonance
NPs	Nanoparticles
OLA	Oleylamine
SEM	Scanning electron microscopy
SAED	Selected area electron diffraction
TOP	Trioctylphosphine
TOPO	Trioctylphosphine oxide
TOPT	Trioctylphosphite
TEM	Transmission electron microscopy
THF	Tetrahydrofuran
UV	Ultra-violet
UV-vis	UV-visible
XPS	X-ray photoelectron spectroscopy
XRD	Powder X-ray diffraction

Table of contents

General Introduction

Copper nanoparticles (CuNPs) have promising applications due to their specific properties (optical, electronic conductivity…) as well as the low cost and high natural abundance of copper metal. The synthesis of CuNPs with controlled shape and size have received increasing interest over the past few years. Indeed, the NPs morphology can alter their catalytic, plasmonic and optoelectronic properties and are thus key for applications.

The main objective of this thesis work is thus to investigate and propose new synthetic routes allowing the preparation of CuNPs with controlled size and shape. Two different chemical methods for the synthesis of CuNPs have been explored in this thesis work: the first one is based on the well-known disproportion of Cu(I) precursors, the other one consists in the thermolysis of organocopper precursors.

This manuscript is divided in five main chapters:

Chapter I gives a quick general overview on the formation (nucleation and growth) of metal NPs and the reaction factors that are able to control the size and shape of NPs, before focusing on the fabrication of CuNPs via some chemical reduction methods described in the literature.

Chapter II describes the synthesis of CuNPs through the disproportionation reaction of copper precursors in the presence of a series of phosphorus ligands. The influence of the phosphorus ligand on the final morphology of CuNPs is studied and an attempt of rationalization presented. In addition, the effect of other reaction parameters on the shape and size of CuNPs prepared is also discussed (heating ramp, amount of phosphorus ligands, nature of the copper precursor, nature of amine solvent, reaction time… to name a few).

Chapter III starts with a quick overview of the synthesis of N-heterocyclic carbenes (NHCs)-stabilized metal nanoparticles reported in the literature, and then reports the preparation of unprecedented CuNPs from a range of cyclic (alkyl)(amino)carbenes (CAACs) -CuCl complexes and via 'one-pot' disproportionation route. The surface of characterization, mainly by XPS, of the CuNPs obtained with of CAACs-CuCl complexes is reported. The shape and size of CuNPs can be tuned by playing with reaction parameters including the steric hindrance of CAACs ligands, the concentration of the copper precursor and the nature of solvent.

Chapter IV focuses on the synthesis of CuNPs with well-defined size and shape CuNPs by a novel chemical route based on the thermal decomposition of organocopper (RCu) or organocuprate ($R_2Cu•MgX$) reagents in the presence of a phosphorus ligand, and the further addition of dodecanethiol. The organocopper precursors are prepared in situ from commercially available copper halides and Grignard reagents. The effects of several reaction

parameters like the amount of phosphine ligand, the temperature, the injection time and amount of DDT, the nature of the phosphorous ligand, the nature and amount of the Grignard reagent on the formation of CuNPs are discussed. Besides, studies aiming at understanding the CuNPs formation pathway are also reported.

Chapter V is related to the experimental section, including chemicals, general characterization techniques and synthetic procedures of CuNPs prepared in this thesis work.

Chapter I. Introduction

I. 1 General overview

Metal nanoparticles (NPs) have been studied for a long time and one of the first example of metal nanoparticle synthesis was described by M. Faraday et al. in 1857,[1] who demonstrated the formation of gold colloids by reducing gold chloride with phosphorus in water. The colloidal solution, also called colloidal suspension, is a solution that contains small particles or materials with possible size ranges from 1 nm to 1 μm. Later on, in 1959, R. Feynman introduced the concept of nanotechnology.[2] Since then, the nanotechnology has been developed as key point in the field of nanoscience and mainly focus on the discovery of new methodologies for preparing NPs, ranging in size from 1 nm to 100 nm, and their further applications.[3-7] The physical and chemical properties of NPs are usually different from material counterparts. NPs have a very large surface area to volume ratio when compared to the corresponding bulk material, such as powder, plate and sheet. This feature enables NPs to possess unexpected optical, physical and chemical properties that strongly depends on their size, as they are small enough to confine their electrons and produce quantum effects. They were thus applied in various application fields, such as catalysis,[8] sensor,[9] electronics[10] and in optical devices.[11-12] Metal NPs became a promising nanomaterial because of their excellent chemical, physical and catalytic properties, including the high conductivity and high surface-to-volume ratio.[13-15] It is noteworthy that most of the unique properties of NPs strongly depend on their size, shape and compositions.[16-18] Therefore, the preparation of metal NPs with strictly controlled size, shape and structure became very important to investigate their properties and enable the discovery of new applications.

A variety of methods, including physical, chemical and biological methods, have been developed to synthetize metal NPs and they have been typically classified into two categories: top-down and bottom-up approaches (Scheme I-1).[19] Typically, the “top-down” approach uses photolithography or electron beam lithography, where the bulk material is split into nanosized particles. This approach is seen as the physical method that involves a milling, a lithography or an attrition process.[20] For the “top-down” approach, it is challenging to synthetize monodisperse NPs of controlled size and shape.[21] The “bottom-up” approach is mostly used for making metal NPs by building up the nanomaterial through atom-by-atom, molecule-by-molecule and cluster-by-cluster strategies.[21-22] This approach is mostly performed by using chemical methods in solution due to their facility in the control of size, shape and polydispersity

of NPs by optimizing the reaction conditions.[23-24] Therefore, the "bottom-up" method is more popular in the nanoparticle synthesis compare to the "top-down" approach.

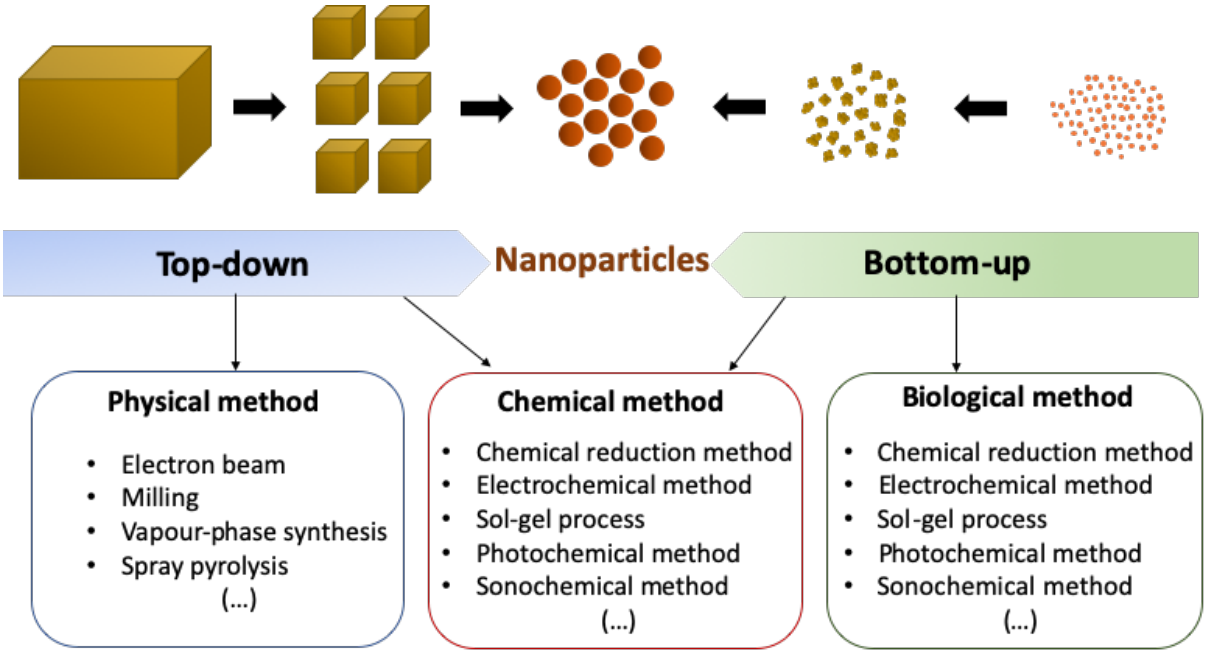

Scheme I-1. *Different approaches and methods for synthetizing NPs.*

In this chapter, we will discuss in details about the chemical reduction method in the NPs synthesis, because these are the methods that we have chosen to use in our work to synthetize copper nanoparticles (CuNPs).

In recent years, CuNPs have attracted increasing attention in the nano-research field because of their high thermal,[25] optical,[26] catalytic,[27] electronic[28,29] properties. Besides, copper is more cost-effective and abundant as compared to silver and gold.[30-31] Up to now, although the preparation of CuNPs was increasingly studied, the number of synthetic routes is still limited as compared to their silver and gold counterparts. One of the reasons for this fact is their spontaneous oxidation when exposed to air. Thus, the exploration of new methodologies to synthetize perfectly defined copper NPs still represents a challenge.

In this thesis work, we propose to address this challenge by investigating synthetic routes leading to CuNPs with controlled size and shape through a simple chemical oxydo-reduction route and by using various ligands (chapters II and III). We have also explored a simple, efficient, low-cost process and scalable process to produce CuNPs from readily available organocopper reagents (chapter IV).

I. 2 Generalities on the synthesis of metal nanoparticles (NPs)

Currently developed synthetic chemical methods are reported in the literature for preparing CuNPs, such as the chemical reduction method,[32] electrochemical method,[33] sonochemical method,[34] microwave assisted method,[35] microemulsion method[36] and thermal decomposition.[37] Among these chemical methods, the chemical reduction method is preferred and has been widely used to synthetize metal nanoparticles usually by reducing metal precursor in the presence of ligands that may next play the role of surfactants or capping agent.[38] This method allows to obtain metal nanoparticles with controlled size by tuning reaction parameters, such as the reaction temperature, the reaction time, the reducing agent, the concentration or type of precursors, the ligands, the injection rate of reactants etc.[39]

For a typical synthesis of metal NPs based on the chemical reduction process, the selected metal precursors are reduced by a molecular reducing agent in the presence of various ligands at an elevated temperature (Scheme I-2). The precursors are usually chosen from metal salts, such as metal halide,[40] acetate,[41] sulfate[42] acetylacetonate[43] and nitrate.[44] The reducing agents are chosen to facilize the chemical reduction of the metal precursor with high oxidation state into zero-valent metallic atoms. They are usually the boranes,[45] hydrazine,[46] acids,[47] and hydrogen.[48]

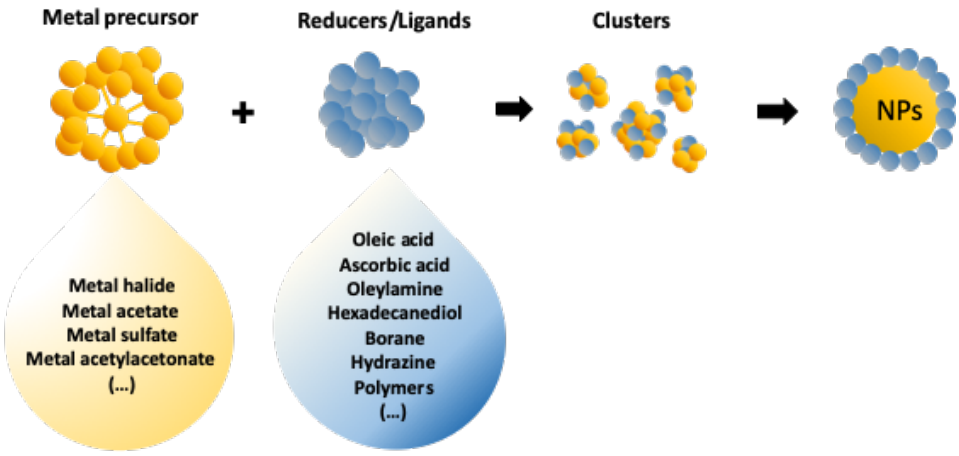

***Scheme I-2**. Schematic illustration of typical synthesis of metal nanoparticles via chemical reduction method.*

Especially, the selection of ligands is extremely important during the metal NPs formation. They often play an important role as capping agent and/or stabilizer and/or dispersing agent[110] for the final NPs. These ligands with different functions are similar but there are some distinct differences among them. At the growth stage, the ligand may influence the final shape and size of the nanoparticle. Once the ligands act as a stabilizing agent, they

prevent the coalescence of the nanoparticles into bulk. The ligands also play the role of dispersing agents to help to form a homogeneous NPs colloidal solution. Sometimes, these three functions can be performed by the same ligand.[49] A variety of ligands were chosen for the metal NPs synthesis, such as organic molecules (e.g., amines, thiols, phosphines, acids),[50] polymers (e.g., PVP, PVA)[51] and ionic salts.[52] It is important to note that their binding affinity, nature, and relative ratio to metal precursor have great influence on the NP size and shape. The effect of ligands during the particle growth will be discussed in details in the subsequent section.

The chemical synthesis of metal nanoparticles with controlled shape and size have been mainly investigated by using nucleation and growth theory. Up to now, a series of theories have been described to explain the crystallization pathways of metal NPs, such as particle-mediated nucleation and growth and atom-mediated nucleation and growth,[53] but most of them were developed based on a nucleation and growth theory, also called LaMer theory which was firstly proposed by LaMer and Dinegar in 1950.[54] The LaMer theory describes the homogeneous nucleation and growth through the evolution of atomic concentration over time, as illustrated in Figure I-1. To sum up, this process of nucleation and growth can be roughly divided into three major stages: i) the formation of zero valent atoms in solution ii) the subsequent nucleation from atoms aggregation and iii) the growth of the seeds into well-defined nanostructures.[54,55] In the synthesis of NPs, each stage plays its proper role to influence the final size and shape of final nanoparticles.

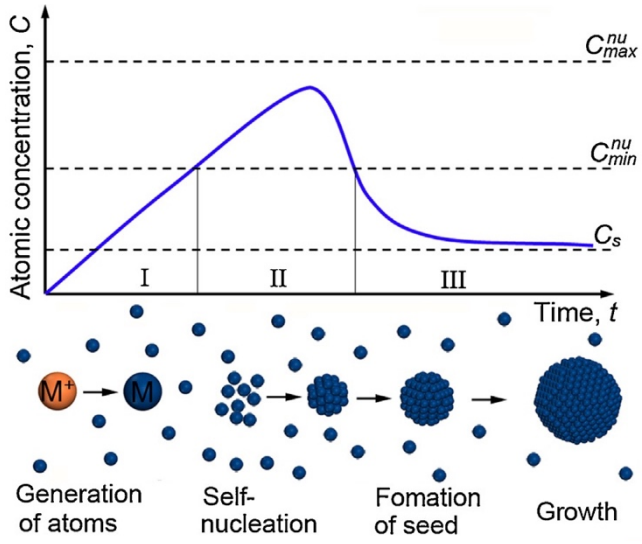

C^{nu}_{max} : Maximal concentration for nucleation
C^{nu}_{min} : Nucleation threshold for seed formation
C_s: solubility level

***Figure I-1**. Schematic illustration of LaMer curve. (Copyright from Ref.[53])*

In a typical solution-phase synthesis of metal NPs, the metallic zero-valent atoms are produced in the early stage of a synthesis through either a reduction by using reducing agent, or through a decomposition of metal precursor compounds.[53] The increase of the concentration of monomers (metal atoms) with time is described in stage I of Figure I-1. It reaches a saturation state. Arrived at this threshold, the atoms start to aggregate to form small nuclei, namely clusters, by self-nucleation (stage II, Figure I-1). However, the formation of a thermodynamically stable nucleus is indeed only possible beyond a critical size. The energy involved in the homogeneous nucleation results from two competitive processes: the surface creation which is unfavorable and a favorable term related to the volume of the nuclei. The free enthalpy of nucleation is therefore negative beyond this critical radius, which corresponds to the nucleation concentration C_{min}^{nu}. The faster this process is as compared to the growth, the more the germs will be homogeneous in size and shape. Consequently, the appearance of nuclei leads to the gradual decrease in the monomer concentration. Nucleation continues as the concentration of reactants falls from critical limiting saturation (C_{max}^{nu}) to C_{min}^{nu}, from which further nucleation is suppressed. The size of nuclei gradually increased through the continuous addition of metallic atoms in solution. This growth is thermodynamically favorable since the volume term prevails over the surface term. The seeds continuously grow into the final nanoparticles until the C_s (solubility concentration of nanoparticles), as shown in stage III (Figure I-1). LaMer's model shows that the size polydispersity of nanoparticles depends on the homogeneity of the nucleation step.

The general procedure of metal NPs formation is schematically illustrated by Y. Xia's and Y. Xiong's groups,[56,57] as shown in Figure I-2. As we can see, the metal precursor is reduced or decomposed in a first stage to produce the nuclei, as soon as the nuclei has grown past a certain size, the seeds could be formed with a single-crystal, singly twinned, or multiply twinned structure. Noteworthy, the introduction of stacking faults leads to plate-like seeds.[56,57] In the next stage, each different types of seed grows into different shapes of nanocrystals.

From single-crystal seeds, this type of seeds can grow into octahedrons, cuboctahedrons, or cubes which depend on the ratio of growth rates (R) along the (111) and (100) directions.[58,59] As a result of the induction of uniaxial growth, the cuboctahedral seeds may evolve into octagonal rods and cubic seeds will grow into rectangular bars, respectively.[59] From the single twinned seeds, these seeds can grow into right bipyramids, a nanocrystal that consists of two right tetrahedrons symmetrically placed base-to-base, with the (100) facets stabilized.[60] Similarly, the induction of anisotropic growth allows the pyramid seeds grow into nanobeams.[61] When the seeds are multiple twinned, icosahedrons, decahedrons and pentagonal nanorods can be formed depending on whether or not the (100) planes on the side surface can be stabilized.[60,62,63] For the seeds with stacking faults, they will grow into thin plates with the top and bottom faces whose are (111) facets, and side surfaces are enclosed by a

mix of (100) and (111) facets.[64,65] In this case, the seeds grow into hexagonal-shaped thin plates due to the six-fold symmetry of an *fcc* (face-centered-cubic) system. Following a continuous growth, the triangular shape can be produced by eliminating the (111) facets from the side surfaces.[65] Therefore, the seeds play very important role as a bridge between the nuclei and final nanocrystals. The selected production of seeds is thus one of the key points to obtain a metal NP of desired shape.[57,66]

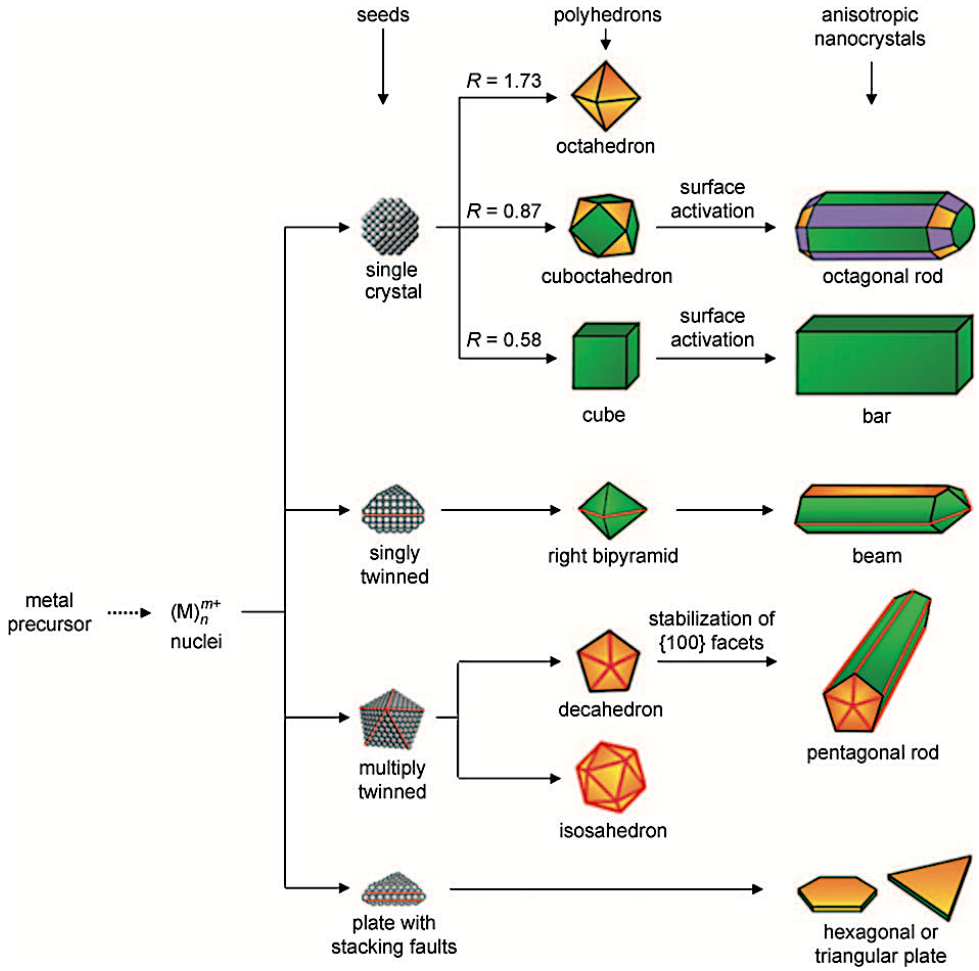

Figure I-2. *Synthetic pathways to form metal nanocrystals with various shapes. R is defined as the ratio between the growth rates along the (100) and (111) axes. The green, orange, and purple colors represent the (100), (111), and (110) facets, respectively. (Copyright from Ref.[56,57])*

Y. Xia *et al.*[57] have demonstrated that the crystallinity of seed is mainly directed by the reduction rate, which is critical to the size growth of seeds in the case of PdNPs. They show that single crystal seeds were produced due to the quick reduction of the Pd precursor that

induces a fast increase of the size resulting from a rapid aggregation of the Pd atoms. Once the reduction rate was substantially slowed down, the multiple-twinned seeds at small sizes were formed due to the slow addition of Pd atoms. As a result, a slow reduction rate of metal precursor promotes the formation of multiple-twinned seeds and possible single-twinned seeds.

In a general synthetic system for preparing metal NPs, the reduction rate of precursor salts greatly depends on the selected reducing agents and/or reaction temperature. In addition to the reduction rate, there are other ways to selectively control the seeds formation. Xia's group[68] has reported other processes of particle formation, the oxidative etching, which enables to manipulate the distribution of single-crystal and twinned seeds (as shown in Figure I-3). A combination of the ligands (e.g. Cl^-, Br^-) and of the O_2 already present in the reaction solution plays the role of a strong oxidative etchant that enable to selectivity reduce the twinned seeds and yields high concentration of single crystal seeds. By this way, nanoparticles of controlled shape were formed.[67,68] The oxidative etching process have been widely applied with a range of noble metals to obtain desirable metal nanoparticles, such as Ag,[69] Pd,[68] Au,[70,71] Cu[72] and Rh.[73]

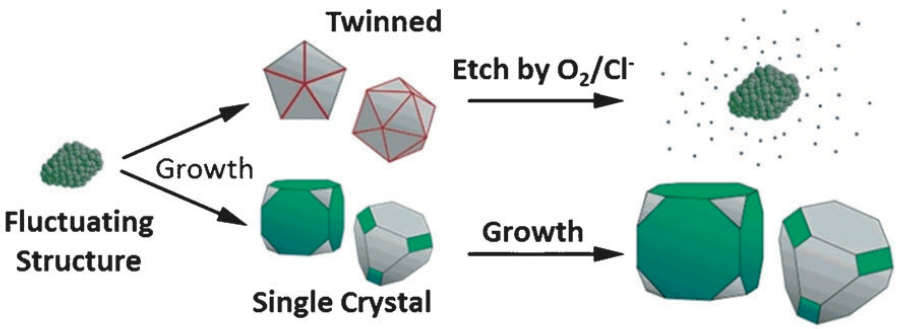

Figure I-3. *Schematic illustration of oxidative etching process. Gray, green, and red represent the (111) facets, (100) facets, and (111) twin planes, respectively. (Copyright from Ref.[68])*

In addition to the selected-production of seeds, another important factor is the control of the growth stage. The growth stage is a deterministic process, it is highly dictated by the initial reaction parameters including temperature, concentration of monomers and competition of growth rate at different facets of seeds.[74,75] It is important to note that the growth rate of NPs is strongly affected by the concentration of monomers. In a typical solution-phase synthesis process, the concentration of monomers can be affected by certain reaction conditions, such as the nature and amount of reducing agents and/or temperature.[75,76] Additionally, the relative growth rates at different facets of seeds can be directly influenced by the introduction of ligands which will be described below.[77]

In order to understand the influence of the reaction parameters on the growth rate of NPs, the investigation of the growth mechanism is required. The growth of NPs may occur through two mechanisms: *i)* monomer addition to seeds and *ii)* coalescence of smaller nanoparticles, as shown in Scheme I-3.[78,79,80] The growth pathway by monomer addition promotes the formation of single crystalline particles whereas the coalescent growth leads to the multiple twin structures with larger size.[81] In our work, we promoted the monomer growth and tried to avoid the coalescence by optimizing reaction parameters. Here, the monomer growth will be discussed in details.

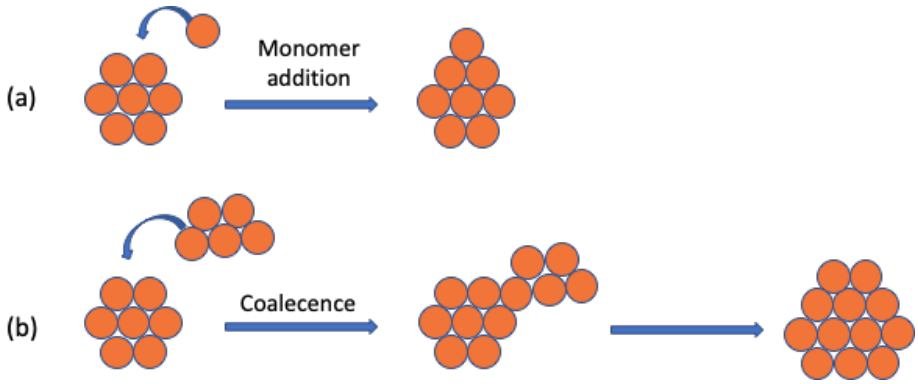

Scheme I-3. *Growth mechanisms of nanoparticles (a) growth by monomer addition (b) growth by coalescence of smaller particles.*

I. 2.1 Effect of concentration of monomers on the NPs growth

The narrowing of size distribution can be studied by considering the dependence of growth rate on the average size of nanoparticles. Based on the LaMer theory, H. Reiss has improved the details of LaMer growth model and proposed “size focusing” and “defocusing” process.[82] The size focusing is a process of growth by consuming the monomers which were formed through the reduction of precursor salts. For the defocusing process, large NPs grow at the expense of dissolving smaller ones. Because the very small NPs have active surface atoms due to curvature and strain, they thus can be dissolved back into reaction solution. Therefore, when the small NPs have size below a certain critical size their growth rate is negative (see in Figure I-4). At the critical size, the NPs neither grow nor shrink. Once above the critical size, the NPs grow and become larger through the monomer addition growth instead of dissolving back into solution. This is due to the fact that these NPs have a small active surface to volume ratio, which lead to the continuous growth. The two curves in Figure I-4 depict the dependence of growth rate on the monomer concentration (red: high monomer

concentration; blue: low monomer concentration). In the growth of NPs, the relative smaller particles grow faster than bigger ones due to their higher surface energy. A high concentration of monomer in the early stage will thus dictate the formation of NPs with small size.

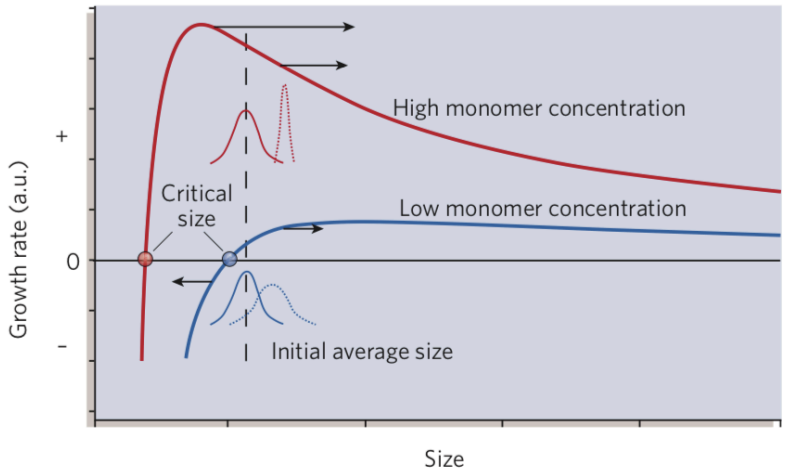

Figure I-4. *Graph illustrating growth rate dependence on the particle size for high and low monomer concentration in solution. (Copyright from Ref.[65])*

In the red curve, the high monomer concentration leads to very small critical size, which allows all the particles to grow. Subsequently, the size distribution of NPs can be reduced. This phenomenon corresponds to the "size focusing process" described before. It is worth noting that the "size focusing" is a kinetically controlled growth process, as the small nanoparticles with higher energy surface grow faster than larger ones that have lower energy surfaces.[75,76] At the opposite, for low monomer concentration (blue curve) small nanocrystals disappear as larger ones grow as a result of Oswald ripening and the size distribution broadens. This effect is known as the "size defocusing" process.

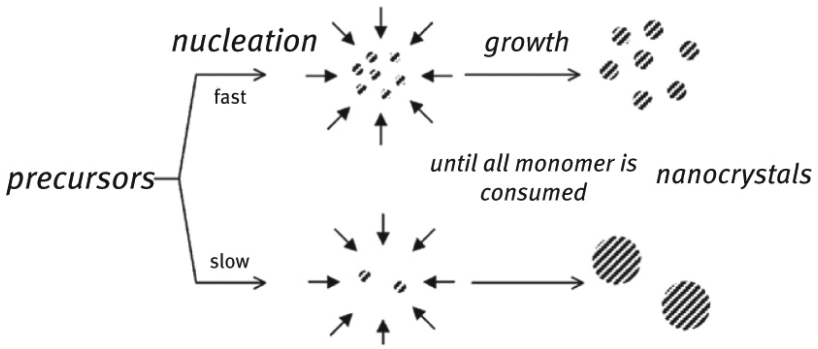

Figure I-5: *Schematic representation of nanocrystal synthesis. (Copyright from Ref.[83])*

In general, a high monomer concentration often occurs by a rapid nucleation step and vice versa,[83] as shown in Figure I-5. In the reduction process, the size of NPs is strongly affected by the nucleation rate. A fast nucleation yields more particle seeds and serve as nucleation centers which leads to small size of NPs. In contrast, a slow nucleation rate promotes less nucleation seeds and nanoparticles of larger size will be formed. To realize the nucleation on a short time, several factors could be optimized such as the use of a fast reacting reducing agent, a high temperature and a high concentration of initial precursor. For example, K. Asadi and co-workers[84] have investigated the influence of monomer concentration on the size and shape control synthesis of iron oxide NPs by thermal decomposition of iron acetylacetonate ($Fe(acac)_3$) in benzyl ether in the presence of oleic acid and oleylamine used as surfactants (Figure I-6). Changes in iron oxide NPs size were observed by increasing the amount of $Fe(acac)_3$ from 0.6 to 6 mmol. In this study, two different size regimes were observed, as shown in Figure I-6a. An increase of the amount of precursor from 2 to 6 mmol induced as expected a decrease of the particle size from 13.1 nm to 6.6 nm, as shown in regime II (green). However, for an amount of precursor less than 2 mmol (here, 2 mmol produce the standard sample with a mean size 13.1 ± 1.1 nm), the size of NPs increased from 6 nm to 13.1 nm when the precursor amount increases from 0.6 to 2 mmol (in the first regime (blue)). They explained this observation by the concept of the diffusion-limited nanoparticle growth in a fixed reaction volume. According to this, the relative high concentration of precursor leads to a relatively high concentration of monomers for which the diffusion distance is shorter, which promotes a higher mass transfer and a higher growth rate. Subsequently, larger nanoparticles were produced at a relative high concentration of precursor in a fixed volume synthetic system.

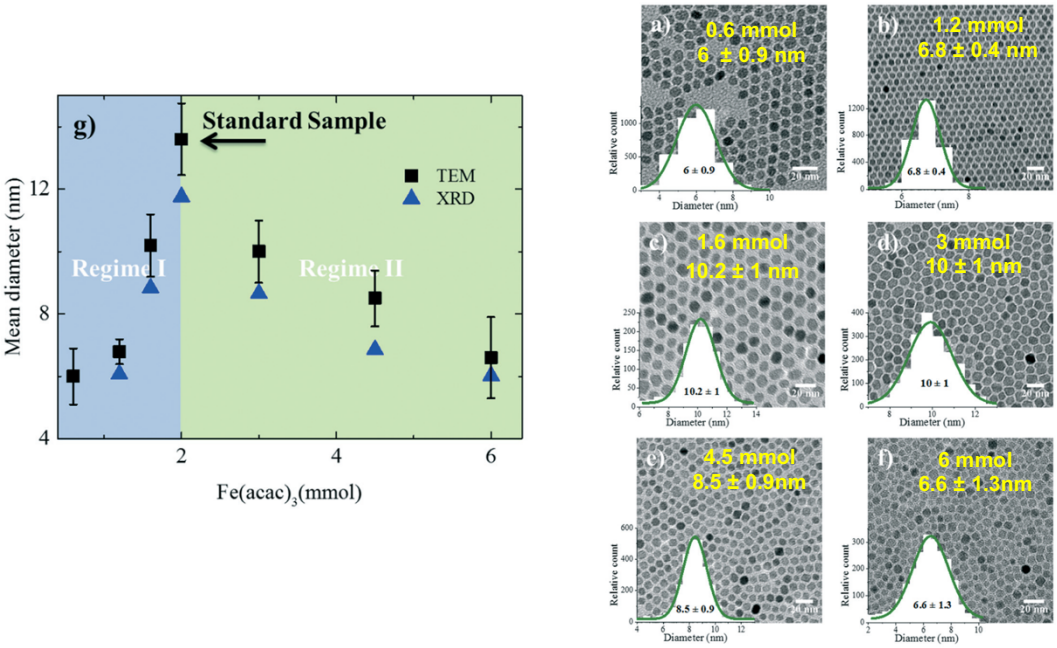

Figure I-6. *Evolution of the nanoparticles size as a function of precursor amount. (Copyright from Ref.[84])*

I. 2.2 Effect of surface ligands

As nanoparticles are finely divided compared to bulk materials, they are thermodynamically unstable with respect to agglomeration. Therefore, they need to be stabilized during the growth stage by one or more ligands that will act as capping agents to prevent their precipitation. But beside this role of stabilizer, these ligands are also important to control the final shape of nanoparticles and thus make possible the design of their chemical and physical properties.[85] The surface energy of crystal facet is a crucial parameter in the growth stage. Indeed, as the energy barrier to monomer addition is inversely proportional to the surface energy, the crystal facets of higher energy grow faster than the lower ones. In a solution-phase synthesis of NPs, the presence of ligands is able to modify the free energies of the different facets by selectively binding to specific ones through their preferential affinities. This reduces the free energy of this facet thus inhibits its growth. Contrarily, the growth of unbound facet is favored, which leads to different crystallographic growth along the planes.[86] Consequently, the shape control of NPs could be achieved with the addition of selective ligands such as amines, thiols, phosphines and polymers.[87] For example, D. L. Peng *et al*.[88] reported a highly shape selective preparation of CuNPs with cubic and wire-like shape in the presence or absence of trioctylphosphine (TOP) via a Galvanic replacement reaction between Ni^0 and Cu^{2+} ions. The presence of TOP plays a critical role in the synthesis of nanocubes (with an edge length of 60 ± 8 nm) to form the single crystal seeds and selectively stabilize the (100)

facets. When the TOP was removed from the reaction, the obtention of final shape of NPs was dominated by nanowires instead of nanocubes. As shown in Figure I-7, the shape selective formation of nanocubes and nanowires was observed in the presence (Figure I-7a) and absence (Figure I-7b) of the TOP ligand respectively.

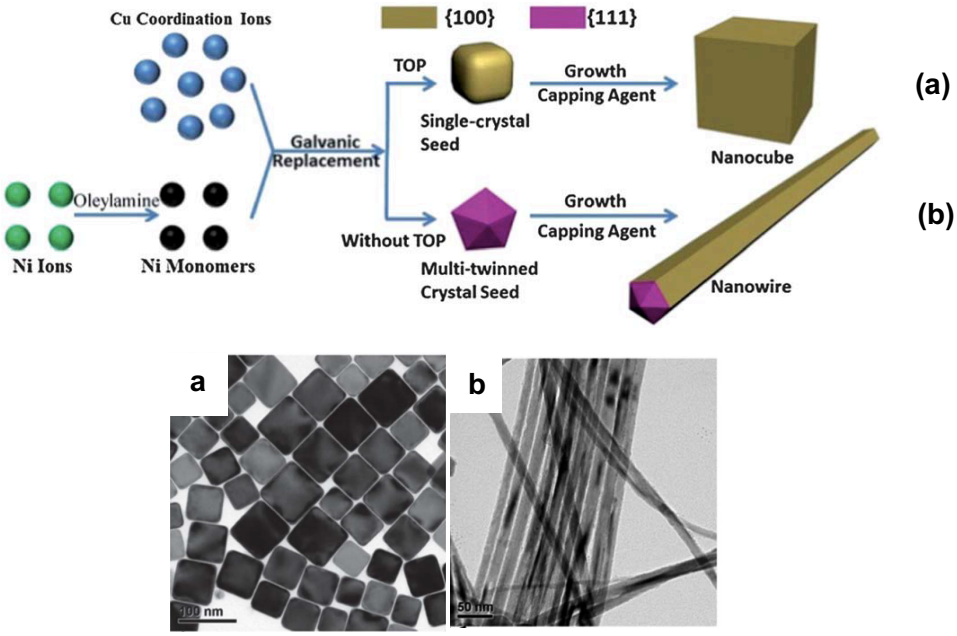

Figure I-7. *Schematic illustration for the shape-selective formation of (a) Cu nanocubes and (b) nanowires with the corresponding TEM images. (Copyright from Ref.[88])*

This effect of surface ligands on shape control was also shown in the synthesis of silver nanowires obtained by the reduction of $AgNO_3$ by ethylene glycol in the presence of poly(vinyl pyrrolidone) (PVP), which was reported by Y. Xia and co-workers.[89] In this synthesis, PVP acts as a polymeric surface ligand during the nanowire synthesis. The PVP has strong affinity to (100) facet of crystal through the oxygen (or nitrogen) atoms of the pyrrolidone. Due to the weak interaction between the PVP and the (111) facet, the Ag atoms preferentially added to the (111) facet, which led to the final shape of wire, as shown in Figure I-8.

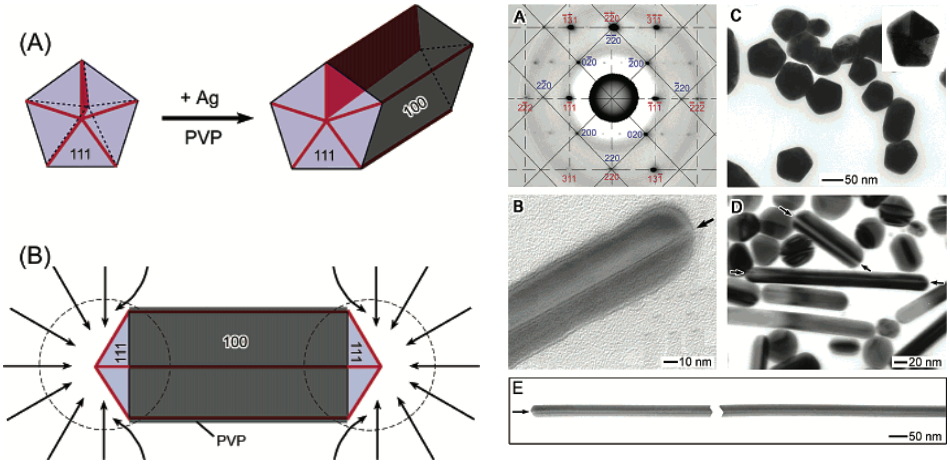

Figure I-8. *Schematic illustration the growth pathway of Ag nanowires and the corresponding TEM images. (Copyright from Ref.[89])*

In addition to play a crucial role in controlling the shape of the NPs, the ligands may still play a role as stabilizers to prevent the NPs coalescence by creating a steric (e.g. thiol, amine) or an electrostatic (i.e. via a double layer structure of a surfactant) barrier as shown in Figures I-9.[90] Additionally, they also influence the solubility of the NPs and define in which solvent they can form a colloidal solution. It is worth noting that the nature and the strength of the interactions between the surface ligands and the NPs play an important role in modulating the catalytic property of metal particles. Surface ligands can indeed change the NP activity and selectivity for a particular reaction.

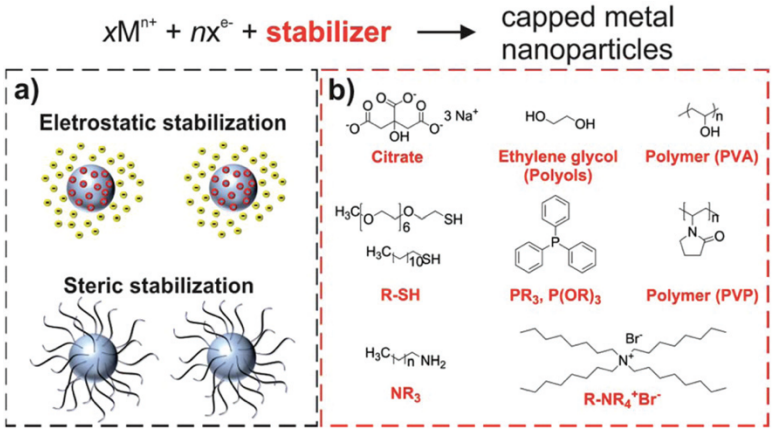

Figure I-9. *Most often used capping ligands in the synthesis of colloidal NPs. (Copyright from Ref.[90])*

In addition to their role as stabilizers and dispersants, the ligands can also help to protect metal NPs from oxidation. This is particularly interesting in the case of CuNPs which oxidize spontaneously in contact with air. K. Kontturi *et al.*[91] have demonstrated that the long chain ligands are able to increase resistance to oxidation of CuNPs. They prepared thiols-coated CuNPs by ligands exchange starting from lauric acid-stabilized CuNPs, and they investigated their behavior towards oxygen by studying their surface plasmon absorbance (SPR) in an air-exposed colloidal solution. The spectra of Cu NPS protected by lauric acid, oleic acid or octanedanethiol are reported in Figure I-10. In all cases, the SPR decreases in intensity and a red shift is observed indicating an oxidation process. As a result, the oxidation resistance of CuNPs was improved by increasing the alkyl chain length of the ligands. Oleic acid and octadecanethiol are observed to improve the oxidation stability of CuNPs relative to lauric acid. Nevertheless, dodecanethiol is shown to be more effective than oleic acid in preventing O_2 diffusion to the surface of CuNPs than oleic acid.

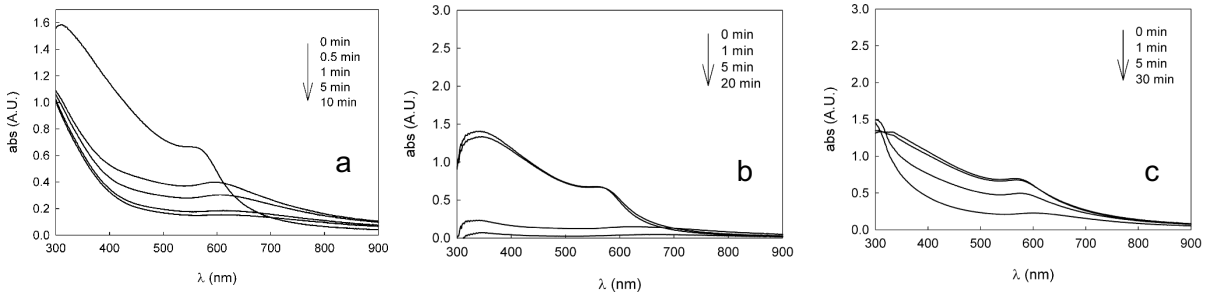

Figure I-10. *Evolution of UV-vis spectra of ligand-exchanged copper nanoparticles after air exposure (a) lauric acid (C_{12}) (b) oleic acid (C_{18}) (c) octadecanethiol (C_{18}). (Copyright from Ref.[91])*

I. 3 Optical properties of copper nanoparticles

Unlike bulk copper metal or atoms, the CuNPs suspension has often reddish or brownish color.[92] Changing the size or shape of NPs results in a change in the color of the colloidal solution. Similarly, as the other noble metal NPs (e.g., Au, Ag), the specificity of CuNPs is the presence of conduction electrons. Those electrons create a cloud of delocalized electrons in the metal. Those electrons will oscillate collectively under excitation by an external electromagnetic wave, leading to light absorption (as shown in Figure I-11).[93-95] This effect is called localized surface plasmon resonance, or LSPR.[96] The position of LSPR wavelength peak depends on various parameters, namely: material, size, shape and environment.[97]

Au, Ag and Cu NPS have the particularity of presenting a LSPR in the vis-NIR spectral range reveals their corresponding plasmon absorbance at a visible range of 400-800 nm. This

special optical property of metal NPs can be used to estimate the synthesis of NPs in solution medium and studied by UV-visible absorption spectroscopy. From those optical properties these particles called “plasmonic particles” have drawn interest for researchers.

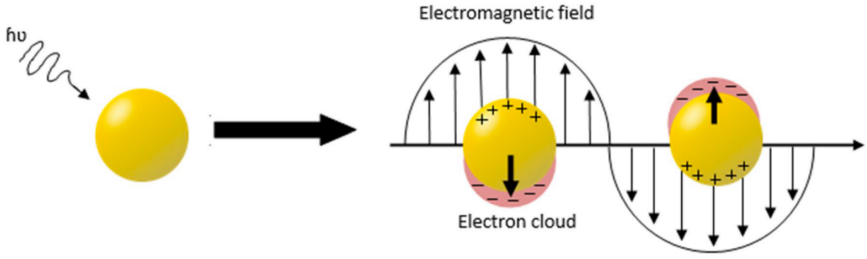

Figure I-11. *Schematic representation of the conduction electrons oscillating across the metal NP under an external electromagnetic field of incident light. (Copyright from Ref.[95])*

As shown in Figure I-12, J. Chen’s group[98] demonstrated the LSPR of Cu-SiO_2 core-shell nanoparticles strongly depended on the shape of NPs. They investigated the LSPR of Cu-SiO_2 nanoparticles through the discrete dipole approximation (DDA) simulation by using two geometries with the same volume: cubes (Figure I-12a) and spheres (Figure I-12b). The nanocubes with an edge length of 30 nm exhibits an extinction peak at 600 nm while the sphere shows an extinction maximum at 560 nm (with a mean size of 37 nm in diameter). Also, they found that the peak position of cube shifted by 14 nm by removing the sharp corners, and the rounded cube has an extinction maximum around to 586 nm (Figure I-12c). These LSPR result indicates that the plasmon peak red shifts for nanocubes of the same volume when compared to corresponding nanospheres.

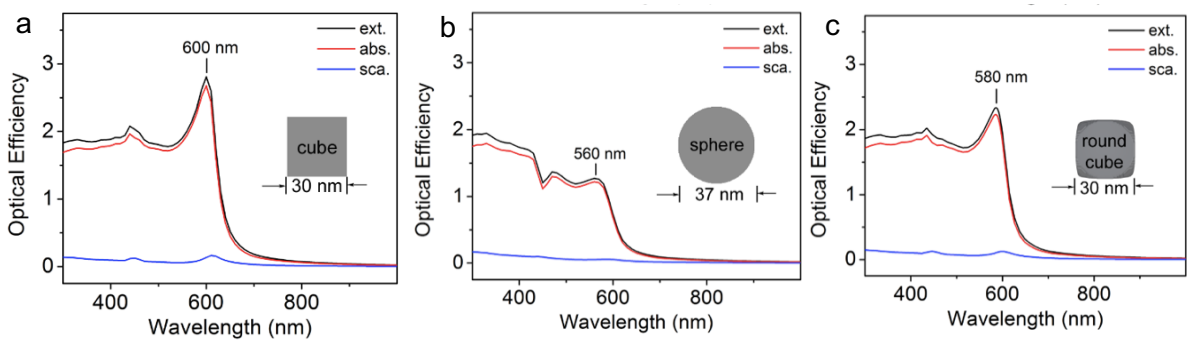

Figure I-12. *UV-vis spectra of the Cu-SiO_2 core-shell nanoparticles with different shapes: (a) Cu nanocubes with an edge length of 30 nm; (b) Cu nanospheres with an average diameter of 37 nm and (c) rounded Cu nanocubes. (Copyright from Ref.[98])*

Furthermore, the LSPR of Cu nanostructures can be tuned away from the interband transitions of Cu to the near infrared (NIR) region by tuning their compositions, such as copper sulfides ($Cu_{2-x}S$)[99] and copper phosphides ($Cu_{3-x}P$)[100] nanocrystals.

I. 4 Chemical reduction methods for preparing CuNPs

Among the various synthesis methods, the chemical reduction one is the simplest and easiest for the preparation of CuNPs. This method enables the control of the size, the size distribution and the morphology of NPs by an optimization of the experimental parameters, such as the nature of the reducing agent, the metal salt ligand, the precursor salt, the reaction time and the temperature.[101] In this thesis work, the CuNPs were synthetized by chemical reduction methods, which can be grouped into two different routes: a direct reduction reaction of copper salts (Cu(I) or Cu(II)) by a reducing agent and a disproportionation reaction of Cu(I) (Figure I-13). The disproportionation reaction is a reduction-oxidation reaction in which the same element is oxidized and reduced simultaneously. In this section, we present some direct reduction methods used in the literature for the synthesis of CuNPs.

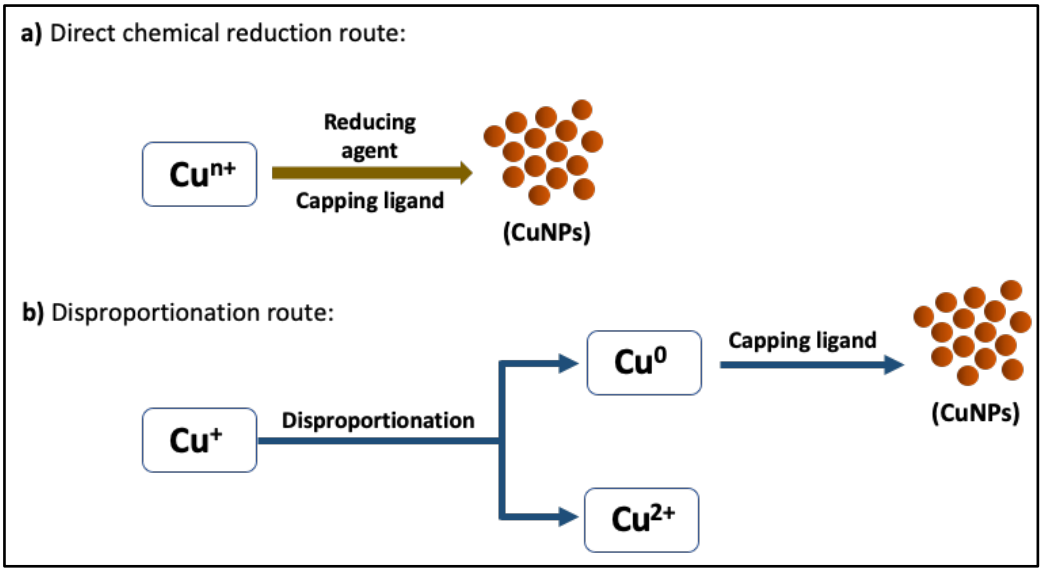

Figure I-13. *Different chemical reductive synthesis routes for preparing CuNPs.*

In the chemical reduction technique, the copper salts are reduced by a reducing agent such as boranes,[102] hydrazine (N_2H_4),[103] ascorbic acid,[104] glycol[105] and glucose[106] in the presence of ligands that play the role of capping agents or/and stabilizer or/and dispersing agent, as described in section 1.2.2. Here, we present some of the published methods to

prepare CuNPs by chemical reduction in solution using various type of reducers, and the corresponding NPs formation rate. (Table I-1).

Table I-1. *Selected examples of methods to synthesize CuNPs by chemical reduction in solution.*

Precursor	**Reducing agent**	**Ligands**	**Solvent**	**Formation rate**[109]
$CuCl_2$•$2H_2O$ $CuSO_4$•$5H_2O$ CuSO4 $Cu(NO_3)_2$ $CuCl(PPh_3)_3$ Cu(II)acetylacetonate $CuCl_2$ $Cu(CH_3COO)_2$	Boranes[102] (e.g. $NaBH_4$ *t*-$BuNH_3Cl$)	PVP, PEG, Amines, Phosphines, Ascorbic acid, CTAB, Oleic acid, Lauric acid	Water, Toluene, Ethylene, Glycol	Fast
	H_2[103]			-
	Amine[104]			-
	Hydrazine[105]			Medium
	Ascorbic acid[106]			Medium
	Glycol[107]			Slow
	Glucose[108]			Slow

CTAB: cetyltrimethylammonium bromide; PVP: polyvinylpyrrolidone; PEG: polyethylene glycol.

Over the past several years, the boranes compounds have been widely used for the synthesis of CuNPs due to their relative high reduction rate compare to others. However, there are still very few methods to obtain highly monodisperses CuNPs. The exploration of new routes to synthetize the CuNPs with narrow size attribution is thus still challenging. Here, we present two examples of synthetic reduction routes using boranes as reducing agent from the literature that yield small and high uniform CuNPs. In 2015, J. Chakraborty *et al.*[110] have reported the preparation of monodisperse CuNPs through a two-step synthetic methodology using digestive ripening. This is a postsynthesis size modification method that convert the large polydisperse NPs into small and monodisperse NPs by refluxing them in the presence of added capping ligand.[111] In their protocol, the first step is the reduction of $CuCl_2$•$2H_2O$ by $NaBH_4$ in the presence of tetraoctylammonium bromide (TOAB) and dodecanethiol (DDT) in toluene, which lead to large and polydisperse CuNPs with a mean size of 13.63 nm. Subsequently, the digestive ripening was used to narrow down polydispersity and size of NPs. After 24 h of digestive ripening in DDT, the NPs had a narrower polydispersity and a well-defined spherical shape, their size had decreased from 13.63 to 5.3 nm (Figure I-14).

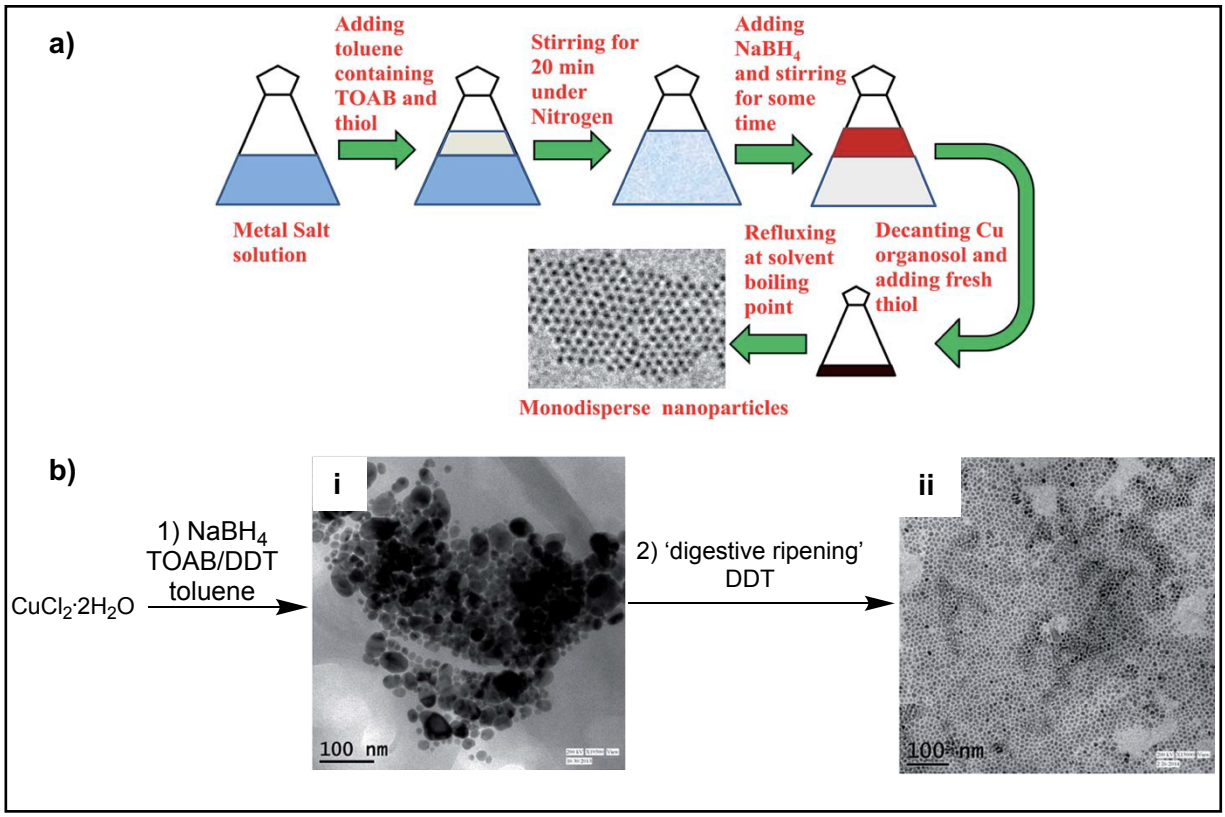

Figure I-14. *(a) Schematic illustration of the digestive ripening process for obtaining monodisperse CuNPs synthesis (b) TEM images of copper nanoparticles in toluene (i) before digestive ripening and (ii) after digestive ripening for 24 h. (Copyright from Ref.[110])*

Although the digestive ripening process favors the formation of monodisperse CuNPs as described as above, this method lacks of efficiency due to its long reaction time. Hence, there is another reduction route using borane as reducer to synthetize monodisperse CuNPs with tunable size and well-defined spherical shape that is more efficient and simpler (Figure I-15). This highly efficient reduction method was reported the same year by A. Courty and co-worker.[112] They have synthetized high-quantity of small CuNPs with narrow size distribution (<10%) through the reduction of the $CuCl(PPh_3)_3$ complex by *tert*-butylamine borane (TBAB) in the presence of alkylamine. After completion of the reaction, oleic acid (OA) was added in the reaction mixture to act as a CuNPs stabilizer and to prevent their coalescence. Indeed, the precipitation of as-synthetized CuNPs without addition of OA were observed after only 24h. An optimization of the reaction parameters as the temperature (50 °C, 80 °C and 100 °C) and the DDA to copper precursor ratio (from 8:1 to 16:1) enable the synthesis of CuNPs with tunable sizes from 3 nm to 11 nm. This study shows that the temperature is an important factor to tune the nanoparticle size. In this reaction, the increase in temperature promotes an increase in the nanoparticle size. The amount of capping agent has also been found to affect the NPs size.

The smaller CuNPs was obtained by increasing the concentration of capping ligands. This may be due to the high coverage of DDA on the particle surface that could hinder the growth of nanoparticles. They also investigated the influence of the amine chain length on the CuNPs morphology. The DDA was replaced with oleylamine (OLA) by maintaining the reaction condition at same temperature (50 °C, 80 °C and 100 °C), and a morphological evolution was observed. When reaction temperature is maintained at 50 °C, the size of CuNPs was increased from 3.5 nm to 7.4 nm. Once the temperature was increased to 80 °C and 100 °C, the CuNPs changed from spherical shape to triangle-shaped and nanodisks shapes. In their synthetic conditions, the reaction was carried out in toluene that is an apolar solvent. The increase of the length of the hydrocarbon chain allows to increase the chain-chain interaction between the solvent and ligands, which favors the particle growth. As a result, the nature of the amines ligands not only influences the size of the CuNPs, but also their shape. In this thesis work, a similar phenomenon has been observed (see Chapter II).

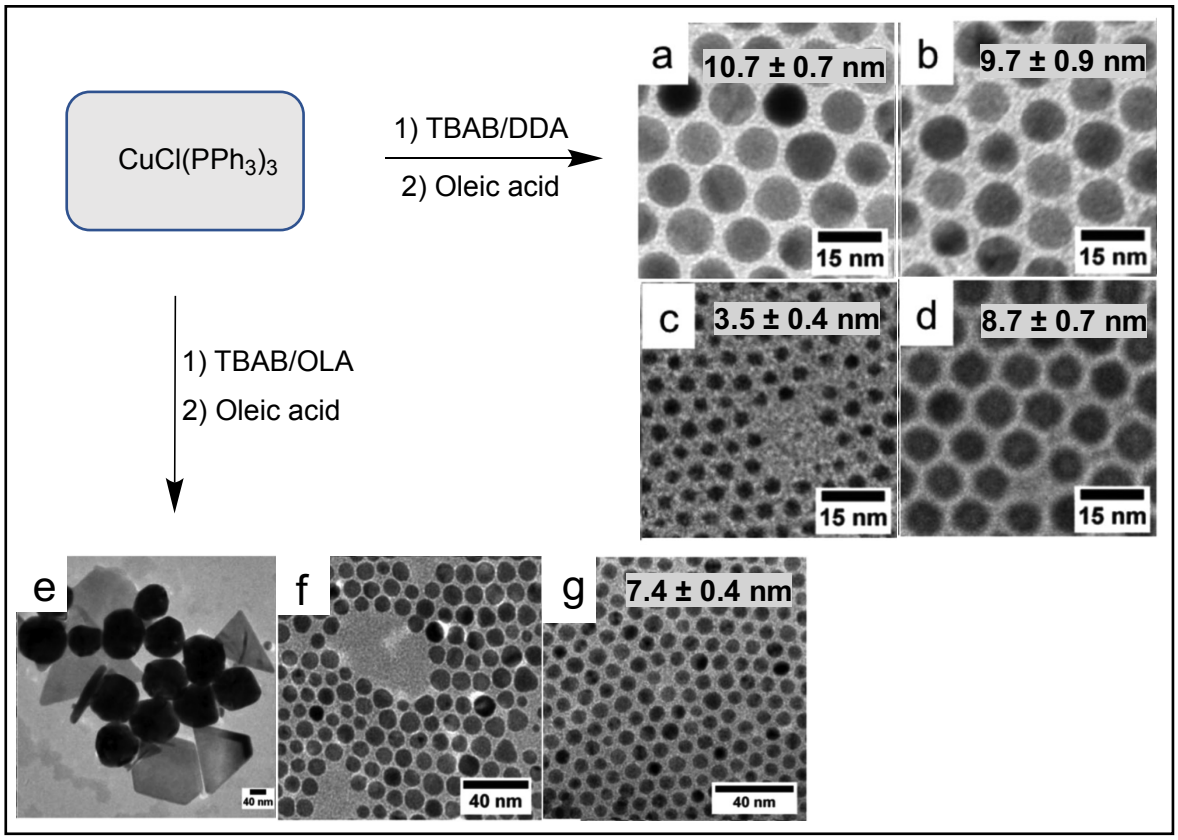

Figure I-15. *TEM images CuNPs stabilized by mixed ligands dodecylamine/oleic acid or oleylamine/oleic acid and prepared via the reduction of $CuCl(PPh_3)_3$ by TBAB. The molar ratio of dodecylamine to copper precursor is of 8 :1 at (a-e) 100 °C; (b-f) 80 °C and (c-g) 50 °C and (d) of ratio 16 : 1 at 100 °C. (Copyright from Ref.[112])*

In addition to the synthesis of CuNPs using boranes reducers seen above, other reduction methods using other types of reducers are reported in the literature as shown in Table I-2.

Table I-2. *Representative synthetic reduction route to CuNPs using various reducing agents*.

$CuCl_2 \cdot 2H_2O$ → **N_2H_4**, Ascorbic acid, Glycerol	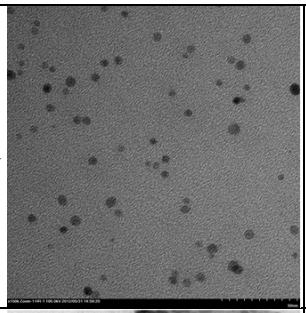	(R. Yunus *et al.* 2014)[105c] Mean size: 2-10 nm Spheroids
$CuSO_4$ → **Ethylene glycol**, PVP	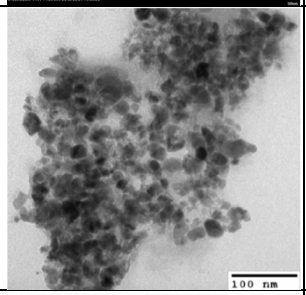	(C. Zhang *et al.* 2010)[107c] Mean size: 18 nm Spheroids
$Cu(CH_3COO)_2$ → **L-Ascorbic acid**, H_2O	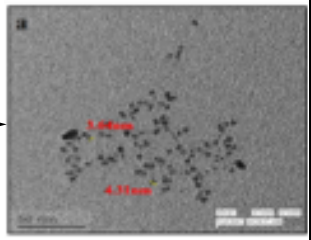	(Y. Li *et al.* 2014)[9] Mean size: 3 nm Spheroids
$CuCl_2 \cdot 2H_2O$ → **Glucose**, H_2O, OA, OLA, EtOH	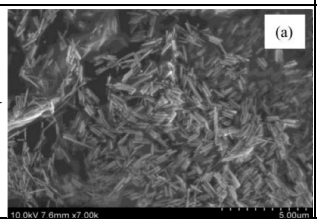	(D. Pan *et al.* 2014)[108] Mean size: 45 ± 3 nm Wires

The reduction of copper salts by a reducing agent is an efficient and convenient method to synthetize controlled size and monodisperse CuNPs. However, few different shapes are currently accessible by this method, which limits the number and type of their possible applications.[113] Up to now, although the synthesis of shape-controlled CuNPs has been increasingly studied, the variety of available shapes is less than for other noble metals such as gold or silver. Recently, another simple chemical method, the disproportionation reaction of copper salts in organic solvent under high temperature, has been developed to synthetize CuNPs. This methodology has been shown to be effective for the synthesis of tunable size-controlled CuNPs and offers the possibility of simple access to a greater diversity of shapes.

The bibliographic introduction of the disproportionation reaction for the synthesis of metallic NPs will be presented in chapter II.

I. 5 Conclusion

To conclude, this chapter presented a brief overview of the most recent analyses showing how noble metal nucleate and grow in solution. We thus focused on the reaction factors that are able to influence the final size and shape of the nanoparticles. We also presented some examples of methods reported in the literature of synthetizing CuNPs through the chemical reduction route. As shown in this last section, this strategy enables a fast and easy access to monodisperse CuNPs with tunable size and shape.

The aim of this thesis is to investigate and to develop new chemical synthetic methods for the synthesis of CuNPs that allow a size and shape control. Two different chemical reduction routes have been explored in this thesis work.

- In the Chapter II, the disproportionation reaction has been used for size and shape control synthesis of CuNPs by tuning a series of reaction parameters. Particularly, we focused on the investigation of the influence of the phosphine ligand and of the copper salt precursor on the final CuNPs size and shape.

- For Chapter III, the disproportionation route was also applied to realize the shape control synthesis of CuNPs by using a range of new source precursors, the Cu-CAACs complexes.

- In Chapter IV, a novel process of chemical reduction route based on the thermolysis of organocopper reagents was developed to synthetize with well-defined size and shape CuNPs in large amount.

I.6 References

(1) M. Faraday, *Philos. Trans. R. Soc. London*, **1857**, *147*, 145-181.
(2) R. P. Feynman, There's plenty of room at the bottom. *Eng. Sci.* **1960**, *23*, 22-36.
(3) K. Mallick, M. J. Witcomb, M. S. Scurrell, *Mater. Sci. Eng: B*, **2005**, *123*, 181.
(4) M. Grzelczak, J. Pérez-Juste, P. Mulvaney, L. M. Liz-Marzán, *Chem. Soc. Rev.* **2008**, *37*, 1783-1791.
(5) M. Abdulla-al-Mamun, Y. Kusumoto, M. Muruganandham, *Mater. Lett.*, **2009,** *63*, 2007.
(6) R. Das, S. S. Nath, R. Bhattacharjee, *J. Lumin.*, **2011**, *131*, 2703.
(7) C. Sauerbeck, M. Haderlein, B. Schürer, B. Braunschweig, W. Peukert, R. N. Klupp Taylor, *ACS Nano.*, **2014**, *8*, 3088-3096.
(8) a) P. Zhang, Z-A. Qiao, X. Jiang, G. M. Veith, S. Dai, *Nano Lett.,* **2015**, *15*, 823−828; b) M. R. Axet, K. Philippot, *Chem. Rev.,* **2020**, *120*, 1085-1145.
(9) J. Lawrence, J. T. Pham, D. Y. Lee, Y. Liu, A. J. Crosby, T. Emrick, *ACS Nano.*, **2014**, *8,* 1173-1179.
(10) Y. Wu, Y. Li, P. Liu, S. Gardner, B. S. Ong, *Chem. Mater*., **2006**, *18*, 4627-4632.
(11) L. Tong, R. R. Gattass, J. B. Ashcom, S. He, J. Lou, M. Shen, I. Maxwell, E. Mazur, *Nature.*, **2003**, *426*, 816-819.
(12) Y. Nakayama, P. J. Pauzauskie, A. Radenovic, R. M. Onarato, R. J. Saykally, J. Liphardt, P. Yang, *Nature.*, **2007**, *447*, 1098-1102.
(13) J. E. Millstone, S. J. Hurst, G. S. Métraux, J. I. Cutler and C. A. Mirkin, *Small.*, **2009**, *5*, 646-664.
(14) J. Watt, G. C. Bleier, M. J. Austin, S. A. Ivanov and D. L. Huber, *Nanoscale.*, **2017**, *9*, 6632-6637.
(15) C. Jing, F. J. Rawson, H. Zhou, X. Shi, W.-H. Li, D.-W. Li and Y. T. Long, *Anal. Chem.*, **2014**, *86*, 5513-5518.
(16) C. B. Williamson, D. R. Nevers, T. Hanrath, R. D. Robinson, *J. Am. Chem. Soc.*, **2015**,*137*, 15843-15851.
(17) M. A. El-Sayed, *Acc. Chem. Res.*, **2004**, *37*, 326-333.
(18) a) C. Amiens, B. Chaudret, D. Ciuculescu-Pradines, V. Collière, K. Fajerwerg, P. Fau, M. Kahn, A. Maisonnat, K. Soulantica, K. Philippot, *New. J. Chem.*, **2013**, *37*, 3374-3401; b) I. Lignos, R. Maceiczyk, *Acc. Chem. Res.*, **2017**, *50*, 1248-1257.
(19) J. K. Patra, K-H. Baek, *J. Nanomater.,* **2014**. Article ID 417305.
(20) a) T. Prasad Yadav, R. Manohar Yadav, D. Pratap Singh, *J. Nanosci. Nanotechnol.*, **2012**, *2,* 22-48; b) P. Colson, C. Henrist, R. Cloots, *J. Nanomater.*, **2013**, Article ID 948510.
(21) P. F. M. de Oliveira, R. M. Torresi, F. Emmerling, P. H. C. Camargo, *J. Mater. Chem. A.,* **2020**, *8*, 16114-16141.
(22) S. Eustis, *M. A.* El-Sayed, *Chem. Soc. Rev*., **2006**, *35*, 209-217.
(23) A. Adlim*, Indo. J. Chem.*, **2006**, *6,* 1-10.
(24) P. Pattekari, Z. Zheng, X. Zhang, T. Levchenko, V. Torchilin, Y. Lvov, *Phys. Chem. Chem. Phys*., **2011**, *13* (19*)*, 9014-9019.
(25) W. Yu, H. Xie, L. Chen, Y. Li, *Powder Technology.*, **2011**, *197*, 218-221.
(26) a) T. M. D. Dang, T. T. T. Le, E. Fribourg-Blanc, M. C. Dang, *Adv. Nat. Sci.: Nanosci. Nanotechnol.,* **2011**, *2*, Article ID 015009; b) G. H. Chan, J. Zhao, E. M. Hicks, G. C. Schatz, and R. P. Van Duyne, *Nano Lett.*, **2007,** *7*, 1947-1952.
(27) K. Judai, S. Numao, J. Nishijo, N. Nishi, *J. Mol. Catal. A: Chem.*, **2011**, *347*, 28-33.

(28) A. O. Musa, T. Akomolafe, M. J. Carter, *Sol. Energy Mater. Sol. Cells.*, **1998**, *5*, 305-316.
(29) B. K. Park, D. Kim, S. Jeong, J. Moon, J. S. Kim, *Thin Solid Films*, **2007**, *515*, 7706-7711.
(30) T. M. D. Dang, T. T. T. Le, E. Fribourg-Blanc and M. C. Dang, *Adv. Nature. Sci. Nanosci. Nanotechnol.*, **2011**, *2,* 015009.
(31) D. Tomotoshi, H. Kawasaki., *Nanomater.,* **2020**, *10*, 1689.
(32) a) C. Wu, B. P. Mosher, T. Zeng, *J. Nanopart. Res.,* **2006**, *8*, 965; b) H. X. Zhang, U. Siegert U, R. Liu, W. B. Cai, *Nanoscale Res. Lett.*, **2009**, *4*, 705; c) X. Zhang, H. Yin, X. Cheng, H. Hu, Q. Yu, A. Wang, *Mater. Res. Bull.**, 2006**, 41*, 2041; d) W. Yu, H. Xie, L. Chen, Y. Li, C. Zhang, *Nanoscale Res. Lett.,* **2009***, 4*, 465; e) P. Pulkkinen, J. Shan, K. Leppanen, A. Kansakoshi, A. Laiho, M. Jarn and H. Tenhu, Appl. Mater. Interfaces, **2009**, *2*, 519; f) X. Cheng, X. Zhang, H. Yin, A. Wang, Y. Xu, *Appl. Surface Sci.*, **2006**, *253*, 2727; g) Q. L. Zhang, Z. M. Yang, B. J. Ding, X. Z. Lan, Y. J. Guo, *Trans. Nonferrous Met. Soc. China.*, **2010**, *20*, 240-244.
(33) a) R. Zhou, X. Wua, X. Hao, F. Zhou, H. Li, W. Rao, *Nucl. Instrum. Methods Phys. Res.* B., **2008**, *266,* 599; b) W. K. Han, J. W. Choi, G. H. Hwang, S. J. Hong, J. S. Lee, S. G. Kang, *Appl. Surface Sci.*, **2006**, *252*, 2832.
(34) a) D. Tomotoshi, H. Kawasaki, *Nanomater.,* **2020**, *10*, 1689; b) R. V. Kumar, Y. Mastai, Y. Diamant, *J. Mat. Chem.*, **2001**, *11*, 1209.
(35) N. Sreeju, R. Alex, D. Philip, *J. Mol. Liq.,* **2016**, *221*, 1008-1021.
(36) J. N. Solanki, R. Sengupta, Z. V. P. Murthy, *Solid State Sciences.*, **2010**, *12*, 1560-1566
(37) a) F. B. Effenberger, M. A. Sulca, M. T. Machini, R. A. Couto, K. K. Pedro, M. Giovanna, M. R. Liane, *J. Nanopart. Res.,* **2014***. 16***,** 2588; b) M. Salavati-Niasari, F. Davar, *Mater. Let.*, **2009**, *63*, 441-443.
(38) A. Heuer-Jungemann, N. Feliu, I. Bakaimi, M. Hamaly, A. Alkilany, I. Chakraborty, A. Masood, M. F. Casula, A. Kostopoulou, E. Oh, K. Susumu, M. H. Stewart, I. L. Medintz, E. Stratakis, W. J. Parak, A. G. Kanaras, *Chem. Rev.*, **2019**, *119*, 4819−4880.
(39) S. B. Yaqoob, R. Adnan, RM. Rameez Khan, M. Rashid M, *Front. Chem.,* **2020**, *8*, 376.
(40) X. Song, S. Sun, W. Zhang, Z. A. Yin, *J. Colloid Interface Sci.,* **2004**, *273,* 463−469.
(41) A. M. El Sayed, S. El-Gamal, W. Morsi, G. Mohammed, *J. Mater. Sci.*, **2015**, *50*, 4717-4728.
(42) H. T. Zhu, C. Y. Zhang, Y. S. J. Yin, *Cryst. Growth Des.*, **2004**, *270*, 722−728.
(43) D. Mott, J. Galkowski, L. Y. Wang, J. Luo, C. J. Zhong, *Langmuir.*, **2007**, *23*, 5740-5745.
(44) J. C. Yu, F. G. Zhao, W. Shao, C. W. Ge, W. S. Li, *Nanoscale.,* **2015**, *7*, 8811-8818.
(45) K. Liu, Y. Song, S. Chen, *J. Power Sources.*, **2014**, *268*, 469-475.
(46) I. Lisiecki, M. P. Pileni, *J. Phys. Chem.,* **1995,** *99*, 5077-5082.
(47) A. Wang, L. Chen, F. Xu, Z. Yan, *RSC Adv.,* **2014**, *4*, 45251-45257.
(48) F. Chahdoura, C. Pradel, M. Gómez, *Chem. Cat. Chem.*, **2014**, *6*, 2929-2936.
(49) K. An, S. Alayoglu, T. Ewers, G. A. Somorjai, *J. Colloid Interface Sci.,* **2012**, *373*, (1-13).
(50) a) I. Lisiecki, F. Billoudet, M. P. Pileni, *J. Phys. Chem.*, **1996**, *10*, 4160-4166; b) M. A. Ben Aissa, B. Tremblay, A. Andrieux-Ledier, E. Maisonhaute, N. Raouafi, A. Courty, *Nanoscale*, **2015**, *7*, 3189-3195; c) D. Mott, J. Galkowski, L. Y. Wang, J. Luo, C. J. Zhong, *Langmuir*, **2007**, *23*, 5740-5745; d) A. Sharma, R. K. Dutta, *RSC Adv.,* **2015**, *5*, 43815-43823.
(51) a) N. Zhang, X. Zhu, *Phys. Rev. Lett.*, **2008**, *101*, Article ID 099702; b) A. P. LaGrow, L. Sinatra, A. Elshewy, K. W. Huang, K. Katsiev, A. R. Kirmani, A. Amassian, A. D. H. Anjum, O. M. Bakr, *J. Phys. Chem. C.*, **2014**, *118*, 19374-19379.

(52) a) R. Venkatasubramanian, J. He, M. W. Johnson, I. Stern, D. H. Kim, N. S. Pesika, *Langmuir,* **2013**, *29,* 13135-13139; b) W. Songping, M. Shuyuan, *Mater. Lett.,* **2006**, *60*, 2438-2442.
(53) H. J. You, J. X. Fang, *Nanotoday*, **2016**, *11*, 145-167.
(54) V. K. LaMer, R. H. Dinegar, *J. Am. Chem. Soc.,* **1950**, *72*, 4847-4854.
(55) J. Polte, R. Erler, A. F. Thunemann, S. Sokolov, T. T. Ahner, K. Rademann, F. Emmerling, R. Kraehnert, *ACS Nano*., **2010**, *4*, 1076.
(56) Y. N. Xia, X. J. Xiong, B. Lim, S. E. Skrabalak, *Angew, Chem. Int. Ed.,* **2009**, *48*, 60-103.
(57) a) Y. Xiong, Y. Xia, *Adv. Mater.*, **2007**, *19*, 3385; b) B. Wiley, T. Herricks, Y. Sun, Y. Xia, Nano Lett., **2004**, *4*, 1733-739.
(58) Y. Xiong, J. Chen, B. Wiley, Y. Xia, S. Aloni, Y. Yin, *J. Am. Chem. Soc.,* **2005**, *127*, 7332.
(59) Y. Xiong, H. Cai, B. J. Wiley, J. Wang, M. J. Kim, Y. Xia, *J. Am. Chem. Soc.,* **2007**, *129*, 3665.
(60) Y. Xiong, H. Cai, Y. Yin, Y. Xia, *Chem. Phys. Lett.,* **2007**, *440*, 273.
(61) B. J. Wiley, Z. Wang, J. Wei, Y. Yin, D. H. Cobden, Y. Xia, *Nano Lett*., **2006**, *6,* 2273.
(62) Y. Xiong, J. M. McLellan, Y. Yin, Y. Xia, *Angew. Chem. Int. Ed.,* **2007**, *46*, 790.
(63) Y. Sun, B. Mayers, T. Herricks, Y. Xia, *Nano Lett*., **2003**, *3*, 955.
(64) Y. Xiong, J. M. McLellan, J. Chen, Y. Yin, Z.-Y. Li, Y. Xia, *J. Am. Chem. Soc.* **2005**, *127* (17), 118.
(65) Y. Yin, A. P. Alivisator, *Nature*, **2005**, *437*, 664-670.
(66) Y. Xiong, I. Washio, J. Chen, H. Cai, Z.-Y. Li, Y. Xia, *Langmuir,* **2006**, *22*, 8563.
(67) a) B. Wiley, Y. Sun, B. Mayers, Y. Xia, *Chem. Eur. J.,* **2005**, *11*, 454; b) B. Wiley, Y. Sun, J. Chen, H. Cang, Z.-Y. Li, X. Li, Y. Xia, *MRS Bull.,* **2005**, *30*, 356; c) B. Wiley, Y. Sun, Y. Xia, *Acc. Chem. Res*., **2007**, *40*, 1067; d) A. R. Tao, S. Habas, P. Yang, *Small,* **2008**, *4*, 310.
(68) B. Wiley, T. Herricks, Y. G. Sun, Y. N. Xia, *Nano Lett*., **2004**, *4* (9), 1733-1739.
(69) K. K. Caswell, C. B. Bender, C. J. Murphy, *Nano Lett.,* **2003**, *3*, 667.
(70) B. J. Wiley, Y. Xiong, Z.-Y. Li, Y. Yin, Y. Xia, *Nano Lett.,* **2006**, *6*, 765.
(71) B. J. Wiley, Y. Chen, J. McLellan, Y. Xiong, Z.-Y. Li, D. Ginger, Y. Xia, *Nano Lett.,* **2007**, *7*, 1032.
(72) H. Yuan, K. P. F. Janssen, T. Franklin, G. Lu, L. Su, X. Gu, H. Uji-i, M. Roeffaers, J. Hofkens, *RSC Adv*., **2015**, *5*, 6829-6833.
(73) G. D. M. R. Dabera, M. Walker, A. M. Sanchez, H. J. Pereira, R. Beanland, R. Hatton, *Nature Com.***, 2017**, *8*, 1894.
(74) a) Y. Xiong, J. Chen, B. Wiley, Y. Xia, S. Aloni, Y. Yin, *J. Am. Chem. Soc*., **2005**, *127,* 7332; b) Y. Xiong, B. Wiley, J. Chen, Z.-Y. Li, Y. Yin, Y. Xia, *Angew. Chem.,* **2005**, *117*, 8127; *Angew. Chem. Int. Ed.,* **2005**, *44*, 7913; c) N. Zettsu, J. M. McLellan, B. Wiley, Y. Yin, Z.-Y. Li, Y. Xia, *Angew. Chem*., **2006**, *118*, 1310*; Angew. Chem. Int. Ed.,* **2006**, *45*, 1288; d) Y. Xiong, H. Cai, B. J. Wiley, J. Wang, M. J. Kim, Y. Xia, *J. Am. Chem. Soc.,* **2007**, *129*, 3665.
(75) a) A. Holden, P. Singer, Crystals and Crystal Growing, Double- day, Garden City, **1960**; b) J. W. Mullin, Crystallization, Butter-worths, London, **1961**; c) J. Hulliger, *Angew. Chem*., **1994**, *106*, 151; d) *Angew. Chem. Int. Ed. Engl*., **1994**, *33*, 143.
(76) Y. Yin, A. P. Alivisarors, *Nature*, **2005**, *437*, 664-670.
(77) N. Razgoniaeva, A. Acharya, N. Sharma, P. Adhikari, M. Shaughnessy, P. Moroz, D. Khon, M. Zamkov, *Chem. Mater.,* **2015**, *27* (17), 6102-6108.
(78) A. Pimpinelli, J. Villain, *Phys. Crys. Growth*, Cambridge University Press, UK, **1998**.
(79) T. Sugimoto, *J. Colloid Interf. Sci.,* **1992**, *150*, 208-225.

(80) a) H. Zheng, R. K. Smith, Y. W. Jun, C. Kisielowski, U. Dahmen, *Science*, **2009**, *324,* 1309-1312; b) Y. T. Zhu, J. Narayan, J. P. Hirth, S. Mahajan, X. L. Wu, X. Z. Liao, *Acta Materialia*, **2009,** *57*, 3763-3770; c) D. Li, M. H. Nielsen, J. R. Lee, C. Frandsen, J. F. Banfield, J. J. De Yoreo, *Science*, **2012**, *336*, 1014-1018; d) H. G. Liao, L. Cui, S. Whitelam, H. Zheng, *Science*, **2012**, *336*, 1219185.
(81) a) C. Besson, E. E. Finney, R. G. Finke, *J. Am. Chem. Soc.,* **2005**, *127,* 8179-8184; b) G. D. Barmparis, Z. Lodziana, N. Lopez, I. N. Remediakis, J. Beilstein, *J. Nanotechnol.,* **2015**, *6*, 361.
(82) H. Reiss, J. Chem. Phys., **1951**, *19*, 482-487.
(83) J. Zhang, Y. Yu, B. Zhang, *Phys. Sci. Rev.*, **2019**, 20180046.
(84) H. S. Dehsari, A. H. Ribeiro, B. Ersöz, W. Tremel, G. Jakob, K, Asadi, *Cryst. Eng. Comm*, **2017**, *19*, 6694-6702.
(85) C. J. Murphy, A. M. Gole, S. E. Hynyadi, J. W. Stone, P. N. Sisco, A. Alkilany, B. E. Kinard, P. Hankins, *Chem. Comm.,* **2008**, *5*, 544-557.
(86) C. Boukouvala, J. Daniel, E. Ringe, Approaches to modelling the shape of nanocrystals. *Nano Converg.*, **2021**, *8*, 26.
(87) A. Heuer-Jungemann, N. Feliu, I. Bakaimi, M. Hamaly, A. Alkilany, I. Chakraborty, A. Masood, M. F. Casula, A. Kostopoulou, E. Oh, K. Susumu, M. H. Stewart, I. L. Medintz, E. Stratakis, W. J. Parak, A. G. Kanaras. *Chem. Rev*., **2019**, *119,* 4819-4880.
(88) H. Guo, Y. Chen, H. Ping, J. Jin, D-L. Peng, *Nanoscale*, **2013**, *5*, 2394.
(89) Y. Sun, B. Mayers, T. Herricks, Y. Xia, *Nano. Lett*., **2003**, *3*, 995.
(90) L. M. Rossi, J. L. Fiorio, M. A. S. Garcia, C. P. Ferraz, *Dalton Trans.*, **2018**, *47*, 5889-5915.
(91) P. Kanninen, C. Johans, J. Merta, K. Kontturi, *J. Colloid Interface Sci.,* **2008**, *318*, 88-95.
(92) M. A. El-Sayed, Acc*. Chem. Res*., **2001**, *34*, 251-264.
(93) A. J. Henglein, *J. Phys. Chem.*, **1993**, *97*, 5457-5471.
(94) S. Eustis, M. A. El-Sayed, *Chem. Soc, Rev*., **2006**, *35*, 209-217.
(95) M.A. Fuller, I. Köper, *Nano Converg.,* **2019***, 6***,** 11.
(96) J. J. Mohindroo, U. K. Garg, A. K. Sharma, *AIP Conf. Proc.*, **2016**, *1728*, 020534.
(97) P. S. S. dos Santos, J. M. M. M. de Almeida, I. Pastoriza-Santos, L. C. C. Coelho, *Sensors*. **2021**, *21* (6), 2111.
(98) C. C. Crane, F. Wang, J. Li, J. Tao, Y. Zhu, J. Chen, *J. Phys. Chem. C.* **2017**, *121* (10), 5684-5692.
(99) K. Young-Tae, L. Gu-Dam, K. Seil, R. Seung Han, H. Tae-Yeon, P. Kee-Ryung, C.Yong-Ho. *J. Mater. Chem. C.*, **2018**, *6*, 754-760.
(100) L. De Trizio, R. Gaspari, G. Bertoni, I. Kriegel, L. Moretti, F. Scotognella, L. Maserati, Y. Zhang, G. C. Messina, M. Prato, S. Marras, A. Cavalli, L. Manna, *Chem. Mater.,* **2015**, *27* (3), 1120-1128.
(101) A. Umer, S. Naveed, N. Ramzan, M. S. Rafique, *NANO: Brief Reports and Reviews,* **2012**, *7* (5), 1230005.
(102) a) Z. Song, J. Hrbek, and R. Osgood, J. phys. Nano Lett., **2005**, 5, 228; b) Z. Li, Y. Ding, X. Wu, J. Ge, P. Ouyang, Z. Liu, *RSC Adv.*, **2016**, *6,* 20772.
(103) C. Barrière, K. Piettre, V. Latour, O. Margeat, C. O. Turrin, B. Chaudret, P. Fau, *J. Mater. Chem.,* **2012**, *22*, 2279-2285.
(104) X. Frogneux, F. Borondics, S. Lefrançois, F. D'Accriscio, C. Sanchez, S. Carenco, *Catal. Sci. Technol.*, **2018**, *8*, 5073-5080.
(105) a) X. Su, J. Zhao, H. Bala, Y. Zhu, Y. Gao, S. Ma, and Z. Wang, The Journal of Physical Chemistry C, **2007**, *111*, 14689; b) T. Karaca, M. Sevim, O. Metin, *Chem. Cat. Chem*.,

2017, *9*, 4185; c) H.R. Ong, M. R. Khan, R. Ramli, R. Yunus, *Appl. Mechanics Mater.,* **2014**, *481*, 21-26.

(106) a) C. Wu, B. P. Mosher, T. Zeng, *J. Nanopart. Res*., **2006**, *8*, 965; b) D. Gyasi-Antwi, A. O. Boansi, P. K. Mensah, *J. Appl. Sci. Tech*., **2019**, *23,* 46; c) Q. M. Liu, Y. Takehiro, K. Kensuke, O. Masazumi, Trans. Nonferrous Met. Soc. China, **2012**, *22*, 2198−2203; d) R. Phul, C. Kaur, U. Farooq, T. Ahmad, *Material Sci. Eng. Int. J.,* **2018**, *2* (4), 90-94.

(107) a) B. K. Park, S. Jeong, D. Kim, J. Moon, S. Lim, J. S. Kim, *J. Colloid Interface Sci.,* **2007,** 311, 417; b) N. Hikmah, N. F. Idrus, J. Jai, A. Hadi, **2016**, *InIOP Conf. Ser.: Earth Environ. Sci*., **2011**, *36,* 012050; c) W. Yu, H. Xie, L. Chen, C. Zhang, *J. D. Sci. Tec.*, **2010**, *31*, 364-367.

(108) S. J. Li, Y. Y. Chen, L. J. Huang, D. C. Pan, *Inorg. Chem.,* **2014**, *53*, 4440-4444.

(109) A. Umer, S. Naveed, N. Ramzan, M. S. Rafique, *NANO: Brief Reports and Reviews,* **2012**, *7* (5), 1230005.

(110) A. H. Shaik, J. Chakraborty, *RSC Adv.,* **2015**, *5*, 85974-85977.

(111) J. R. Shimpi, D. S. Sidhaye, B. L. V. Prasad, *Langmuir,* **2017,** *33*, 9491-9507.

(112) M. Ali Ben Aissa, B. Tremblay, A. Andrieux-Ledier, E. Maisonhaute, N. Raouafi, Alexa Courty, *Nanoscale*, **2015**, *7*, 3189.

(113) a) N. N. Hoover, B. J. Auten, B. D. Chandler, *J. Phys. Chem. B*, **2006**, *110*, 8606-8612; b) H. Kim, S. R. Dhage, D. Shim, H. T. Hahn, *Appl. Phys. A*, **2009**, *97*, 791-798; c) Y. Lee, J. Choi, K. J. Lee, N. E. Stott, D. Kim, *Nanotechnology*, **2008**, *19*, 415604-415610.

Chapter II. Synthesis of copper nanoparticles with controlled size and shape using various phosphorus ligands

II. 1 Introduction

As discussed previously, the synthesis of copper nanoparticles (CuNPs) with controlled shape and size has attracted increasing interest due to their particular chemical and physical properties. Moreover, the control of the morphology of CuNPs allows to improve their reactivity and selectivity towards specific catalytic reactions, their special plasmon signal in spectroscopic reaction and their application for plasmonic devices.[1-5] However, compared to other noble metal NPs of the same group such as gold and silver, the development of shape-controlled CuNPs synthesis is still in its infancy. This may be explained by the fact that the CuNPs possess a very low redox potential and are thus easily oxidized by air, which makes their preparation and use more difficult because they must be synthesized under inert gas such as N_2 or Ar.[6,7]

The synthesis of CuNPs from copper salts using molecular reducers has been previously presented in Chapter I. The salt reduction method is robust, convenient, and enable a good control of the size. However, the variety of accessible shapes is limited.

The aim of this chapter is to study the synthesis of CuNPs whose shape and size are controlled by another simple and practical route, the disproportionation reaction. Up to now, very few studies are reported in the literature about the selective shape synthesis of CuNPs by this way, and they all only use the two most common phosphorus ligands: trioctylphosphine (TOP) and trioctylphosphine oxide (TOPO).[13-15] These works will be presented in details in the next section. Based on these seminal works, we wanted to try to rationalize the effect of the phosphorous ligand on the synthesis of CuNPs, in particular whether it was possible to find a simple and predictive relationship between the pKa and the steric hindrance of the phosphorus ligand on the one hand, and the shape and the size of the yielded nanoparticle on the other hand. We thus expanded the disproportionation reaction by using various phosphorus ligands owning different steric and electronic properties in order to obtain CuNPs with various original shapes and tunable sizes. Beside the various phosphorus ligands, other reaction parameters have been also studied, including the amount of phosphorus ligands, the nature of copper precursor and the reaction temperature.

II. 2 Bibliographic introduction on the synthesis of CuNPs via disproportionation

In the typical salt reduction method for CuNPs synthesis, strong reducing agents and/or high temperature are usually required to realize the synthesis of CuNPs due to the low redox potential of copper. However, the nucleation and growth of NPs are not easily controlled in these reaction conditions.[7,8] To face this challenge, the development of synthetic routes by reducing Cu precursor into Cu(0) with controllable nucleation and growth steps became the major task for chemists. In recent years, an alternative non-aqueous method to produce CuNPs via the disproportionation of copper (I) salts, which would be able to easily control the morphology and size of NPs was increasingly studied.

In 2011, the first investigation of CuNPs synthesis through a disproportionation of a ligand-free copper salt in an organic solvent was reported by M. Y. Han and co-workers.[9] In this seminal work they have synthetized copper NPs through the controlled disproportionation of Cu(I)Cl into metallic Cu(0) and bivalent Cu(II) at 200 °C in oleylamine (OLA) (Figure II-1). They obtained high-quality oleylamine-coated copper nanowires with an average size of 50 nm in diameter and a length greater than 10 μm. In this work, the oleylamine played not only the role of an organic solvent, but also of capping agent. To improve the air-stability of the nanowires obtained, they have exchanged the oleylamine on surface with trioctylphosphine (TOP) after the synthesis of the CuNPs. The TOP-coated CuNPs nanowires obtained shown a better resistance to oxygen than their OLA-coated NPs analogs as exposed to air. This result also shown that the binding between the NPs surface and the TOP ligand is stronger than with oleylamine. During the ligand-exchange procedure, they found no significant change in size or shape of CuNPs from TEM results.

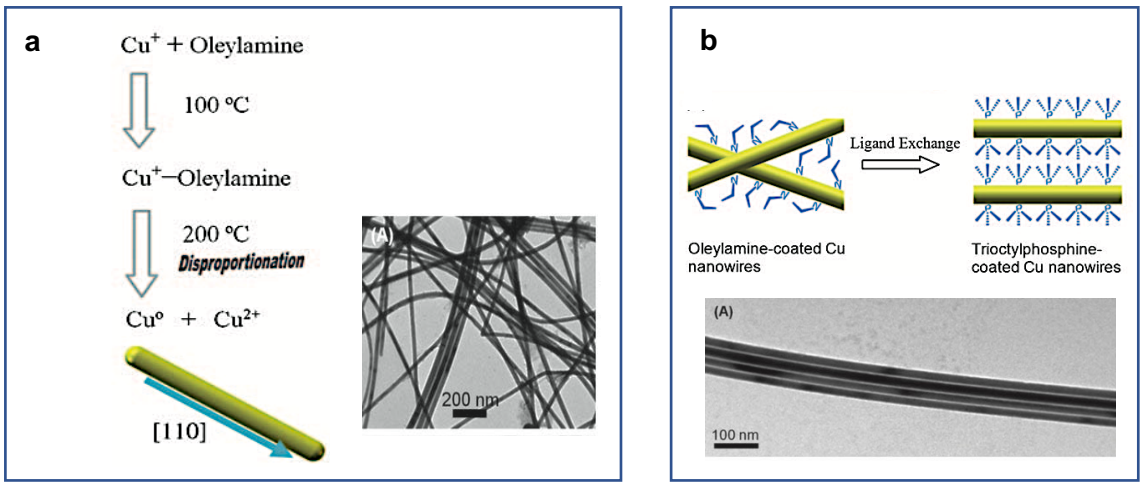

Figure II-1. *(a) Schematic disproportional reaction for the formation of oleylamine-stabilized copper nanowires (b) Schematic self-assembly of OLA- and TOP-coated copper nanowires. (Copyright from Ref.[9])*

In 2013, H. Guo's group[10] has developed a synthetic route via a disproportionation reaction of a CuBr•TOP complex in oleylamine, increasing the reaction temperature from 100 °C to 260 °C. These modified conditions yield monodisperse spherical CuNPs with an average size of 23 nm in diameter (Figure II-2a). For studying the role of TOP ligand, they have performed this reaction in the same conditions but without addition of TOP. A reddish solution was observed at a lower temperature of 210 °C compared to the reaction with TOP (for which the color of the solution changed at 250 °C) and larger and polydispersed nanocrystals were obtained. As a result, the presence of TOP and Br^- is required to form monodisperse CuNPs in this work. They proposed that the presence of TOP ligand could prevent a fast reduction of Cu(I) to Cu(0), which allows to accumulate enough reactant species to reach the critical nucleation concentration, and thus to achieve an instantaneous nucleation leading to the formation of monodisperse NPs. It must be pointed out that this hypothesis is in contradiction with a more recent study by M. Strach *et al*.[11] who showed that the disproportionation of the CuBr•TOP complex started from 150 °C. These monodisperse Cu nanospheres were used to prepare a SiO_2@Cu nanocatalyst by mixing silica aerogel with CuNPs colloidal solution in toluene, that was used for A_3 coupling reaction (Figure II-ii).[10]

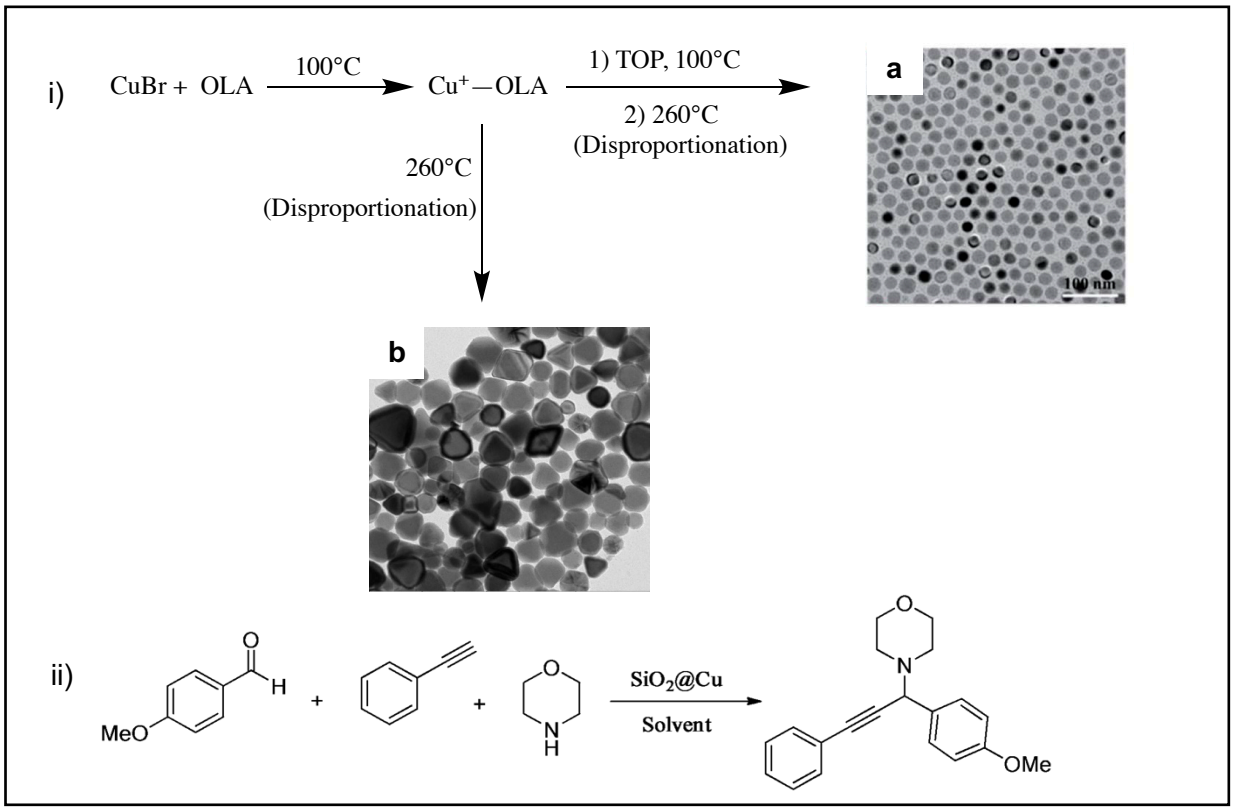

Figure II-2. *i) Disproportional reaction for the formation of CuNPs in the presence (a) or absence (b) of TOP ligand and ii) A_3 coupling reaction. (Copyright from Ref. [10])*

One-year later, the same group[12] reported a shape-controlled synthesis of CuNPs by using two different phosphine ligands via a disproportionation reaction route, and the possible formation mechanism of these CuNPs has been first discussed. In addition to the TOP, the trioctylphosphine oxide (TOPO) was also selected as phosphorus ligand to synthetize CuNPs. In this work, the presence of TOP yielded the sphere-shaped NPs with an average size of 23.4 ± 1.5 nm which have a narrow size distribution of 6% (Figure II-3a). However, in the case of TOPO (Figure II-3b), cubic CuNPs were obtained with a mean size of 46.8 nm in length. They found that the different shape-selective effect between the TOP and TOPO is due to their different coordination mode to Cu ions and their different nucleation temperatures. As seen above, they postulated that the role of TOP was to prevent a fast reduction of Cu(I) which enables an instantaneous nucleation process at a high temperature (260 °C).[12] They claimed that isotropous crystals with low selective adsorption of Br^- have been formed at high temperature, which allows to the seeds to grow identically in all direction, thus leading to spherical NPs.

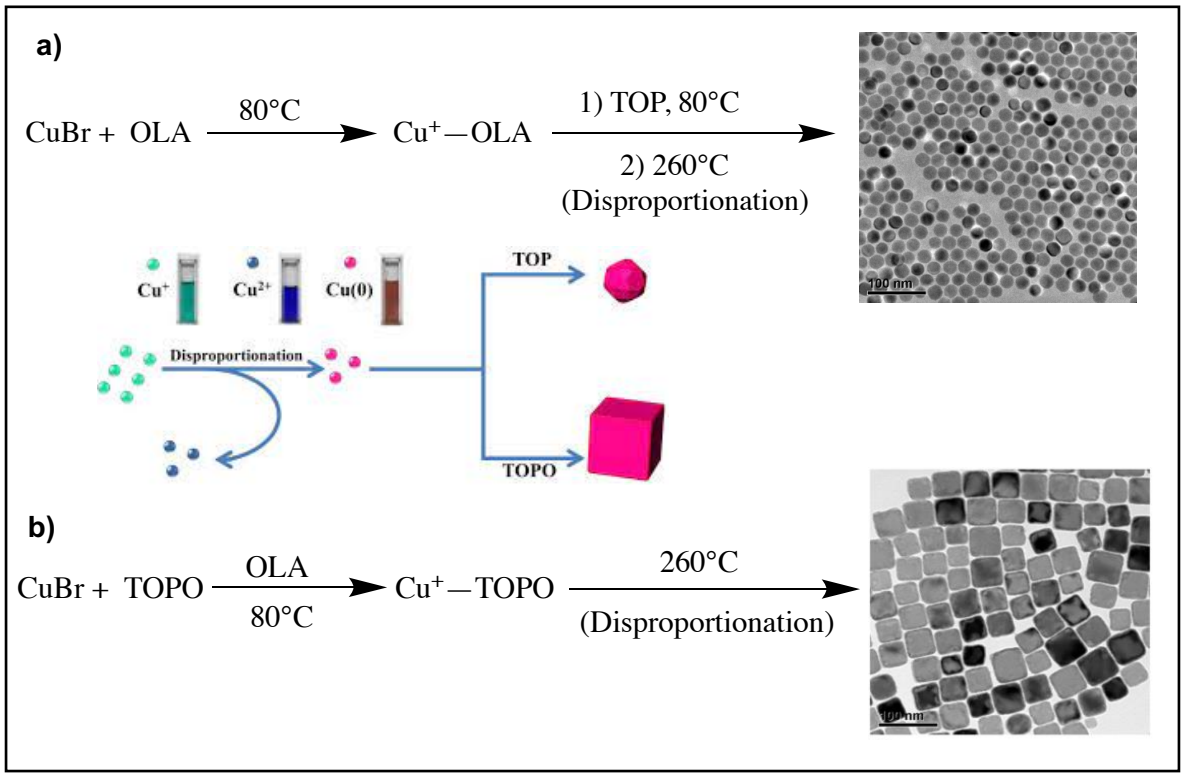

Figure II-3. *Shape-selective Formation of Cu nanospheres (a) and Cu nanocubes (b) via the disproportionation reaction route with the corresponding TEM images. (Copyright from Ref.[12])*

The authors argued that in the case of the use of TOPO, its weak coordination of Cu(I) promotes the occurrence of nucleation at a lower temperature (170 °C), and the low

temperature could reduce the growth rate of NPs and enable the Br^- to be selectively bound on the (100) facet of the crystal seeds. As a result, the cubic shape of CuNPs would be obtained by a kinetic control mode, other facets growing faster than the (100) one. Once again, this explanation is in contrast to the more recent study by M. Strach's group (2019)[11] that shows that hemolytic dimer $(CuBr•(TOP)_2)_2$ complex disproportionate at a lower temperature (150 °C) than the $CuBr•(OLA)_2TOPO$ complex (255 °C) (see in Figure II-15). It is not clear whether these differences are due to the analytical and reactive monitoring methods employed by these two groups. It is also interesting to note that these two groups used different amounts of phosphine ligands (2 equiv. TOP (M. Strach) vs 1.6 equiv. TOP (H. Guo)). As a minimum of 2 equivalents of TOP are required to form the $(CuBr•(TOP)_2)_2$ complex, it may be argued that the amount of TOP is not enough to make it in Guo's reaction conditions which also may explain the differences. Similar remark can be made for the differences reported in the case of TOPO (8 equiv. TOPO (M. Strach) vs 2.5 equiv. TOPO (H. Guo)).

In the H. Guo's work, they also found that the size of nanocubes could be tuned from 24.1 to 76.4 nm, depending on the amount of TOPO. Indeed, CuNPs of smaller size were obtained for the use of higher amount of TOPO.

The same year (2014), H. Tuan and co-workers[13] reported a disproportionation reaction of a Cu(I)•TOP complex using a "hot-injection" synthetic process and leading to the formation of copper nanocubes. In their work, cubic CuNPs with a mean size of 75.7 nm were produced by a hot-injection of the solution of CuCl in octadecylamine (ODA) into the mixture of oleylamine (OLA) and TOP at 330 °C (Figure II-4). They investigated the crystalline structure and surface compounds of these nanocubes by using a series of characterization analysis, including X-ray diffraction (XRD), selected area electron diffraction (SAED) and X-ray photoelectron spectroscopy (XPS). They postulated that TOP and ODA play a critical role in the nucleation and growth of Cu nanocubes through the formation of single crystal seeds by selective stabilization the (100) facets.

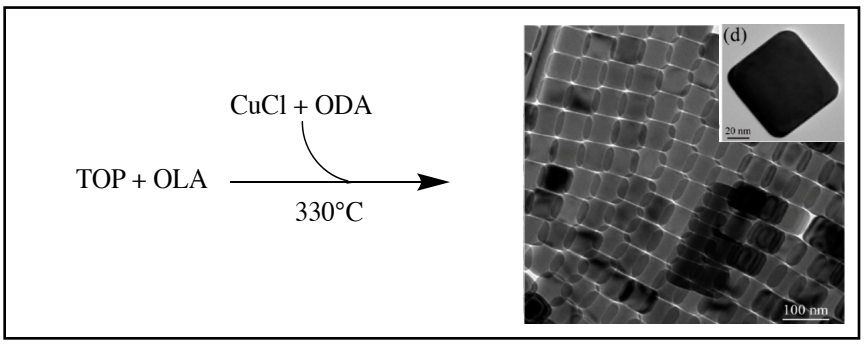

Figure II-4. *Synthesis of Cu nanocubes by hot-injecting Cu precursor solution in ODA via the disproportionation reaction route with the corresponding TEM images. (Copyright from Ref.* [13]*)*

The authors deduced from the study of the FTIR analysis the presence of OLA, ODA and TOP on the nanoparticle surface, based on the observation of stretching peaks corresponding to the symmetric (2848 cm^{-1}) and asymmetric (2908 cm^{-1}) CH_2 stretches from OLA and ODA, as well as symmetric rocking mode of terminal methyl group at 1454 cm^{-1} and 1504 cm^{-1} and the C-P stretch (1108 and 1158 cm^{-1}) from TOP. The XRD pattern shown a significantly higher diffraction density of (200) compared to (111) and (220) and more than the value obtained from a conventional powder sample. This result indicates the cubes tend to preferentially orient parallel to the supporting substrates (silicon substrate). Interestingly, these Cu nanocubes are able to self-assemble by van der Waals interaction into supracrystals with rhombohedral structure (RS). In addition, these nanocubes have been used to prepare dense copper nanocubes films which have high electrical conductivity.

Based on these studies, the advantage of the disproportionation reaction is the possibility to control the nucleation and growth steps and thus to produce CuNPs with tunable size and shape. The shape of NPs depends on many reaction factors such as the nucleation reaction, the temperature and the nature of the ligand used. More specifically, the nucleation and growth of CuNPs strongly depend on the ability of the ligand to selectively stabilize specific crystal facets. Therefore, we selected a small library of phosphorus ligands to investigate the effect of their pKa and steric hindrance on the size and shape of the CuNPs. Our results are reported in the next section.

II. 3 Study of the effect of the phosphine ligands on the morphology of the CuNPs

As discussed in the Chapter I (section I.2.2), ligands are molecules or ions that bind to a metal atom to yield a coordination complex. They are often used in the synthesis of NPs and play multiple roles during the steps of reduction, nucleation, growth and stabilization stages of the final NPs.[14-17] In addition, the ligands may contribute to the formation of NPs colloidal solution and prevent their oxidation and coalescence.[18] Thus, ligands are of fundamental importance for the chemical synthesis of nanoparticles.[19]

Indeed, the nature and strength of the bonding between the ligands and the copper salt precursor and the resulting seed intermediate strongly influence the nucleation and growth of the nanoparticles, and consequently influences the final size and shape of NPs. Importantly, it could also change their physical and chemical properties.[20] The ligand should not bond too strongly to the nuclei, which would prevent the growth of the nanoparticle, and also the bond should not be too weak otherwise the nanoparticles would continuously grow until becoming bulk.[21] Most of the time, ligands chemically bind to metal atoms through the donation of one of their free electron pair, and also through the π-interaction between one of their functional

groups such as a double or a triple bond and the metallic surface.[20] It is interesting to note that their steric hindrance will also play an important role in the strength of the coordination to the surface. Various organic ligands with high metal surface affinity were used in CuNPs synthesis, such thiols, carboxylates, amines and phosphines.[22-25] Particularly, the phosphorus ligands (such as TOP, TOPO, PPh_3) have been often employed in the preparation of copper nanoparticles.[26]

A detailed study of the steric and electronic properties of phosphorus ligands is required to better understand their steric and electronic effects on the CuNPs synthesis. The steric effect of ligand was schematically illustrated as shown in Figure II-5.

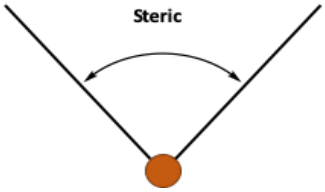

***Figure II-5**. Definition scheme of steric effect.*

In general, the electronic properties of phosphorous ligands can be modified by the transmission of inductive and/or mesomeric effects of their substituents. The steric effect could be adjusted when the shape or size of the molecule changes. The most frequently used parameter to measure the steric effect of the phosphine ligands is the Tolman cone angle (θ), which was quantified by Tolman based on the Corey-Pauling-Koltun model in 1977.[27] This parameter is defined as the apex angle of a cylindrical cone centered at a distance of 2.28 Å (metal-phosphorus distance) from the center of the phosphorus atom, which just touching the van der Waals radii of outermost atoms on each of three substituents.[27-29] Additionally, Tolman has correlated the electronic properties of phosphine ligands to the carbonyl stretching frequency (ν(CO)) of the type $[NiL(CO)_3]$ complexes. This frequency is dependent on the combination of σ-donating and π-accepting characteristics of L (L = Ligand) with respect to the center P atom. Electron density donated by L enhances back donation from the metal center into the LUMO orbital of the CO ligand, which leads to a decrease of ν(CO). A lower carbonyl stretching frequency is required to accord with a higher donating strength of the phosphine.[27]

Nevertheless, tuning the steric effect can produce a significant electronic effect and vice versa. The increase of angles between substituents will reduce the amount of *s*-character in the phosphorus lone pair, which leads to a change of the electronic properties of the phosphine ligands. Changing the electronegativity of the substituents may also affect the bond distance and angles at P atom.[30a] Phosphorus ligands owning a lone pair of electrons can play a role as nucleophiles and as Brønsted bases. Generally, the basicity of phosphorus ligands

bearing alkyl substituents lie in the order: $PR_3 > PR_2H > PRH_2 > PH_3$.[30b] Among the PR_3 ligands, the order of the decreasing basic character is: $PMe_3 \approx P(NR_2)_3 > PAr_3 > P(OMe)_3 > P(OAr)_3 > PCl_3$. In our study, we used the pKa values of PR_3 to compare their electronic properties.

In this thesis work, we started by using trioctylphosphine (TOP) and trioctylphosphine oxide (TOPO) ligands to investigate the CuNPs synthesis via a disproportionation reaction route, based on the seminal work reported by H. Guo et co-workers[12] (Table II-1, entry 1 and 6). Besides these two common phosphorus ligands, TOP and TOPO, we have also explored the use of various phosphorus ligands which own different steric and electronic properties, namely the triphenylphosphine (PPh_3) (Table II-1, entry 10), the tris(trimethylphenyl)phosphine ($P(PhMe_3)_3$) (Table II-1, entry 12), the trimethylphosphite ($P(OMe)_3$) (Table II-1, entry 13), the trioctylphosphite (TOPT) (Table II-1, entry 14), the Hexamethylphosphorous triamide (HMPT, $P(NMe_2)_3$) (Table II-1, entry 15), and the hexamethylphosphoramide (HMPA, $P(O)(NMe_2)_3$) (Table II-1, entry 16). Their cone angle and pKa values are reported in Table II-1. Among these phosphorus ligands, the cone angle or pKa of some of them have not been reported in the literature (e.g. TOPO, $P(PhMe_3)_3$, TOPT) thus, we chose similar phosphorus ligands (e.g. $OPPhMe_2$, $OPPh_3$, $OPEt_3$, $P(PhMe)_3$, PMe_3) to compare their steric and electronic properties. Regarding the steric hindrance around the copper center, we first assumed that it should be small for any phosphine oxide (OPR_3) compared to their phosphine analogues.

***Table II-1**. Steric and pKa parameters for selected phosphorus ligands.*[30c,d,e,f]

Entry	Ligands	Molecule structure	Cone angle	pKa
1	TOP	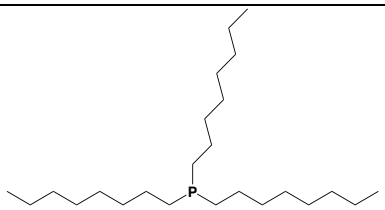	-	8.4
2	PMe_3	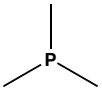	118	8.7
3	PEt_3	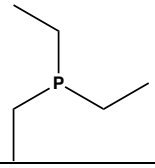	132	-

4	PBu_3	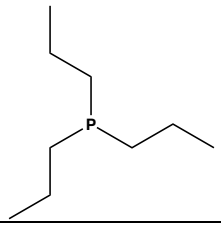	132	-
5	$P(iPr)_3$	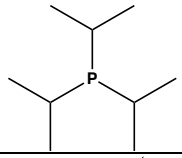	160	-
6	TOPO	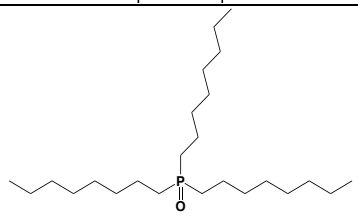	-	-
7	$OPPhMe_2$	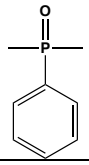	-	- 2.4
8	$OPPh_3$	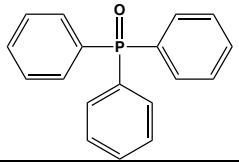	-	3.2
9	$OPEt_3$	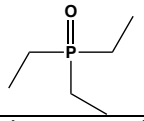	-	3.6
10	PPh_3	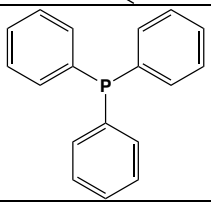	145	2.7
11	$P(PhMe)_3$	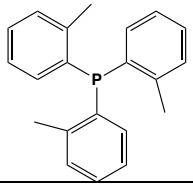	194	-
12	$P(PhMe_3)_3$	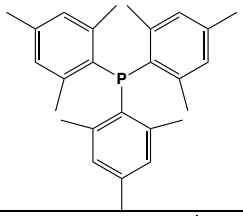	-	-
13	$P(OMe)_3$	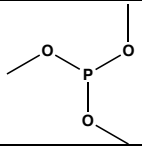	107	2.6

14	$P(OC_8H_{17})_3$	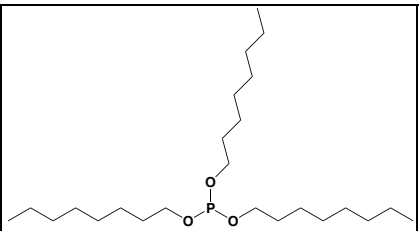	-	-
15	$P(NMe_2)_3$	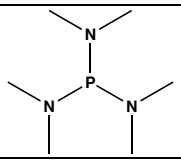	152	8.0 (± 0.7)
16	$P(O)(NMe_2)_3$	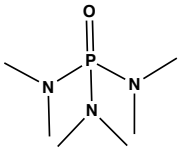	-	4.7 (± 0.7)

Before the investigation of CuNPs synthesis with these several phosphorus ligands, we first studied the effect of the phosphine ligands (L = PR_3) on the energy of first coordination at the $CuCl_n$ (n = 0, 1, 2) and on the disproportionation energy of copper(I)-ligands. All calculated results were achieved by Maya Guillaumont and Hélène Gérard's group from the LCT laboratory of Sorbonne Université.

In order to better understand the affinity of different ligands to copper, the coordination energies between copper (0, I or II) and different types of ligands (L = PR_3 ligands, amine) were studied (see in Figure II-6). The coordination energy was calculated as the energy of reaction by using a simple model as shown in Figure II-6(a). In this work, some simple phosphine ligand models were used, namely PMe_3, PPh_3, $P(O)Ph_3$, $P(O)Me_3$, $P(OMe)_3$, $P(NMe_2)_3$, and NH_2CH_3 as an amine model for the oleylamine (NH_2R). As a result, the coordination abilities between ligands and Cu(0) in the following order: $P(NMe_2)_3 \approx PMe_3 > PPh_3 > NH_2CH_3 > P(O)Me_3 > P(O)Ph_3 > P(OMe)_3$. These theoretical calculations show the affinities of various phosphorus ligands to copper (0, I, II) through their coordination energies. These different coordination energies may affect not only the nucleation and growth of nanoparticle, but also the disproportionation process.

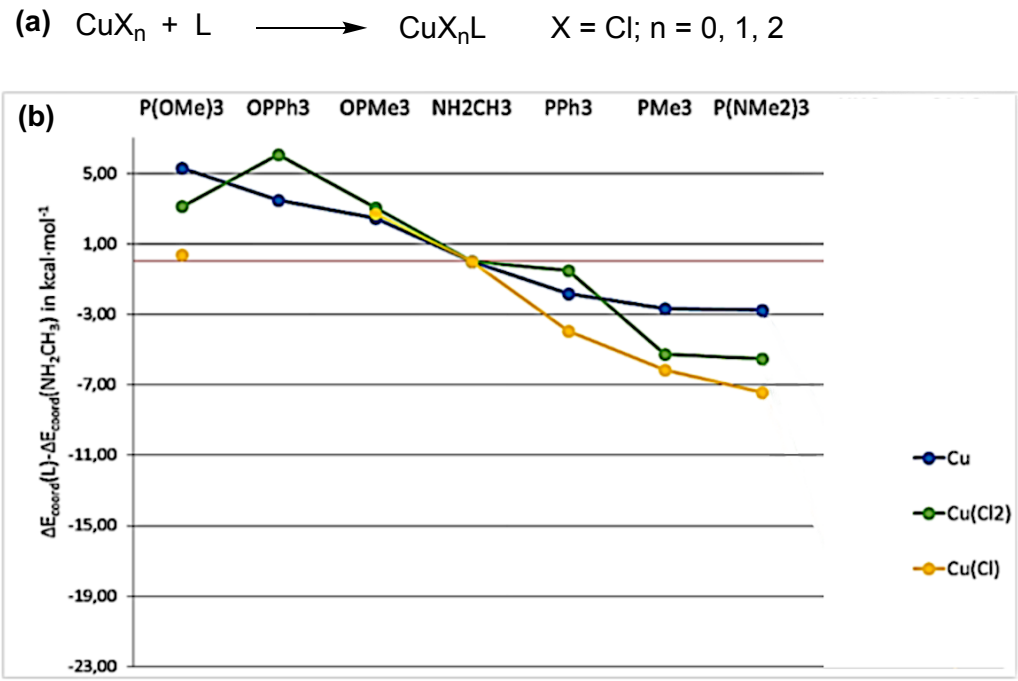

Figure II-6. *(a) Reaction model for calculate the coordination energy between copper and ligands (L = PR_3, $NHCH_3$) (b) comparison of coordination energies between the ligands and $CuCl_n$ (n = 0, I, II).*

Next, the energy of disproportionation of CuCl in the presence of ligands (L) was investigated by using a monomer complex model as shown in Figure II-7(a). As a result, the calculated disproportionation energy ($\Delta E_{\mathrm{dis}}^{\mathrm{CuCl(L)}}$) increases in order of $\Delta E_{\mathrm{dis}}^{\mathrm{CuCl(NH2CH3)}} \approx \Delta E_{\mathrm{dis}}^{\mathrm{CuCl(OPMe3)}}$ (= 63.0 kcal·mol^{-1}) < $\Delta E_{\mathrm{dis}}^{\mathrm{CuCl(PMe3)}}$ (= 67.4 kcal·mol^{-1}) < $\Delta E_{\mathrm{dis}}^{\mathrm{CuCl(PPh3)}} \approx \Delta E_{\mathrm{dis}}^{\mathrm{CuCl(P(OMe)3)}}$ (= 68.5 kcal·mol^{-1}) <$\Delta E_{\mathrm{dis}}^{\mathrm{CuCl(P(NMe2)3)}}$ (= 69.6 kcal·mol^{-1}). Consequently, the disproportionation of CuCl-ligand complexes would occur from easy to hard: $NH_2CH_3 \approx OPMe_3 < PMe_3 < PPh_3 \approx P(OMe)_3 < P(NMe_2)_3$.

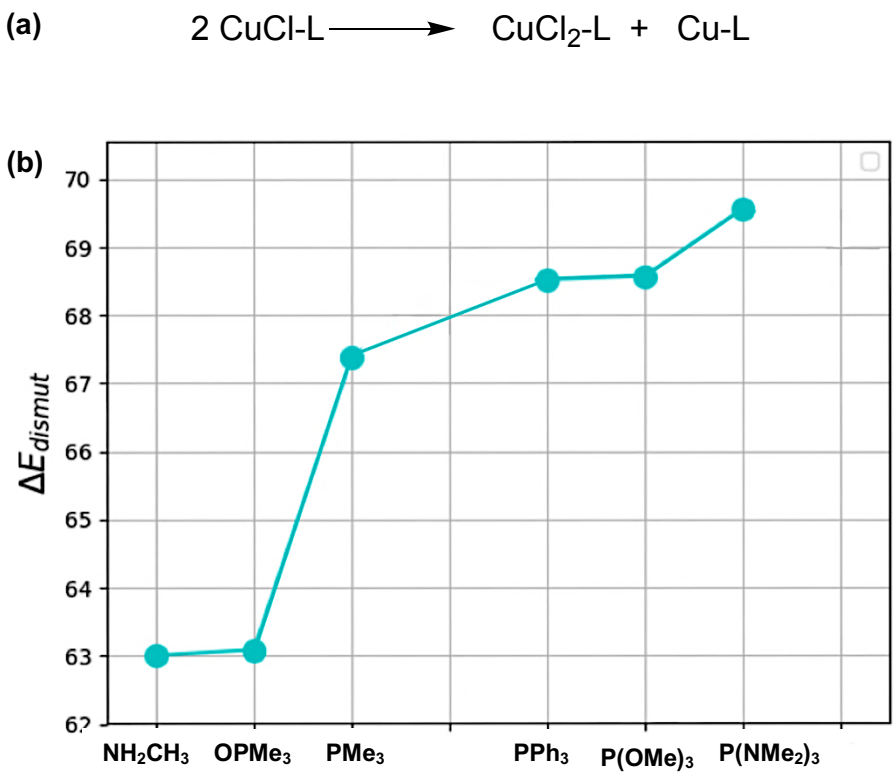

Figure II-7. *(a) Reaction model for calculate the disproportionation energy CuCl-L (L = PR_3, $NHCH_3$) (b)comparison of disproportionation energies of CuCl-L.*

Based on the calculated coordination energies between Cu(0) and ligands (L) and the disproportionation energies of CuCl-L, we could compare the effect of different ligands in the CuNPs synthesis. For example, PMe_3, PPh_3 and $P(NMe_2)_3$, have similar coordination energy to Cu(0) (Figure II-6). However, the disproportionation energy in the presence of PMe_3 (67.4 kcal·mol^{-1}) is lower than PPh_3 (68.5 kcal·mol^{-}1) and $P(NMe_2)_3$ (69.6 kcal·mol^{-1}), thus, the disproportionation reaction in the case of PMe_3 is more favorable. From these results, we assumed that the low disproportionation energy of Cu(I)-L would favor the formation of CuNPs synthesis. Therefore, in the next sections, the synthesis of Cu nanoparticles will be investigated in the presence of different phosphine ligands by the help of the theoretical different copper-ligand coordination energies and the disproportionation energies.

II. 4 Synthesis of CuNPs with controlled shape and size

As seen in section II.2, the nature of the phosphorus ligand plays an important role during the formation of nanoparticles and may enable a high level of control of their size and shape. At the beginning of our study, we expanded the disproportionation reaction developed by H. Guo *et al*[12] by using various phosphorus ligands and also by studying the influence of

different reaction parameters on the size and morphology of NPs, such as the amount of ligands, the temperature, the nature of precursors and of solvents. These systematic studies could also help to better understand the growth process of CuNPs and develop methodologies to tune their morphology and size. Our first standard reaction conditions are schematically described in Scheme II-1. The copper salt was first heated in OLA at 100 °C in order to form the corresponding Cu-OLA complex, which was followed by the injection of the phosphine ligands (PR_3) at this temperature. The temperature of the reaction mixture was increased until the observation of a color change indicating the disproportionation of Cu(I) and the subsequent formation of CuNPs. In the subsequent sections, the synthesis of CuNPs was carried out by the different family of phosphorus ligands: TOP/TOPO (section II.4.1), PPh_3/$(PPhMe_3)_3$ (section II.4.2), $P(OMe)_3$/$P(OC_8H_{17})_3$ (section II.4.3), $P(NMe_2)_3$/$OP(NMe_2)_3$ (section II.4.4).

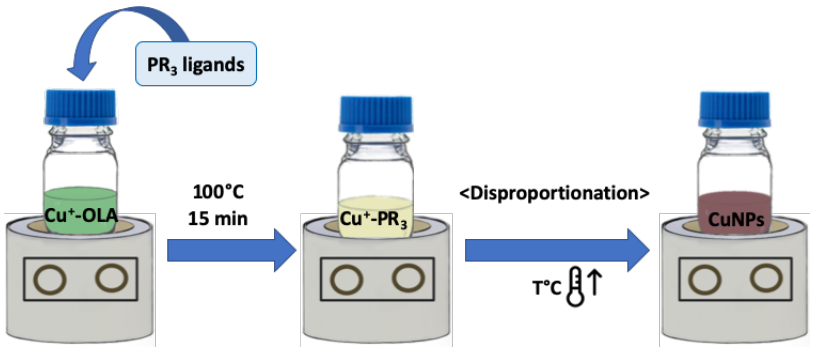

***Scheme II-1**. Schematic description of CuNPs synthesis process in our work.*

II. 4.1 CuNPs preparation using TOP and TOPO

Among the various phosphine ligands, the TOP and TOPO have been often used for the preparation of copper nanoparticles. In the previous section, we have described the seminal synthesis of CuNPs reported by the H. Guo's[12] and H. Yang's[13] groups using these phosphorous ligands. In the work of H. Guo's group, the TOP ligand was showed to promote the formation of spherical NPs, whereas cubic NPs were obtained in the presence of TOPO (Figure II-3). On the contrary, cubic CuNPs where synthetized by H. Yang's group when the copper precursor was injected in the reaction mixture of TOP/OLA at a high temperature (namely hot-injection method) (Figure II-4). In order to understand the difference between these two results, our study of CuNPs synthesis was carried out with TOP and TOPO ligands by tuning the reaction parameters.

II. 4.1.1 Synthesis of CuNPs in the presence of TOP

In our work, monodisperse copper nanocubes with an average size of 59.8 ± 5.8 nm with a low polydispersity of 10% (Figure II-9a, b) were prepared through an extended method from H. Guo's group[12] as follows (Figure II-8, see Chapter V experimental section 3.1A): 0.6 mmol of copper (I) chloride (CuCl) was weight in an N_2-filled glovebox and transferred inside a Pyrex 25mL vial along with 7 mL of oleylamine, the mixture was heated to 100 °C under inert gas (N_2) for 15 min. The change of color of the solution into green indicated the formation of a Cu(I)-oleylamine complex[12] which was characterized by IR spectroscopy, as shown in Figure II-10. Indeed, the IR spectra of oleylamine (Figure II-10a) shows a weak peak observed at 1650 cm^{-1} that corresponds to the C=C stretching mode, and the N-H stretching vibration can be detected at about 3338 cm^{-1}.[31] In the IR spectrum of Cu(I)-oleylamine complex (Figure II-10b), two new peaks appeared at 3377 cm^{-1} and 3281 cm^{-1} which may be due to the coordination of the amine group of oleylamine with Cu(I).[32] In addition, a blue shift of the NH_2 bending (1632 cm^{-1}) was shown in the complex of Cu(I)-OLA compared to that in pure oleylamine (1574 cm^{-1}).[12,32]

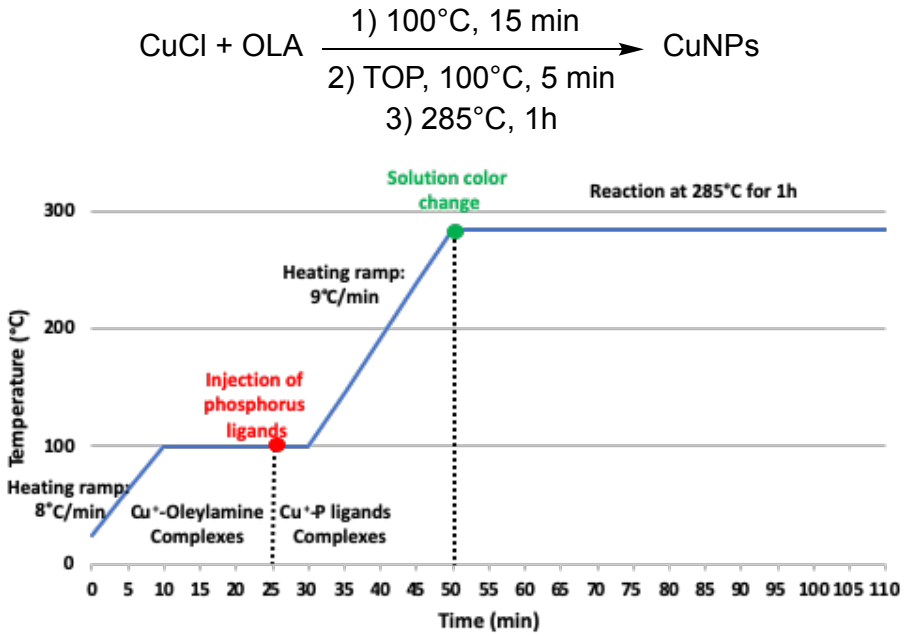

***Figure II-8**. Description of synthesis process of CuNPs via disproportionation reaction of CuCl in oleylamine in the presence of TOP ligand.*

Subsequently, 1 mmol of trioctylphosphine (TOP) was quickly added and the solution mixture becomes instantly colorless. After 5 min of stirring at this temperature, the colorless mixture was heated up to 285 °C, and held at this temperature for 1 hour. The formation of

CuNPs was evidenced by a slow color change of the solution from colorless to orange and finally to red-purple. After the reaction was stopped, the NPs were purified by dispersing the reaction mixture in an excess of absolute ethanol, followed by a centrifugation of the resulting suspension at 2500 rpm for 10 min to remove all organic compounds. The supernatant containing the organic compounds was discarded and the precipitate was dispersed in hexane or chloroform, before a centrifugation at 4000 rpm for 5 min. As expected, the blue color of the supernatant observed after the washing procedure demonstrates the presence of Cu(II) in the solution, and thus suggests that a disproportionation reaction took place. The resulting copper nanocubes were then stored up in a glove box as a red powder.

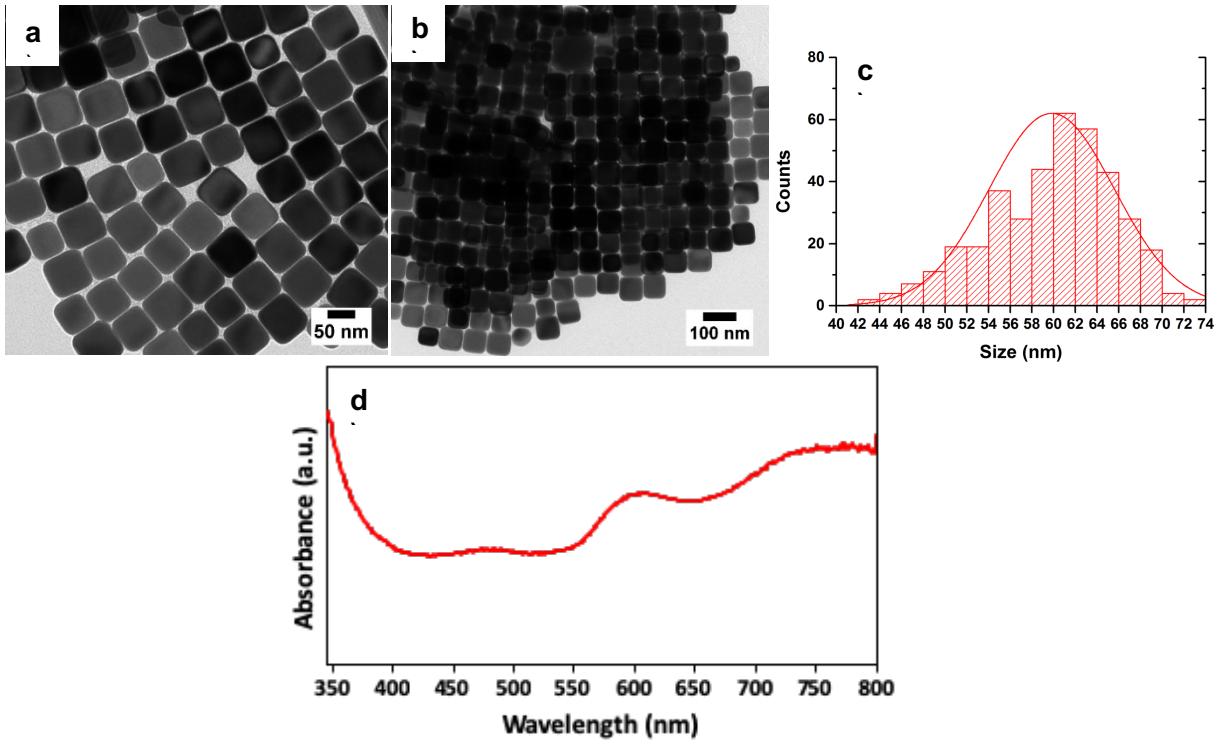

***Figure II-9**. (a) Typical TEM image of copper nanocubes obtained in the presence of TOP (b) self-assembly (c) the corresponding size distribution histograms and d) UV-vis absorbance spectrum (*603 nm, 725 nm).

The UV-visible spectroscopy is often used to detect the presence of CuNPs in colloidal solution due to the presence of local surface plasmon resonance (LSPR). The width and the position of the plasmon band depend on the size, shape, composition, and environment of nanoparticle.[33] According to Mie theory,[34] a single LSPR peak was attributed to spherical copper nanoparticles due to their spherical symmetric geometry, and two or more LSPR peaks could be observed for anisotropic morphology (non-spherical structures, e.g., rods, prisms) of particles depending to the particle shape. As shown in Figure II-9d, two characteristic LSPR

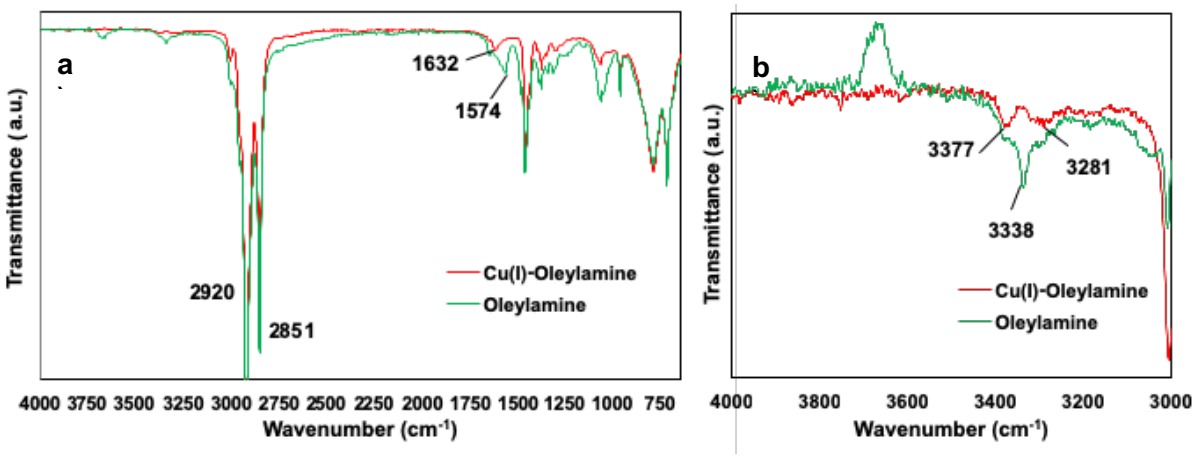

***Figure II-10**. IR spectra of Cu(I)-Oleylamine complex (red) and Oleylamine (green) (a) 4000-650 cm^{-1} (b) 4000-3000 cm^{-1}.*

peaks of copper nanocubes located at 603 nm and 725 nm were observed. The main peak at 603 nm is mostly attributed to the monodisperse CuNPs in solution, and the peak at 725 nm may belong to the aggregation of nanocubes through the Van der Waals attraction between the particles as shown in Figure II-9b. A similar phenomenon has also been reported in H. Guo's work where the nanocubes with tunable size exhibit their size-dependent optical property.[12] In their work, a tiny red shift from 576 nm to 585 nm (SPR peaks) was observed as the edge length of nanocubes increases from 24.1 nm to 26.4 nm. Furthermore, for the largest cubes with a mean edge length of 46.8 nm, two SPR peaks located at about 670 and 858 nm were observed the second one being attributed to aggregation.

Influence of the nature of the glassware and of the heating plates:

At the beginning of this thesis work, we observed that the preparation of cubic CuNPs (as shown in Figure II-9a) using TOP as phosphorus ligand were poorly reproducible. After verifying that this was not related to the nature of the additives or the quality of the inert gas used, we realized that it might due to the characteristics of the different hotplates used. We will hereinafter call "heating plate A" the standard heating plates, and "heating plate B" the high-performance plates mostly used in inorganic chemistry, as shown in Figure II-11d.

In the typical procedure described above, the synthesis of Cu nanocubes (59.8 ± 5.8 nm, σ% = 10%) (Figure II-9a) were carried out with hotplate A (Figure II-11d). Interestingly, when the synthesis of CuNPs using TOP as ligand was performed in a vial heated with hotplate B (Figure II-11d), Cu nanooctahedra (quasi-spherical) with a mean size of 35.9 ± 4.8 nm (σ% = 13%) in diagonal and a few triangular and hexagonal NPs were obtained (Figure II-11b) instead of the Cu nanocubes. Using the same hotplate B, but a three-neck flask as glassware

leaded to the formation of Cu nanospheres with an average size of 59.5 ± 2.8 nm (σ% = 5%) in diameter (Figure II-11c) were formed. Figure II-11e shows the UV-vis absorption bands of synthetized CuNPs with different shapes, there is a tiny bleu shift from 603 to 595 nm was observed as the size of Cu nanooctahedra (major, 35.6 nm) is smaller than the one of Cu nanocubes (59.8 nm). And also, a narrower LSPR peak located around 600 nm was observed in the case of nanospheres (59.5 nm) due to their lower polydispersity (σ% = 5%). Due to the equivalent size between the Cu nanospheres and Cu nanocubes, no remarkable evolution of wavelength was observed.

Obviously, the type of hotplates and glass materials used in our work which plays a very important role in determining the shape and size of CuNPs synthetized in the presence of TOP.

In the literature, the selective formation of cubes or spheres are rationalized through the concept of kinetic and thermodynamic control.[35-39] Indeed, when the NPs synthesis is under thermodynamic control, the most stable NPs will be formed. The NPs will assume its equilibrium shape corresponding to the global minimum in Gibbs free energy, thus a spherical form. On the contrary, if a synthesis is kinetically driven, the nanocrystal will assume different shapes of higher Gibbs free energy but corresponding to local minima, i.e., polyhedral forms.[35] The competition between thermodynamic and kinetic products can be directed by tuning the reaction parameters, such as the temperature and the reduction or decomposition rate of the precursor.[35-39] In practice, high monomer flux and/or low temperature[35-41] favor the kinetic product, while low monomer flux and/or high temperature lead to the thermodynamic product.[35-39]

For a *fcc* structure, such as Cu, the energetic sequence of the specific surface energies of the low-index crystallographic facets is $\gamma(111) < \gamma(100) < \gamma(110)$.[42] This sequence implies that a single-crystal seed should be thermodynamically stable as an octahedral shape which allows for maximizing the expression of (111) facets and minimizing the total surface energy. Octahedral shape, however, possess a larger surface area than a cube of the same volume. As a result, the thermodynamically stable seeds are expected to exist as truncated octahedrons (or Wulff polyhedrons) enclosed by a mix of (111) and (100) facets, which can be regarded as quasi-sphere thus the smallest surface area to minimize the total interfacial free energy.[35,42,43] Based on the discussion above, the cubic shape of NPs will be kinetic products.

In order to get a clear observation in these different shapes obtained from different hotplates (A and B), we next studied the heating ramp of each hotplate by monitoring the temperature directly in the reaction solution and in the sand bath of the heat-on, for a VWR glass vial and a traditional three neck flask glassware (Figure II-12).

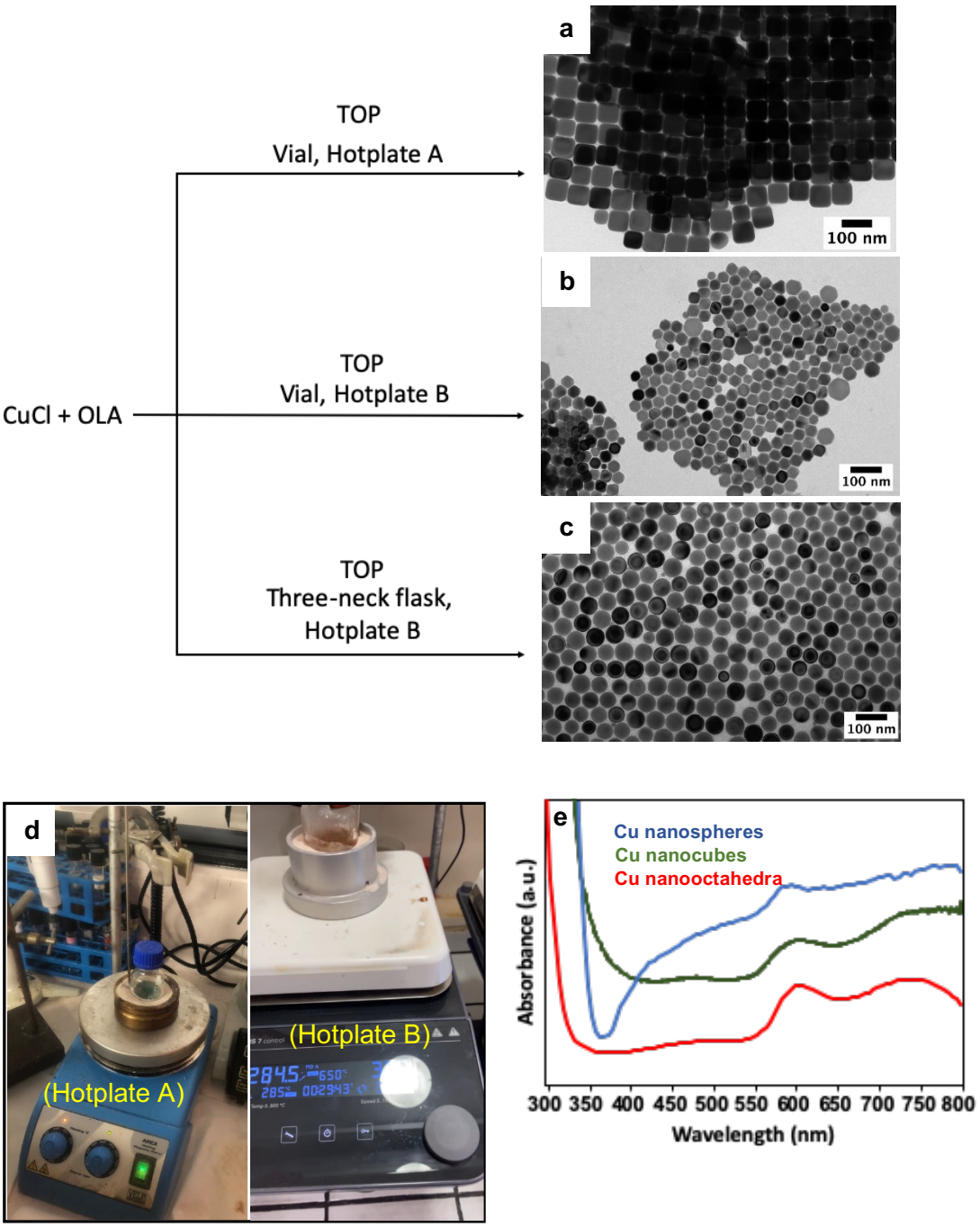

***Figure II-11**. Synthesis of CuNPs using different magnetic hotplate stirrers A and B (d) and the corresponding TEM images of the (a) Cu nanocubes (b) Cu nanooctahedra (c) Cu nanospheres in our work and (e) the corresponding UV-vis absorbance spectra (bleu: 600 nm; green:* 603 nm, 725 nm; red: 595 nm, 724 nm).

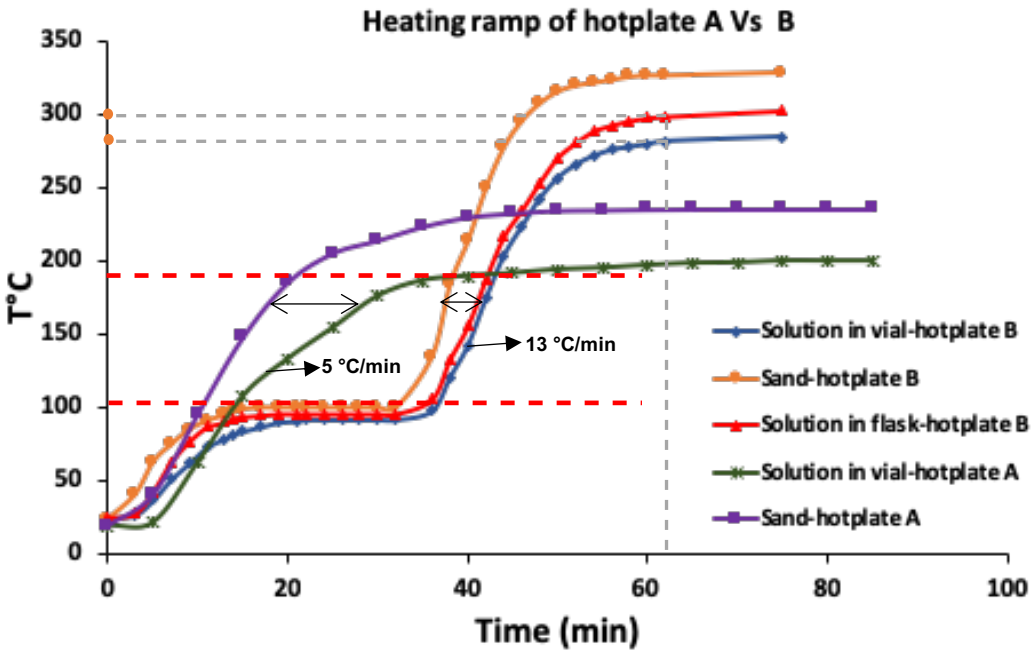

Figure II-12. *Investigation of heating ramps for the oleylamine solution in a vial or in a three-neck flask and the sand.*

The tests of heating ramp in solution was performed using 7 mL of oleylamine, in accordance with our standard reaction conditions. The tested temperature ranges of these two hotplates being different (hotplate A: from 20 to 230 °C; hotplate B: from 20 to 330 °C), we chosen the temperature range from 100 °C to 180 °C to compare the heating ramps.

As shown in Figure II-12 (green and blue curves), a heating ramp of 5 °C/min was observed using hotplate A (oleylamine, in a vial, green curve), which is far much slower than the 13 °C/min measured with hotplate B (oleylamine, in a vial, blue curve). Although this test of heating ramp is slightly different from the real synthetic reaction, it highlights the dramatic effect of the heating ramp on the morphology of the synthetized NPs.

Therefore, the use of hotplate B (13 °C/min) for the CuNPs synthesis may induce a change in the final shape and size of NPs due to its high heating ramp. Especially, the difference of temperature between the sand (Figure II-12, purple curve) and the solution (Figure II-12, green curve) is relative larger in the case of hotplate A, and this may also influence the growth of NPs, and thus may affect the final size and shape of the resulting CuNPs. It is important to note that the heating temperatures in our experimental works correspond on the temperatures measured in the sand bath, and they are determined by the change of color of the solution color. The large difference between the real temperature in solution and the temperature determined in the sand bath makes thus extremely difficult to determine the exact reaction temperature. Additionally, in the case of hotplate B, the slight

difference of heating ramp between the vial and three-neck flask also influences the final shape and size of CuNPs. As seen in Figure II-12 (red, blue), a higher solution (OLA) temperature was measured in a three-neck flask (red curve) than the one in a (blue curve) for a same reaction time. Due to the different material nature of three-neck flask and vial, the solution in the three-neck flask would be heated faster than the one in vial. This may show the formation of monodispersed copper nanospheres due to the relative higher heating rate which promotes a thermodynamic control. But, the difference in size between Cu nanospheres and Cu nanooctahedra (quasi-spherical) is still unclear.

Effect of the nature of ligands: XPS analysis

The nature of the ligands absorbed on the surface of NPs was further characterized by X-ray photoelectron spectroscopy (XPS) analysis by Pr. Vincent NOEL from ITODYS laboratory of Paris University. The experimental XPS spectra were recorded using a K-Alpha$^+$ system (ThermoFisher Scientific, East-Grinsted, UK) fitted with a micro-focused and monochromatic Al K_α X-ray source (1486.6 eV, spot size of 400 µm). The spectrometer pass energy was set to 150 and 40 eV for the survey and the narrow high-resolution regions, respectively. Spectral calibration was determined by setting the main C_{1s} component at 285 eV.

To understand the correlation between the nature of surface ligands and different shapes of NPs, XPS analysis was carried out on two samples: Cu nanocubes prepared by using hotplate A and Cu nanospheres (Figure II-11a) synthetized from hotplate B (Figure II-11c). The results are reported in Table II-2 and Figure II-13. In both samples, the Cu/OLA, Cu/TOP and OLA/TOP ratios used in synthetic reaction were 1/35, 1/1.6 and 21/1 respectively.

The XPS survey scan of synthetized Cu nanocubes shows peaks attributed to C_{1s}, Cu_{2p}, O_{1s} and small signals corresponding to N_{1s} (see Table II-2 and Figure II-13a). There is no peak detected in the 130-140 eV regions which indicates an absence of P on the NPs surface. In addition, the presence of Cl^- has not also been detected. The N_{1s} peak at 399.21 eV is the signature of OLA (At% = 1.26%), The $Cu_{2p1/2}$ and $Cu_{2p3/2}$ peaks at 932 and 952 eV respectively are the signature of Cu(0) and/or Cu(I).

Previous studies have reported the selective binding of Br^- to the (100) facets which results the cubic shape of CuNPs (H. Guo *et al.,* 2014).[12] In our case, the equivalent cube-shaped CuNPs were also produced when CuCl was used as the copper precursor instead of CuBr. Furthermore, the presence of Cl^- on the surface of Cu nanocubes was not detected by XPS. We deduce that the shape of the particles is not controlled by the selective adsorption of the halides in our experiments.

For Cu nanospheres (Figure II-13b), the formation of metallic copper is evidenced by the Cu_{2p} signal at 934.47 eV. The N_{1s} peak at 400.11 eV corresponds to the NH_2 of oleylamine (At% = 1.26%). Interestingly, the At% (= 1.26%) of N_{1s} is equivalent in both Cu nanocubes and Cu nanospheres but with different At% of Cu_{2P} (cubes: 6.35% and spheres: 1.23%). In the case of Cu nanocubes, the ratio between OLA and copper deduced from the N_{1s} and Cu_{2p} peaks respectively is around 0.2 (= 1.26/6.35) which is 5 times less than the measured ratio on Cu nanospheres around 1 (= 1.26/1.23). These results demonstrated the high surface coverage of OLA on the spherical shape CuNPs which corresponds to the volume of spherical nanoparticles is generally 4 times bigger than that of cubes.

Table II-2. *XPS data analysis of Cu nanocubes and Cu nanospheres*

Sample	Element	Peak BE	FWHM eV	Area (P) CPS.eV	Atomic %
Cu nanocubes	C1s	284.57	1.22	94791.09	65.21
	C1s A	285.87	1.60	6366.87	4.38
	C1s B	288.25	1.63	2040.93	1.41
	Cu LM2	569.47	3.14	90591.26	0.00
	Cu2p	932.11	1.25	137819.64	6.35
	N1s	399.21	2.01	2840.24	1.26
	O1s	532.00	1.83	75108.65	21.38
Cu nanospheres	C1s	284.96	2.03	237904.23	85.65
	C12p	198.70	0.94	774.34	0.12
	Cu2p	934.47	3.28	68818.89	1.23
	N1s	400.11	2.01	6135.62	1.26
	O1s	532.72	2.83	89864.31	11.71

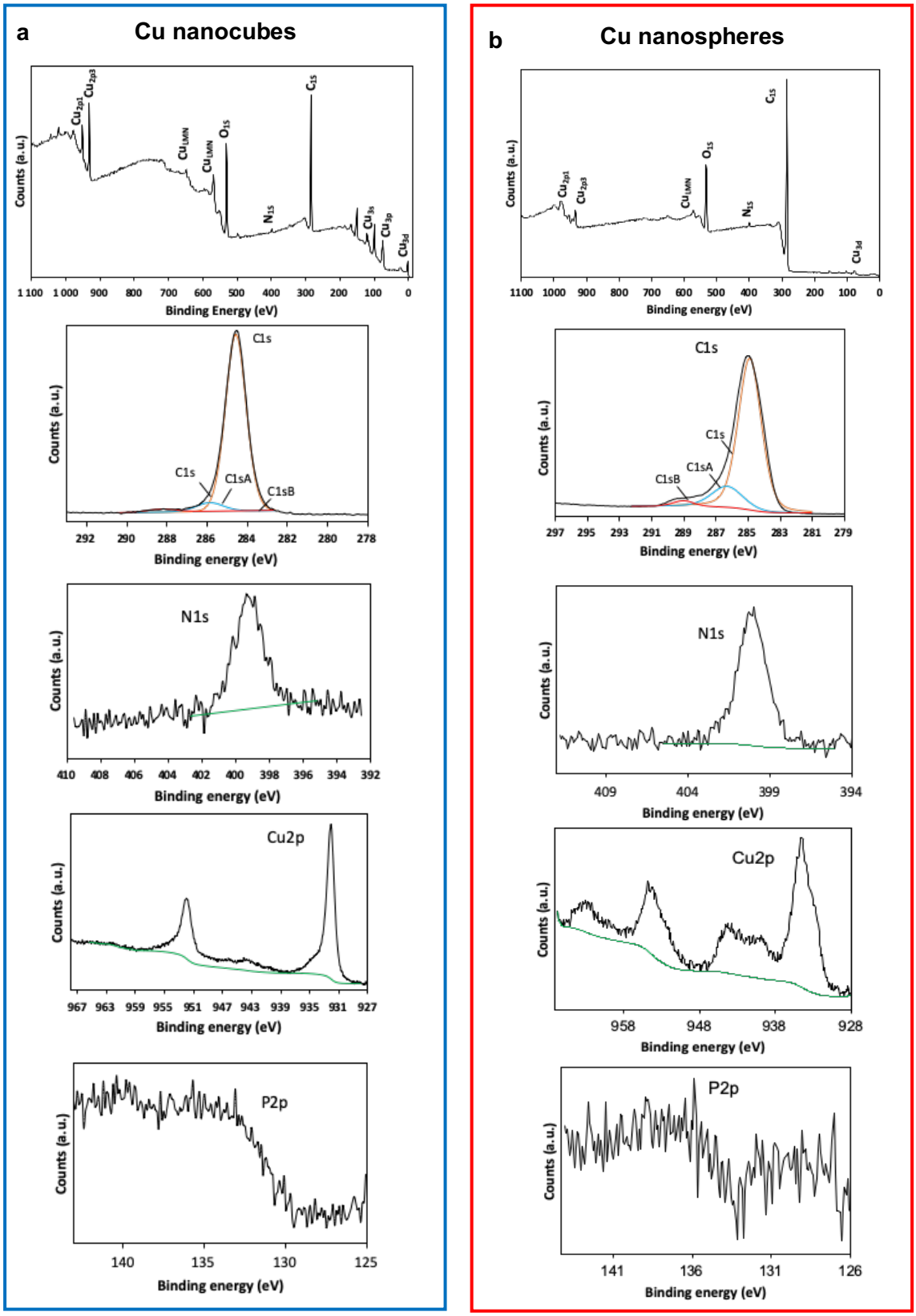

Figure II-13. *XPS survey spectra and High resolution XPS spectra of $C_{1s,}$ $N_{1s,}$ Cu_{2p} and P_{2p} of (a) Cu nanocubes (b) Cu nanospheres obtained in the presence of TOP ligands.*

In 2019, M. Strach *et al.*[11] reported an investigation on the synthetic pathway of shape-controlled CuNPs by using TOP and TOPO via the disproportionation reaction route (Figure II-14). This study shed an interesting light on our own observations on the effect of the heating ramp on the shape of the CuNPs.

In their study, they obtained CuNPs of a series of shapes including spheres, cubes, octahedra and tetrahedra by varying the reaction and/or injection temperature of the Copper-phosphine complex (as shown in Figure II-14).

In the first part of their work, they have investigated the reaction intermediates formed at 80 °C, at the beginning stage of the synthesis, between the CuBr, the phosphine and the OLA through X-ray Absorption Spectroscopy (XAS) and Nuclear Magnetic Resonance (NMR) analyses. They found that the pseudotetrahedral $CuBr(OLA)_3$ complex was formed when CuBr dissolved in OLA (Figure II-15a). When TOPO is used as ligand, it reacted with this $CuBr(OLA)_3$ complex to yield the monometallic and heteroleptic $CuBr(OLA)_2(TOPO)$ complex after a ligand-exchange of one OLA molecule by one TOPO (Figure II-15a (up)). However, in the case of TOP, all the three OLA of ($CuBr(OLA)_3$) were replaced by the TOP, which led to the bimetallic $\{CuBr(TOP)_2\}_2$ complex, as shown in Figure II-15a (down). The following two steps of heating ramp from 100 °C to 260 °C and 1 h of heating at 260 °C have also been investigated by XAS. They showed that the disproportionation of copper (I) to metallic atoms was carried out during the heating ramp for the synthesis of Cu spheres in the presence of TOP, and during the 1 h of heating at 260 °C for the Cu cubes synthesized in the case of TOPO. Once again, this work demonstrated that the disproportionation of the Cu(I)-TOP occurs at lower temperature compared to Cu(I)-TOPO complex which is in contrast to the work reported by H. Guo's group in 2014 (section II.2).[12] They claimed that the bimetallic $(CuBr(TOP)_2)_2$ complex favors the disproportionation of Cu(I) into Cu(0) by a direct inner-sphere electron transfer (Figure II-15b), which induces a slow formation of monomers in the reaction mixture, and thus a low concentration of them. On the contrary, a high temperature is required to promote the disproportionation of Cu(I)-TOPO. When this temperature is reached, all the complexes disproportionate at the same time, which lead to a high concentration of monomers in the medium. According to LaMer theory,[45] they thus assumed that the reaction in the presence of TOP is under thermodynamic control due to low monomer concentration, which induces the formation of quasi-spheres, whereas the reaction of TOPO is under kinetic control due to the high monomer concentration and lead to kinetic anisotropic shapes such as cubes.

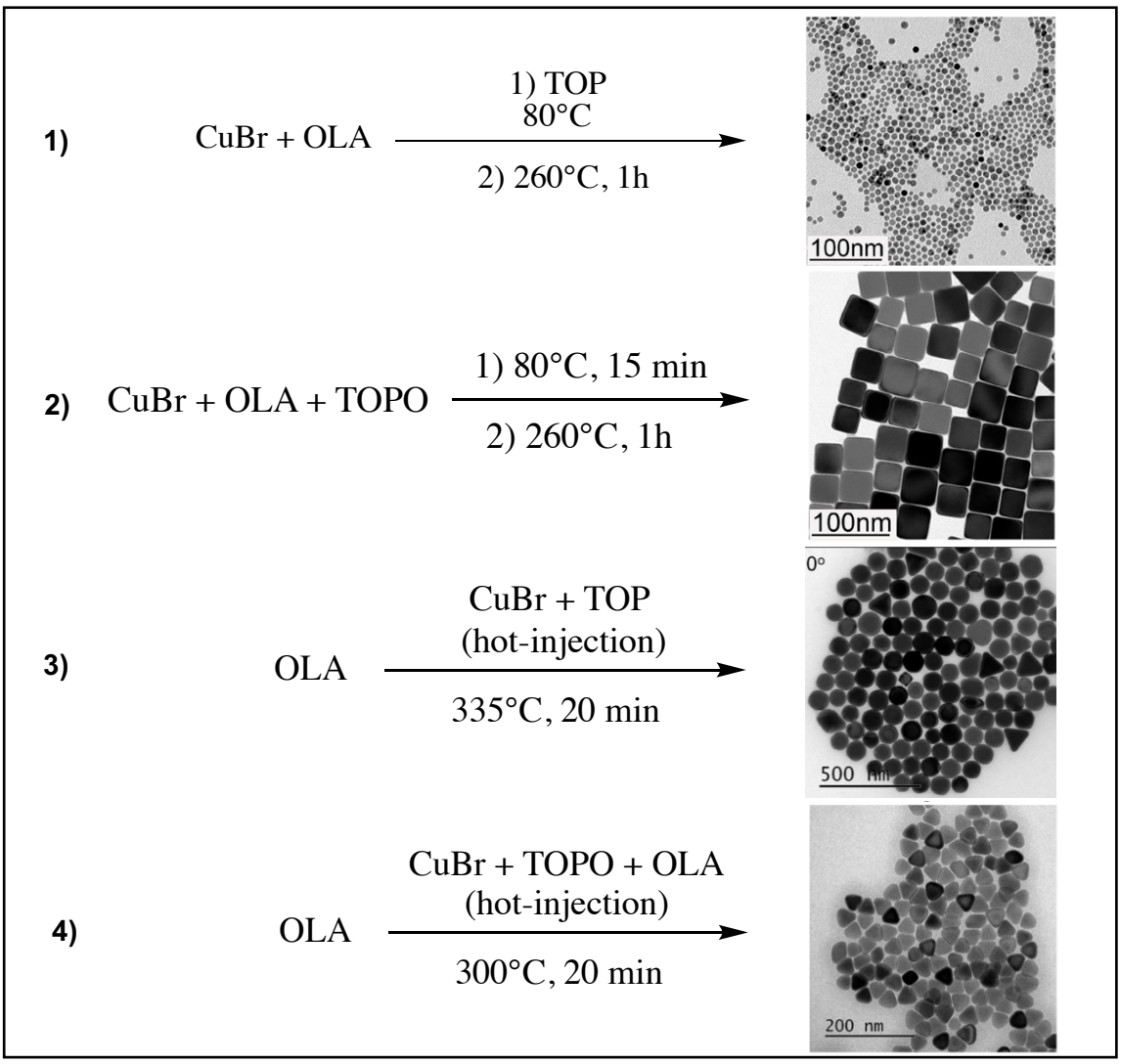

Figure II-14. *Reaction schemes and representative TEM images of 1) Cu spheres 2) Cu cubes 3) Cu octahedra 4) Cu tetrahedra studied in M. Strach's work. (Copyright from Ref.[11])*

They have also investigated the effect of the injection rates of copper complex with TOP and TOPO into OLA at different temperatures (260 °C, 300 °C and 335 °C) on the monomer flux and their effects on the final shape of the CuNPs (Figure II-16). In the case of the Cu(I)-TOP complex, Cu nanocubes were formed with both slow and rapid injection at 260 °C (Figure II-16A, B). Once the temperature increased to 335 °C, the rapid injection rate yielded the Cu cubes (Figure II-16D) but Cu spheres (Figure II-16C) were formed with the slow one. For the Cu(I)-TOPO complex, spherical NPs were obtained both with a low and with a high injection rate at 260 °C (Figure II-16E, F). As discussed above, the high monomer flux and/or low temperature[35-41] favor the kinetic product as polyhedral or cubic NCs, while high temperature and/or low monomer flux lead to an end product dictated by the thermodynamic regime and result thus the quasi-spherical NCs.[35-39]

Interestingly, large spherical NPs (Figure II-16G) were obtained with a slow injection at a higher temperature of 335 °C. However, a rapid injection leads to Cu octahedra (Figure II-16H). Based on the condition for the octahedra synthesis, they also produced Cu tetrahedra by decreasing the temperature to 300 °C with rapid injection of Cu(I)-TOPO complex, as shown in Figure II-14(4).

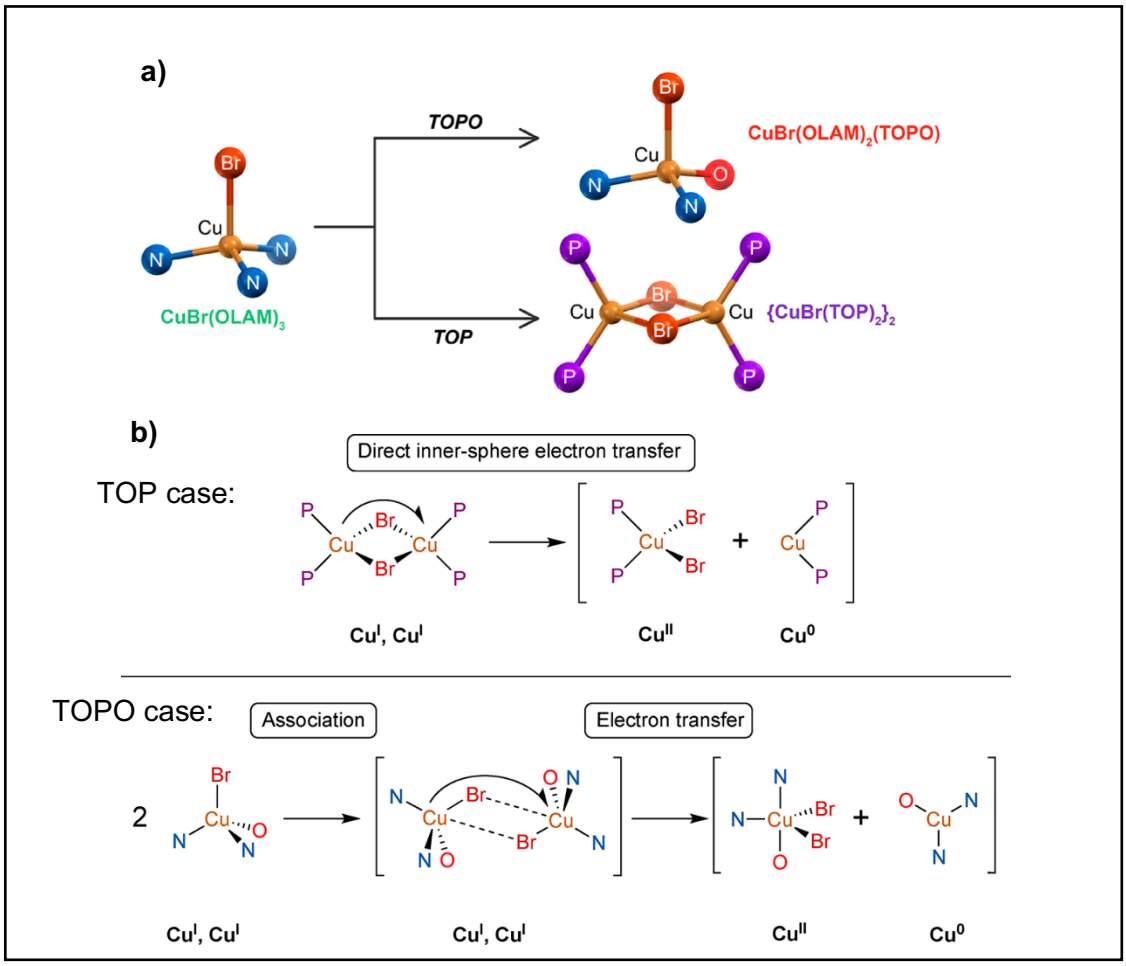

Figure II-15. *Complexes formed at 80 °C from reactions of $CuBr(OLA)_3$ with TOPO and TOP b) Summary of the Disproportionation Pathways of $\{CuBr(TOP)_2\}_2$ and $CuBr(OLA)_2(TOPO)$ Complexes, where TOP, TOPO, and OLA Ligands are represented by their donor atoms P, O, and N. (Copyright from Ref.[11])*

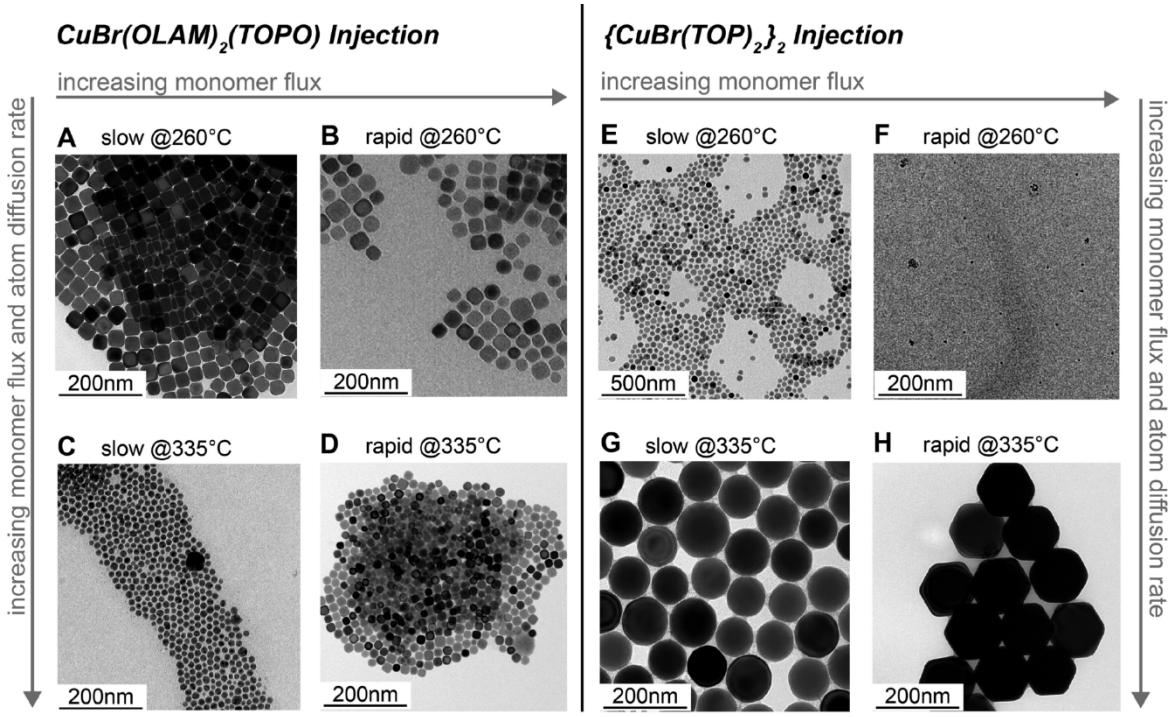

Figure II-16. *Representative TEM images of CuNPs synthetized after (A, B) dropwise and rapid injection of $CuBr(OLA)_2(TOPO)$ at 260 °C; (C, D) dropwise and rapid injection of $CuBr(OLA)_2(TOPO)$ at 335 °C; (E, F) dropwise and rapid injection of $\{CuBr(TOP)_2\}_2$ at 260 °C and (G, H) dropwise and rapid injection of $\{CuBr(TOP)_2\}_2$ at 335 °C. (Copyright from Ref.[11])*

In our work, the formation of different morphologies (cubes and spheres) of CuNPs were observed in the presence of TOP using the different hotplates A and B (see Figure II-11a, c). Based on the study of heating ramp of these hotplates, we found that the heating ability of hotplate A is less efficient than the one of hotplate B. In the reaction with the use of hotplate A, the reaction temperature of the solution could be better controlled compared to hotplate B due to its lower heating ramp (A: 5 °C/min vs B: 13 °C/min), thus a kinetic regime was favored which resulted in the formation of cubic CuNPs. Nevertheless, when the synthesis of CuNPs was carried out using the hotplate B, the control of the temperature of reaction solution became difficult for a short time due to the fast heating ramp. We hypothesized that the higher reaction temperature leads a thermodynamic control during the NPs formation and promoted the spherical shape.

Considering that reaction conditions such as the nature of the copper precursor, the amount of ligands and the reaction time could affect the size and shape of the CuNPs,[46] we undertook a general study to measure and to better understand their effects on the CuNPs synthesis.

II. 4.1.1.1 Effect of the nature of precursor

We first addressed the effect of the nature of the halide stemming from the copper salt precursor. The TEM images depicted in Figure II-17a, b show the effect of halide ions from copper precursor on the final size of CuNPs synthetized by the typical synthetic condition described as Figure II-8 (see Chapter V experimental section 3.1A). As a result, monodisperse Cu nanocubes with an average size of 55.6 ± 4.9 nm (σ% = 9%) in edge length were obtained from CuBr as the copper precursor instead of CuCl. The size of the CuNPs slightly decreased from 59 nm (Cl^-) to 55 nm (Br^-) under identical reaction conditions. As shown in Figure II-17d, two characteristic LSPR peaks of copper nanocubes at 607 nm and 711 nm also can be observed. As mentioned previously, the main peak at 603 nm is attributed to the monodisperse CuNPs, and the second one is a redshift at 711 nm may due to the formation of NPs aggregates in solution.

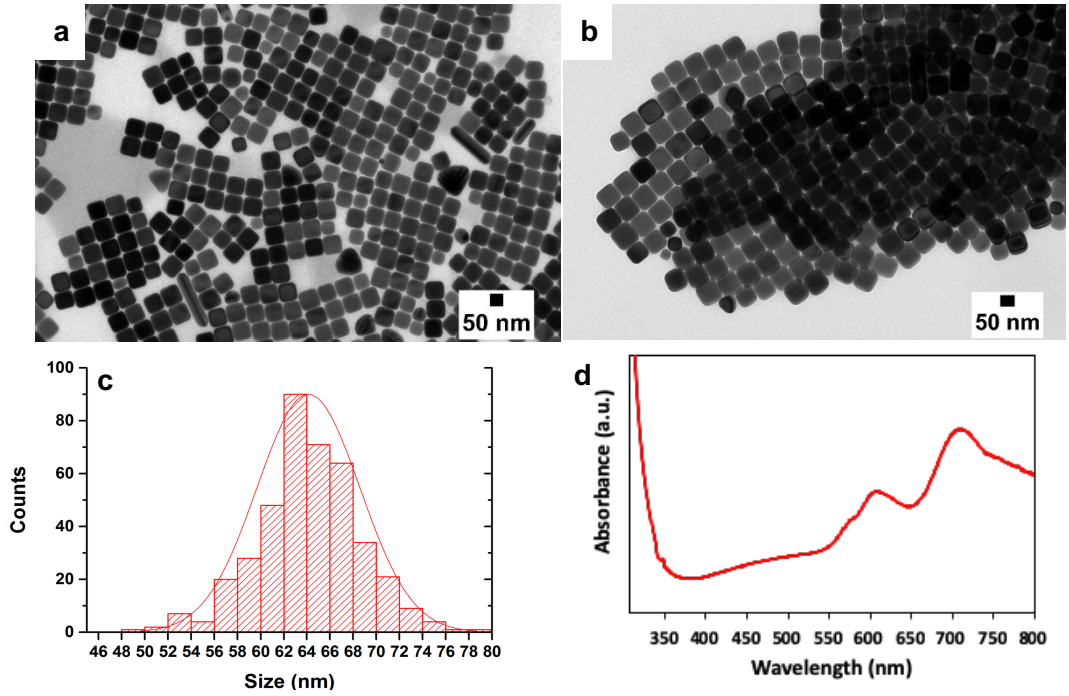

Figure II-17. *(a) Typical TEM image of CuNPs obtained with CuBr as precursor (b) self-assembly (c) the corresponding size distribution histograms and (d) UV-vis absorbance spectra (609 nm, 711 nm).*

We assumed that this size variation could be explained by the difference of the copper-halide bond strength and the different nucleation temperatures in the cases of CuCl and CuBr.

Indeed, the stronger affinity of Br^- ions to Cu(I) compared to Cl^- ions would induce an increase of the disproportionation temperature in the beginning stage of the reaction. This could be confirmed by the different nucleation temperatures observed through the color change of the reaction solution depending on the copper precursor used. Indeed, we observed a faster color change from colorless to orange at 285 °C for the use of CuCl as precursor than for the use of CuBr. For both reactions using CuCl and CuBr salts, we heated the reaction mixture until 285 °C and keep it at this temperature for 1 hour. As we discussed in the last section (see in Figure II-12), there is a significant difference of temperature between the solution and the sand bath, the first one being lower than the second one. In these experiments, the temperature was measured in the sand bath. As the reaction temperature reached 285 °C in the sand, the temperature of the solution was in fact lower and needed more time to increase to 285 °C. We could thus not detect the exact nucleation temperature in solution. The color change suggested that the disproportionation of CuCl is faster than for CuBr. The CuNPs stemming from CuCl would thus have a longer time to grow than the one from CuBr. This may therefore explain why the size of the CuNPs prepared from CuCl (59 nm) is slight bigger than for the use of CuBr (55 nm).

The effect of the difference of the copper-halide bond strength in the NPs formation, is in good accordance with the result obtained for the use of CuI as Cu(I) source instead of CuCl or CuBr. Indeed, the TEM and UV-vis analyses shown that no CuNPs were formed using CuI as precursor. Additionally, no change of solution color was observed during this reaction as the cases of CuCl or CuBr. This mostly due to the high strength of the copper-iodide bond that do not allow the disproportionation of Cu(I) into Cu(0) under the reaction conditions used in our work. We therefore found that the bond strength between the copper and the halide ions not only affect the growth of the CuNPs, but also have a dramatic effect on the early stages of reduction and nucleation.

It is important to note that when $CuBr_2$ or $CuCl_2$ was used as copper precursor in this reaction under identical conditions (285 °C/OLA), we did not observe the formation of CuNPs by UV-vis analysis. Knowing that their standard potentials are greater than the one of CuCl and CuBr (and that they are therefore easily reducible), this would confirm that there are no competitive reduction paths to the disproportionation reaction in these transformations. H. Guo *et al*.[12] showed that the direct reduction of Cu(II) into Cu(0) by the OLA used as solvent is possible. Indeed, the heating of a $CuBr_2$ in OLA at 300 °C for 6 h produces a micrometer-scale size and chaotic shape particles. Higher reaction temperatures than the one we used to be thus required to promote this reduction reaction.

XPS analysis

The XPS was carried out on the Cu nanocubes obtained from the disproportionation of CuBr. The survey spectrum shows peaks attributed to C_{1s}, $Cu_{2p,}$ $O_{1s,}$ $N_{1s,}$ P_{2p} and small signal corresponding to Br_{3d}, as shown in Table II-3 and Figure II-18. The ratio between oleylamine and metallic copper deduced from the N_{1s} and Cu_{2p} peaks at 400.11 eV (At% = 0.78%) and at 934.73 eV (At% = 3.75%) respectively is 0.21, which is similar to that measured on Cu nanocubes prepared from CuCl (Table II-2, Figure II-13a). For Cu nanocubes prepared from CuBr, the peak at 69.43 eV is the signature of Br_{3d}. The atomic percentage ratio between Br and Cu is equal to 0.016. However, the Cl^- peak was not detected on the surface of Cu nanocubes prepared from CuCl. Finally, the presence of TOP ligands on the particle surface of nanocubes stemming from CuBr was also confirmed by the detection of P_{2P} peak at 132.8 eV, it was also not detected from the sample prepared from CuCl. The ratio between phosphine ligand and metallic copper deduced from the P_{2p} and Cu_{2p} peaks at 132.80 eV (At% = 0.29%) and at 934.73 eV (At% = 3.75%) is 0.08, and the OLA-to-TOP ratio deduced from the N_{1s} and P_{2p} peaks at 400.11 eV (At% = 0.78%) and at 132.80 eV (At% = 0.29%) is 2.7. As a result, the coverage ratio of OLA is significantly higher than the one of TOP. In the high-resolution spectra for Cu_{2p} (Figure II-18), $Cu_{2p3/2}$ and $Cu_{2p1/2}$ peaks of Cu^{2+} at 934.6 eV and 954.6 eV in combination with satellite peaks at range from 930 eV and 948 eV were observed, which indicate the presence of CuO.[44] The detected Cu-O may due to the oxidation of the surface of the NPs that occurred during the sample transportation.

Table II-3. *XPS data analysis of Cu nanocubes obtained from CuBr.*

Sample	Element	Peak BE	FWHM eV	Area (P) CPS.eV	Atomic %
Cu nanocubes	Br3d	69.43	0.16	571.47	0.06
	C1s	284.96	1.49	263085.34	82.03
	Cu2p	934.73	2.81	241995.27	3.75
	N1s	400.11	1.73	4402.26	0.78
	O1s	532.00	1.88	115951.52	13.09
	P2p	132.80	2.31	1131.92	0.29

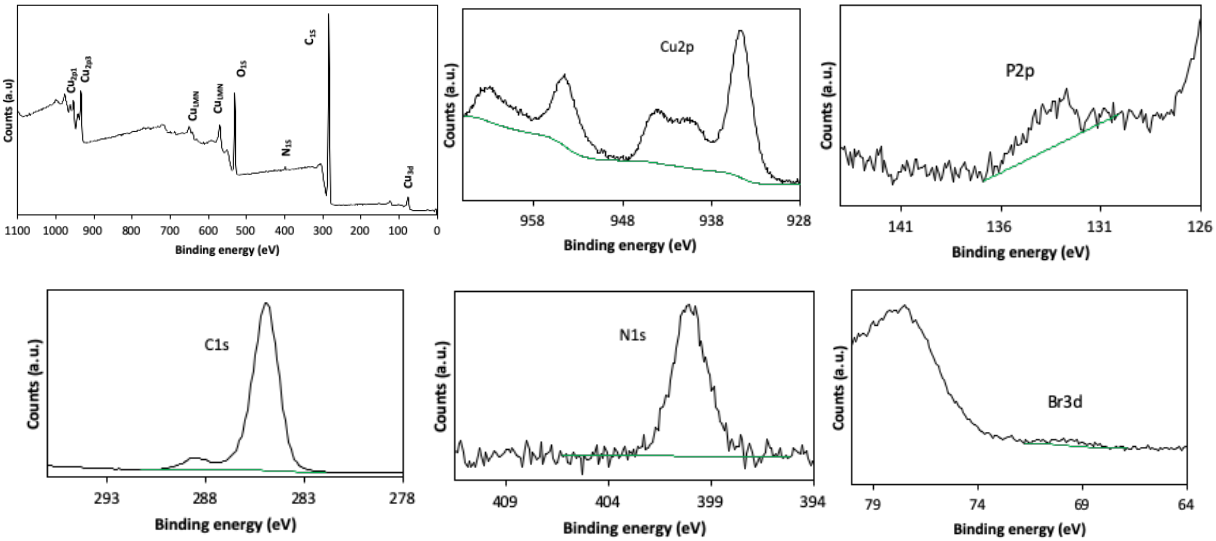

Figure II-18. *XPS survey spectra and High resolution XPS spectra of Cu_{2p}, P_{2p}, C_{1s}, N_{1s}, and Br_{3d} of Cu nanocubes obtained from CuBr in the presence of TOP ligands.*

In addition to the copper halide, others Cu salts were tested as copper precursor, such as $[Cu(CH_3CN)_4]PF_6$, CuCN, $Cu(CH_3COO)$ and $Cu(CH_3COO)_2$. All next experiments were performed using our standard reaction conditions described in Figure II-8 with a range of reaction temperature from 240 °C to 265 °C (see Chapter V experimental section 3.1.B). The typical TEM images of CuNPs obtained from these copper salts are shown in Figure II-19. In the case of $[Cu(CH_3CN)_4]PF_6$, large Cu crystals with mixed triangular and spherical shapes are observed (Figure II-19a). Monodisperse spherical CuNPs with an average size of 15.8 ± 1.6 nm and a low polydispersity of 10% were produced when CuCN was used as Cu(I) source. For the use of $Cu(CH_3COO)$, quasi-spherical and a few rod-shaped NPs were observed (Figure II-19c). The mean size of theses Cu quasi-spheres is 38.3 ± 8.3 nm with a size distribution of 21%. Surprisingly, the reaction of $Cu(CH_3COO)_2$ also produced the Cu quasi-spheres with a mean size of 66.9 ± 16.1 nm. Beside the role of capping agent and surfactant, it was shown that oleylamine can also play the role of a weak reducing agent in high-temperature solution phase syntheses of metal NPs.[17,47] In our work, the CuNPs obtained from $Cu(CH_3COO)_2$ could be formed by a direct reduction of Cu(II) into Cu(0) by OLA instead of a disproportion reaction. But it is still unclear why $Cu(CH_3COO)$ and $Cu(CH_3COO)_2$ nucleate at the same heating temperature (245 °C) to form the NPs.

Based on the results obtained from different copper precursors, it seems that the nature of copper precursor remarkably influences the final morphology of CuNPs. This may be due to the different nucleation temperatures that occurred under the influence of precursor nature.

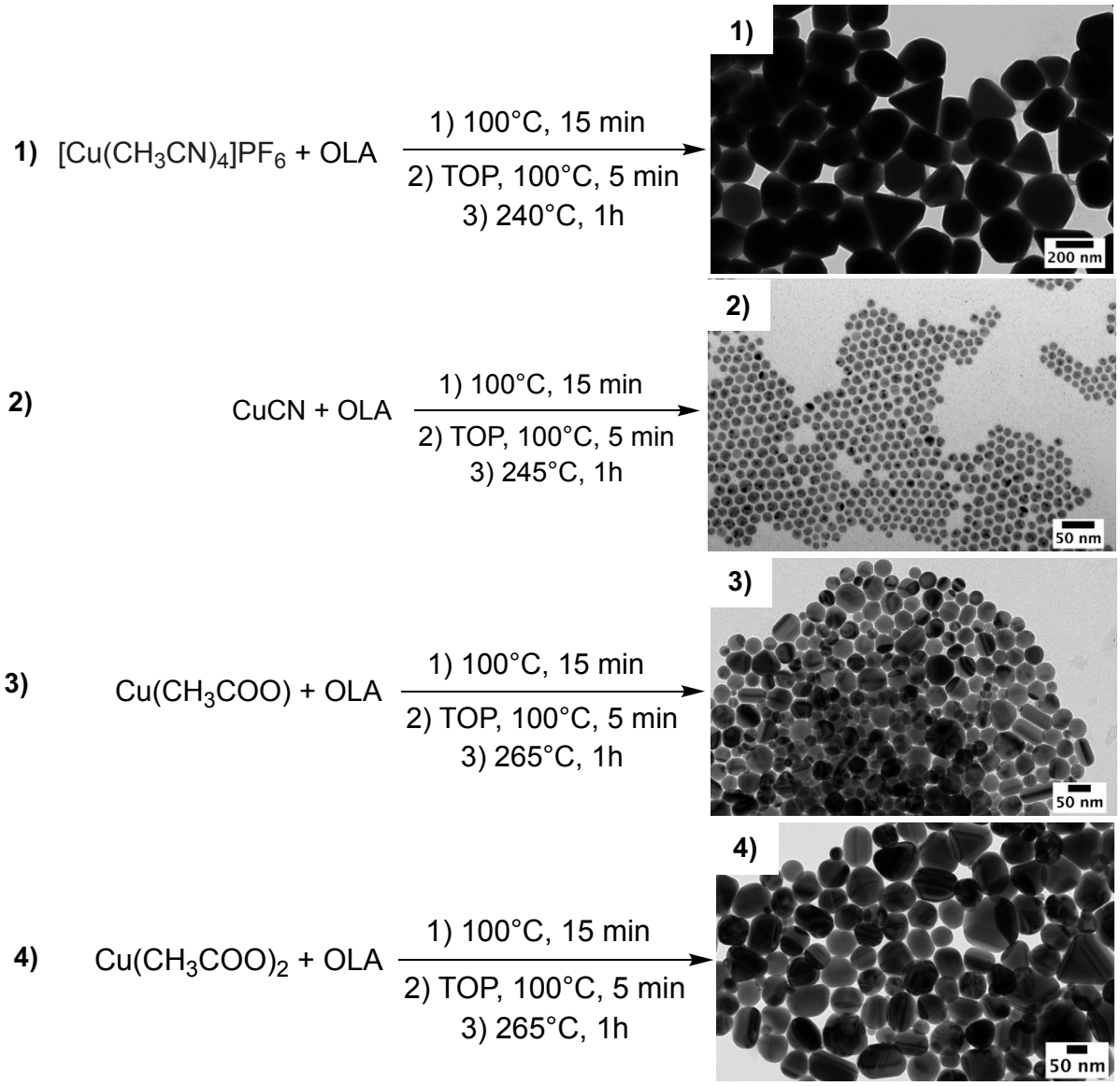

Figure II-19. *Synthesis of CuNPs with various copper salts: 1) $[Cu(CH_3CN)_4]PF_6$ 2) CuCN 3) $Cu(CH_3COO)$ 4) $Cu(CH_3COO)_2$ and the TEM images of the corresponding CuNPs.*

II. 4.1.1.2 Effect of reaction time and amount of phosphorus ligands

We next addressed the effect of the reaction time on the size of the CuNPs. Increasing the reaction time from 1 h to 2 h resulted in an increase of the NPs size whatever the nature of the halide used. Figure II-20a, b show the typical TEM images of CuNPs obtained after 2 hours starting from CuCl as the precursor with a mean size of 80.6 ± 5.3 nm (vs 59.8 ± 5.8 nm at 1 h, see Figure II-9) or from CuBr (average size of 67 ± 5.8 nm at 2 h vs 55.6 ± 4.9 nm at 1 h, see Figure II-17). Both syntheses present a size low polydispersity of 9%. As shown by

these results, the reaction time play important role for the size control in the synthesis of CuNPs, but not greatly affected their polydispersity.

The effect of the number of equivalents of the phosphine ligand was next studied. As we can see in Figure II-20c, the Cu nanocubes prepared from CuBr by using 3 equivalents of TOP have a size of 33.8 ± 2.0 nm instead of 55.6 ± 4.9 nm for the use of 1.6 equivalents in the same reaction conditions. It is well known that the amount of ligands introduced at the beginning of the synthesis can affect the final size of the nanoparticles. A high ratio of phosphine ligands to copper precursor was shown to lead smaller particles than a lower one in the disproportionation route.[12] Interestingly, a slight change in nanoparticle shape was observed from cube-shaped to round cube in the presence of a larger amount of TOP. The size distribution is expected to depend on the ligands surface coverage, because high cover of ligands on the surface of nuclei reduces the fraction and the reactivity of the free surface site.[46,47] In our case, the change of shape may be due to the face-selective adsorption of TOP that would affect the facets growth rate.[11,21] Additionally, when the equivalent of TOP increased to 4 or 5 equiv. at 285 °C, the formation of CuNPs was not observed by UV-vis analysis. CuNPs sizes and corresponding size distribution in function of TOP amount are reported in Table II-4.

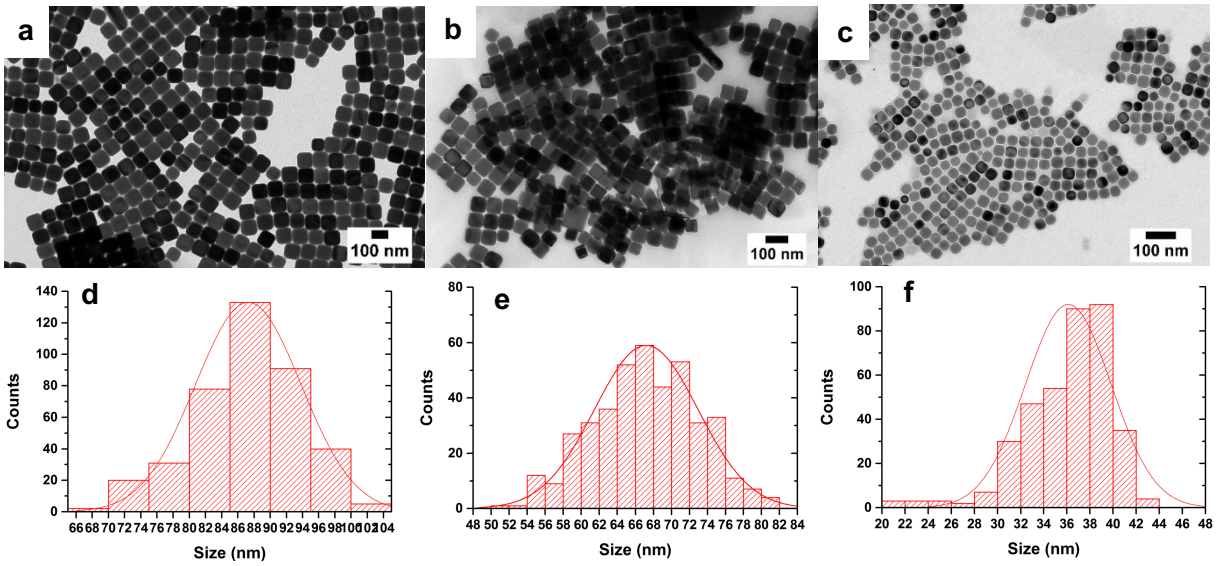

***Figure II-20**. TEM images of CuNPs synthesized from (a) CuCl/1.6 equiv. TOP/2 h (b) CuBr/1.6 equiv.TOP/2 h (c) CuBr/3 equiv.TOP/1 h and (d, e, f) the corresponding size histograms.*

***Table II-4**. Experimental conditions were used for preparing CuNPs (TOP) with the corresponding size distributions.*

Precursor (1 mmol)	**TOP (eq.)**			**Reaction time (h)**		**NPs Size (nm)**	**σ* (%)**
	1,6	3	4 or 5	1	2		
CuCl	✓			✓		59.8 ± 5.8	10
	✓				✓	80.6 ± 5.3	7
		✓		✓		33.8 ± 2.0	6
			✓	✓		-	-
CuBr	✓			✓		55.6 ± 4.9	9
	✓				✓	67.2 ± 5.8	9
CuI	✓			✓		-	-
$CuCl_2$	✓			✓		-	-
$CuCl_2$	✓			✓		-	-
$[Cu(CH_3CN)_4]PF_6$	✓			✓		250 - 500	-
CuCN	✓			✓		15.8 ± 1.6	10
$Cu(CH_3COO)$	✓			✓		38.3 ± 8.3	22
$Cu(CH_3COO)_2$	✓			✓		66.9 ± 16.1	24

**: Polydispersity*

In this section, we have investigated the effects of nature of the precursor, the heating ramp, the amount of TOP and the reaction time on the size and shape of CuNPs synthetized. These different factors allow the formation of shape-controlled (cubes, octahedra, spheres) and size tunable (c.a. 15 to 80 nm) copper nanoparticles via robust and convenient disproportionation reactions. Especially, the efficient temperature ramp-controlled procedure has been studied to obtain the NPs with morphological evolution from cube to octahedra and sphere. It worth noting that this shape control realized by tuning the heating ramp was mainly observed for the use of TOP ligand.

II. 4.1.2 CuNPs synthesized in the presence of TOPO

In this section, the formation of CuNPs was achieved in the presence of TOPO using two different protocols, the "hot-injection" and the "heating-up" methods, as shown in Figure II-21. In our work, we call "hot-injection" method the addition of phosphorus ligand into the copper-OLA complexes at 100 °C, which is different from the method reported by Strach's group who added the mixture of copper salt and phosphorus ligand into OLA at high temperatures (as shown in Figure II-14).

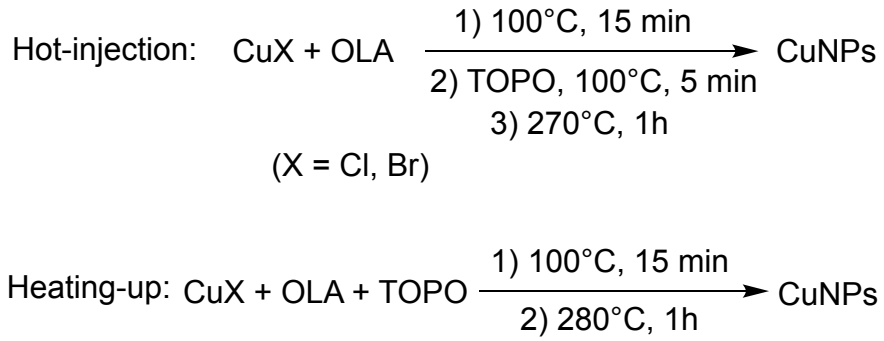

Figure II-21. *Synthesis of CuNPs in the presence of TOPO by "hot-injection" and "heating-up" routes.*

1) Hot-injection

A typical synthesis of copper NPs in the presence of TOPO was performed with the same hot-injection procedure described above for the use of TOP (Figure II-8), but with a lower heating temperature of 270 °C instead of 285 °C (see in Chapter V experimental section 3.1.C). The formation of CuNPs was evidenced by a slow color change of the solution from colorless to orange and finally to red-purple. As seen in Figure II-22a, CuNPs with mixed shapes of wires (mean size of 35 ± 12.6 nm in diameter) and a few quasi-spheres (~ 68.6 nm) were obtained for the use of CuCl as the Cu(I) source in the presence of TOPO. As previously observed for the use of TOP, a higher amount of phosphorus ligands induced a decrease of the nanoparticle size. Indeed, increasing the amount of TOPO from 1.6 to 3 equiv. resulted in the formation of homogeneous nanowires with an average size of 21 ± 4.4 nm (σ% = 21%) in diameter (see in Figure II-22b). Next, CuBr was used as Cu(I) precursor in the presence of different amounts of TOPO: 1.6 and 3 equivalents. In these reaction conditions, well-defined nanowires were obtained with a mean size of 41.5 ± 13.5 nm (σ% = 33%) with 1.6 equiv. of TOPO, and a smaller average size of 30.1 ± 5.7 nm (σ% = 19%) with 3 equiv. (see in Figure II-22c, d).

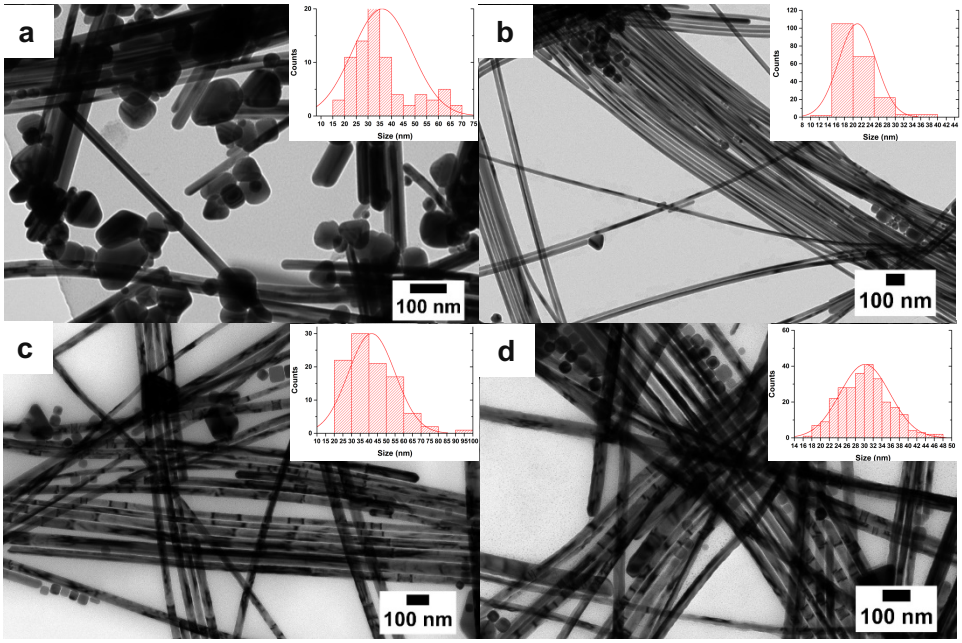

***Figure II-22**. Typical TEM images of CuNPs obtained from different amounts of TOPO starting from: i) CuCl, (a) 1.6 equiv. (b) 3 equiv. and ii): CuBr, (c) 1.6 equiv. (d) 3 equiv.*

2) Heating-up

In this heating-up procedure (see in Chapter V experimental section 3.1.D), the copper nanoparticles were produced by a modified synthetic procedure as shown in Figure II-23. 1 mmol of TOPO ligands was added into a 0.6 mmol of CuX (X= Cl, Br) in 7 mL of oleylamine solution at room temperature (rt). The reaction mixture was next heated at 100 °C and kept at this temperature for 15 min until a greenish solution was obtained. The temperature was then increased to 285 °C until the solution color changed to orange. After 1 h at 285 °C the resulting red-purple solution was cooling to room temperature, and the copper nanoparticles were purified by dispersing the reaction mixture in an excess of absolute ethanol and using centrifugation. As a result, monodisperse cubic shape nanoparticles were obtained instead of nanowires, as shown in Figure II-24a, b.

As in the case of TOP, the blue color of the supernatant was also observed in both procedures after the standard washing procedure which showing the presence of Cu(II) in the solution, and thus demonstrated that a disproportionation reaction underwent when TOPO was used as phosphine ligand.

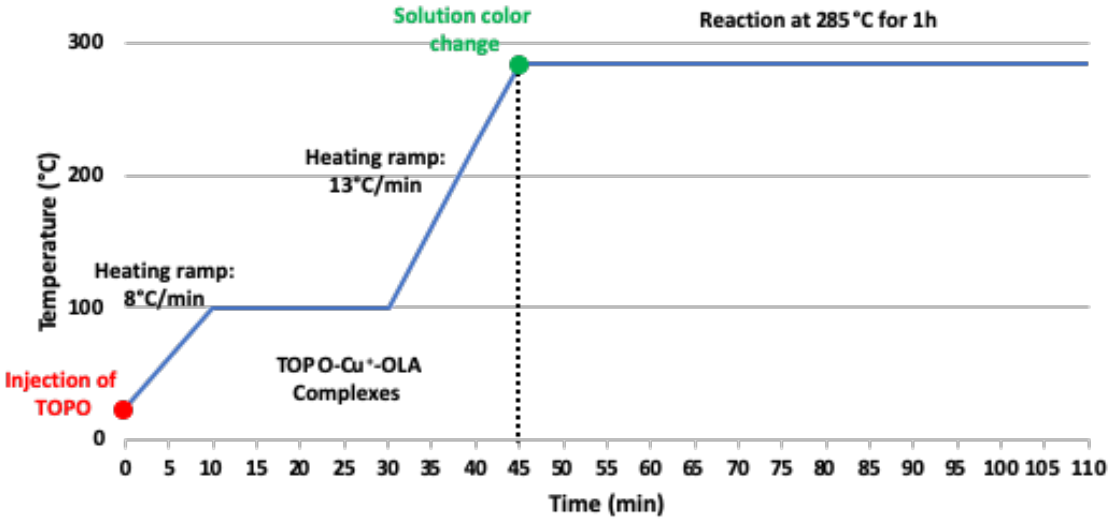

Figure II-23. *Schematic illustration of CuNPs synthesis in the presence of TOPO through heating-up procedure.*

Figure II-24a shows the copper nanocubes obtained with an average size of 75.2 ± 8.7 nm and a low polydispersity of 11% when CuCl was used as the precursor. As shown in Figure II-24b, the CuBr allows to produce smaller nanocubes with a mean size of 49.9 ± 10.4 nm (σ% = 21%). This result shows that it is possible to tune the final size of the nanoparticles through a judicious choice of the copper halide ligands. A similar observation was reported by the Strach's group but was not discussed.[11]

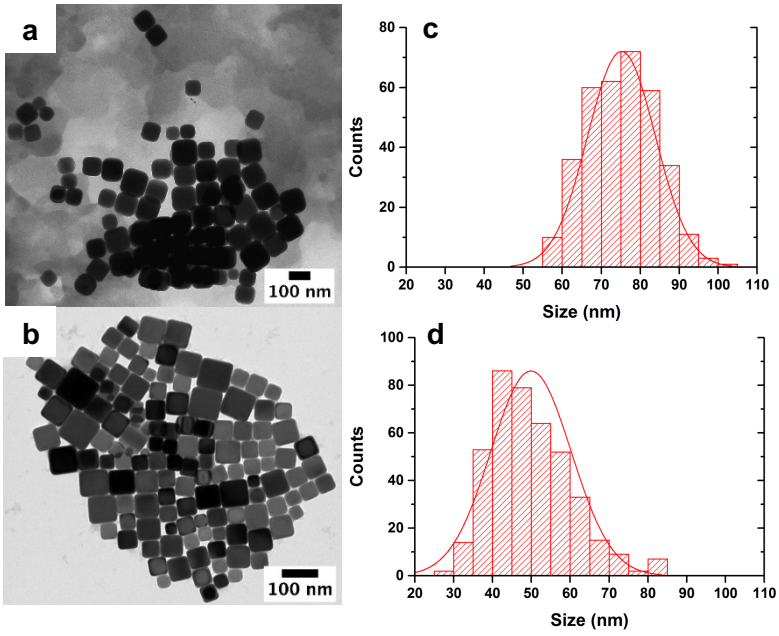

Figure II-24*. TEM images of Cu nanocubes stemming from the heating-up of TOPO in oleylamine with different copper precursors: (a) CuCl (b) CuBr and (c-d) the corresponding size distribution histograms.*

In the case of TOPO, the results obtained using different synthetic procedures show that the injection temperature of TOPO enables to control the morphology of the nanoparticles. The hot-injection method promotes the formation of nanowires whereas a cubic shape was obtained using the heating-up procedure.

As reported in the Strach's work (Figure II-15),[11] the nature of the complex intermediate is one of the key factors influencing the disproportionation temperatures, thereby affecting the size and shape of CuNPs synthetized. We assumed that the formation of $CuCl(OLA)_{3-x}(TOPO)_x$ (x = 0, 1) may depend on the starting reaction temperature in our study. During the heating-up procedure, the monometallic $CuBr(OLA)_2(TOPO)$ was yielded during heating ramp from rt to 100 °C which promotes the followed production of cubic shape CuNPs. In the case of hot-injection of TOPO at 100 °C, the $CuCl(OLA)_3$ was yielded during the temperature raises and the substitution of TOPO might not completely occurred due to the TOPO relatively is a weaker ligands compared to TOP.[11] Therefore, in our reaction conditions $CuCl(OLA)_3$ may be mainly formed in the reaction mixture, which would lead to the synthesis of nanowires. The formation of copper nanowires in the sole presence of OLA via a disproportionation reaction has indeed been reported in the literature.[4, 49]

Interestingly, when the synthesis of CuNPs in the presence of TOP (instead of TOPO) was carried out by "heating-up" procedure, no CuNPs formed was observed by TEM and UV-vis analyses under identical reaction conditions (1.6 equiv. of TOP/285 °C).

XPS analysis

The XPS analysis was carried out on the CuNPs obtained from CuCl and CuBr in the presence of TOPO (1.6 equiv.) through the heating-up route. The results were collected in Table II-5 and Figure II-25.

For CuNPs prepared from CuCl, the formation of metallic copper is evidenced by the Cu_{2p} signal at 932.55 eV (At% = 5.22%). The N_{1s} peak at 399.25 eV (At% = 2.67%) is the signature of the presence of OLA on the particle surface. Also, P_{2p} and Cl_{2p} peaks are observed at 132.10 eV (At% = 0.4%) and at 197.78 eV (At% = 0.53%) which are attributed to the P form TOPO ligand and Cl^- ions from initial precursor. The ratio between OLA and phosphine ligand deduced from the N_{1s} and P_{2p} peaks at 399.25 eV (At% = 2.67%) and at 132.10 eV (At% = 0.4%) respectively is 6.7.

For CuNPs synthetized from CuBr, the XPS signals of N_{1s} and P_{2p} at 399.59 eV (At% = 1.49%) and at 132.96 eV (At% = 0.99%) were also detected which indicate the presence of OLA and TOPO ligands on the particle surface, the OLA-to-TOPO ratio is 1.5. Comparison with the OLA-to-TOPO ratio detected from NPs obtained from CuCl, the coverage of amine ligand is lower (1.5 < 6.7) on the NPs surface prepared with CuBr. Also, Br_{3d} peak is observed

at 68.63 eV (At% = 0.45%) which shows the Br^- as a surfactant or capping agent on the particle surface.

As in the previous XPS studies for the use of TOP, the presence of Br^- was detected on the surface on the NPs, but not Cl^-.

Table II-5. *XPS data analysis of Cu nanoparticles prepared from CuCl and CuBr in the presence of TOPO via heating-up route.*

Sample	Element	Peak BE	FWHM eV	Area (P) CPS.eV	Atomic %
CuNPs (CuCl)	C1s	284.74	1.14	148994.91	74.97
	C1s A	285.87	1.49	10700.49	5.39
	C1s B	288.17	1.80	3510.16	1.77
	Cl2p	197.78	1.66	3048.69	0.53
	Cu2p	932.55	2.55	154882.43	5.22
	N1s	399.25	1.62	8229.43	2.67
	O1s	531.10	3.52	43498.97	9.05
	P2p	132.10	0.94	1173.43	0.40
CuNPs (CuBr)	Br3d	68.63	1.97	1974.61	0.45
	C1s	284.75	1.26	73591.79	51.68
	C1s A	286.14	1.62	6058.96	4.26
	C1s B	288.58	1.80	4156.64	2.93
	Cu2p	932.49	1.23	363516.29	17.11
	N1s	399.59	1.37	3291.84	1.49
	O1s	530.84	2.36	72725.61	21.11
	P2p	132.96	1.71	2081.05	0.99

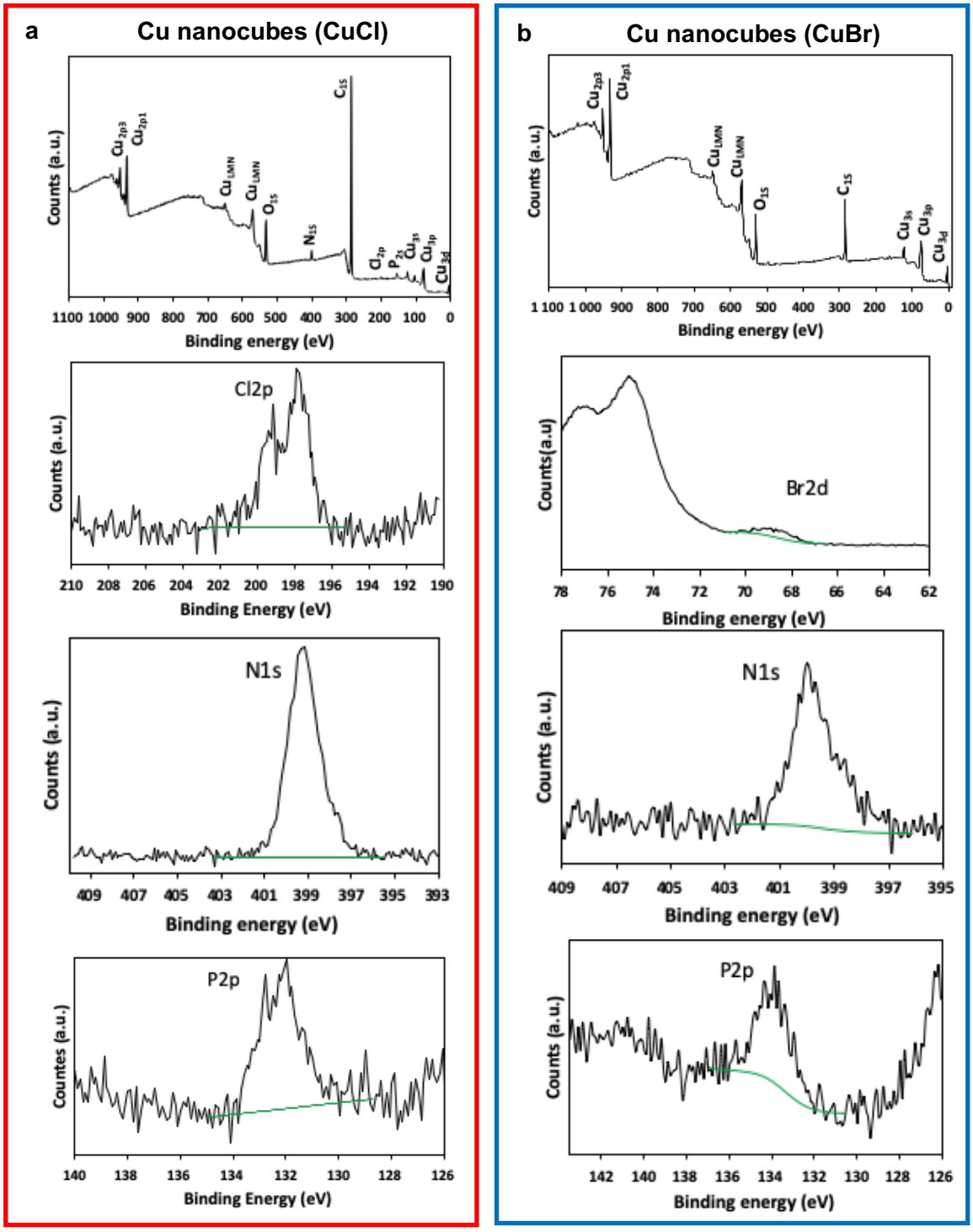

Figure II-25. *XPS survey spectra and high resolution XPS spectra of Cl_{2p}, Br_{3d}, N_{1s}, P_{2p} of Cu nanocubes obtained from (a) CuCl and (b) CuBr in the presence of TOPO (1.6 equiv.).*

The different synthetic conditions of CuNPs in the presence of TOPO were overall described in Table II-6.

***Table II-6**. Summary of the different experimental conditions used for preparing CuNPs from CuCl or CuBr and TOPO with the size distribution of the corresponding CuNPs.*

Precursor (1 mmol)	**TOPO (equiv.)**		**Reaction method**		**NPs shape**	**NPs Size (nm)**	**σ* (%)**
	1.6	3	Hot-injection	Heating-up			
CuCl	✓		✓		Wires (Maj)	35.0 ± 12.6	36
	✓			✓	Cubes	75.2 ± 8.7	12
		✓	✓		Wires	21.0 ± 4.4	21
CuBr	✓		✓		Wires	41.5 ± 13.5	33
	✓			✓	Cube	49.9 ± 10.4	21
		✓	✓		Wires	30.1 ± 5.7	19

* : Polydispersity

These results show that the injection temperature of TOPO critically influence the final shape of CuNPs in this present work. Additionally, the amount of TOPO and the nature of the halide of copper precursor play an important role in the final size of CuNPs prepared. As a result, a high phosphorus ligand-to-copper ratio leads to a decrease of the NPs size. The Cu nanocubes synthetized from CuCl are larger than CuBr. However, an opposite trend of the NPs size was observed in the synthesis of nanowires in the cases of CuCl and CuBr. The reason is still unclear. On the other hand, an increase in the amount of TOPO leaded to a decrease in the size of nanowires.

II. 4.2 CuNPs preparation using PPh_3 and $P(PhMe_3)_3$.

As TOP and TOPO ligands, the PPh_3 has often been reported as a capping agent and a stabilizer of metallic nanoparticles.[50] As seen in Chapter I, A. Courty *et al.*[51] reported the synthesis of spherical CuNPs with tunable size through the reduction of the $CuCl(PPh_3)_3$ complex by *tert*-butylamine borane. In this reaction, the free PPh_3 derived from the copper precursor acted as stabilizer of the NPs products. Also, L. M. Rossi *et al.*[52] synthetized PPh_3-stabilized Rh NPs and shown that the use of PPh_3 as capping ligands induced an increase of the catalytic selectivity of these nanoparticles in the hydroformylation.

In the previous section II.3 (Table II-1), we have studied the electronic (pKa) and steric (Tolman cone angle) properties of various phosphorus ligands, as well as their coordination energy to copper and the disproportionation energy of Cu(I)-PR_3 complexes. Comparing to TOP ($P(C_8H_{17})_3$, pKa = 8.4), PPh_3 is more acid (pKa = 2.73, θ = 145°). The PMe_3 (pKa = 8.65, θ = 118°) was used as the PR_3 (R = alkyl) model (i.e., TOP model) to calculate the theoretical coordination and disproportionation energy. From the calculated results (Figure II-6), the PMe_3 has a higher coordination ability to copper than the PPh_3 and the disproportionation energy of its corresponding complex with copper is also higher than the one of PPh_3. Compare to their Tolman cone angle (θ = 118° vs θ = 145°), the greater difference between PMe_3 and PPh_3 is in their pKa (8.65 vs 2.73). Thus, we presumed that a lower pKa ligand facilitates the disproportionation reaction. In order to investigate this hypothesis, a series of experiences were carried out.

In our work, CuNPs were also prepared from a Cu(I)-PPh_3 complex using the following procedure (see in Chapter V experimental section 3.1.E): 0.6 mmol of copper salts CuX (X=Cl, Br) was weighted in an N_2-filled glovebox and transferred inside a Pyrex 25 mL glass vial along with 7 mL (35 equiv.) of OLA. The mixture was vigorously stirred and heated up to 100 °C under inert gas (N_2) to completely dissolve all solids. After 15 min of stirring, 1 mmol of PPh_3 was quickly added to the resulting greenish solution, inducing its immediate discoloration. After 5 minutes of stirring the colorless mixture was heated up to 270 °C and held at this temperature for 1 hour (Figure II-26). The formation of CuNPs was evidenced by a slow color change of the solution from colorless to pink and finally to pink-purple. The resulting CuNPs were purified and isolated by dispersing the reaction mixture in excess absolute ethanol and using centrifugation. Also, the blue color of the supernatant was also observed after the standard washing procedure which suggesting the presence of Cu(II) in the solution, and thus shown the occurrence of a disproportionation reaction when PPh_3 was used as phosphine ligand.

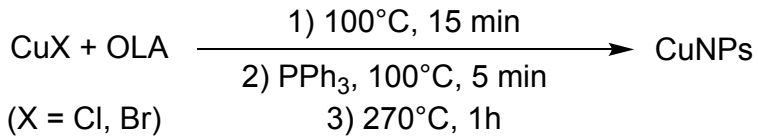

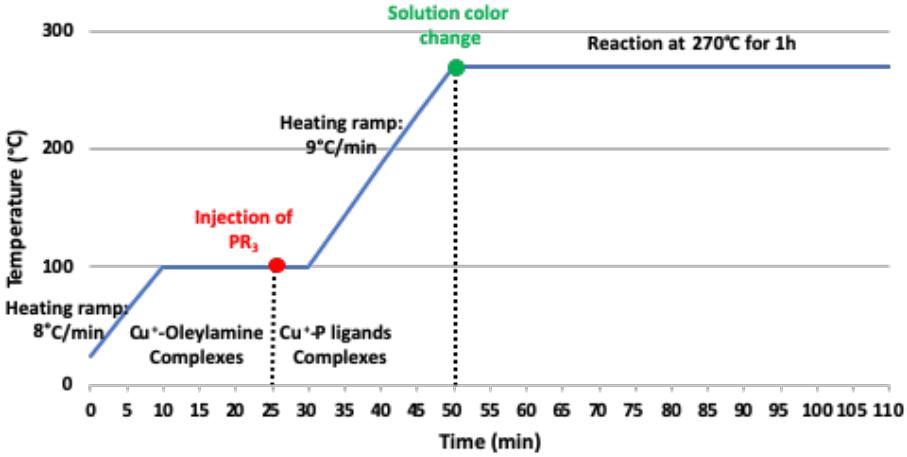

***Figure II-26**. Description of the synthesis procedure of CuNPs via disproportionation reaction of Cu(I)X (X = Cl, Br) in oleylamine in the presence of PPh_3 ligand.*

As shown in Figure II-27a, the use of CuCl in the presence of 1.6 equivalents of PPh_3 yielded cubic copper nanoparticles with an average size of 88.5 ± 16.0 nm (σ% = 18%). When CuBr was used as Cu(I) source instead of CuCl, cubic nanoparticles with a larger size of 110.8 ± 15.3 nm (σ% = 14%). Interestingly, a few well-defined nanorods (~ 96.8 nm in diameter) were observed along with nanocubes in the reaction with CuBr (Figure II-27b). Considering that the reaction time could be a key factor, the heating time at 270 °C was increased from 1 h to 2 hours. Under these reaction conditions, well-defined nanowires with a mean size of 36.4 ± 7.3 nm in diameter (σ% = 20%) were produced (Figure II-27c). We found that the reaction time has thus a dramatic effect on the CuNPs morphologies in this reaction.

One of possible explanations could be that the nanowires stem from the continuous growth of the small nanorods or the oriented attachment of small nanocubes already present in the CuNPs mixture formed after 1 hour.[53-55] Another hypothesis could be the formation of different nanocrystal seeds (single crystal and multiply twinned) during the nucleation stage and thus might lead to different morphologies.[56] A possible explanation of these different seeds may be the formation of $CuCl(OLA)_{3-x}(PPh_3)_x$ (x = 0, 1, 2, 3) when the PPh_3 was used as the phosphorus ligand. Based on the calculated coordination energies (see Figure II-6), we found that the coordination abilities to copper between PPh_3 and NH_2CH_3 (i.e., OLA) are very close, especially, the oleylamine is in excess (35 equiv. OLA vs 1.6 equiv. PPh_3). Accordingly, there was a possible competition between them which leaded to different complexes $CuCl(OLA)_{3-x}(PPh_3)_x$ (x = 0, 1, 2, 3) and thus resulted incontrollable formation of initial nanocrystal seeds.

As mentioned before, Cu nanowires could be produced in the presence of only OLA (i.e., $CuCl(OLA)_3$) which is used as solvent and capping agent via a disproportionation reaction.[4,49] Thus, the cubic shape of NPs was may obtained from the growth of single crystal at 1 hour, and the multiply twinned possibly grown up to nanorods at 1 hour or nanowires at 2 hours.[57,58]

Additionally, these different complexes could have different disproportionation rates which influence the monomer concentration and the consequent nucleation and growth of NPs would be affected thus leads to different final nanoparticle shapes. This phenomenon has been illustrated by Strach's work,[11] the bimetallic $\{CuBr(TOP)_2\}_2$ complex slow down the disproportionation rate at a low temperature (150 °C) lead to the spherical shape of CuNPs and a burst disproportionation monometallic $CuBr(OLA)_2(TOPO)$ complexes occurs at 255 °C.

In these cases, the large mass difference between the nanowires and the nanocubes means that the last may have been eliminated during the washing step and are therefore missing from the TEM images. Also, the formation of nanowires may be due to an oxidative etching of nanocubes formed in the first 1 hour. In Chapter I, the oxidative etching process which enables to re-dissolve the nanoparticles formed in the solution and the new "nuclei" regrow and yield new shape of NPs.[59] The halide ions and O_2 present in solution which could act a strong oxidative etchant to promote the oxidative etching process.[60]

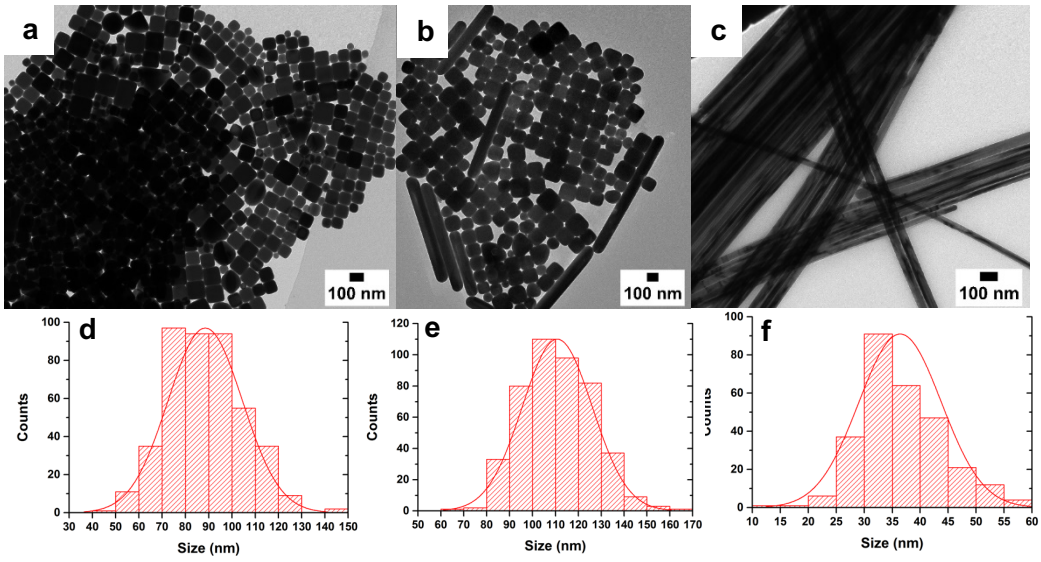

Figure II-27. *TEM images of Cu nanocubes synthetized by hot-injection of PPh_3 starting from copper precursor (a) CuCl (b) CuBr (c) CuBr with an increased reaction time to 2h (d, e, f) the corresponding size distribution histograms.*

XPS analysis

XPS was carried out on the nanoparticles obtained from CuCl in the presence of PPh_3. The survey spectrum shows peaks attributed to C_{1s}, $Cu_{2p,}$ O_{1s} and small signal corresponding to N_{1s} (see Table II-7 and Figure II-28). Furthermore the peaks at 932.24 and 952.08 eV correspond to $Cu_{2p1/2}$ and $Cu_{2p3/2}$ BE of Cu(0) and/or Cu(I), respectively. The presence of oleylamine was confirmed by the N_{1s} peak at 399.09 eV (At% = 0.89%). Although the phosphorus (P) is not observed in the high-resolution spectrum of P_{2p}, but, the high-resolution spectrum for C_{1s} shows a low component at 288.23 eV may corresponding to the C-P bond on the surface of NPs. However, the presence of Cl^- ions is also not detected by XPS analysis.

Table II-7. *XPS data analysis of Cu nanoparticles prepared from CuCl in the presence of* PPh_3.

Element	Peak BE	FWHM eV	Area (P) CPS.eV	Atomic %
C1s	284.48	1.18	96515.12	67.34
C1s A	285.90	1.53	6575.56	4.59
C1s B	288.23	1.54	2039.24	1.43
Cu LM2	569.49	3.34	111658.33	0.00
Cu2p	932.24	1.28	178332.00	8.34
N1s	399.07	2.09	1988.80	0.89
O1s	531.85	2.01	60316.26	17.41
Si2p	99.29	1.09	14265.11	0.00

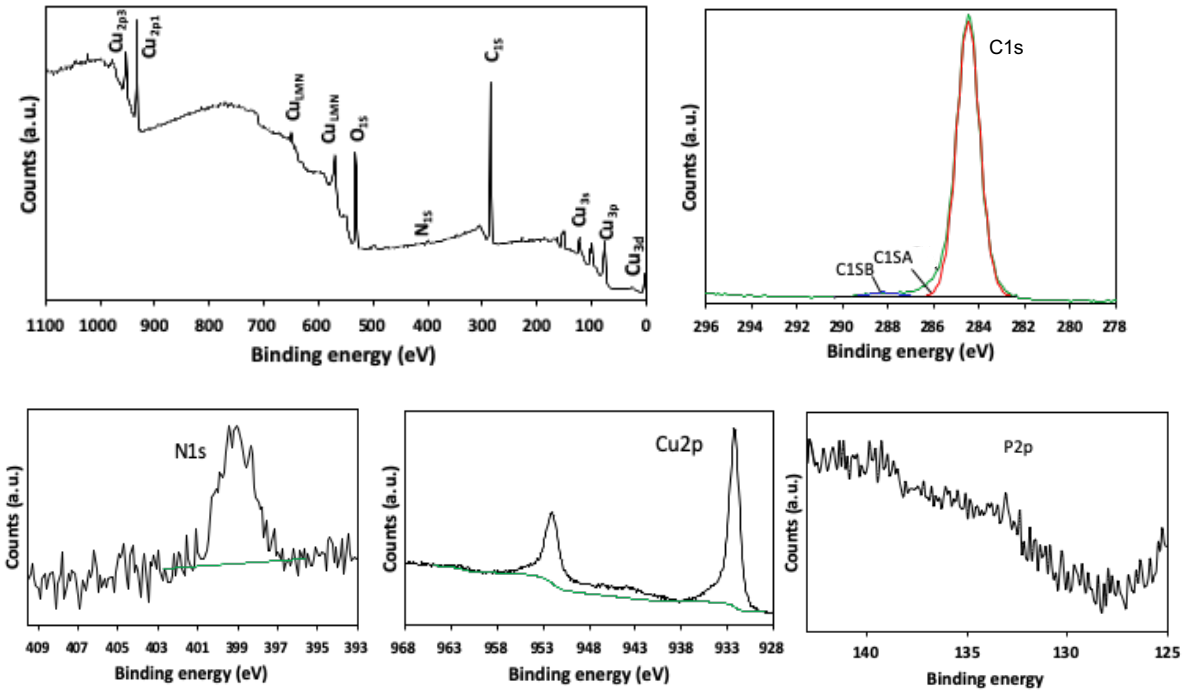

Figure II-28. *XPS survey spectra and high resolution XPS spectra of C_{1s}, N_{1s}, Cu_{2p}, P_{2p}, of Cu nanocubes obtained from CuCl in the presence of PPh_3.*

In order to study the steric effect of phosphorus ligands on the formation of nanoparticles, PPh_3 was replaced by the $P(PhMe_3)_3$ which has a similar pKa but a greater steric hindrance. Figure II-29 shows the typical TEM images of the copper nanoparticles synthesized from CuX (X = Cl, Br) in the presence of $P(PhMe_3)_3$ using the heating-up procedure described above (Figure II-26) (see in Chapter V experimental section 3.1.F). As seen in Figure II-29a, nanowires with an average size of 103.9 ± 24.6 nm (σ% = 24%) in diameter are obtained for the use of CuCl in the presence of 1.6 equiv. of $P(PhMe_3)_3$. As shown in Figure II-29b, replacing CuCl by CuBr in the same reaction conditions leads to the formation of nanoparticles of poorly defined shapes. In the case of $P(PhMe_3)_3$, we thus observed that the nature of the halide ions (Cl^- and Br^-) greatly affects the final size and shape of the resulting nanoparticles. By comparison with Cu nanocubes obtained from PPh_3 (Figure II-27a), these different NPs shapes show that the difference of the steric hindrance between PPh_3 and $P(PhMe_3)_3$ plays a remarkable role in the final shape of the synthetized CuNPs.

As previously, we have studied the effect of reaction time on the final shape of the nanoparticles. Hence, the reaction time was increased to 2 h in the presence of $P(PhMe_3)_3$ (1.6 equiv.) and CuBr as the precursor, which led to well-defined nanowires with an average diameter of 47.8 ± 11.8 nm (σ% = 25%) in diameter (Figure II-29c). A similar phenomenon was observed for the use of PPh_3 at 2 h (Figure II-27c).

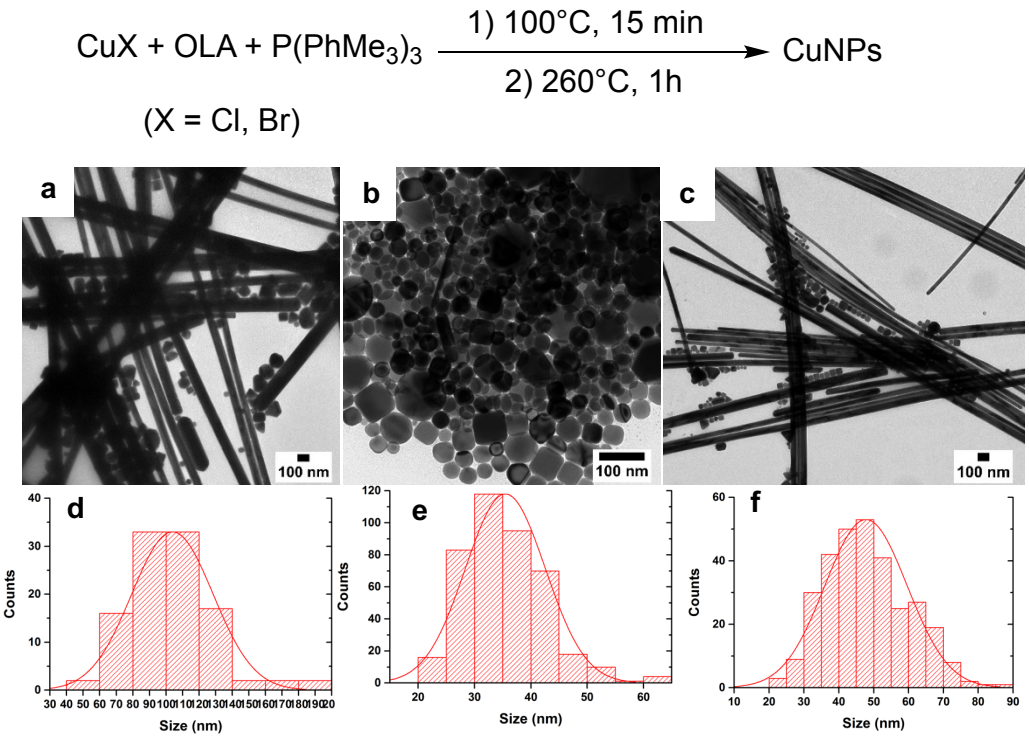

Figure II-29. *TEM images of CuNPs synthetized from (a) CuCl/1h (b) CuBr/1h (c) CuBr/2h and (d, e, f) the corresponding size distribution histograms.*

Table II-8. *Experimental conditions used for preparing CuNPs in presence of PPh_3 and $P(PhMe_3)_3$ with the corresponding size distributions.*

Precursor (1 mmol)	**Phosphorus ligands**		**Reaction time (h)**		**NPs Shape**	**NPs Size (nm)**	**σ* (%)**
	PPh_3	**$P(PhMe_3)_3$**	1	2			
CuCl	✓		✓		Cubes	88.5 ± 16.0	18%
		✓	✓		Wires	103.9 ± 24.6	24%
CuBr	✓		✓		Cubes (major), nanorods (minor)	Cubes: 110.8 ± 15.3 Rods: 96.8	Cubes: 14%
	✓			✓	Wires	36.4 ± 7.4	20%
		✓	✓		Mixed Shape	-	-
		✓		✓	Wires	47.8 ± 11.8	25%

**: Polydispersity*

These results show that the steric hindrance of phosphorus ligands has an important effect on the morphology of CuNPs. Indeed, Cu nanocubes could be produced by using the PPh_3 with both CuCl and CuBr at 1 h of stirring time. In the case of $P(PhMe_3)_3$, Cu nanowires were mainly observed instead of nanocubes. Noteworthy, the change of color indicating the nucleation process occurred at lower temperature (270 °C) for the use of PPh_3 and $P(PhMe_3)_3$ compared to TOP and TOPO (285 °C). This is contrast to the calculated disproportionation energies (see in Figure II-7) where $\Delta E_{dis}^{CuCl(OPMe3)}$ (= 63.0 kcal·mol^{-1}) < $\Delta E_{dis}^{CuCl(PMe3)}$ (= 67.4 kcal·mol^{-1}) < $\Delta E_{dis}^{CuCl(PPh3)}$ (= 68.5 kcal·mol^{-1}). These energies values were calculated starting from a simple CuCl-L (L = PR_3, amine) model. As shown by Strach's group,[11] the real copper complexes in solution include several equivalents of OLA and/or phosphine. This may have a great impact on these disproportionation energies, which could explain the differences between the experimental observations and the calculated disproportionation energies.

II. 4.3 CuNPs preparation using $P(O\text{-}C_8H_{17})_3$ and $P(OMe)_3$.

In order to get further insights on the effect of the nature of the phosphine ligand used on the shape and the size of the CuNPs, the next investigations focused on the use of phosphite ligands $P(OR)_3$ that had never been used so far. The trioctylphosphite ($P(O\text{-}C_8H_{17})_3$, TOPT) and the trimethylphosphite ($P(OMe)_3$) were chosen due to the similarity of their pKa with the tri-aryls phosphines (pKa $P(OMe)_3$: 2.6; pKa PPh_3: 2.76), but their lower steric hindrance (θ $P(OMe)_3$: 107°; θ PPh_3: 145°) (see Table II-1). Our standard hot injection protocol was used as depicted in Figure II-30:

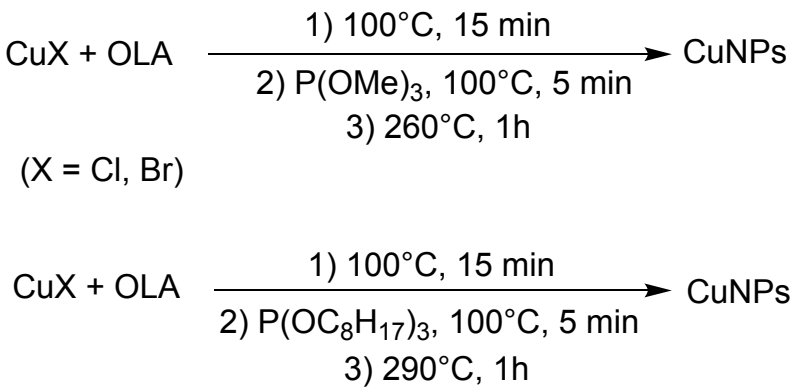

***Figure II-30**. Synthesis of CuNPs from CuX (X = Cl, Br) in the presence of $P(OMe)_3$ and $P(O\text{-}C_8H_{17})_3$ ligands.*

In this section, the CuNPs with triangle and cube-shaped were produced by using $P(OMe)_3$ and $P(O\text{-}C_8H_{17})_3$ as the phosphine source in the reaction (see in Chapter V experimental section 3.1.G-H). Figure II-31(a-c) sum up the representative TEM images of the CuNPs synthetized via the disproportionation of CuX (X = Cl, Br) in oleylamine with 1.6 or 3 equiv. of $P(OMe)_3$. Figure II-31a clearly shows monodispersed nanotriangles with an average size of 39.3 ± 3.0 nm in edge length (σ% = 7%) were obtained from 1.6 equiv. of $P(OMe)_3$ and CuBr as the precursor. These CuNPs were also characterized by UV-visible spectroscopy, a LSPR peak located at 606 nm may indicate their isotropic morphology[61] (Figure II-32a, bleu). When increasing the amount of $P(OMe)_3$ from 1.6 to 3 equiv., we obtained round nanotriangles with round edges and with a smaller mean size of 37.2 ± 5.6 nm but a higher polydispersity (σ% = 15%), as shown in Figure II-31b. The decrease of the NPS size with the amount of ligands has already been observed. The effect of the nature of the halide ions has also been studied. The use of CuCl instead of CuBr led to larger round nanotriangles with a mean size of 62.2 ± 7.8 nm in edge length (σ% = 12%) (Figure II-31c).

In order to get clear observation of the steric effect of phosphite ligand on the CuNPs synthesis, the $P(O\text{-}C_8H_{17})_3$ (TOPT) was next used as phosphine source due to its longer chain than $P(OMe)_3$. Interestingly, the TOPT gave cubic nanoparticles with an average size of 50.5 ± 6.3 nm (σ% = 12%) when the CuBr was used as precursor, as shown in Figure II-31g. Once the CuCl was used as the Cu(I) source in the synthesis, bigger nanocubes were yielded with a mean size of 62.1 ± 9.2 nm (σ% = 15%) (Figure II-31h). This phenomenon of size increasing by tuning the halide of copper salts has already been observed previously. The halide ions were demonstrated to may influence the final size of nanoparticles and the Cl^- ions often tend to favors the larger particle. Additionally, the formation of Cu nanocubes from TOPT was also characterized by UV-vis spectroscopy. A LSPR band is bleu shifted at 582 nm in comparison to the nanotriangles synthetized from $P(OMe)_3$, is observed in Figure II-32a (red). This result indicates that the differences in the LSPR band position can also be inferred the shape of nanoparticles.

In addition, the blue color of the supernatant was also observed after the washing procedure in all experiences with the use of $P(OMe)_3$ and $P(OC_8H_{17})_3$ as phosphine ligands. The presence of Cu(II) in the solution demonstrates the disproportionation reaction took place.

To confirm the crystalline structure of Cu nanotriangles, powder X-ray diffraction (XRD) was performed and the corresponding diffraction pattern (Figure II-32b) obtained from CuBr/1.6 equiv. of $P(OMe)_3$, is characteristic of face-centered cubic (*fcc*) crystalline structure. The diffraction peaks located at 43.32°, 50.45°, 74.09°, 89.89°, and 95.09° can be indexed to the (111), (200), (220), (311) and (222) planes of Cu respectively in good agreement with the conference JCPDS No. 03-1018 (Table II-9).

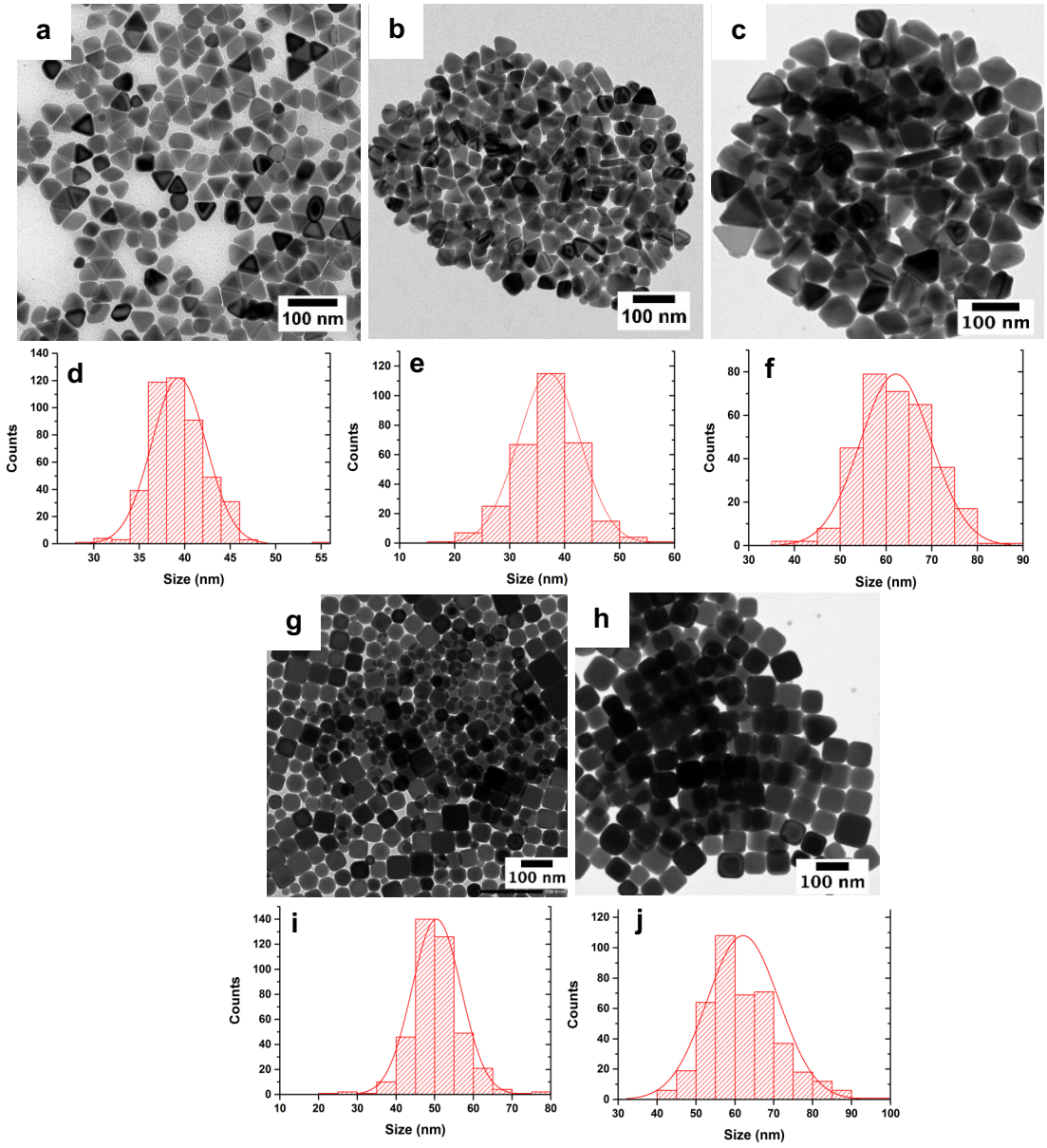

Figure II-31. *Typical TEM images of Cu nanoparticles obtained from (a) 1.6 equiv. $P(OMe)_3$/CuBr (b) 3 equiv. $P(OMe)_3$/CuBr and (c) 1.6 equiv. $P(OMe)_3$/CuCl (d, e, f) the corresponding size distribution histograms and TEM images of CuNPs were synthetized from 1.6 equiv. of TOPT with different copper precursor (g) CuBr (h) CuCl and (I, j) the corresponding size distribution histograms.*

Table II-9. *XRD data of Cu nanotriangles synthetized in the presence of $P(OMe)_3$.*

Diffraction peak	43.32°	50.45°	74.09°	89.89°	95.09°
Plane	(111)	(200)	(220)	(311)	(222)

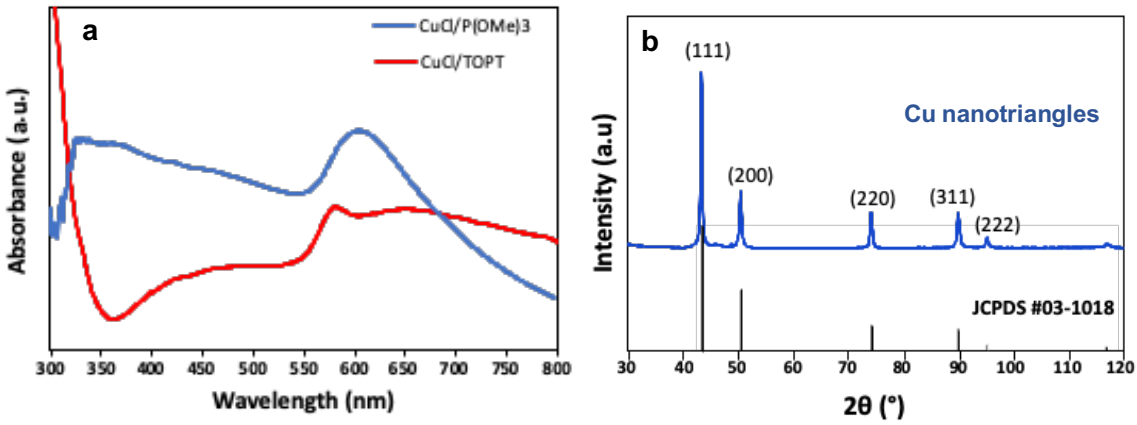

Figure II-32. *(a) UV-vis absorption spectra of CuNPs obtained from CuCl/TOPT (blue curve) and CuCl/P(OMe)$_3$ (red curve) (b) powder XRD pattern (up: experimental; down: theoretical) of CuNPs prepared from CuBr/1.6 equiv. P(OMe)$_3$.*

Table II-10*. Experimental conditions used for preparing CuNPs in presence of P(OMe)$_3$ and TOPT with the corresponding size distributions.*

Precursor 1 mmol	**Phosphorus ligands**			**NPs Shape**	**NPs Size (nm)**	**σ* (%)**
	P(OMe)$_3$ (equiv.)		**TOPT (equiv.)**			
	1.6	3	1.6			
CuBr	✓			Triangles	39.3 ± 3.0	8
		✓		Triangles	37.2 ± 5.6	15
			✓	Cubes	50.5 ± 6.3	12
CuCl	✓			Triangles	62.1± 7.7	12
			✓	Cubes	62.1 ± 9.2	15

** : Polydispersity*

The results summarized in the table II-10 demonstrated that the steric effect of phosphine ligands is extremely important to control the final shape of CuNPs. The higher steric hindrance resulted the cubic shape of CuNPs from TOPT (P(OC$_8$H$_{17}$)$_3$ and the shape of tetrahedra could be obtained in the presence of P(OMe)$_3$ with lower steric hindrance. As

mentioned before, the pKa of $P(OMe)_3$ and PPh_3 are similar (pKa: 2.73 vs 2.6) but their steric hindrances (θ angle $P(OMe)_3$: 107°; θ angle PPh_3: 145°) are very different. As a result, the use of $P(OMe)_3$ resulted the formation of nanotriangles, whereas the obtention of nanocubes was observed for the use of PPh_3. This result may indicate that the steric effect of phosphorus ligand plays an important role in the final shape of NPs.

XPS analysis

The XPS was used to detect the nature of ligands at the surface of nanoparticles prepared in the presence of $P(OMe)_3$ and $P(OC_8H_{17})_3$ ligands.

The results concerning the CuNPs synthetized from the reaction of $P(OMe)_3$ were collected in the Table II-11 and Figure II-33,34. Two peaks at 932 and 952 eV were observed which correspond to the $Cu_{2p1/2}$ and $Cu_{2p3/2}$ BE of Cu(0) and/or Cu(I), respectively. The XPS signals show the presence of amine from oleylamine with a N_{1s} at 399.61 eV (At% = 1.74%). The presence of P and Cl which come from the $P(OMe)_3$ ligand and initial copper precursor, have also been detected by the P_{2p} and Cl_{2p} peaks at 132.9 eV (At% = 0.61 %) and 198.71 eV (At% = 0.49%) respectively.

For the CuNPs obtained from $P(OC_8H_{17})_3$ ligands (Table II-11 and Figure II-34, 34), as was the case for NPs prepared from $P(OMe)_3$, the presence of C, Cl and P were detected. However, the observation of large satellite peaks of Cu_{2p} at range of 938-948 eV are the signature of Cu-O bond mostly due to the oxidation of sample, during the sample transportation. Also, the presence of P and Cl which come from the $P(OMe)_3$ ligand and CuCl, have also been detected by the P_{2p} and Cl_{2p} peaks at 132.83 eV (At% = 0.35 %) and 197.72 eV (At% = 0.64%), respectively.

After comparing the ratio of Chloride-to-Copper and Phosphine-to-Copper (deduced from the Cl_{2p}, P_{2p} and Cu_{2p} peaks) between these two types of CuNPs prepared from $P(OMe)_3$ and $P(OC_8H_{17})_3$, we found that the Cl-to-Cu ratio of Cu nanotrangles ($P(OMe)_3$) is lower (0.07) than that of Cu nanocubes ($P(OC_8H_{17})_3$) (0.2). Interestingly, the Phosphine-to-Copper ratios are equivalent (around 0.1) in both cases of Cu triangles and Cu cubes.

Table II-11. *XPS data analysis of CuNPs prepared from CuCl in the presence of $P(OMe)_3$ and $P(OC_8H_{17})_3$.*

Samlpe	Name	Peak BE	FWHM eV	Area (P) CPS.eV	Atomic %
Cu triangles ($P(OMe)_3$)	Cu2p	932.77	2.09	182421.38	6.75
	C1s	284.70	1.40	82840.28	45.75
	N1s	399.60	1.98	6193.92	2.20
	O1s	531.70	2.86	85072.05	19.43
	P2p	132.90	2.28	1639.58	0.61
	Cl2p	198.71	3.46	2545.83	0.49
	C1s A	286.07	1.73	30340.06	16.77
	C1s B	287.86	1.74	14441.68	7.99
Cu cubes ($P(OC_8H_{17})_3$)	C1s	284.53	1.08	185553.03	87.45
	Cl2p	197.72	1.15	3904.14	0.64
	Cu LM2	569.69	4.50	55610.61	0.00
	Cu2p	932.83	3.40	101942.38	3.22
	N1s	399.07	1.51	10794.89	3.28
	O1s	530.61	2.10	26023.16	5.07
	P2p	132.83	1.81	1089.84	0.35

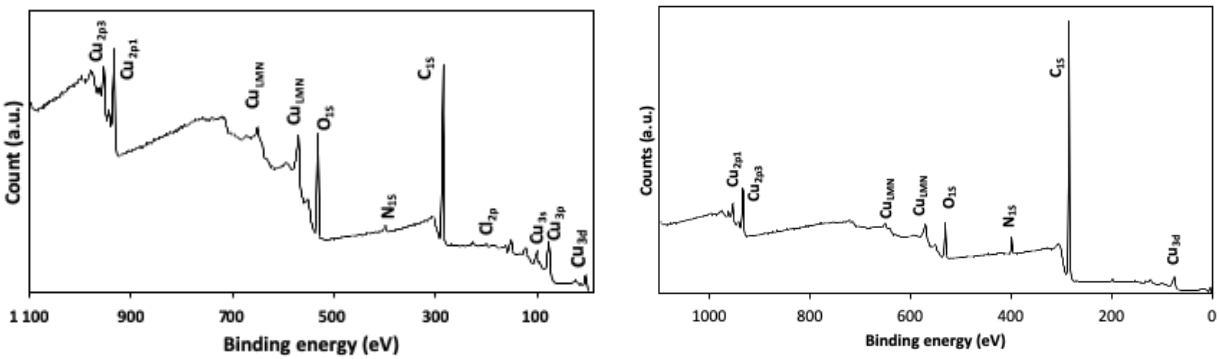

Figure II-33*. XPS survey spectra of (a) Cu nanotriangles and (b) Cu nanocubes.*

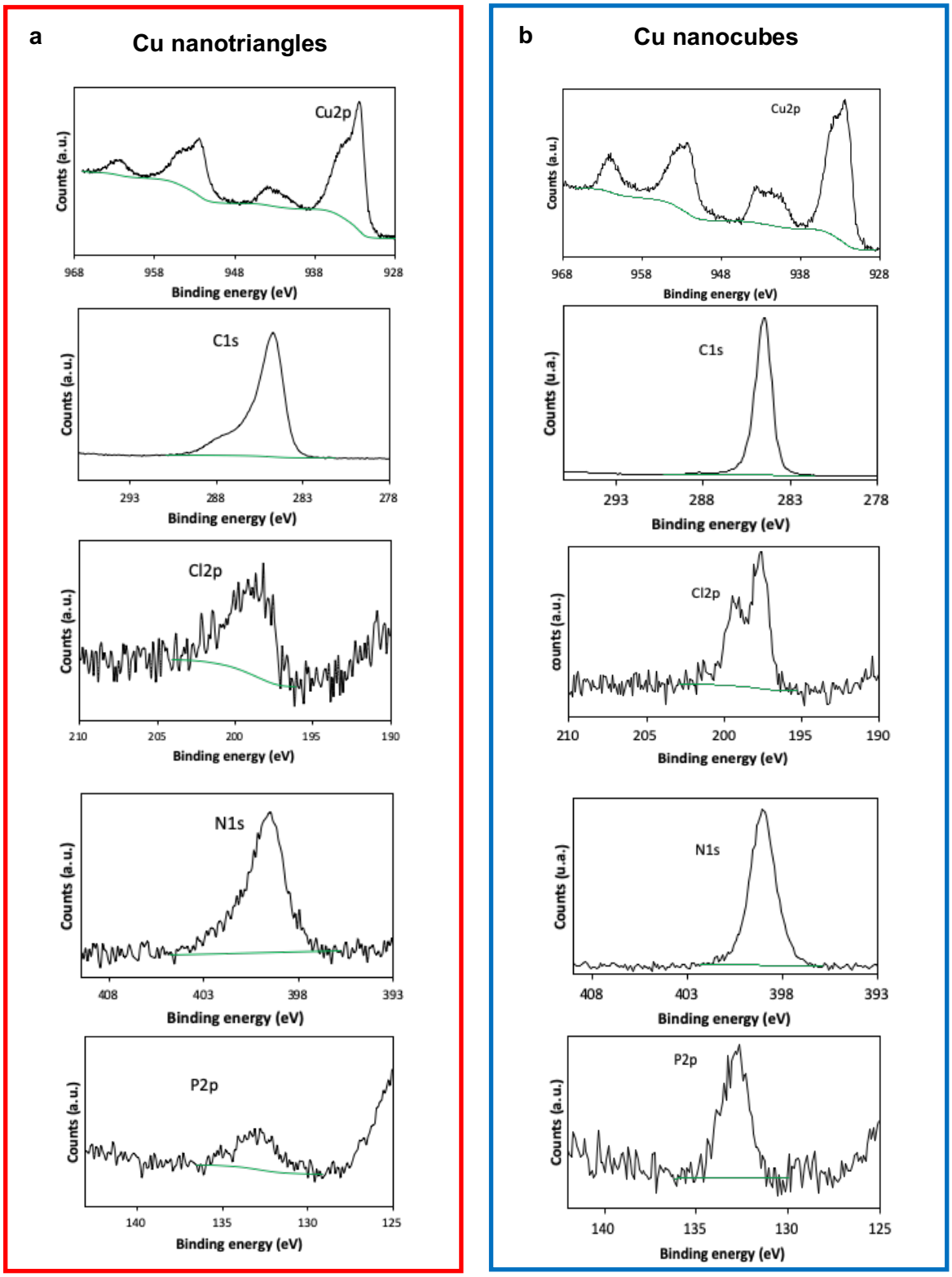

Figure II-34. *High resolution XPS spectra of C_{1s}, Cu_{2P}, $N_{1s,}$ Cu_{2p}, Cl_{2p} and $P_{2p,}$ of (a) Cu nanotriangles and (b) Cu nanocubes obtained from $P(OMe)_3$ and $P(OC_8H_{17})_3$ ligands.*

II. 4.4 CuNPs preparation using HMPT and HMPA.

To complete our study on the steric and electronic effects of phosphorus ligands on the size and shape of Cu nanoparticles, two other phosphorus ligands, the tris(dimethylamino)phosphine oxide (HMPA) and the tris(dimethylamino)phosphine (HMPT), were used for the following experiments. The HMPA was chosen to compare its effects with the TOPO, and the HMPT as an example of phosphine owning a pKa value close to a trialkyl phosphine (pKa HMPT: 8.03 vs pKa PMe_3: 8.65) and an θ angle close to a triaryl phosphine (θ angle HMPT: 152° vs θ angle PPh_3: 149°) (see in Table II-1).

II. 3.4.1 CuNPs synthetized in the presence of $P(O)(NMe_2)_3$ (HMPA).

The HMPA was first used as ligand in our typical hot-injection procedure as described above (see Figure II-35): 0.6 mmol of copper saults CuCl was weighted in an N_2-filled glovebox and transferred inside a Pyrex 25 mL glass vial along with 7 mL (35 equiv.) of OLA. The mixture was heated up to 100 °C under inert gas (N_2) by strong magnetic stirring to completely dissolve all solids which led to a greenish solution. After 15 min of stirring at this temperature, 1 mmol of $P(O)(NMe_2)_3$ was quickly added and the mixture solution turned instantly colorless. After additional 5 minutes of stirring the colorless mixture was heated up to 290 °C, and the reaction was held at this temperature for 1 hour. The formation of CuNPs was evidenced by a slow color change of the solution from colorless to brownish and finally to gray-purple. The CuNPs synthetized were purified by dispersing the reaction mixture in excess absolute ethanol and using centrifugation. We isolated triangle-shaped NPs with an average size of 119.7 ± 27.2 nm in perpendicular height and a few quasi-spheres (85 nm) as shown in Figure II-36a. In the previous work, the use of TOPO as the ligands promoted the mixed shapes of wire (35 nm in diameter) and a few quasi-spheres (68.6 nm) under the same reaction conditions (Figure II-22a).

In this reaction, the formation of Cu(0) NPs was evidenced by a change color of the reaction solution from brown to purple, and the LSPR absorption spectroscopy demonstrated the presence of Cu(0) NPs in the colloidal solution by the presence of a signal at around at 580 nm, as shown in Figure II-36c. The broad band observed at 580 nm is may be due to the mixed shape of synthetized NPs. Additionally, the blue color of the supernatant observed after the standard washing procedure suggesting the presence of Cu(II) in the solution, and thus suggested that a disproportionation reaction took place.

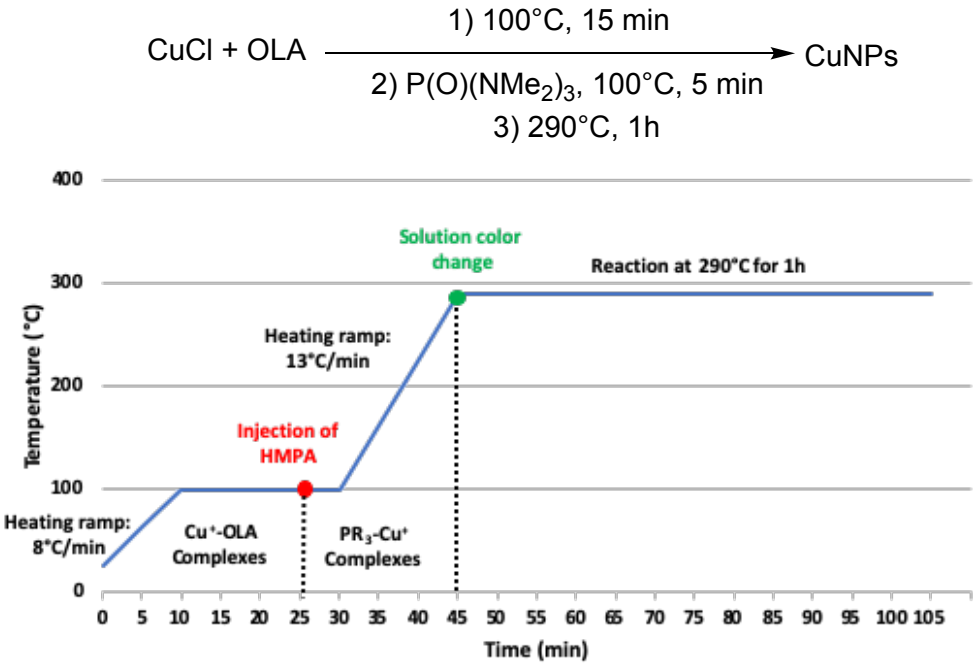

***Figure II-35**. Synthesis of CuNPs in the presence of HMPA.*

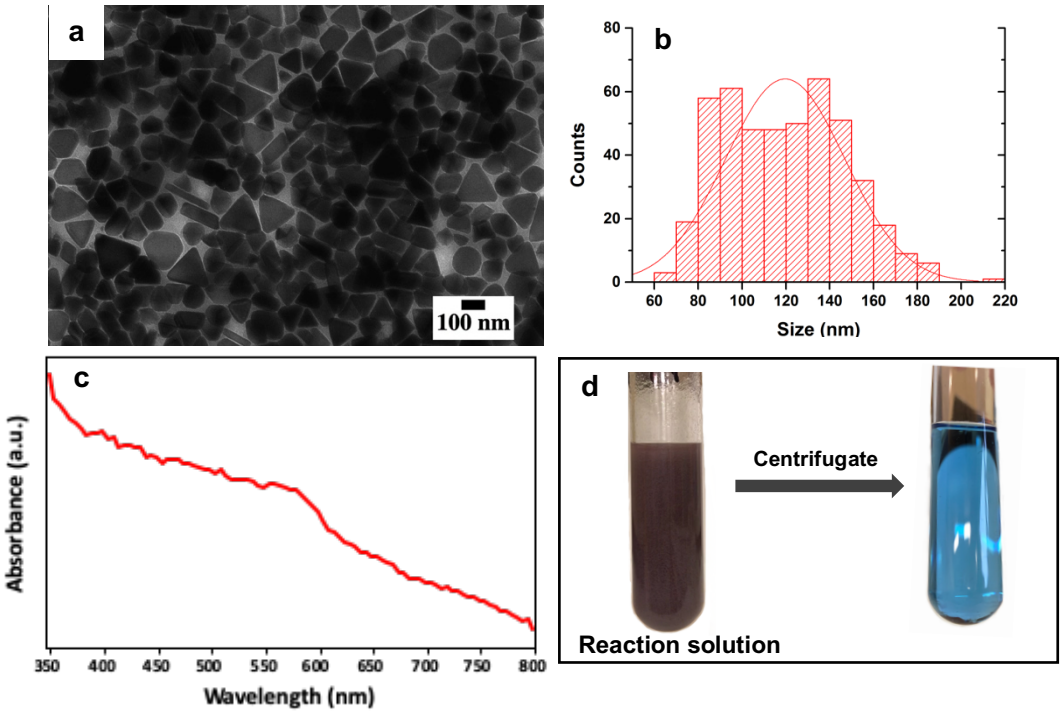

***Figure II-36**. (a) Typical TEM images of Cu nanoparticles obtained in presence of HMPA (b) the corresponding distribution histogram and (c) UV-vis absorbance spectra diapered in chloroform (d) picture of the copper nanoparticles reaction solution before and after centrifugation.*

II. 3.4.2 Copper phosphide synthetized in the presence of $P(NMe_2)_3$ (HMPT)

We next turned our attention to the use of HMPT in the same reaction conditions but at a lower reaction temperature (265 °C, 13 °C/min) (see in Chapter V experimental section 3.1.J). A slow color change of the solution from colorless to brown and finally black was observed when the reaction was maintained at 265 °C. After cooling, the nanoparticles were purified by dispersing the reaction mixture in excess absolute ethanol and using centrifugation. Unexpectedly, the resulting supernatant was yellower instead of blue, which suggested the absence of Cu(II) (Figure II-37).

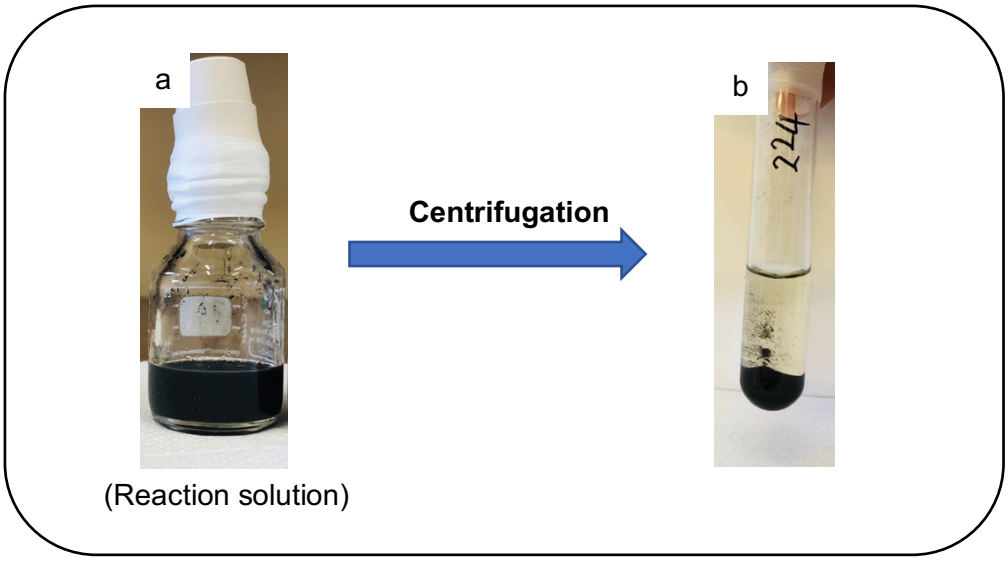

Figure II-37. *Pictures of dark reaction solution obtained from HMPT (a) before and (b) after precipitation with ethanol.*

In order to investigate this reaction in more details, a series of analyses (TEM, XRD, ICP-MS, HRTEM and XPS) were carried out on the precipitate and the obtained supernatant. The TEM images confirmed the formation of nanoparticles as shown Figure II-38a,b. They are monodispersed, hexagonal in shape with an average size of 22.5 ± 2.1 nm and a narrow size distribution of 9%. Figure II-38d shows the UV-vis spectra of these Cu nanohexagons dispersed in oleylamine showed a plasmon peak at 1626 nm, which may unexpectedly correspond to nanocrystal copper phosphide Cu_3P instead of Cu(0) NPs according to recent papers.[62,63] In a typical synthesis of Cu(0) NPs via disproportionation reaction of Cu(I) precursor, theoretically, the disproportionation of Cu(I) into Cu(0) and Cu(II) with stoichiometric ratio is 1:1. This is why the presence of Cu(II) can be usually detected in CuNPs solution (as shown in Figure II-36). To investigate the absence of copper, the ICP-MS analysis was used to study the separated supernatant and the dark precipitates. ICP-MS (inductively coupled

plasma-mass-spectrometry) is an analytic method that allows to determine low-concentrations (range: ppb = parts per billion = µg/L) of elements. Here, the ICP-MS analysis was used to determine the concentration of copper element in the supernatant. The same analyses were carried out in parallel on the supernatant of a previous disproportionation reaction using the TOP as ligand for comparison.

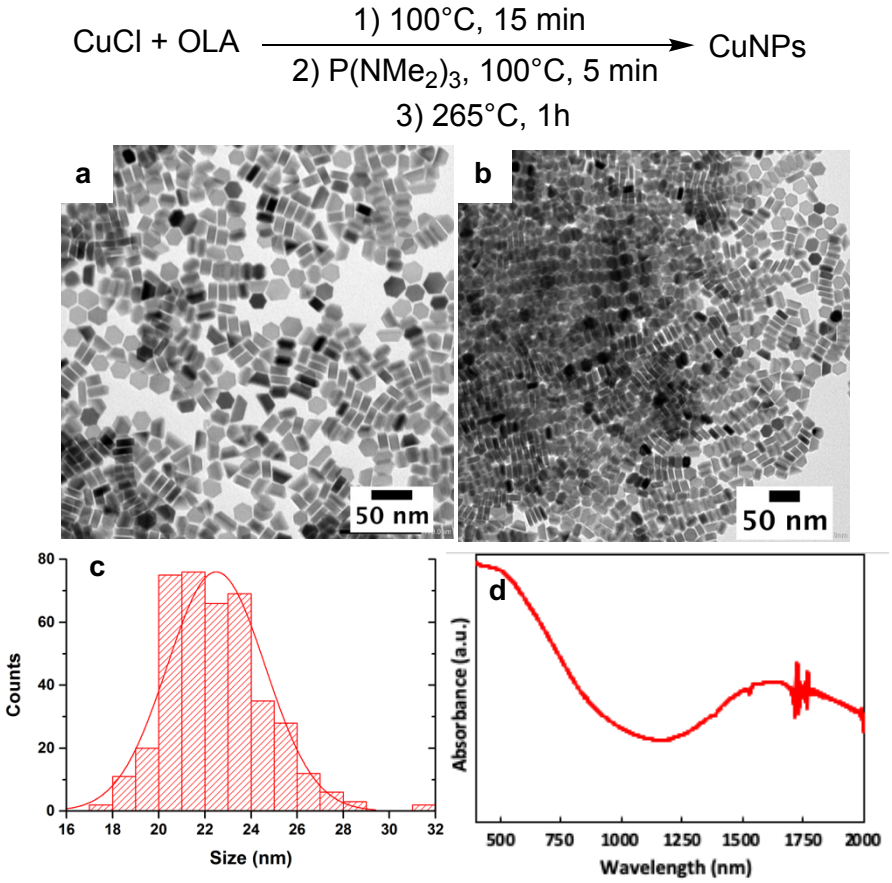

***Figure II-38**. (a, b) TEM images of Cu nanohexagons by hot-injection of $P(NMe_2)_3$ in the presence of CuCl and self-assembly and (c) the corresponding size distribution histograms (d) UV-Vis-NIR absorption spectra.*

As seen in Table II-12, in the case of the supernatant obtained from the reaction with TOP, the measured molar mass (n) of Cu is around 0.4 mmol (starting from 0.6 mmol of Cu(I) precursor). The experimental molar mass value is beyond the expected theoretical value of 0.3 mmol. This probably due to the presence of smaller NPs in the supernatant that didn't fully precipitate during the washing step. For the reaction performed in the presence of HMPT, the molar mass of copper element in the supernatant is around 0.01 mmol, which is far below the expected theoretical value. These first results indicated that the synthesis of CuNPs in the presence of HMPT is not a disproportionation reaction.

***Table II-12**. ICP-MS results obtained of supernatants from reaction TOP and HMPT.*
(All samples were diluted by a factor of 1000: 100 µL *of solution was diluted to 100 mL with* deionized water. *The concentration of added acids for all samples were 1% H_2SO_4, 1% H_2O_2, 2% HCl and 1% HNO_3.)*

Sample	**^{63}Cu[He]**			**n_{exp}** (mmol)
Name	**Conc. (ppb)**	**CPS**	**RSD**	
Supernatant (TOP)	**4 770**	79 822 646	5,6	**0.4**
Supernatant (HMPT)	**122**	2 045 555	2,6	**0.01**

High-resolution transmission electron (HRTEM) and X-ray diffraction analysis were next carried out to further analyze the nanohexagons obtained and to determine their crystalline structure. Figure II-39a, b show the HRTEM images of copper nanohexagons and a selected single platelet. The calculated d-spacing of 0.201 nm agrees well with the (300) lattice pacing of Cu_3P with hexagonal phase.[64,65] Figure II-39c shows the corresponding selected area electron diffraction (SAED) pattern which demonstrate the polycrystalline structure of Cu_3P.[49] The hexagons were further characterized using X-ray diffraction (XRD). Figure II-39d shows that all diffractions peaks well agree with the polycrystalline structure of Cu_3P (PDF # 01-071-2261) (Table II-13). The diffraction peaks located at 28.5°, 36.1°, 39.1°, 41.7°, 45.2°, 46.3°, 47.4°, 53.6°, 56.6°, 59.2°, 66.7°, 73.5° and 78.3° can be assigned to the (111), (112), (202), (211), (300), (113), (212), (104), (311), (222), (223), (322) and (314) planes of space group $P6_3cm$, respectively.[66]

***Table II-13**. XRD data of hexagonal Cu_3P synthetized from CuCl in the presence of $P(NMe_2)_3$.*

Diffraction peak	28.5°	36.1°	39.1°	41.7°	45.2°	46.3°	47.4°
Plane	(111)	(112)	(202)	(211)	(300)	(113)	(212)
Diffraction peak	53.6°	56.6°	59.2°	66.7°	73.5°	78.3°	
Plane	(104)	(311)	(222)	(223)	(322)	(314)	

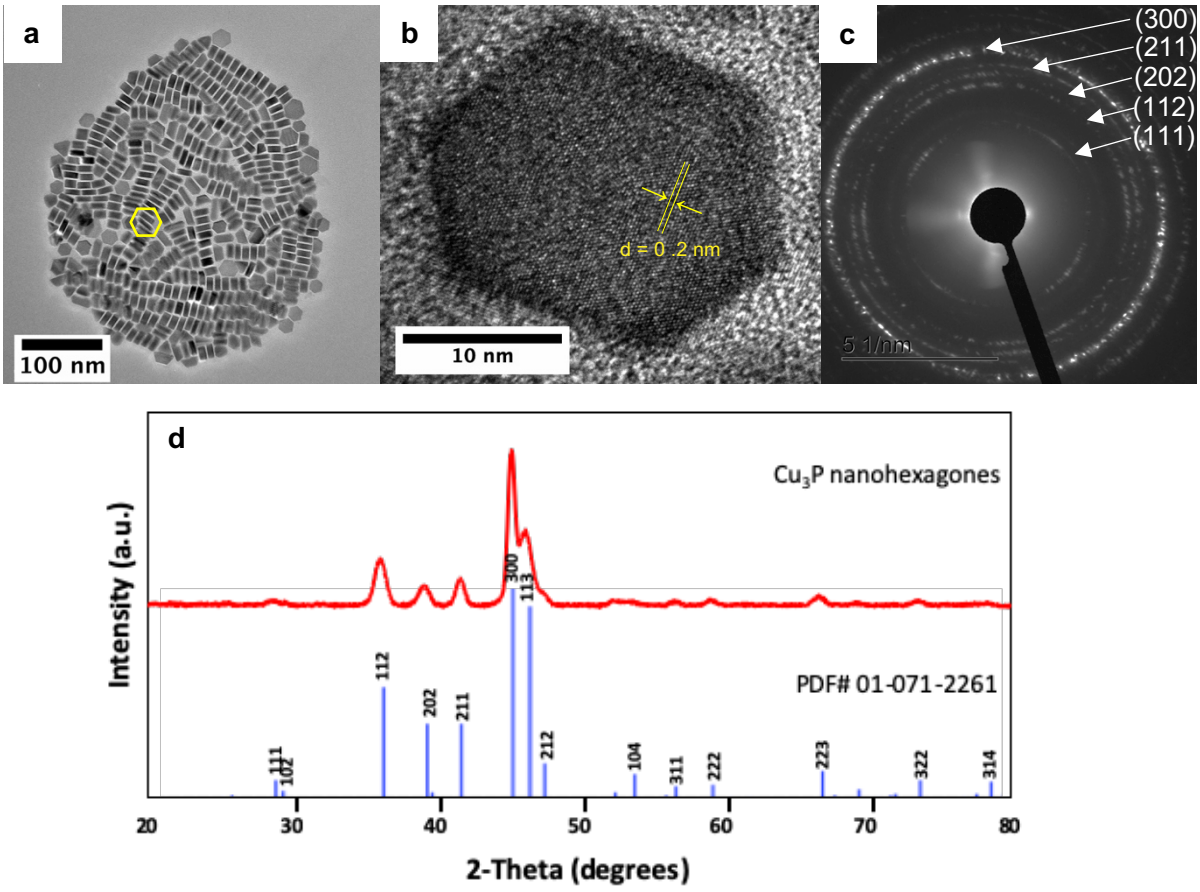

***Figure II-39**. (a-c) Typical HRTEM image, a selected platelet and SAED pattern of Cu_3P synthetized from CuCl/1.6 equiv. $P(NMe_2)_3$ (d) powder XRD patterns (the reference* PDF# 01-071-2261*) of Cu_3P platelets.*

The energy-dispersive X-ray spectroscopy (EDX) was carried out to investigate the nature of ligands on the Cu_3P surface and the corresponding element mapping is given in Figure II-40b. It shows that the nanocrystals contain 4 elements (Cu, P, Cl, N) that are evenly distributed across the surface of the particles. A uniform distribution of copper atoms and phosphorus was observed in each of nanoparticles, which indicates that the composition of the particles matches to that of Cu_3P. A large amount of phosphor (P) has been detected across the NPs surface that is in good accordance with Cu_3P structure. The presence of Cl and N atoms on nanoparticle surface may stem from the copper precursor, the HMPT and the oleylamine (NH_2R) solvent. The nanoscopic hexagonal morphology 3D of Cu_3P and their self-assembly were characterized by Scanning Electron Microscope (SEM) analysis as shown in figure II-40c.

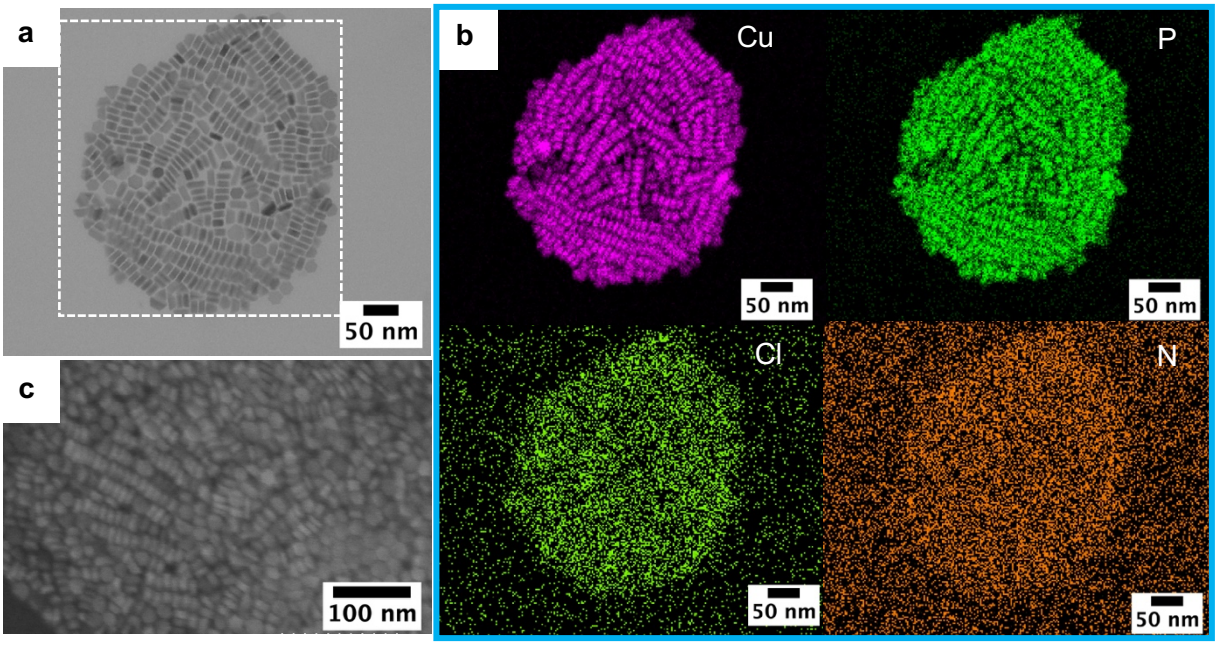

Figure II-40. *(a) Representative STEM image and (b) corresponding element mapping of Cu, P, Cl, N and (c) typical SEM images of Cu_3P nanohexagons.*

XPS analysis

XPS analysis was carried out to further investigate the chemical composition at the surface of Cu_3P NCs. All the results were collected in Table II-14 and Figure II-41. As shown in Figure II-41, the XPS survey spectra shows peaks attributed to C_{1s}, Cu_{2p} O_{1s} N_{1s} and P_{2p}. Figure II-41 shows a P_{2p} peak at 129.7 eV (At% = 3.01%) corresponding to the binding energy (BE) of $P_{2P3/2}$ coming from P-Cu bond.[67] However, the peak at 134.09 eV can be attributed to the P-O bond as a result of oxidation of P from air contact. The XPS signal of Cu is showed in Figure II-41, the Cu_{2p} peak at 933.7 eV (At% = 1.66%) was detected which corresponding the $Cu_{2P3/2}$. In the literature, the BE of Cu and P are reported at 932.26 eV and 130.2 eV, respectively[68,69] In our work, the detected BE of P_{2P} (129.7 eV) is lower than the one of phosphorus reported in the literature (130.2 eV). These results reveal the charge transfer between the P and Cu which demonstrate the BE of $P_{2P3/2}$ shifts to low energy (from 130.2 to 129.7 eV) and that of $Cu_{2P3/2}$ shifts to higher energy (from 932.6 to 933.7 eV), therefore, the negative charge of P and positive charge of Cu are indicated. The signal of O could be originated from the absorbed oxygen or surface oxidation of the nanocrystal in air. The N_{1s} spectrum presents one peak with two components at 402.11 eV and 400.29 eV accounting for N-P from $P(NMe_2)_3$ and amine from oleylamine. Additionally, the strong peak of C also confirms the presence of long chain alkyl group from oleylamine.

Table II-14. *XPS data analysis of Cu_3P prepared from CuCl as copper precursor in the presence of HMPT ($P(NMe_2)_3$).*

Name	Peak BE	Height CPS	FWHM eV	Area (P) CPS.eV	Area (N) KE^0.6	Atomic %
Cu2p	933.70	11669.43	3.17	134936.21	0.06	1.66
P2p	134.09	5916.87	2.14	14873.67	0.10	3.01
C1s	284.93	150185.56	1.84	329147.11	2.82	81.45
N1s	401.68	2325.26	3.29	8765.98	0.04	1.24
N1s A	402.11	2238.02	1.59	4218.67	0.02	0.59
N1s B	400.29	1943.73	1.92	4401.70	0.02	0.62
O1s	532.35	48648.45	2.77	141186.32	0.44	12.65

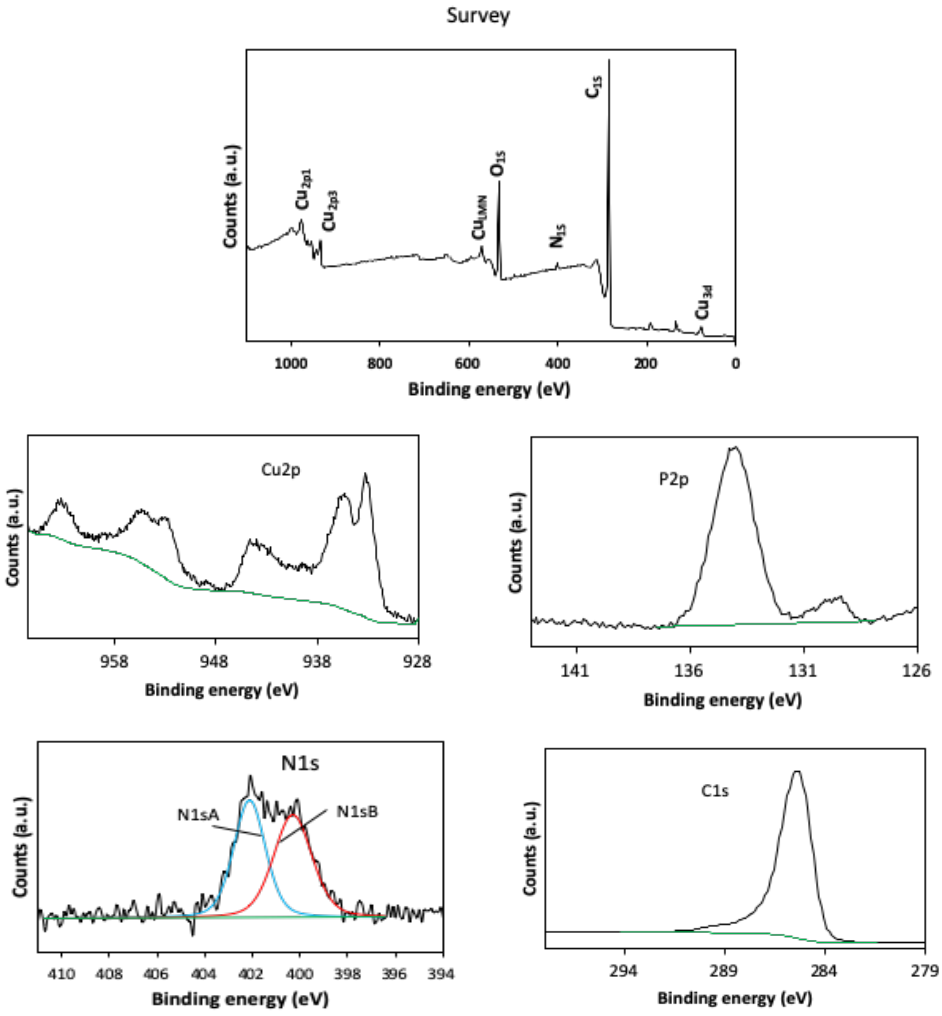

Figure II-41. *XPS survey spectrum and high resolution XPS spectra of Cu_{2p}, P_{2p}, N_{1s} and C_{1s} of Cu nanohexagons obtained in the presence of $P(NMe_2)_3$ ligand.*

As a conclusion, all these analyses show that the use of HMPT as additive under our standard disproportionation reaction conditions do not lead to the expected Cu(0) nanoparticles but instead to nanocrystals of copper phosphide Cu_3P.

In recent years, metal phosphides have attracted attention as a promising class of nanomaterials due to their magnetic, catalytic and electronic properties.[70-72] Specifically, copper phosphide (Cu_3P) has become a relevant important nanomaterial for colloidal semiconductor,[73] and has been demonstrated as an alternative anode material for lithium ion batteries.[74-76]

Two possible approaches:

Few methods have been reported for the synthesis of Cu_3P, as for example solvothermal reaction,[77,78] solid-vapor transport[79] and solution-based methods.[73,80,81] However, few of these methods allow a good control of size and polydispersity. Regarding solution-based methods, the synthesis of copper phosphide has often been performed by using TOP and/or TOPO as phosphine source. For example, N. Pradhan *et al*. (2013)[64] reported the synthesis of Cu_3P with a large tunable size (10-1000 nm in width) by using CuCl as the precursor in a mixture of alkylamine and TOPO as solvent, and using TOP as nucleation controlling agent (see in Figure II-42). In this work, an increase of the particle size was observed when the amount of TOP increased. They have demonstrated the plasmonic nature of these hexagonal Cu_3P by studying near-infrared (NIR) analysis (as shown in Figure II-42h).

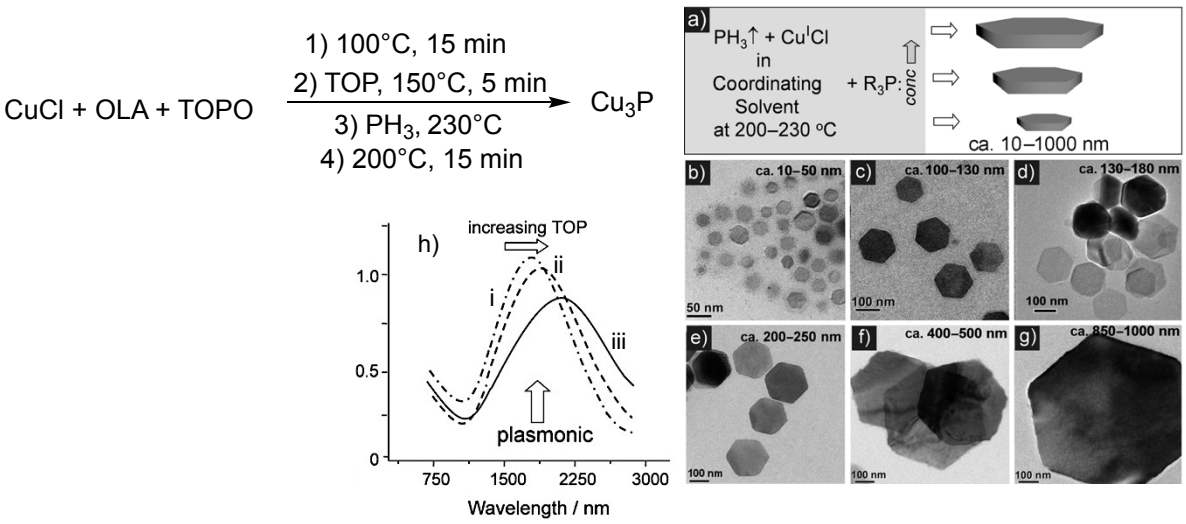

***Figure II-42**. a) Reaction Scheme and the TOP (trioctylphosphine) concentration dependent tunability of the Cu_3P nanoplatelets width and b-g) TEM images of different Cu_3P platelet sizes obtained from different reaction conditions h) the plasmonic absorption for platelets of (i) 10-50 nm, (ii) 200-250 nm and (iii) 400-500 nm. (Copyright from Ref.[64])*

Later on, L. Manna *et al*.[66] also reported a synthesis approaches that produced poly-dispersed Cu_3P nanocrystal (NCs) with a diameter ranging from 10 nm to 50 nm (Figure II-43a), by using TOP and TOPO as the phosphine source and CuCl in OLA and ODA (octyldodecylamine) at high temperature (350 °C). A plasmonic absorption located around 1500 nm was also observed which corresponds to the hexagonal $Cu_{3-x}P$ NCs, as shown in Figure II-43b.

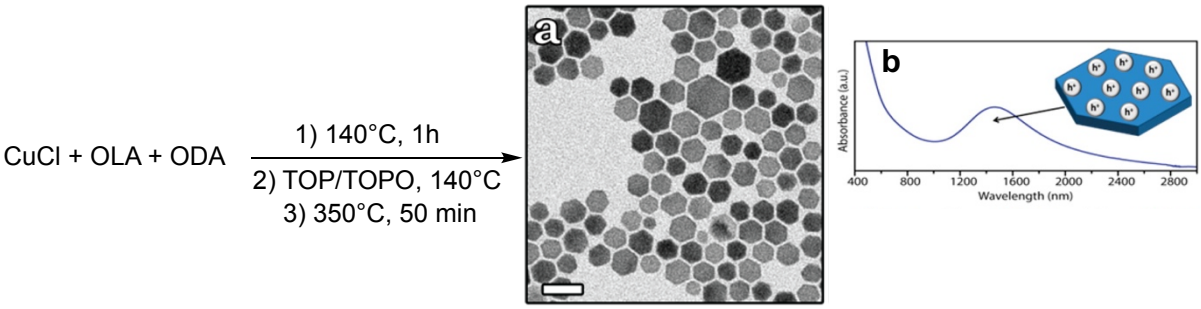

Figure II-43. *Synthesis of Cu_3P by using a mixture of TOP/TOPO as phosphine sources (a) typical TEM image of Cu_3P synthetized and (b)the corresponding plasmonic absorption. (Copyright from Ref.[66])*

After comparison with methods reported in the literature, our synthetic method (CuCl/OLA/HMPT/265 °C) has the advantage of being a one-pot procedure using $P(NMe_2)_3$ as the only phosphine source, occurring under mild reaction conditions and giving a well-defined hexagonal and high monodisperse Cu_3P NPs (22.5 ± 2.1 nm, σ% = 9%) in good yield. We were thus keen to further explore the potential of this new Cu_3P NCs synthesis reaction.

II. 4.4.2.1 Control of Cu_3P size and shape

In order to study the influence of reaction parameters on the formation of Cu_3P, several reaction conditions such as the reaction temperature, the reaction time, the amount of phosphorus ligands and the nature of the solvent were next investigated.

II. 4.4.2.1.1 Influence of reaction temperature

We first turned our attention to the influence of the reaction temperature. We thus performed a set of experiments in our standard reaction conditions but with a range of reaction temperatures from 245 °C to 290 °C (see in Chapter V experimental section 3.1.K). The TEM

analysis of the resulting Cu_3P is showed in Figure II-44(a-c). As shown by these TEM images, an increase of the reaction temperature induced the formation of larger Cu nanohexagons. Indeed, the average size of the hexagonal Cu_3P increases from 17.7 ± 1.2 nm for a reaction temperature of 245 °C, to 22.5 ± 2.1 nm at 265 °C and to 29.9 ± 2.5 nm at 290 °C, with in all cases a low polydispersity (< 10%).

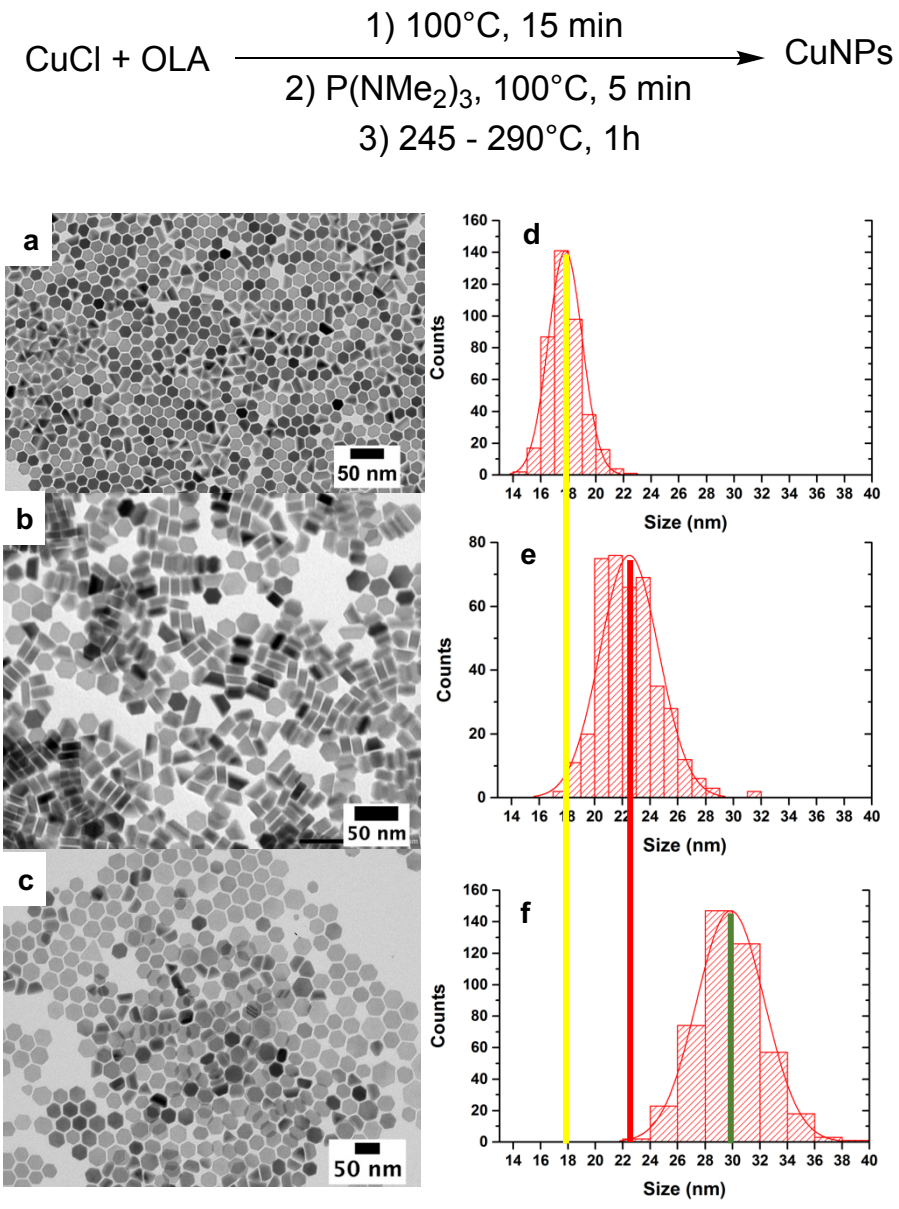

Figure II-44. *Representative TEM images of Cu_3P nanohexagons prepared from different reaction temperatures: (a) 245 °C (b) 265 °C (c) 290 °C and (d, e, f) the corresponding size histograms.*

II.4.4.2.1.2 Influence of the different P/Cu ratios

The effect of the P/Cu ratios on the particle size of Cu_3P nanohexagons was also studied (see in Chapter V experimental section 3.1.L). Figure II-45 shows the typical TEM images of nanocrystals synthetized at 265 °C with a range of P/Cu ratios from 1 to 5, which leads to particles size from 17 nm to 29 nm. For a low P/Cu ratio of 1 (1:1), small and uniform Cu_3P nanohexagons with an average size of 17.4 ± 1.2 nm and a low polydispersity of 7% were obtained, as shown in Figure II-45a. Increasing the P/Cu ratio to 3 (3:1) resulted in an increase of the Cu nanohexagons size to 27.6 ± 1.9 nm with a low polydispersity (σ% = 9%) (Figure II-45c). Similarly, hexagonal Cu_3P with a larger size of 28.6 ± 2.8 nm (σ% = 10%) were produced from the P/Cu ratio = 5, as shown in Figure II-45d. Accordingly, as the increase of nanohexagons size, UV-vis absorption spectrum shows a red shift of the peaks from 1516 nm to 1617 nm, as depicted in Figure II-46. It is in good accordance with the study of UV-vis absorption of Cu_3P reported by N. Pradhan and co-workers,[64] as shown in Figure II-24h. We have shown that increasing the $P(NMe_2)_3$/Cu ratio induce the formation of bigger copper phosphide nanocrystals. This is in contrast to the results obtained for the synthesis of copper nanocubes in presence of TOP realized in the same reaction conditions for which the opposite trend was observed, as seen above. This difference in behavior will be discussed in the subsequent sections.

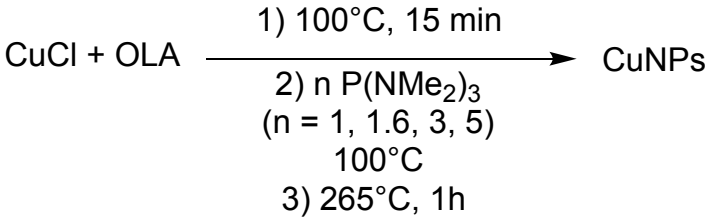

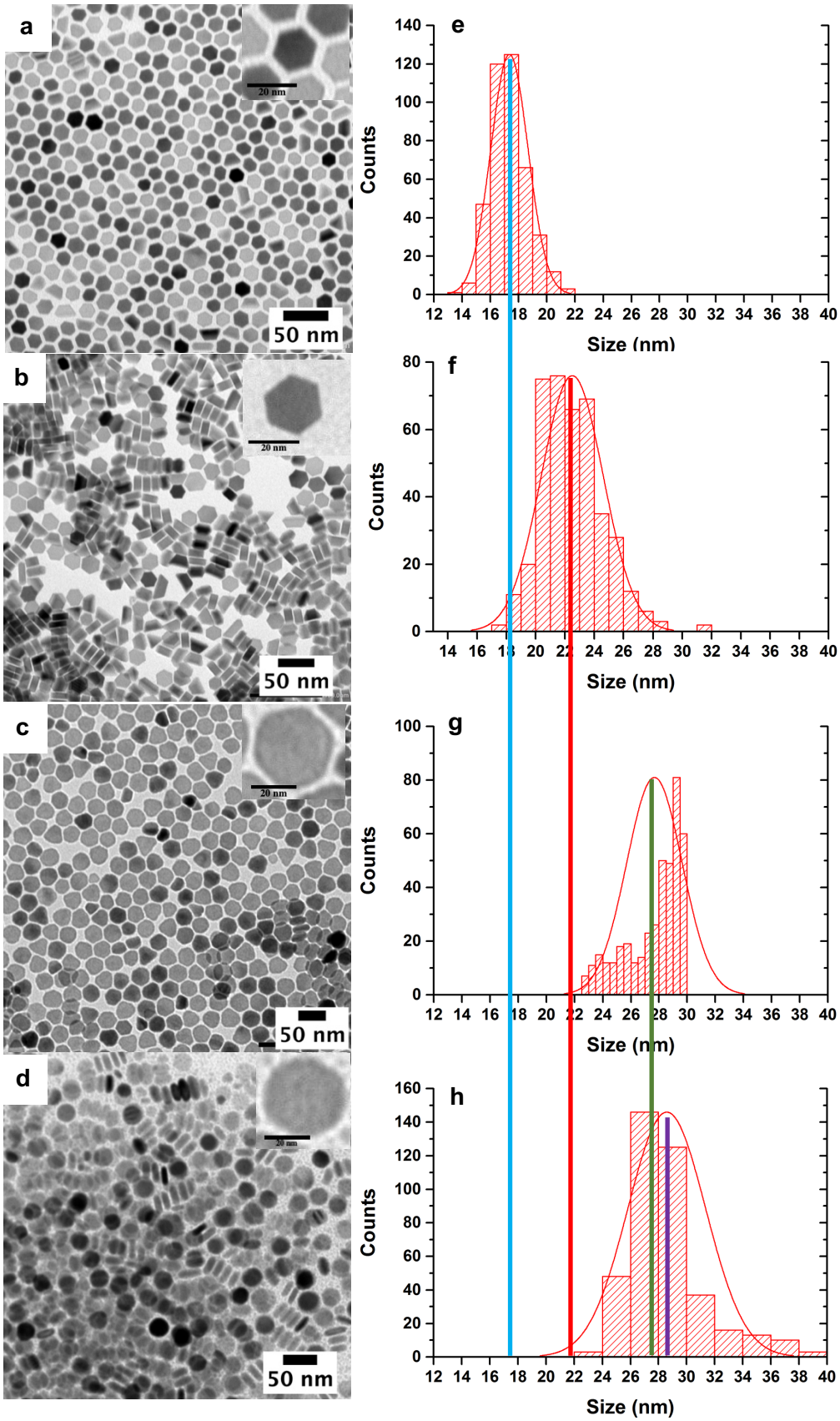

Figure II-45. *Representative TEM images of nanohexagonal Cu_3P prepared with varying $P(NMe_2)_3$/Cu rations (a) P/Cu =1 (b) P/Cu = 1.6 (c) P/Cu = 3 (d) P/Cu = 5 and (e, f, g, h) the corresponding size histograms.*

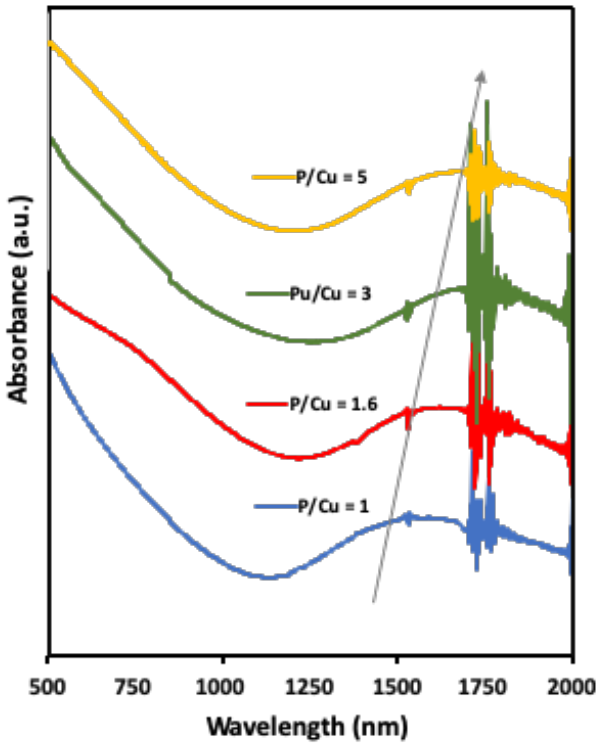

Figure II-46. *Absorbance spectra of copper nanohexagons synthetized from different $P(NMe_2)_3$/Cu ratios (P/Cu = 5, 3, 1.6, 1).*

II.4.4.2.1.3 Effect of the nature of copper salts

The effect of the nature of the precursor salt on the formation of Cu_3P nanocrystals was next studied. The following reactions were performed with a series of copper salts including Cu(I)X (X = Cl, Br, I, CN) and Cu(II)X (X=Cl, Br) (see in Chapter V experimental section 3.1.J).

Figure II-47 shows the typical TEM images of Cu_3P nanohexagones of various sizes that were obtained from different Cu(I) precursor salts: CuBr, CuI and CuCN. As seen above for the disproportionation reaction, the halide ions are one of the factors that influence the size of the CuNPs. We were keen to check their effects on the Cu_3P synthesis. The use of CuBr and CuI allows the formation of Cu_3P nanohexagons, and their size increased from 22.5 ± 2.1 nm for the use of CuCl to 24.4 ± 2.6 nm for the use of CuBr (Figure II-45a) and 47.7 ± 4.9 nm (Figure II-45b) for the use of CuI, with in all cases a low size polydispersity (< 10%). These results are in contrast with those reported by Hens and co-workers[82] for the preparation of InP crystals where the opposite trend was observed. In their work, the final size of InP crystals tend to decrease by following the order $Cl^- > Br^- > I^-$. The authors explained these results by a better absorption of Br^- and I^- ions on the surface of the particles compare to Cl^-, which hinders

their growth. In our study, the final size of Cu_3P synthetized tends to increase on the opposite order ($Cl^- < Br^- < I^-$).

A possible explanation of our results could be that the higher stability of the Cu-I bond compared to Cu-Cl decreases the reduction rate and modifies the nucleation kinetic, thus leading to a low nuclei concentration. According to LaMer theory,[45] a low concentration of metal nuclei induces the formation of larger nanoparticles (see Chapter I section I.2.1). This phenomenon was experimentally observed by a slower color change of the solution from yellow to brown in comparison with CuCl and CuBr. This Cu_3P reaction synthesis would thus follows the LaMer model.

In addition to copper halide, CuCN was also tested as the copper (I) source to produce Cu_3P, and monodisperse copper nanohexagones with an average size of 27.4 ± 2.7 nm (σ% = 10%) were obtained (Figure II-47c). It seems that the CN^- ions from copper precursor is able to affect the size of nanocrystal but not their shape.

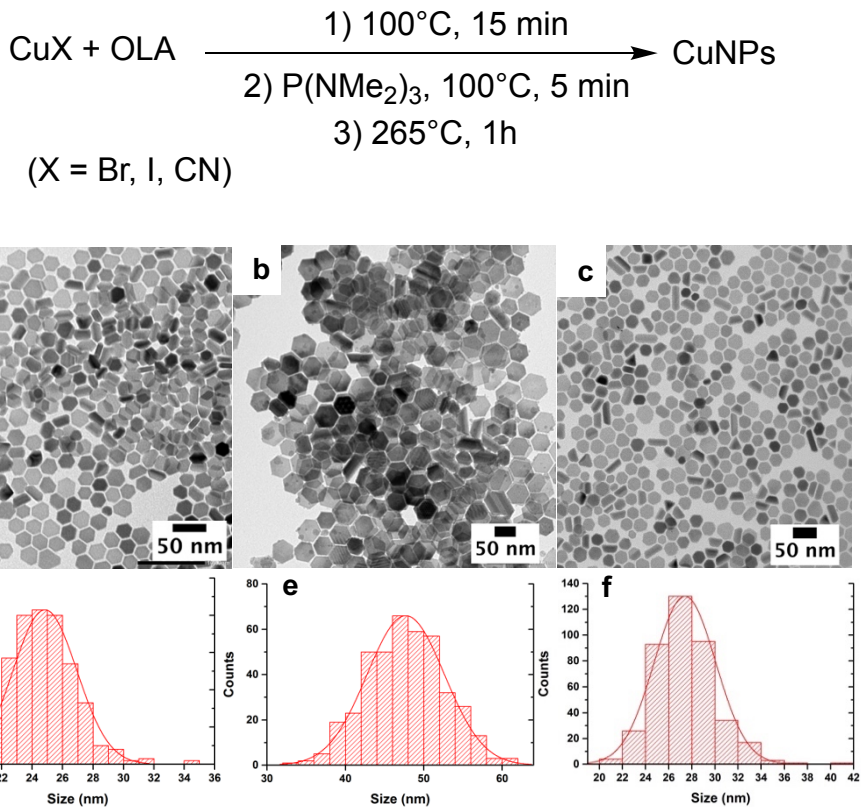

***Figure II-47**. TEM images of Cu_3P obtained from different precursors (a) CuBr (b) CuI (c) CuCN and (d, e, f) the corresponding size histograms.*

Besides Cu(I) salts, we also used Cu(II) salts to synthetize copper phosphide nanocrystals. Once again Cu_3P with hexagonal nanoplatelet shape were produced when $CuCl_2$ and $CuBr_2$ were used as copper precursors, with an average size of 51.5 ± 6.4 nm (σ% = 12%) and 50.6 ± 6.4 nm (σ% = 13%) respectively, as shown in Figure II-48a, b. In order to investigate the crystallographic nanostructure of these Cu nanocrystals, the powder XRD patterns was carried out on the Cu nanohexagons prepared from $CuCl_2$. Figure II-49 shows that all diffraction peaks are in accordance with hexagonal structure of Cu_3P, which is the same as the result obtained using Cu(I) salts as precursor, with reference to PDF# 01-071-2261, respectively. Indeed, the diffraction peaks located at 28.6°, 36.1°, 39.1°, 41.6°, 45.1°, 46.1°, 47.3°, 53.5°, 56.5°, 59.0°, 66.6°, 73.3° and 78.3° can be assigned to the (111), (112), (202), (211), (300), (113), (212), (104), (311), (222), (223), (322) and (314) planes of space group $P6_3cm$ (Table II-15).[64,66]

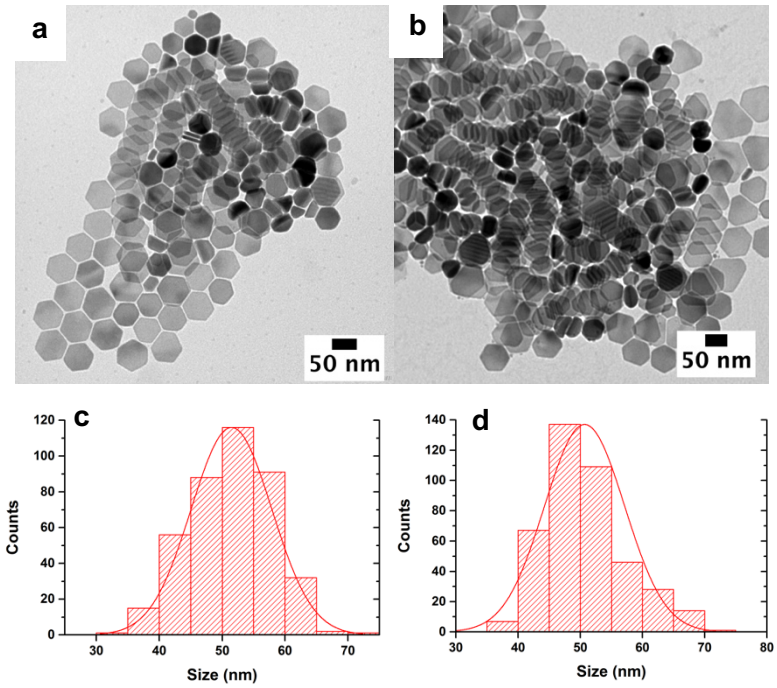

***Figure II-48**. Typical TEM images of Cu_3P nanohexagons obtained from different copper precursors (a) $CuCl_2$ (b) $CuBr_2$ and (c, d) the corresponding size histograms.*

***Table II-15**. XRD data of hexagonal Cu_3P synthetized from $CuCl_2$ in the presence of $P(NMe_2)_3$.*

Diffraction peak	28.6°	36.1°	39.1°	41.6°	45.1°	46.1°	47.3°
Plane	(111)	(112)	(202)	(211)	(300)	(113)	(212)
Diffraction peak	53.5°	56.5°	59.0°	66.6°	73.3°	78.3°	
Plane	(104)	(311)	(222)	(223)	(322)	(314)	

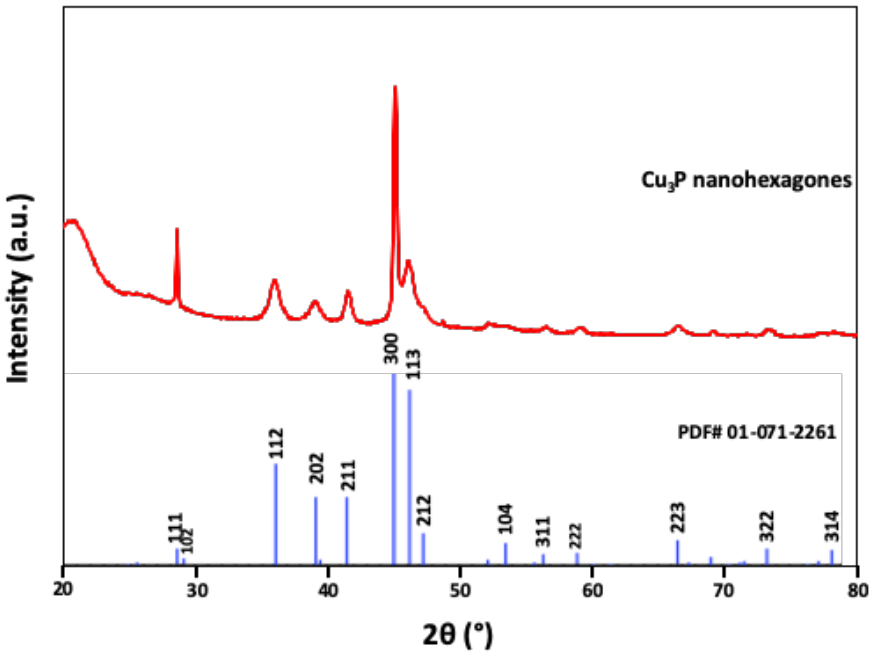

Figure II-49. *Representative powder XRD pattern of hexagonal Cu_3P synthetized using $CuCl_2$ as the copper precursor (with the reference PDF# 01-071-2261).*

As discussed above, the precursors and ligands are expected to affect the size and the morphology of the nanoparticle during the nucleation and growth steps. The energy barrier of decomposition of the salt-ligands complex depends on the interaction between copper atom and its ligands, which may influence the nucleation (K_N) step. Relying on the La Mer theory,[45] a fast nucleation allows to produce a high concentration of monomer which leads to the formation of numerous nuclei. Consequently, smaller nanoparticles could be formed with a fast growth process. Compare to $CuCl_2$ precursor, CuCl decomposes easily due to the lower bonding energy between Cu(I) and Cl^-. On the other hand, the reactivity of CuCl is higher than $CuCl_2$, which can be corroborated by the enthalpy of formation ($\Delta_f H°$) reported for the copper salts ($\Delta_f H°_{298k}$ for CuCl = 1.42 eV, for $CuCl_2$ = 2.28 eV).[83] Due to the additional reduction step of Cu(II) to Cu(I), the monomer release may be slower than for the use of CuCl, which would decrease the rate of the nucleation step, thus the number of nuclei, and would consequently yield nanocrystals of larger size. The general mechanisms about the effect of the salt precursor on the particle size is described in Figure II-50.

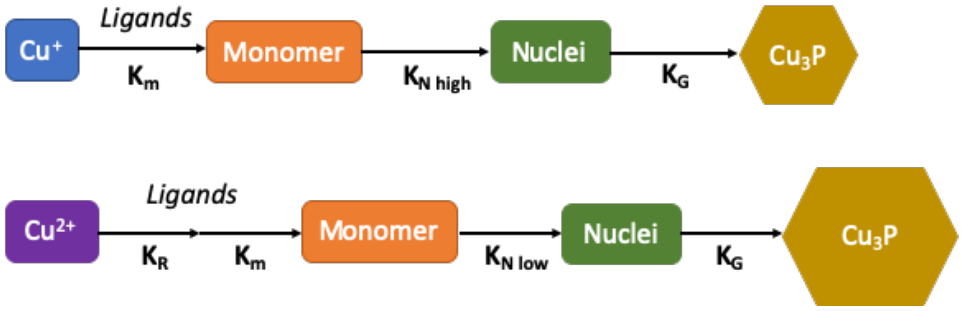

Figure II-50. *Description of possible mechanisms allow to obtain controlled size of Cu_3P by using Cu(I)X and Cu(II)X_2 as copper precursors. (K_m corresponds to the rate of monomer formation, K_R is the rate of redaction Cu(II) to Cu(I), K_N is the rate of nanoparticle nucleation and K_G corresponds to the rate of nanoparticle growth.)*[83]

As mentioned in the previous sections, the Cu(II) salts has been also tested to form Cu nanoparticles in the presence of TOP ligands via disproportionation reaction, however, the formation of NPs was not observed in our standard reaction conditions (1.6 equiv. TOP/290 °C/1 h). Contrarily, the Cu(II) salts were successfully reduced in the presence of $P(NMe_2)_3$ at a low temperature and yielded the Cu_3P nanocrystals.

In order to better understand the formation mechanism of Cu_3P, we tried to characterize by ^{31}P NMR the reaction intermediates in the supernatants separated from different reaction solutions (Figure II-50).

The ^{31}P NMR spectra of all reaction supernatants show two major peaks at 18 ppm and 29 ppm, with no signal at 121 ppm corresponding to $P(NMe_2)_3$. These two peaks may be assigned to phosphoniums products of general formula $P^+((NMe_2)_3)_n(NHC_{18}H_{35})_m$ (n + m = 4; n = 0, 1 or 2; m = 2, 3 or 4). The formation of similar aminophosphonium cations was observed in a previous study on aminophosphine-based InP nanocrystals synthesis.[54,84] In 2016, the B. Dubertret's group[84] reported the synthesis of InP from $InCl_3$ using HMPT and oleylamine as solvent, as shown in Figure II-52. They demonstrate that the transamination of the $P(NMe_2)_3$ by the oleylamine (RNH_2) converts $P(NMe_2)_3$ into the aminophosphine species ($P(NHR)_3$) that next coordinates with the $InCl_3$ salt, which yield the In-P through an acid-base process. Based on the B. Dubertret's work (Figure II-52A), the ^{31}P NMR peak at 29 ppm observed in our work was attributed to the $P(NHR)_4^+$ species. In order to characterize the transamination of aminophosphine, the mixture solution of $P(NMe_2)_3$ in oleylamine in the absence of CuCl was carried out by ^{31}P NMR and mass spectroscopy (MS) after heating at 265 °C for 1 h. In the blank test (Figure II-51f), these two peaks at 29 ppm and 18 ppm have also been observed. The MS peaks show a major peak at m/z = 1096, which is assigned to $P(NHC_{18}H_{35})_4^+$. There

was not only the transamination reaction occurred, but also the oxidation of phosphine into phosphonium.

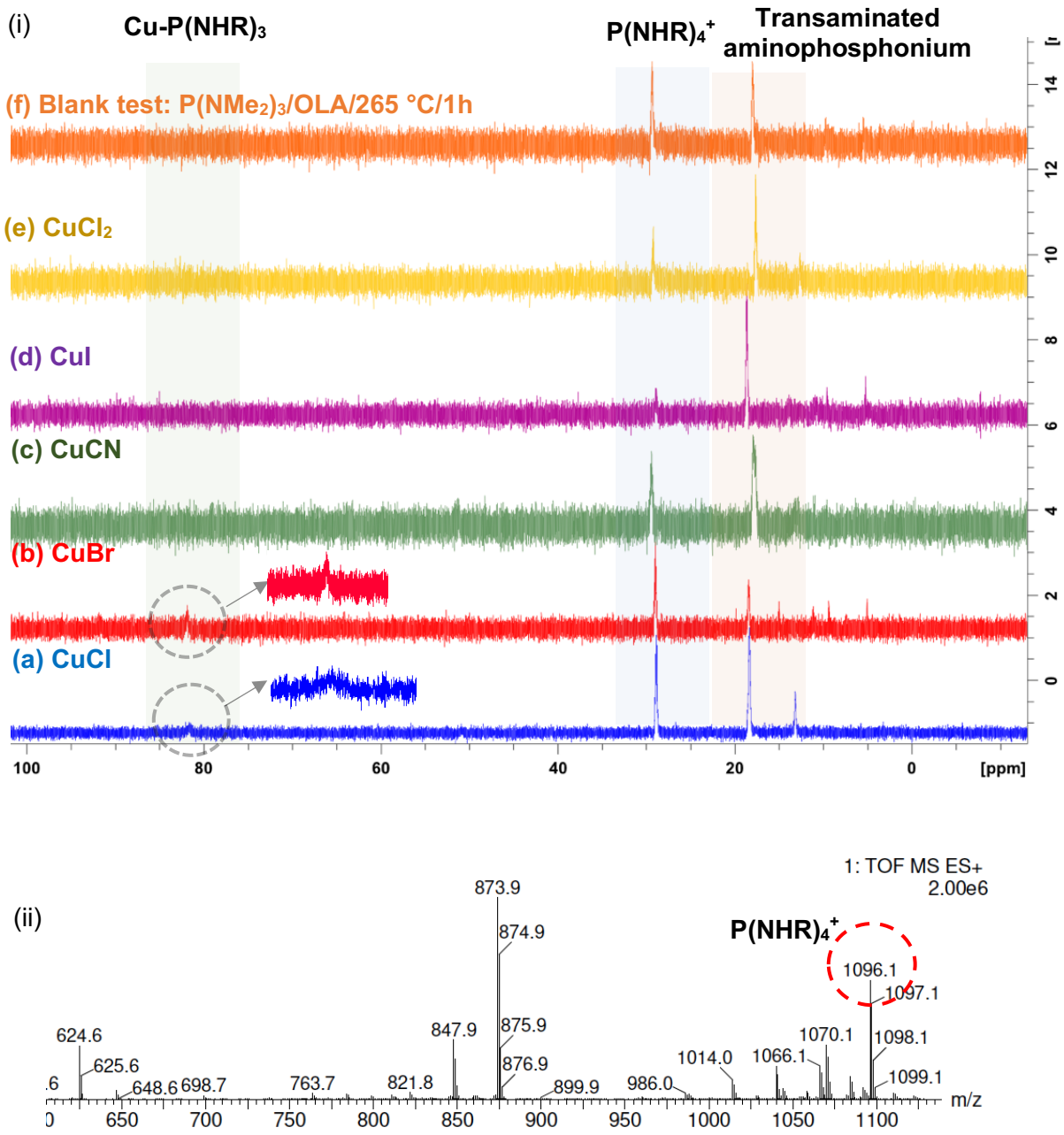

Figure II-51. *(i) ^{31}P-NMR spectra of reaction supernatant obtained from Cu_3P synthesis using different copper precursors (a) CuCl (b) CuBr (c) CuCN (d) CuI (e) $CuCl_2$ at the reaction temperature of 265 °C for 1 h in our work (f) blank test: solution mixture of $P(NMe_2)_3$ in oleylamine heated at 265 °C for 1 h and (ii) the corresponding MS. (In the beginning of this work, oleic acid has been used as stabilizer in Cu_3P synthesis, thus, to reproduce the experimental conditions, the OA is added into the blank test).*

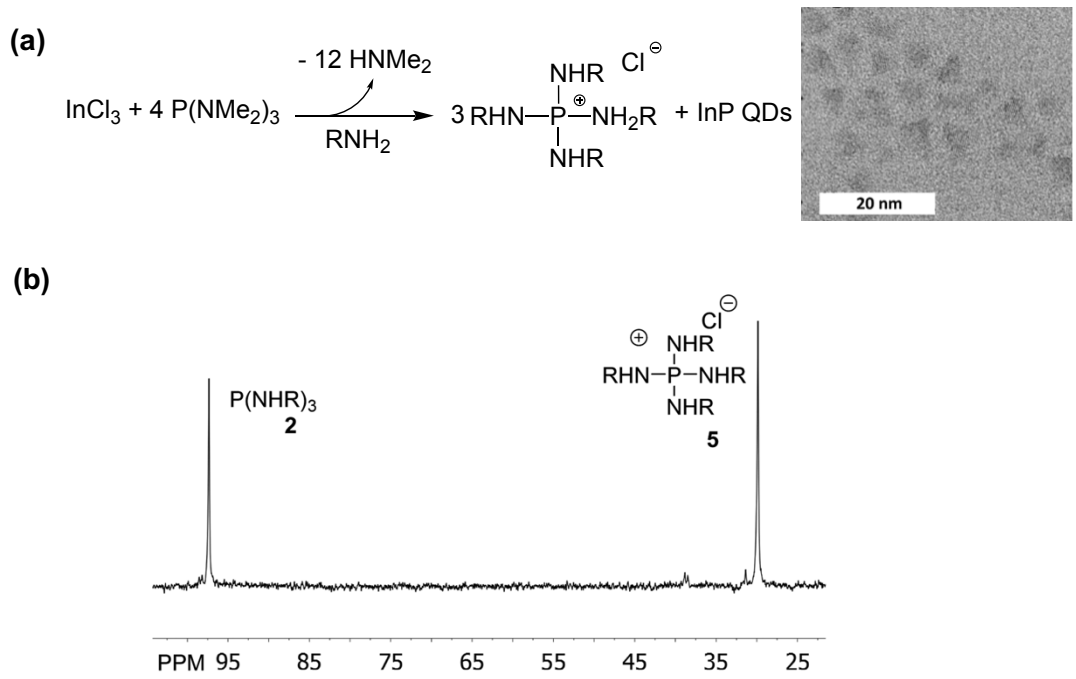

Figure II-52. *(a) Proposed chemical equation for InP synthesis and (b) typical [31] P{1H} NMR recording during the reaction between $P(NMe_2)_3$, OLA, and $InCl_3$. (Copyright from Ref.[84])*

During our research work, A. M. Schimpf *et al.* (2021)[85] reported the preparation of $Cu_{3-x}P$ nanocrystals from copper halides and $P(NEt_2)_3$ in the presence of oleylamine and trioctylamine (Figure II-53), and mechanistic investigations was provided. As the InP synthesis described above, they have also observed the transamination of aminophosphonium during the $Cu_{3-x}P$ nanocrystals reaction by ^{31}P NMR study. Therefore, they proposed the formation mechanism of $Cu_{3-x}P$ nanocrystals is similar to that observed for InP nanocrystal. Here, we studied this work as bibliographic part to help understand the formation of Cu_3P nanocrystals in our wok.

The reaction conditions developed by the Schimpf's group differ significantly from ours. Indeed, their protocol start by 3 h heating of a mixture of CuCl and $P(NEt_2)_3$ (1/3) in oleylamine at 125 °C under vacuum to generate the $(CuCl•(P(OLA)_3)_2$. The reaction conditions used in our work is simpler and faster (1 h 20 total reaction time in our synthesis vs > 3 h of Schimpf's work), also the Cu_3P nanocrystals obtained from our reaction conditions have higher uniformity and well-defined hexagonal shape compared to the ones synthetized in their work.

The Schimpf's group has also investigated various reactions parameters for tuning the size of copper phosphide nanocrystals, including the reaction temperature and the amount of oleylamine, phosphine and copper. About the reaction temperature, they reported that a lower temperature promotes smaller size of nanocrystals, and vice versa. In their reaction conditions, an increase of the reaction temperature from 220 °C to 285 °C resulted in an increase of the average size of the nanocrystals from 6.1 ± 0.8 nm to 17 ± 1 nm. This result is in good

accordance with our own observations, but under our reaction conditions the Cu_3P obtained are bigger: from 17.7 nm to 29.9 nm for the similar range of reaction temperature (from 245 °C to 290 °C) (see Figure II-44). The effect of the amount of phosphorus ligands was also investigated by A. M. Schimpf and co-workers.[85] They reported the larger copper nanocrystals were yielded by increasing the $P(NEt_2)_3$/Cu ratio (P/Cu = 1.4, 11 ± 2 nm; P/Cu = 2.2, 13 ± 2 nm; P/Cu = 3.8, 17 ± 1 nm). This phenomenon was also observed in our work (see in section II.3.4.2.1.2): P/Cu = 1, 17.4 ± 1.2 nm; P/Cu = 1.6, 22.5 ± 2.1 nm; P/Cu = 3, 27.6 ± 1.9 nm; P/Cu = 5, 28.6 ± 2.8 nm). In the A. M. Schimpf's study, the Cu-P bond formation pathway was firstly proposed (as seen in Figure II-54).[85] In their work, the formation of reaction intermediates was studied and the transamination of aminophosphines derived which could alter the growth rate of copper phosphide formation was demonstrated. They reported that a ratio of $P(NHC_{18}H_{35})_3$/Cu ≥ 3 is required to have one free and two metal-bound aminophosphines to promote an efficient redox disproportionation leading to the Cu_3P formation (Figure II-54). They concluded that a high concentration of phosphorus ligands increases the reactivity of Cu-P bond formation. The small size of Cu_3P synthetized by the low P/Cu ratio is yielded by an incomplete reactivity (i.e., incomplete consumption of CuCl) and does not represent the atom-efficient size tuning.

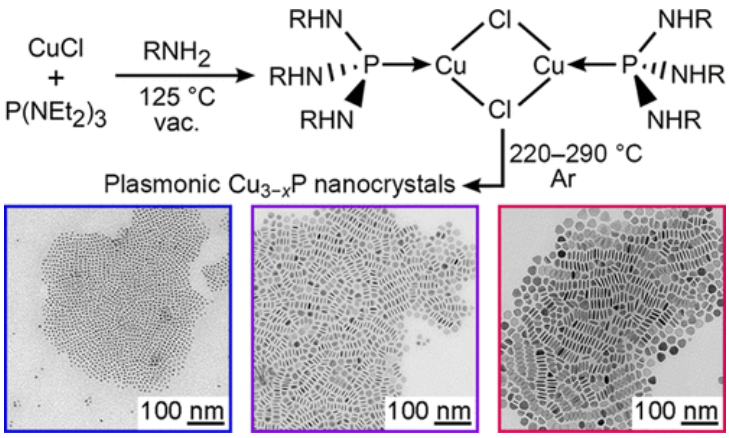

Figure II-53. *Synthesis of Cu_3P from CuCl and $P(NEt_2)_3$ in alkylamine (RNH_2) with the corresponding TEM images of Cu_3P obtained from different temperatures (220-290 °C). (Copyright from Ref.[85])*

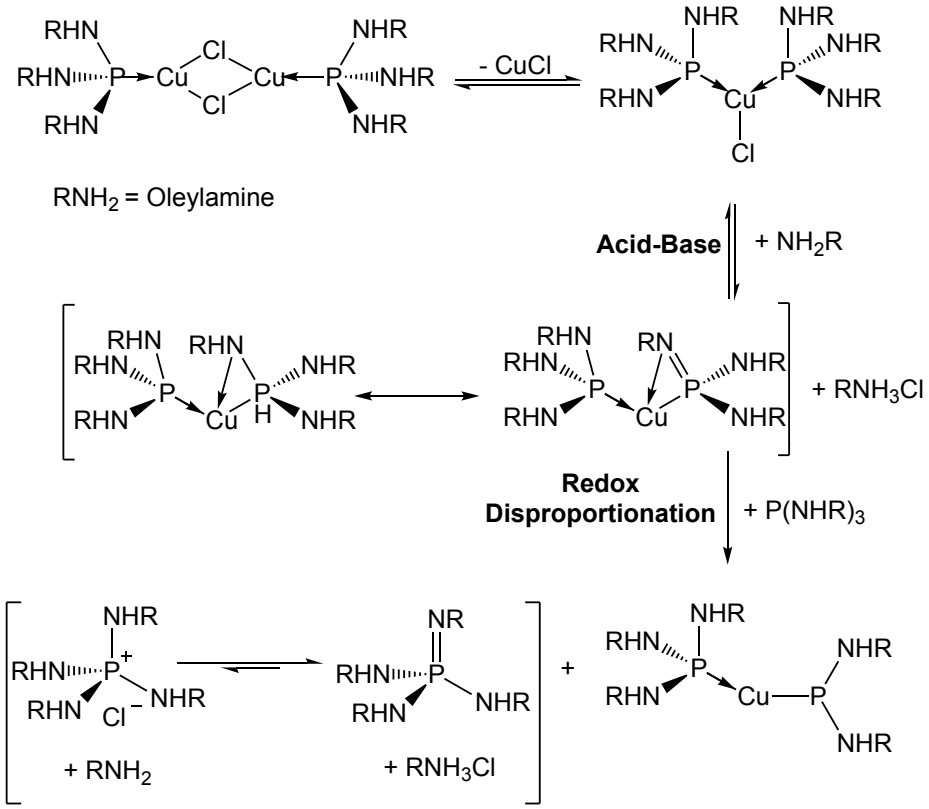

***Figure II-54**. Pathway for Cu−P Bond formation based on that previously proposed for In−P. (Copyright from Ref.[85]).*

^{31}P NMR and masse spectroscopy (MS) analysis were carried out to investigate the intermediates formed during Cu_3P synthesis in their work. The ^{31}P NMR spectra of the reaction supernatant shows that the $P(NMe_2)_3$ (120 ppm) exchanged its dimethylamino groups with the oleylamine (NH_2R), a peak at 29 ppm was observed which indicate a tetra(alkylamino)phosphonium ($P(NHC_{18}H_{35})_4^+$), furthermore, it was confirmed by MS (m/z = 1096). Based on their results, the observed peak at 29 ppm (Figure II-48) in our study can be confirmed to correspond to the $\{P(NHR)_4^+\}Cl^-$. As discussed before, this aminophosphonium cation has been shown as the byproduct in the synthesis of InP nanocrystals,[55] they reported this substitution reaction can be happened at low temperature (50 °C) due to the evaporation of dimethylamine (NMe_2) with a very low boiling point (Bp = 7 °C). Sequentially, another reaction intermediate also was reported in Schimpf's work, a peak observed at 82 ppm which attributes to the complex of Cu-$P(NMe_2)_3$. The peaks at 80 ppm was equally observed in the supernatant of Cu_3P synthesis in our work (Figure II-48). It is important to note that they used different reaction conditions from us (trioctylamine was used as co-solvent) which lead to slightly different results for the reaction. Moreover, somewhat shifted around at 18 ppm and 13 ppm (Figure II-51), which likely some transaminated aminophosphines may also include a small amount of aminophosphine oxide, based on the Schimpf's work.

II.4.4.2.1.4 Effect of the primary amine chain length

Considering the effect of reaction temperature, the amount of phosphorus ligand and the copper precursor nature on the shape and size of CuNPs, the length of the primary amine's chain may have also a significant effect on the CuNPs synthesis. In the literature, the effect of chain length on the metal nanoparticle synthesis has already reported. For example, R. R. Gullapalli *et al.*[86] investigated the influence of carbon chain length on the synthesis of iron-platinum (FePt) NPs, using different amines from 12 to 18 carbons in length (octadecylamine (ODA), hexadecylamine (HDA), tetradecylamine (TDA) and dodecylamine (DDA)), as shown in Figure II-55. They showed that the decrease of polydispersity is resulted by decreasing the chain length. The C_{14} chain amine (TDA) and C_{12} chain amine (DDA) promoted the more uniform FePt NPs in size compared to the other two longer chain amines (C_{18}-ODA and C_{16}-HAD).

$$Fe(NO_3)_3 \cdot 9H_2O + Pt(acac)_2 \xrightarrow[\text{Reflux/30 min}\ (340 - 360°C)]{\text{Alkylamine}} \text{FePt NPs}$$

(Alkylamine: (a)-ODA, (b)-HDA, (c)-TDA or (d)-DDA)

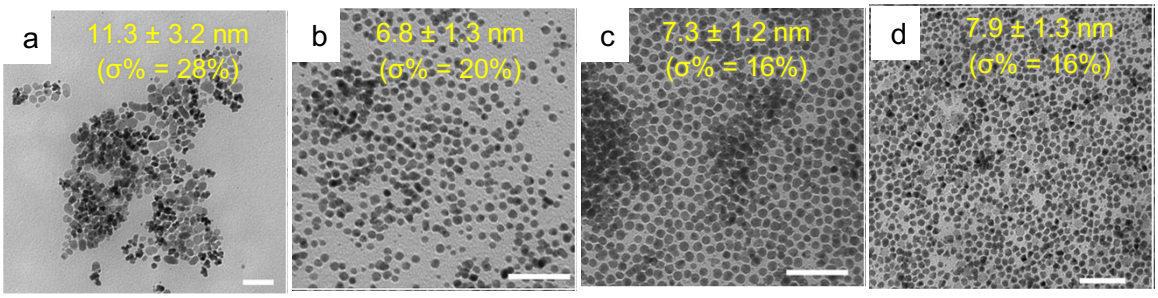

***Figure II-55**. Synthesis of FePt NPs using (a) octadecylamine (ODA) (b) hexadecylamine (HDA) (c) tetradecylamine (TDA) (d) dodecylamine (DDA)) reflux for 30 min with the corresponding TEM images (scale bars are 50 nm). (Copyright from Ref.[86])*

In our work, the effect of primary amine on the formation of NPs was studied by replacing the oleylamine ($C_{18}H_{37}N$) with dodecylamine ($C_{12}H_{27}N$) (Schema II-2) (see in Chapter V experimental section 3.1.M-N). A mixture of oleylamine and dodecylamine was also used as solvent and in the hot-injection of $P(NMe_2)_3$ procedure in the presence of CuCl. The only differences between these two primary amines are their length and the presence of a double bond in OLA.[87]

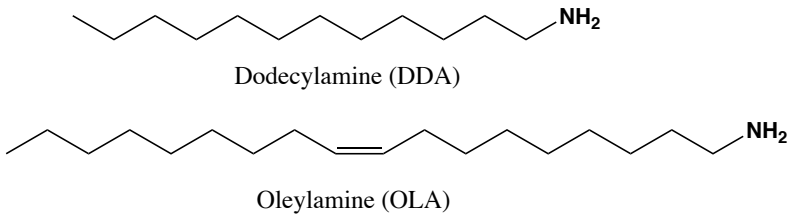

***Scheme II-2**. Molecular structure of dodecylamine (DDA) and oleylamine (OLA)*

In our study, we observed that the nature of the primary amine used affects not only the morphology of the synthetized nanoparticles, but also their chemical composition, as showed by TEM and XRD analysis. Figure II-56a, b show the typical TEM images of quasi-spherical shape and rectangle shape of copper nanoparticles were prepared using DDA alone and a 1/1 (volume ratio) mixture of OLA and DDA.

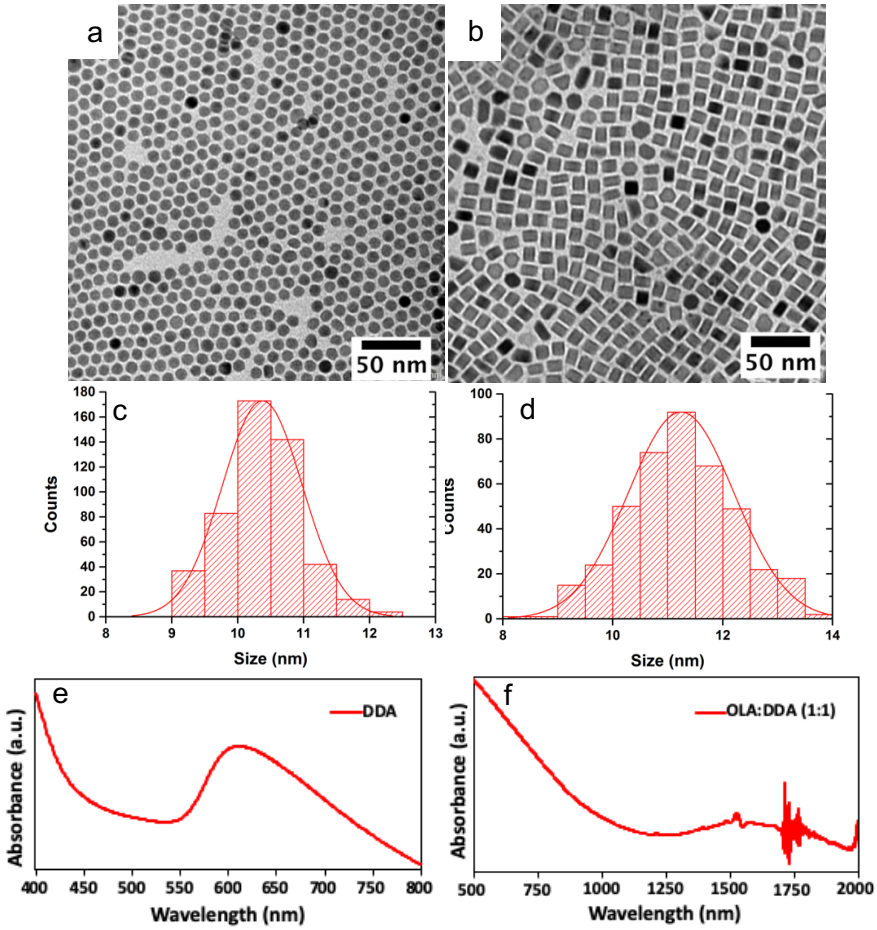

***Figure II-56**. TEM images of copper nanoparticles obtained from different reaction solvents: (a) DDA as solvent (b) DDA/OLA (volume ratio = 1) (c, d) the corresponding size histograms and (e, f) the corresponding UV-vis-NIR absorbance spectra dispersed in OLA.*

A depicted Figure II-56a, quasi-nanospheres with an average size of 10.3 ± 0.8 nm (σ% = 8%) were obtained after a heating of 1 h at 240 °C when the dodecylamine was used as solvent instead of oleylamine (see in Chapter V experimental section 3.1.M). The crystal phase of these nanospheroids were determined by XRD, and further high-resolution TEM (HRTEM) and the energy-dispersive X-ray spectroscopy (EDX) analysis were performed. The respective HRTEM of Cu nanospheres was displayed in Figure II-57a, b. The HRTEM images (Figure II-57b) reveal that the NPs are well crystallized and correspond to a face centered cubic (*fcc*) single crystals. The lattice spacing of one direction is 0.20 nm, accordingly to the (111) planes of *fcc* copper (JCPDS No. 03-1018, Fm-3m, a = 0.3617 nm, d_{111} = 0.20883 nm, d_{200} = 0.18085 nm, d_{220} = 0.12788 nm, and d_{311} = 0.10906 nm). Figure II-57c shows the SAED pattern of the Cu nanospheres, four distinct diffraction rings are clearly observed: (111), (200), (220) and (311).

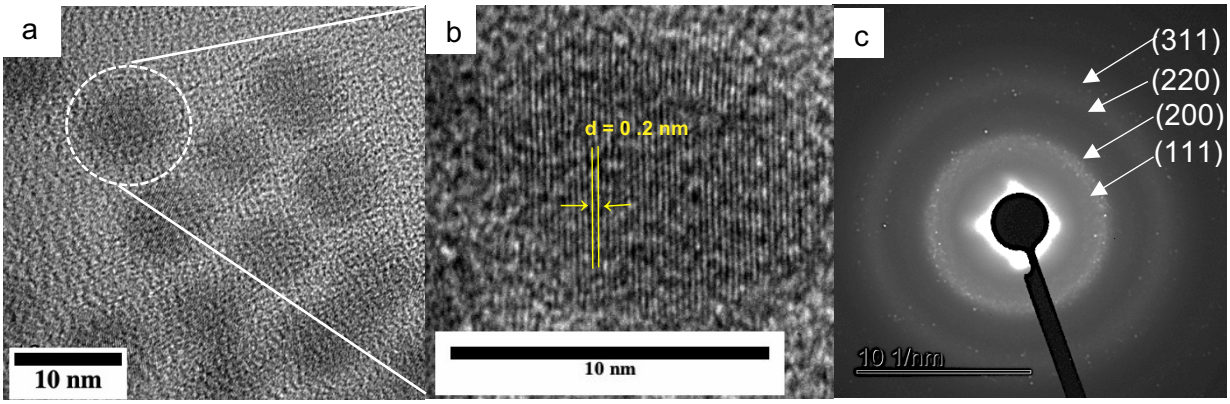

Figure II-57. *(a, b) Typical HRTEM image of Cu nanospheres synthesized in the dodecylamine (DDA) as the solvent, and (c) the corresponding SAED pattern.*

Energy dispersive X-ray spectroscopy (EDX) results of copper nanoparticles are shown in Figure II-58. The chemical composition of the nanospheres was determined by EDX analysis that shows a strong signal in the copper region of 0.93 KeV and confirmed the formation of CuNPs (Figure II-58a). It also shows the presence of Cu, P, O, Cl, C and Ni elements. In addition to the evident peak of element Cu, a significant peak of P was also observed which is mostly from $P(NMe_2)_3$. The C and Ni peaks arise from the lacey carbon-coated nickel TEM, and the element C may come from the alkyl group present in the reaction. Surface O atoms were most probably carried out during the washing step when the washing tube contains the NPs solution was moved out from the glove box. As shown in Figure II-58b, EDX analysis confirmed that copper and phosphine atoms were distributed in each of the nanoparticles and a spot of chloride atoms was also observed. However, the nitrogen atoms of the primary amine

(DDA) were not detected in these products. We propose that dodecylamine as only a role of solvent in this reaction which leads to the formation of Cu(0) instead of copper phosphide.

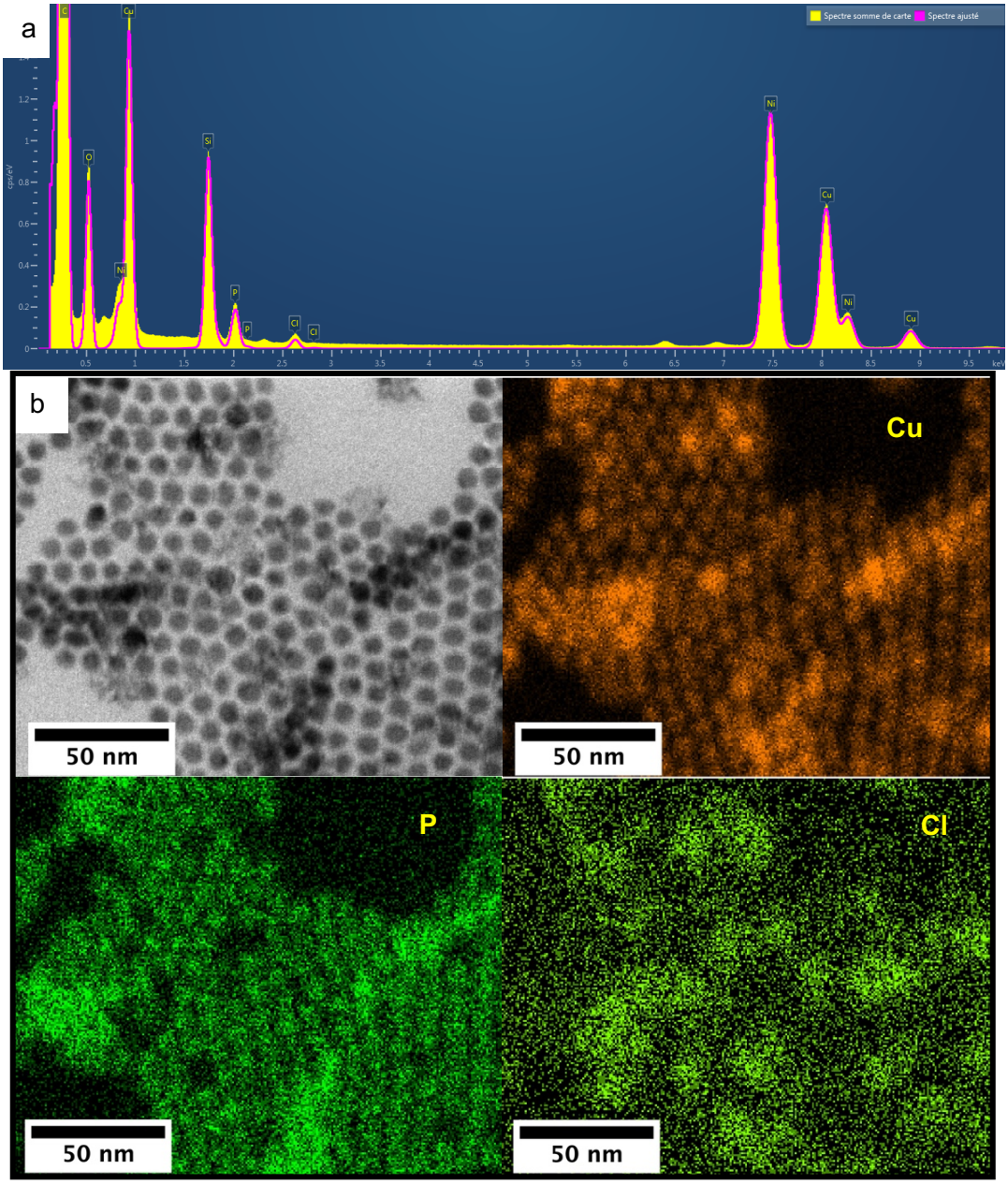

***Figure II-58**. (a) EDX spectra of CuNPs obtained from dodecylamine (DDA) used as the solvent and (b) typical STEM image and the corresponding element mapping of Cu, P and Cl.*

The identification of Cu(0) crystal phase was provided by XRD analysis as indicated in Figure II-59 (red) and Table II-16 show that dodecylamine promoted the formation of shape controlled Cu(0) rather than Cu_3P in presence of HMPT as the phosphorus ligands source. The diffraction peaks located at 43.3°, 50.4°, 74.1°, 89.9°, 95.1° and 117.1° corresponding to the (111), (200), (220), (311), (222) and (400) planes indicate a face-centered cubic (*fcc*)

structure of Cu(0) (Ref: JCPDS # 03-1018). No copper oxides were detected. Figure II-56c shows the optical UV-vis absorption spectrum. A unique absorbance band around 614 nm is observed in agreement with Cu NP spherical shape.

In the next investigation, a mixture of OLA and DDA in a volume ratio of 1:1 (3.5 mL : 3.5 mL) was used as solvent and the reaction mixture was heated at 260 °C for 1 h. These reaction conditions yielded copper nanorectangles characterized by a narrow size distribution (σ% = 6%) and an average size of 10.4 ± 0.6 nm as shown in Figure II-56b (Table II-17). The copper nanorectangles were further characterized using X-ray diffraction (XRD) (Figure II-59 (bleu)) and confirmed to be Cu_3P. The diffraction peaks at 35.9°, 39.0°, 41.4°, 44.9°, 46.2°, 47.0°, 53.44°, 56.6°, 58.9°, 66.3°, 73.2° and 77.9°and correspondent to the (112), (202), (211), (300), (113), (104), (311), (222), (223), (322) and (314) planes of space group $P6_3cm$ (Ref. PDF# 01-071-2261). As shown in Figure II-56f, the Cu_3P was characterized by an absorption peak at around 1525 nm, in agreement with the peak position observed for Cu_3P synthesis in only oleylamine (see previous section).

We have shown that a simple change of the solvent (OLA vs DDA) induced a change of the reaction pathway (Cu_3P vs Cu(0)NPs synthesis). The raison of this crucial influence of the primary amine used as solvent is still unclear. A possible explanation could be related to their boiling points differences. Indeed, the inclusion of phosphorus stemming from the phosphine ligands in Cu_3P NCs requires a high reaction temperature. For example, as seen in Figure II-43, the synthesis of Cu_3P from CuCl and TOP/TOPO in OLA and ODA mixture occurred at 350 °C whereas CuNPs are produced with similar reagents at lower temperature (< 290 °C). It is possible that use of the DDA (DDA Bp = 247 °C vs OLA Bp = 348 °C) induce a decrease of reaction temperature which prevent the formation of Cu_3P. To check this hypothesis, the synthesis was carried out at the same temperature (245 °C) but using OLA instead of DDA as the solvent. Surprisingly, we observed the formation of nanohexagons that are typical of Cu_3P in this reaction condition. It could suggest that the double bond in OLA has a dramatic effect on the reaction pathway. Further experiences are required to confirm this hypothesis as for example using the hydrogenated analogue of oleylamine as solvent at 245 °C and 265 °C. Unfortunately, this test has not yet been performed due to lack of time.

***Table II-16**. XRD data of spherical CuNPs and hexagonal Cu_3P synthetized from the DDA alone and mixed solvent OLA/DDA (1/1) as the solvent in the presence of $P(NMe_2)_3$.*

Spherical CuNPs (DDA)						
Diffraction peak	43.3°	50.4°	74.1°	89.9°	95.1°	117.1°
Plane	(111)	(200)	(220)	(311)	(222)	(400)
Rectangular Cu_3P (OLA/DDA)						
Diffraction peak	35.9°	39.0°	41.4°	44.9°	47.0°	53.44°
Plane	(112)	(202)	(211)	(300)	(113)	(104)
Diffraction peak	56.6°	58.9°	66.3°	73.2°	77.9°	
Plane	(311)	(222)	(223)	(322)	(314)	

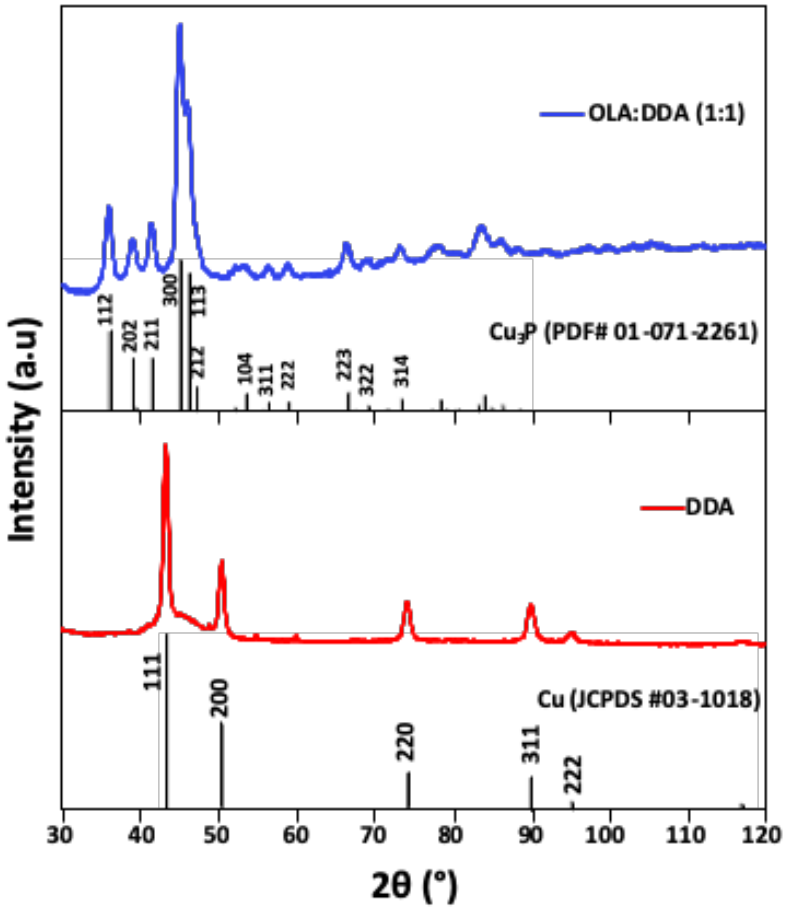

***Figure II-59**. Powder XRD pattern of copper nanoparticles synthesized in different amines: dodecylamine (DDA) (red) and a mixture of oleylamine (OLA) and dodecylamine (DDA).*

***Table II-17**. Experimental conditions used for preparing CuNPs in presence of HMPT and HMPA with the corresponding size distributions.*

Precursor (1mmol)	**Phosphorus ligands**					**T** (°C)			**Solvent**			**NPs Size** (nm) **& Shape**
	HMPT (equiv.)				HMPA (equiv.)				OLA	DDA	OLA /DDA (1/1)	
	1	1.6	3	5	1.6	245	265	290				
CuCl	✓						✓		✓			17.4 ± 1.2 Hexagons
		✓				✓			✓			17.7 ± 1.2 Hexagons
		✓					✓		✓			22.5 ± 2.1 Hexagons
		✓						✓	✓			29.9 ± 2.5 Hexagons
			✓				✓		✓			27.6 ± 1.9 Hexagons
				✓			✓		✓			28.6 ± 2.8 Hexagons
		✓				✓				✓		10.3 ± 0.8 Spheres
		✓					✓				✓	10.4 ± 0.6 Rectangles
		✓			✓			✓	✓			119.7 ± 27.2 Hexagons
CuBr		✓					✓		✓			24.4 ± 2.6 Hexagons

CuI		✓					✓		✓			47.7 ± 4.9 Hexagons
CuCN		✓					✓		✓			27.4 ± 2.7 Hexagons
$CuCl_2$							✓					51.5 ± 6.4 Hexagons
$CuBr_2$							✓					50.6 ± 6.4 Hexagons

II. 5 Conclusion

In this Chapter, a general study of CuNPs synthesis with controllable size and shape via the disproportionation reaction in the presence of a series of phosphorus ligands (TOP, TOPO, PPh_3, $P(PhMe_3)_3$, $P(OMe)_3$, $P(OC_8H_{17})_3$, $P(NMe_2)_3$, $P(O)((NMe_2)_3)$ was reported.

Firstly, we tried to find the correlation between the steric and electronic effects of the phosphorus ligands (by using their Tolman cone angle and pKa reported in the literature) and the morphology of CuNPs. During our investigations, we initiated a collaboration with Hélène Gérard's group to get DFT calculations about the coordination energy of these phosphorus ligands to copper and the disproportionation energy of the corresponding PR_3-Cu complexes. Simple monomer models of CuCl-L (L = ligands) complex were used in this theoretical study.

After comparing the steric and electronic properties of phosphorus ligands and the corresponding coordination affinities and the disproportionation energies, there was no obvious relationships among these parameters. Moreover, the calculated disproportionation energies do not always fit well with the experimental nucleation temperature in our work. This may be explained by the real nature of the copper-phosphine ligands complexes in solution that may exist as a dimeric (or more) structure instead of monomeric as the theoretical model used.

In our study, we did not find a simple effective model to predict the effect of phosphorus ligands of different classes. However, our experimental results indicate that for each class of phosphorous ligand, the steric hindrance may help to predict the final type of morphology of the CuNPs synthetized (i.e., PPh_3 and $P(PhMe_3)_3$, $P(OMe)_3$ and $P(OC_8H_{17})_3$).

In the case of TOP, we found that the type of hotplates used, and thus the heating ramp, has dramatical effect on the final shape of CuNPs (i.e., spheres, octahedra, cubes).

About the results obtained using PPh_3 and $P(PhMe_3)_3$ as phosphorus ligands, Cu nanocubes and Cu nanowires were respectively produced under identical reaction conditions.

According to our knowledge we have used for the first time $P(OMe)_3$ and $P(OC_8H_{17})_3$ as phosphine ligands in the CuNPs preparation. Starting from a copper-$P(OMe)_3$ complex enables us to access to an original tetrahedra CuNPs. We also shown that a simple change of the alkyl chain length leads to shape change of the corresponding CuNPs.

In the case of phosphorus oxide ligands, we have investigated the effect of TOPO and $OP(NMe_2)_3$. They gave cubes or mixture of triangle and quasi-spheres, respectively. Thus, these results shown the crucial effect of the nature of the substituents (alkyl vs amine) on P(V) ($R_3P=O$) atom center.

For the CuNPs synthetized with the use of $P(NMe_2)_3$, the morphology of NPs was not only affected, but the reaction itself. Indeed, in our standard reaction conditions, $P(NMe_2)_3$ promoted Cu_3P synthesis reaction instead of disproportionation.

Copper phosphide (Cu_3P) nanocrystals were prepared via a simpler and faster synthetic procedure by using $P(NMe_2)_3$ as the phosphorus source in oleylamine (OLA) and exhibit a low size polydispersity and high chemical yield, compared to the protocol reported in the literature. We found that the nature of the primary amine used as solvent (DDA vs OLA) can change the chemical course of the reaction, and thus changed the nature of the product (Cu_3P vs Cu(0)NPs). Indeed, uniform spherical Cu(0) NPs were obtained when the DDA was used as solvent instead of OLA under identical reaction temperature at 245 °C. Interestingly, once the binary solvent OLA/DDA (volume ratio 1:1) was used for synthesis, well-defined and original rectangle Cu_3P were obtained. It seems that the nature of solvent not only influenced the reaction pathway, but also the morphology of the obtained Cu_3P.

In addition to the nature of ligands phosphines, others reactions parameters also play a remarkable role on the final size of CuNPs. The amount of phosphorus ligand is able to affect the nanoparticle size, an increase in the ligand amount leads to a decrease in size and a rounded shape. The nature of halide ions from initial copper precursor was found to be crucial in modifying the final size of NPs.

This thesis chapter shows that we are able to produce copper nanoparticles with controlled size and shape by a simple procedure through tuning the phosphorus ligands and reaction conditions. These various shape-controlled copper nanoparticles could be used as nanocatalyst. The size, shape and crystallinity of the nanoparticles are well known to influence their catalytic activity.

II. 6 References

(1) A. R. Tao, S. Habas, P. Yang, *small*, **2008**, *4*, No. *3*, 310-325.
(2) X. Zhou, Y. Gan, S. Sun, *Acta Phys. Chim. Sin*., **2012**, *28*, 2071.
(3) H. J. Cho, P. G. Hwang, D. Jung, *J. Phys. Chem. Solids*, **2011**, *72*, 1462.
(4) I. Pastoriza-Santos, A. Sanchez-Iglesias, B. Rodriguez-Gonzalez, L. M. Liz-Marzan, *Small*, **2009**, *5*, 440.
(5) A. Tao, P. Sinsermsuksakul, P. Yang, *Angew. Chem. Int. Ed*., **2006**, *45*, 4597.
(6) B. C. Ranu, A. Saha, R. Jana, *Adv. Synth. Catal.*, **2007**, *349*, 2690-2696.
(7) J. L. Cuya Huaman, K. Sato, S. Kurita, T. Matsumoto, B. Jeyadevan, *J. Mater. Chem.,* **2011,** *21*, 7062.
(8) A. R. Tao, S. Habas, P. Yang, *Small*, **2008**, *4*, 310-325.
(9) E. Ye, S. Zhang, S. Liu, M. Y. Han, *Chem. Eur. J.,* **2011**, *17*, 3074-3077
(10) H. Guo, X. Liu, Q. Xie, L. Wang, D. Peng, P. S. Branco, M. B. Gawande, *RSC Adv.*, **2013**, *3*, 19812.
(11) M. Strach, V. Mantella, J. R. Pankhurst, P. Iyengar, A. Loiudice, ShubhajitDas, C. Corminboeuf, W. van Beek, R. Buonsanti, *J. Am. Chem. Soc.,* **2019**, *141* (41), 16312-16322.
(12) H. Guo, Y. Chen, M. B. Cortie, X. Liu, Q. Xie, X. Wang, D. Peng, *J. Phys. Chem. C.*, **2014**, *118* (18), 9801-9808.
(13) H. Yang, S. He, H. Chen, H. Tuan, *Chem. Mater*., **2014**, *26*, 1785-1793.
(14) I. Chakraborty, A. Jimenez, N. Pazos-Perez, L. Guerrini, A. Masood, R. A. Alvarez-Puebla, N. Feliu, W. J. Parak, *Z. Phys. Chem*., **2018**, *232*, 1307-1317.
(15) Y. Liu, D. Yao, L. Shen, H. Zhang, X. Zhang, B. Yang, *J. Am. Chem. Soc*., **2012**, *134* 7207-7210.
(16) S. Mourdikoudis, L.M. Liz-Marz-an, *Chem. Mater*., **2013**, *25*, 1465-1476.
(17) D. Sharma, S. Kanchi, K. Bisetty, *Arab. J. Chem.,* **2019**, *12*, 3576-3600.
(18) W. Wu, E. V. Shevchenko, *J. Nano. Part. Res*., **2018**, *20*, 255.
(19) a) M. C. Daniel, D. Astruc, *Chem. Rev.,* **2004**, *104* (1), 293-346; b) L. S. Ott, R. G. Finke, *Coord. Chem. Rev.,* **2007**, *251* (9-10), 1075-1100; c) R. A. Sperling, P. Rivera Gil, F. Zhang, M. Zanella, W. J. Parak, *Chem. Soc. Rev.,* **2008**, *37* (9), 1896-1908.
(20) A. Heuer-Jungemann, N. Feliu, I. Bakaimi, M. Hamaly, A. Alkilany, I. Chakraborty, A. Masood, M. F. Casula, A. Kostopoulou, E. Oh, K. Susumu, M. H. Stewart, I. L. Medintz, E. Stratakis, W. J. Parak, A. G. Kanaras, *Chem. Rev*., **2019**, *119*, 4819−4880.
(21) D. C. Onwadiwe, M. Hrubaru, E. E. Ebenso, *J. Nanomater.*, **2015**, *7*, 915.
(22) C. Barrière, K. Piettre, V. Latour, O. Margeat, C. Turrin, B. Chaudret, P. Fau *J. Mater. Chem.,* **2012**, *22*, 2279.
(23) R. Sierra-Ávila, M. Pérez-Alvarez, G. Cadenas-Pliego, C. A. Ávila-Orta, R. Betancourt-Galindo, E. Jiménez-Regalado, R. M. Jiménez-Barrera, J. G. Martínez-Colunga, *J. Nanomate.,* **2014**, Article ID 361791.
(24) P. Kanninen, C. Johans, J. Merta, K. Kontturi, *J. Col. Int. Sci.,* **2008,** *318*, 88-95.
(25) N. Jardón-Maximino, M. Pérez-Alvarez, G. Cadenas-Pliego, L. E. Lugo-Uribe, C. Cabello-Alvarado, J. M. Mata-Padilla, E. D. Barriga-Castro, *Pol.*, **2021**, *13*, 2846.
(26) a) M. B. Gawande, A. Goswami, F. Felpin, T. Asefa, X. Huang, R. Silva, X. Zou, R. Zboril, R. S. Varma, *Chem. Rev.,* **2016**, *116*, 3722-3811; b) V. Mantella, L. Castilla-Amor´os R. Buonsanti. *Chem. Sci.,* **2020**, *11*, 11394-11403.
(27) C. A. Tolman, *Chem. Rev.,* **1977,** *77*, 3, 313-348.

(28) J. Mathew, T. Thomas, C. H. Suresh, *Inorg. Chem.*, **2007**, *46,* 10800-10809.
(29) D. J. M. Snelders, G. van Koten, R. J. M. K. Gebbink, *Chem. Eur. J., **2011***, *17*, 42-57.
(30) a) A. M. Ejgandi, *Measuring the electronic and steric effect of some phosphine ligands,* **2010**. A dissertation submitted to the University of Manchester for the degree of Master of Science by research in the Faculty of Engineering and Physical Sciences; b) T. Hughes, *MSc dissertation "Chemistry in the preparation of phosphine ligands for Pd-catalysed reactions".* **2009**. University of Johannesburg; c) J. Jover, J. Cirera, *Dalton Trans.*, **2019**, *48*, 15036-15048; d) T. P. A. Ruberu, H. R. Albright, B. Callis, B. Ward, J. Cisneros, H. Fan, J. Vela, *ACS Nano.,* **2012**, *6* (6), 5348-5359; e) R. C. Bush, R. J. Angelici, *Inorg. Chem.,* **1988**, *27*, 681-686; f) W. A. Henderson, C. A. Streuli, *Anal. Chem*., **1960**, *32*, 985-987.
(31) W. Erley, J. C. Hemminger, *Surf. Sci*. **1994**, *316*, L,1025-1030.
(32) J. K. Cooper, A. M. Franco, S. Gul, C. Corrado, J. Z. Zhang, *Langmuir*, **2011**, *27*, 8486-8493.
(33) S. A. Maier, Plasmonics Funadamentals and Applications. *Springer Science Business Media LLC.*, **2007**.
(34) G. Mie, Ann. *Phys.*, **1908**, *25* (4), 377-445.
(35) Y. Xia, Y. Xiong, B. Lim, S. E. Skrabalak, *Angew. Chem., Int. Ed.,* **2009**, *48*, 60-103.
(36) R. E. Schaak, M. E. Williams, *ACS Nano.,* **2012**, *6*, 8492-8497.
(37) S. G. Kwon, T. Hyeon, *Small.*, **2011**, *7*, 2685-2702.
(38) J. Lee, J. Yang, S. G. Kwon, T. Hyeon, *Nat. Rev. Mater.*, **2016**, *1*, 16034-16050.
(39) Y. Xia, X. Xia, H. C. Peng, *J. Am. Chem. Soc.,* **2015**, *137*, 7947-7966.
(40) a) P. F. Ho, K. M. Chi. *Langmuir*, **2002**, *18*, 1413-1418; b) Y. Xiong, A. R. Siekkinen, J. Wang, Y. Yin, M. J. Kim, Y. Xia, *J. Mater. Chem.,* **2007**, *17*, 2600.
(41) a) I. Washio, Y. Xiong, Y. Yin, Y. Xia, *Adv Mater.* **2006**, 18, 1745; b) Y. Xiong, I. Washio, J. Chen, H. Cai, Z. Y. Li, Y. Xia, *Langmuir*, **2006**, *22*, 8563.
(42) Z. L. Wang, *J. Phys. Chem. B.,* **2000**, *104*, 1153-1175.
(43) J. Yang, M. K. Choi, D. H. Kim, T. Hyeon, *Adv. Mater.,* **2016**, *28*, 1176-1207.
(44) Z. Jin, C. Liu, K. Qi, X. Cui, Scientific Reports, **2017**, *7*, Article number: 39695.
(45) K. LaMer. H. Dinegar, *J. Am. Chem. Soc.,* **1950**, *72*, 11, 4847-4854.
(46) M. Giancaspro, T. Sibillano, F. Panzarea, C. Giannini, S. Schmitzer, F. Vischio, N. Depalo, A. Agostiano, M. L. Curri, M. Striccoli, E. Fanizza, *Mater. Chem. Front*., **2021**, *5*, 1341-1354.
(47) X. Frogneux, F. Borondics, S. Lefrançois, F. D'Accriscio, C. Sanchez, S. Carenco, *Catal. Sci. Technol.*, **2018**, *8*, 5073-5080.
(48) S. Mozaffari, W. Li, M. Dixit, S. Seifert, B. Lee, L. Kovarik, G. Mpourpmakis, A. M. Karim, *Nanoscale Adv.*, **2019**, *1*, 4052-4066.
(49) T. Sreethawong, K. W. Shah, S. Zhang, E. Ye, S. H. Lim, U. Maheswaran, W. Mao, M. Han. *J. Mater. Chem. A*., **2014**, *2*, 3417-3423
(50) Y. Tang, M. Ouyang, *Nature Mater.,* **2007***, 6*, 754-759.
(51) M. Ali Ben Aissa, B. Tremblay, A. Andrieux-Ledier, E. Maisonhaute, N. Raouafi, A. Courty, *Nanoscale*, **2015**, *7*, 3189-3195.
(52) M. A. S. Garciaa, M. Ibrahimb, J.C.S. Costaa, P. Corioa, E. V. Gusevskayad, E. N. dos Santosd, K. Philippotb, *Appl. Cat. A.: General,* **2017**, *548,* 136-142.
(53) R. Lu, J. Yuan, H. Shi, B. Li, W. Wang, D. Wang, M. Cao, *Cryst. Eng. Comm.*, **2013**,*15*, 3984-3991.
(54) Z. Ji, X. Wang, H. Zhang, *ACS Nano.,* **2012**, *6* (6), 5366-5380.
(55) P. Zhang, I. Wyman, J. Hu, S. Lin, Z. Zhong, Y. Tu, Z. Huang, Y. Wei, *Mater. Sci. Engineering: B*, **2017**, *223*, 1-23.

(56) D. Mott, J. Galkowski, L. Wang, J. Luo, C. Zhong, *Langmuir*, **2007**, *23*, 5740-5745.
(57) Y. N. Xia, X. J. Xiong, B. Lim, S. E. Skrabalak, *Angew, Chem. Int. Ed.,* **2009**, *48*, 60-103.
(58) a) Y. Xiong, Y. Xia, *Adv. Mater.*, **2007**, *19*, 3385; b) B. Wiley, T. Herricks, Y. Sun, Y. Xia, *Nano Lett.,* **2004,** *4*, 1733-739.
(59) R. Chen, Q. N. Nguyen, M. Zhao, Z. Chen, M. Chi, Y. Xia, *Chem. A. Euro. J*., **2020**, *27* (8), 2760-2766.
(60) Y. Xiong, Y. Xia, *Adv. Mater.*, **2007**, *19*, 3385.
(61) C. C. Crane, F. Wang, J. Li, J. Tao, Y. Zhu, J. Chen, *J. Phys. Chem. C.,* **2017**, *121*, 10, 5684-5692.
(62) Z. Liu, H. Mu, S. Xiao, R. Wang, Z. Wang, W. Wang, Y. Wang, X. Zhu, K. Lu, H. Zhang, S. Lee, Q. Bao, W. Ma, *Adv. Mater.*, **2016**, *28*, 3535-3542.
(63) A. E. Henkes, R. E. Schaak, *Chem. Mater.*, **2007**, *19*, 4234-4242.
(64) G. Manna, R. Bose, N. Pradhan, *Angew. Chem. Int. Ed.*, **2013**, *52*, 1-6.
(65) E. J. Sheets, W. Yang, R. B. Balow, Y. Wang, B. C. Walker, E. A. Stach, R. Agrawal, *J. Mater. Res.* **2015**, *30* (23), 3710-3716.
(66) L. Trizio, R. Gaspari, G. Bertoni, I. Kriegel, L. Moretti, F. Scotognella, L. Maserati, Y. Zhang, G. C. Messina, M. Prato, S. Marras, A. Cavalli, L. Manna, *Chem. Mater.,* **2015**, *27* (3), 1120-1128.
(67) X. Frogneux, F. Borondics, S. Lefrançois, F. D'Accriscio, C. Sanchez, S. Carenco, *Catal. Sci. Technol.*, **2018**, *8*, 5073-5080.
(68) R. Lu, J. Yuan, H. Shi, B. Li, W. Wang, D. Wang, M. Cao, *Cryst. Eng. Comm.*, **2013**,*15*, 3984-3991.
(69) Z. Ji, X. Wang, H. Zhang, S. Lin, H. Meng, B. Sun, S. George, T. Xia, A. E. Nel, J. I. Zink, *ACS Nano.,* **2012**, *6(6),* 5366-5380.
(70) S. L. Brock, K. Senevirathne, *J. Solid State Chem.*, **2008**, *181*, 1552-1559.
(71) S. T. Oyama, T. Gott, H. Zhao, Y. K. Lee, *Catal. Today*, **2009**, *143*, 94-107.
(72) J. Wang, Q. Yang, Z. Zhang, T. Li, S. Zhang, *Dalt. Trans*., **2010**, *39*, 227-233.
(73) Y. N. Chouryal, R. K. Sharma, D. Acharjee, T. Ganguly, A. Pandey, P. Ghosh, *J. Chem. Sci.,* **2019**, *131* (93).
(74) A. Wolff, T. Doert, J. Hunger, M. Kaiser, J. Pallmann, R. Reinhold, S. Yogendra, L. Giebeler, J. Sichelschmidt, W. Schnelle, R. Whiteside, H. Q. N. Gunaratne, P. Nockemann, J. J. Weigand, E. Brunner, M. Ruck, *Chem. Mate.,* **2018**, *30*, 7111.
(75) H. Pfeiffer, F. Tancret, T. Brousse, *Electrochim. Acta.*, **2005**, *50*, 4763-4770.
(76) M. C. Stan, R. Klöpsch, A. Bhaskar, J. Li, S. Passerini, M. Winter, *Adv. Energ. Mater.*, **2013**, *3*, 231-238.
(77) H. Su, Y. Xie, B. Li, X. M. Liu, Y. T. Qian, *Solid State Ionics*, **1999**, *122*, 157.
(78) Y. Xie, H. L. Su, X. F. Qian, X. M. Liu, Y. T. Qian, *J. Solid State Chem.,* **2000**, *149*, 88.
(79) C. Villevieille, F. Robert, P. L. Taberna, L. Bazin, P. Simon, L. Monconduit, *J. Mater. Chem.*, **2008**, *18*, 5956.
(80) Z. Liu, H. Mu, S. Xiao, R. Wang, Z. Wang, W. Wang, Y. Wang, X. Zhu, K. Lu, H. Zhang, S. Lee, Q. Bao, W. Ma, *Adv. Mater.*, **2016**, *28*, 3535-3542.
(81) A. E. Henkes, R. E. Schaak, *Chem. Mater.*, **2007**, *19*, 4234-4242.
(82) S. Honary, H. Barabadi, E. Gharaeifathabad, F. Naghibi, *Dig. J. Nanomater. Biostruct.,* **2012**, *7*, 999-1005.
(83) B. H. Juarez, *Z. Phys. Chem.,* **2015**, *229* (1-2),119-137.
(84) A. Buffard, S. Dreyfuss, B. Nadal, H. Heuclin, X. Xu, G. Patriarche, N. Mézailles, B. Dubertret, *Chem. Mater.,* **2016**, *28 (16),* 5925-5934.

(85) A. G. Rachkov, A. M. Schimpf, Colloidal Synthesis of Tunable Copper Phosphide, *Nanocrystals Chem. Mater.*, **2021**, *33*, 1394−1406.
(86) R. M. Taylor, T. C. Monson, R. R. Gullapalli, *Nanoscale Res. Lett.,* **2014***, 9,* 306.
(87) P. J. Shaw, M. Meyns, Y. Zuo, A. Grau-Carbonell, P. G. Lagoudakis, M. D. B. Charlton, S. Martí-Sánchez, J. Arbiol, *Nanomaterials*, **2018**, *8*, 506.

Chapter III. Synthesis of copper nanoparticles from CAACs-CuCl complexes

III. 1 Introduction

Carbenes are compounds that have a neutral divalent carbon atom with six electrons in its valence shell.[1] In 1988, G. Bertrand and co-workers[2] first reported the presence of isolated stable carbene in the singlet state, the phosphinosilylcarbenes (see in Figure III-1a). Then, in 1991, A-J. Arduengo *et al.*[3] showed the preparation of the first metal-free N-Heterocyclic carbene: imidazole-2-ylidene (Figure III-1b), which opened up a new area for investigation of stable N-Heterocyclic carbenes (NHCs). Afterward, the carbenes chemistry has been widely developed and has proved to be an excellent tool in the field of organometallic,[4] organic[5] and inorganic chemistry.[6]

NHCs are heterocyclic species containing a carbene carbon and at least one adjacent nitrogen atom. They exhibit high stability due to their specific electronic structure.[6a] As shown in Figure III-1c, the σ-electron-withdrawing and π-electron-donating nitrogen atoms are next to the carbene carbon atom to stabilize the NHC through the conjugation of the lone pair of the nitrogen with the empty p orbital of the carbon.[7] The lone pair of the carbene carbon atom is in the plane of the heterocyclic ring which makes of the NHCs good σ-donors, so they can easily bind to metallic or non-metallic species.[8] The cyclic nature of NHC favors further stabilization of the singlet sp^2 state.[9] Due to their specific electronic properties, NHCs have attracted considerable attention as promising ligands in various fields. In particular, their great ability to complex with transition metals make of them some ligands of choice in catalysis.[10,11]

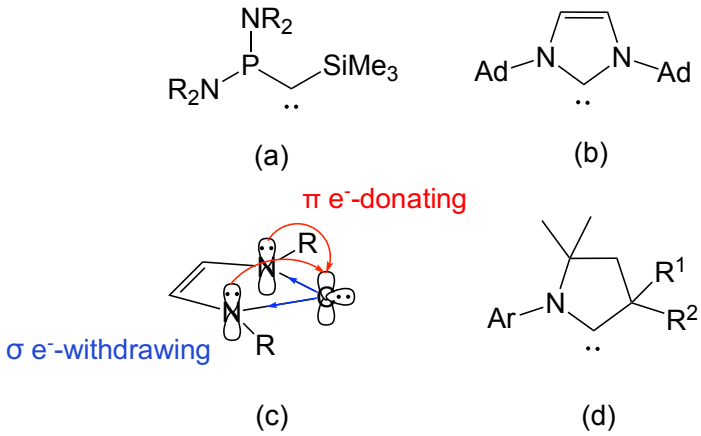

Figure III-1. *(a) First example of an isolated phosphinosilylcarbenes by Bertrand et al.[2] (b) Arduengo's N-Heterocyclic carbene[3] (c) A singlet ground state electronic structure of imidazole-2-ylidene-type NHC* (d) Cyclic (alkyl)(amino)carbenes (CAACs).[12]

A new family of heterocyclic carbenes, called cyclic (alkyl)(amino)carbenes (CAACs) (Figure III-1d), and owning different electronic properties than NHCs, was reported by G. Bertrand et co-workers in 2005.[12] In the structure of CAACs, one of electronegative amino substituent of NHCs was replaced by a strong σ-donor alkyl group, which makes CAACs more nucleophilic (σ-donating) and electrophilic (π-accepting) than classical NHCs.[13]

In recent years, electron-rich NHCs have attracted increasing attention as neutral capped-ligands for the stabilization and functionalization in metal NP synthesis due to their strong covalent bonding to the metal surface.[14] The first research on the interaction between N-Heterocyclic carbene and metal nanoparticles was reported by R. G. Finke's group in 2005.[15] Thereafter, the new field of NHC-functionalized metallic nanoparticles was opened and a range of NHC-metal NPs was explored.

In Chapter III, we first introduce the different methods for synthesizing the NHC-stabilized metal nanoparticles reported in the literatures. Then, we report the preparation of CuNPs by decomposition of CAACs-CuCl complex in oleylamine via a "one-pot" disproportionation reaction. The influence of different reaction factors like the steric effect of CAACs ligands, the CAACs-Cu/OLA ratio and the nature of alkylamine are investigated to obtain tunable shape CuNPs.

III. 2 Bibliographic introduction on metal nanoparticles stabilized by N-Heterocyclic carbenes.

In the last 15 years, NHCs have been used to stabilize metal NPs, such as Au,[16] Ag,[17] Ru,[18] Pt,[19] and Pd.[20] The effect of NHCs ligands in the NP synthesis is highly dependent on their chemical structure, namely the N-substituents and the groups bounded to the C-ring. The tunable structures of NHCs are able to control the morphology and the properties of the NPs, including their size, shape, solubility, catalytic reactivity and surface state.[10] So far, three main approaches have been reported to synthetize NHC-stabilized metal NPs (Scheme III-1): i) the direct decomposition of functionalized metal-NHC complexes,[21] ii) the reduction of metal precursor in the presence of NHCs ligands,[22] and iii) the ligands-exchange.[23]

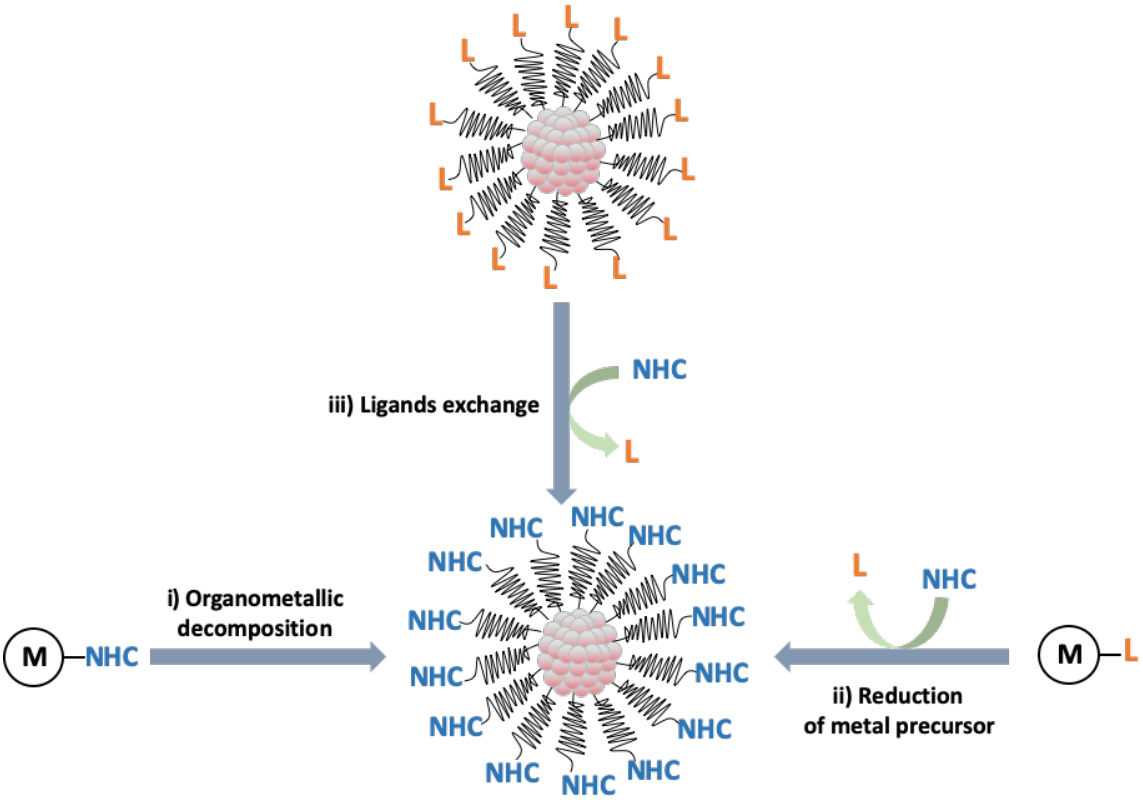

Scheme III-1. *Schematic illustration of different synthesis methodologies for obtaining NHCs-stabilized metal nanoparticles.*

The first method of direct decomposition of organometallic NHC complex (Schema III-1i) belongs to the "bottom-up" approach. The NHC-stabilized NPs are produced by reduction of metal-NHC complex by a reducing agent (e.g., $NaBH_4$, $KBEt_3H$)[24,25] or direct thermal decomposition.[27]

Compared to the direct thermal decomposition, the reduction route allows easier control of the nanoparticle size by varying the nature or the concentration of the reducing agent and/or the steric hindrance of metal-NHC precursor.[25,26] For example, Vignolle and Tilley[25] systematically investigated the influence of reaction parameters, including the nature of reducing agents and the different steric hindrances of NHCs ligands, in the preparation of NHC-stabilized AuNPs. They synthetized different sizes and shapes of NHC-AuNPs using two different reducing agents: $KBEt_3H$ and 9-BBN (9-borabicyclo(3.3.1)nonane) (Figure III-2). In the case of $KBEt_3H$, mainly spherical but some triangularly-shaped AuNPs with an average size of 6.8 ± 1.8 nm were obtained by the reduction of NHC-AuCl complex (Figure III-2a). When the $KBEt_3H$ was replaced by 9-BBN, smaller NPs (5.75 ± 0.49 nm) were obtained with rhombic shape as shown in Figure III-2b. They showed that the simple change of the reducing agent could markedly influence the final nanoparticle size and shape. Furthermore, analysis by FAB mass spectroscopy and ^1H NMR spectra of AuNPs confirmed that NHC are on the NP surface.

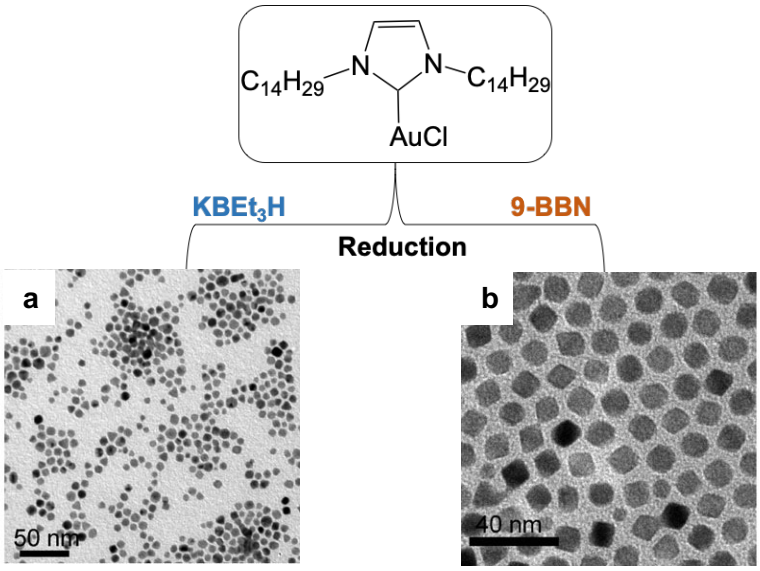

Figure III-2. *Synthesis of NHC-stabilized AuNPs by reduction of NHC-AuCl complex by different reducing agents a) $KBEt_3H$ in THF and b) 9-BBN in Et_2O. (Copyright from Ref.[25])*

They also investigated the steric effect of the N-substituents on NHCs ligands on the final NP size. When the *n*-$C_{14}H_{29}$ substituent are exchanged by isopropyl, a decrease of AuNP size to 2.19 ± 0.47 nm is observed (Figure III-3a). As a result, the flexible long chains ($C_{14}H_{29}$) of N-substituent on NHC ligand favors the formation of bigger Au nanoparticles compared to the bulky and rigid *i*-Pr group.

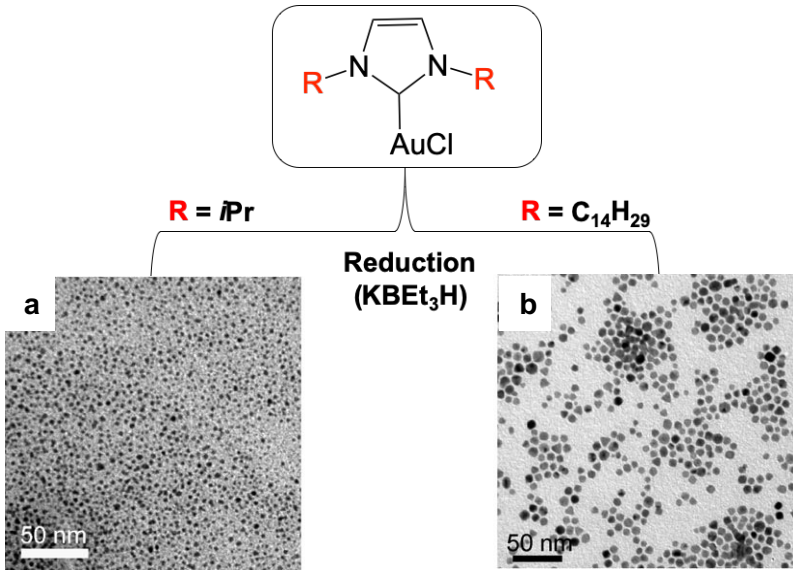

Figure III-3. *Synthesis of NHC-stabilized AuNPs by reduction of NHC-AuCl complex by different N-substituents: a) R = iPr and b) R = $C_{14}H_{29}$. (Copyright from Ref.[25])*

In the case of the direct thermal decomposition, the synthetic "one-pot" procedure is simpler and stable metal NPs are formed.[27] In 2004, the synthesis of highly stable water-soluble NHC-stabilized PtNPs through the thermal decomposition of sulfonated NHC-Pt complex was reported by B. Chaudret and co-workers.[27] In their paper, the obtained NHC-stabilized PtNPs are homogeneous in water and ultra-stable for serval months in air. A series of NHC ligands (1a-d) were investigated to afford small PtNPs with narrow size in the range 1.3-2.0 (± 0.4) nm (Figure III-4). Smallest NPs were formed when the bulkiest ligands (c and b) were used. To investigate the coordination of the surface ligands to the PtNPs, they prepared NPs ^{13}C-2c containing a ^{13}C isotopic labeling in the carbonic carbon atom of the imidazole-ring. These NPs were analyzed by MAS NMR and the ^{13}C-^{195}Pt coupling between the NHC ligands and Pt NPs was firstly observed.

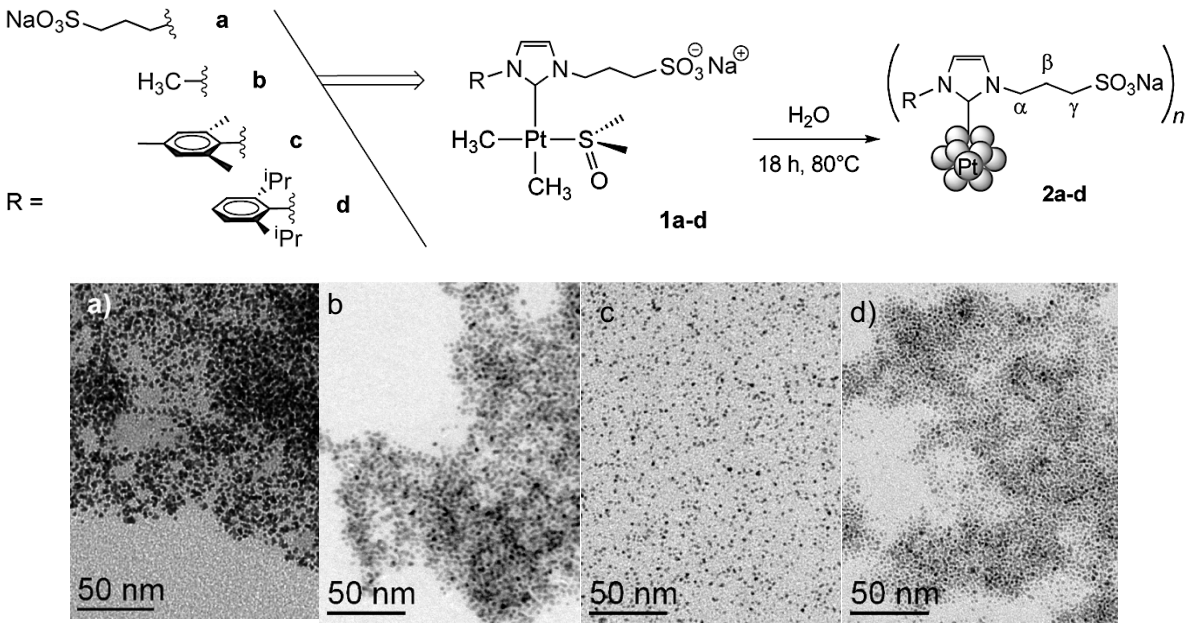

Figure III-4. *Synthesis of small PtNPs (2a-d) by thermal decomposition of different NHC-Pt^{II} complexes (1a-d) in water and (a-d) the corresponding TEM images. (Copyright from Ref.[27])*

Later, E. de Jesús *et al.*[28] reported a similar investigation about the decomposition of the NHC-palladium complexes to prepare stable and water-soluble NHC-PdNPs (Figure III-5). In their work, they found that the most hindered NHC (1a) leads to the formation of smaller NHC-PdNPs (3.4 ± 0.5 nm) compared to ligand 1b (6.3 ± 1.4 nm). Similarly, ^{13}C-isotopic labeling NPs were synthetized to study the coordination of the NHC to the NP surface. They also investigated the organometallic intermediates and the decomposition products during the synthesis by NMR analysis.

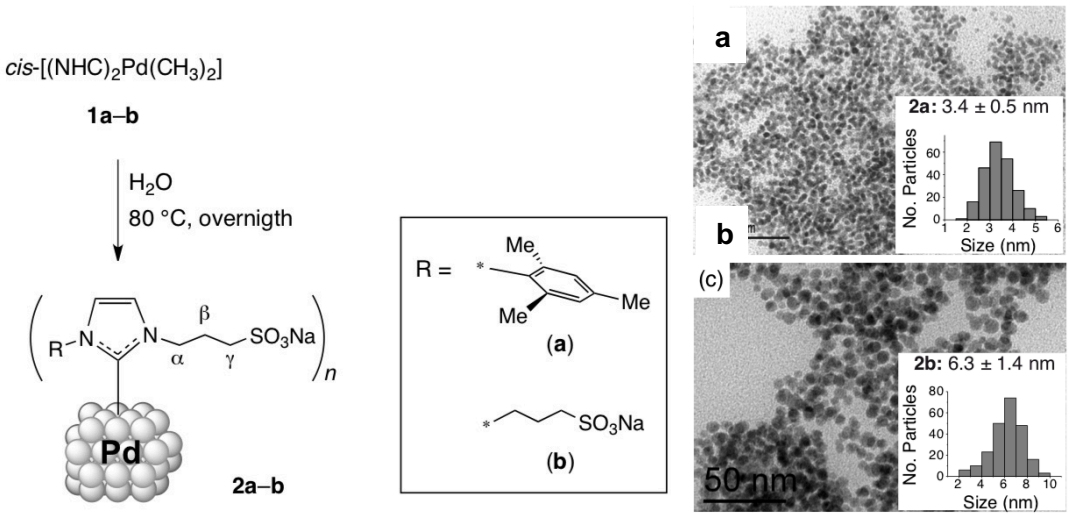

Figure III-5. *Synthesis of water-soluble PdNPs (2a-b) by thermal decomposition of the Pd complexes (1a-b) and (a-b) the corresponding TEM images. (Copyright from Ref.[28])*

The second approach involves the synthesis of NHC-coated NPs through the reduction of a metal precursor in the presence of NHCs ligands (Scheme III-1ii) which is strongly influenced by the nature of the precursor and the stabilizer.[29-31] The reduction rate is also a very important factor in the NHCs-NPs synthesis, which is able to affect the nucleation and growth of NPs. A slow reduction rate of metal precursor leads to limited nucleation, which yields larger NPs compared to a fast reduction rate (see in Chapter I). The capping ligands NHCs binding to the particle surface, a judicious choice of these ligands allows to control the growth of particle to tune their final morphology and size. Therefore, a range of well-defined NHC-stabilized metal NPs with tunable size were prepared using various metal precursors and different types of NHCs ligands through this appoach.[29-31] For example, B. Chaudret *et al*.[22a] presented the synthesis of NHC-stabilized ruthenium NPs by decomposition of Ru precursor at room temperature using H_2 (3 bar) in the presence of variable amount of carbenes ligands (L^1 and L^2; 0.2 or 0.5 equiv.) (Figure III-6). They showed that 0.5 equiv. of ligands L^1 is mandatory to obtain the RuNPs with an average size of 1.7 ± 0.2 nm, whereas a black precipitate was yielded when only 0.2 equiv. of ligand L^1 was present in the reaction mixture. In the case of 0.2 or 0.5 equiv. of ligand L^2, both lead to the formation of stable RuNPs with a decrease in size when the amount of L^2 increased. The higher concentration of NHC ligand thus results in the formation of smaller NPs.

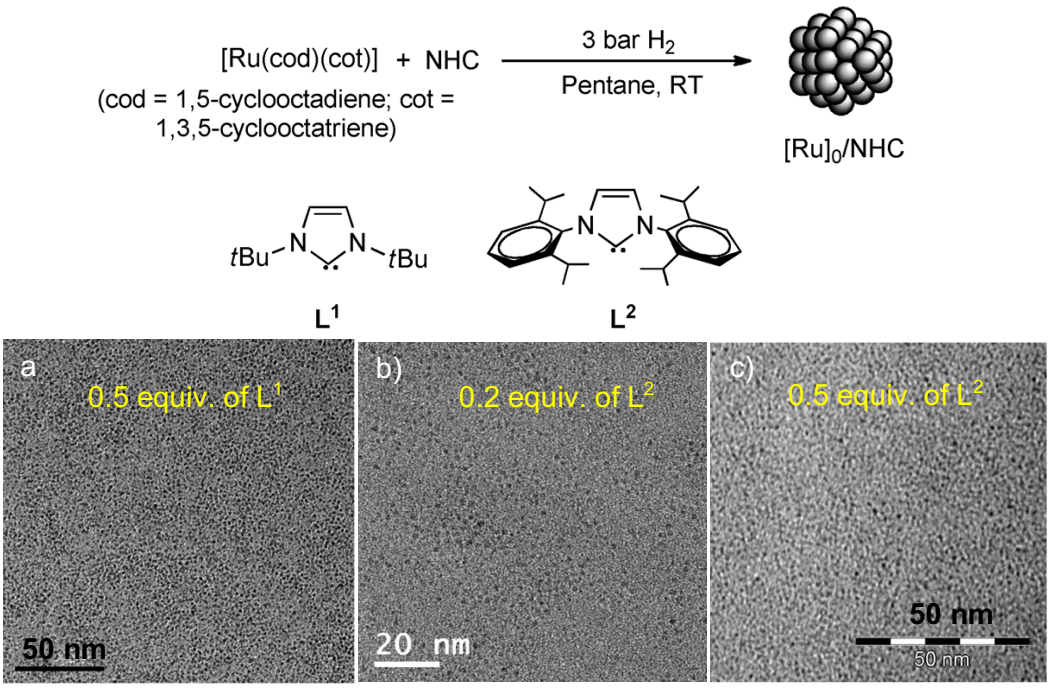

Figure III-6. *The N-heterocyclic carbenes (L^1 and L^2) and reaction conditions used for the synthesis of ruthenium NPs and (a-c) the corresponding TEM images. (Copyright from Ref.[22a])*

As shown in Scheme III-1iii, the preparation of NHC-functionalized metal NPs can be reached via a ligand-exchange process where the capped ligand on the nanoparticle surface are replaced by other better stabilizers which bind more strongly to the NPs. The first investigation of NHC-stabilized metallic NPs via ligands exchange was reported by Chechik *et al.* (2009).[33] They described the preparation of NHC-coated AuNPs by the ligands exchange of thioether-capped AuNPs. After the ligand-exchange, the nanoparticle size (2.6 ± 0.5 nm) was maintained (Figure III-7). However, the obtained NHC-AuNPs was found to be more stable in air compared to the initial thiol-coated AuNPs. The study of the ligands exchange on the surface of nanoparticle was carried out by XPS analysis of NPs, which demonstrated the disappearance of S (S_{2p}) and the appearance of a peak corresponding to N (N_{1s}). The colloidal solution was also analyzed by MS and NMR which showed the presence of $[NHC\text{-}Au\text{-}NHC]^+$.

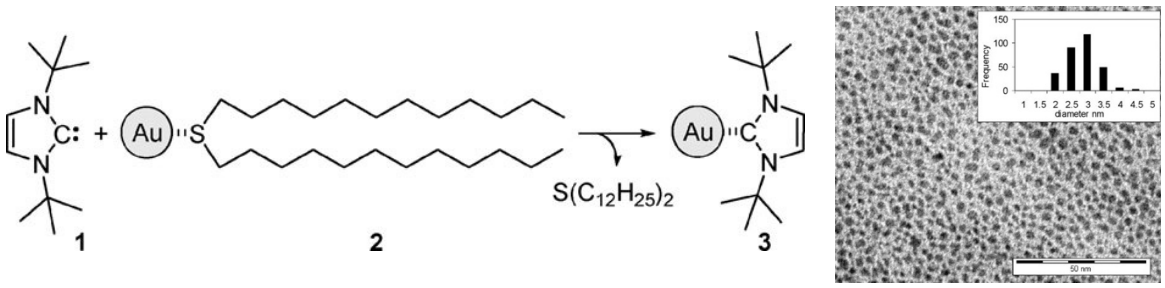

Figure III-7. *Synthesis of NHC-protected Au NPs and the corresponding TEM image. (Copyright from Ref.[33])*

Later on, B. J. Ravoo and co-workers[34] studied the steric effect of N-substituents of NHC in the NHC-stabilized PdNPs synthesis by the same strategy. Two NHCs ligands with different steric hindrances (N-Methyl and N-Bn) were chosen to displace the weaker thioether ligands from PdNPs (4-4.5 nm) (Figure III-8). They observed that the N-Methyl NHC lead to better ligand exchange than the N-Bn analogue. They proved that the small and flexible N-substituents of the imidazole-ring play an important role in the stabilization of PdNPs due to the small steric repulsion between the NPs surface and NHC ligands, while the long alkyl chains would become a protective monolayer that prevents the aggregation of NPs (Figure III-8c).

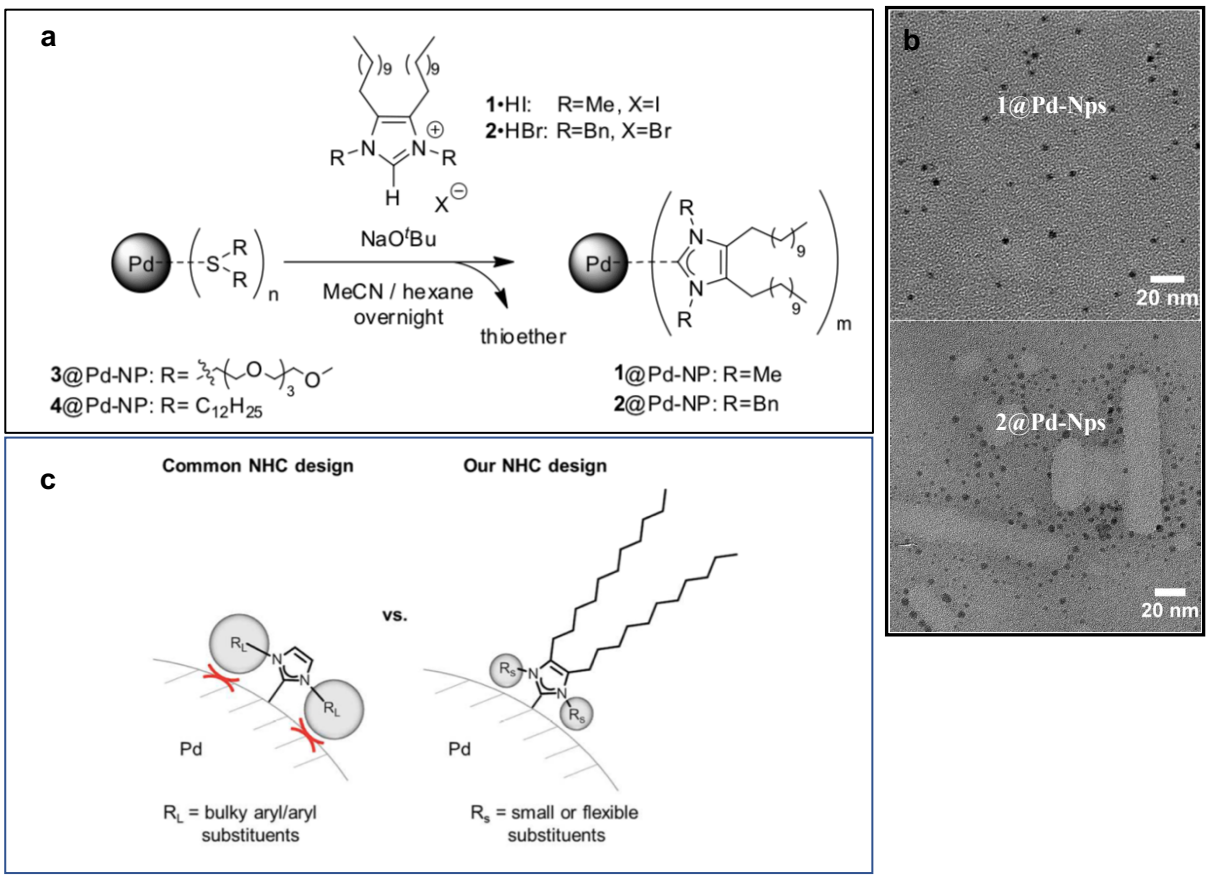

Figure III-8. *(a-b) Ligand exchange reaction on thioether stabilized Pd-NPs with LC-NHCs and the corresponding TEM images of obtained NHC-PdNPs (c) Comparison of different NHC designs. (Copyright from Ref.[34])*

The N-Heterocyclic carbenes are versatile capping agents to stabilize and to functionalize the metal NPs. Compare to others common ligands (e.g., thiols, amines or phosphines), the NHCs ligands present many advantages, such as their strong donating properties and their strong affinity to transition metals. However, the types of NHCs-stabilized metal NPs are not only still limited to few metals, but also the shape control synthesis of NPs was not well developed.[35] Until now, although a number of methods were reported in the synthesis of CuNPs,[36] their high oxygen sensitivity during the preparation is still challenging for the CuNPs synthesis. Due to the specific properties of NHCs ligands (e.g. high stability, specific steric and electronic properties, strong affinity to metal copper),[6,37,38,39] they started to attract increased attention to apply in the CuNPs synthesis, in order to improve the air-stability of CuNPs and also prevent their aggregation over time.

Recently, the first investigation on colloidal NHC-stabilized CuNPs was reported by S. Carenco and co-workers.[39] Their study showed that the NHC-stabilized CuNPs with a size distribution of 11.6 ± 1.8 nm were obtained by the disproportionation of mesitylcopper(I)

precursor in the presence of NHC-boranes in refluxing toluene for 2.5 hours (Figure III-9). They demonstrated by XPS that the nature of bond between NHC ligand and the nanoparticle surface is covalent. Also, they proposed that the NHCs ligands play a role to be trapping the mesityl radical consequently release the Cu(0), meanwhile, they stabilize CuNPs as the major capping agents.

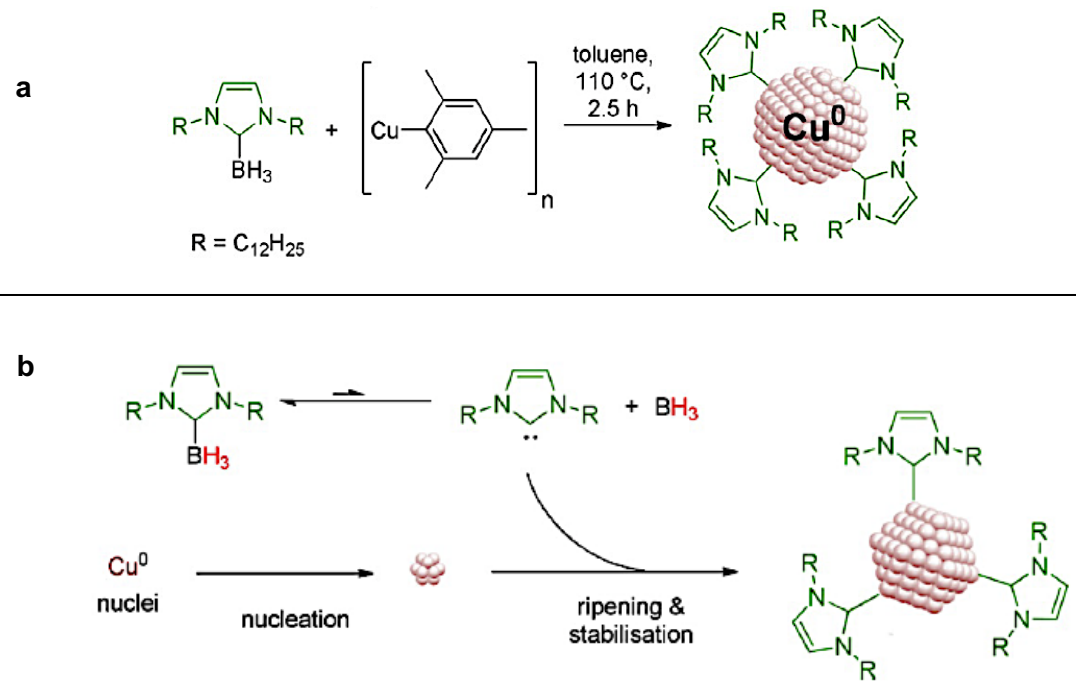

***Figure III-9**. (a) Proposed synthetic pathway using NHC-BH_3 adducts for the direct formation of copper NPs stabilized by NHC. (b) proposed pathway from Cu(0) nuclei to NHC-stabilized NPs by S. Carenco's group. (Copyright from Ref.[39])*

In Chapter II, copper NPs of tunable shape were synthesized using various phosphine ligands via a disproportionation route. In this chapter, a similar synthetic approach was used for synthetizing size- and shape-controlled CuNPs by using a range of CAACs-copper complexes as initial copper precursors.

In the previous work (Chapter II), we have compared the coordination energies between copper (0, I or II) and different types of ligands (e.g., PR_3 ligands, amine), herein, we also studied the ones of CAAC and NHC to copper, as seen in Figure III-10. As a result, the coordination between ligands and copper(0) increases in the following order : CAAC > NHC > $P(NMe_2)_3$ ≈ PMe_3 > PPh_3 > NH_2CH_3 > $P(OMe)_3$ > $P(O)Ph_3$ > $P(OMe)_3$. The CAACs ligands thus show their great potential as stabilizers in the synthesis of copper NPs.

$$CuXn + L \longrightarrow CuXnL\ (X = Cl,\ n = 0, 1, 2) \qquad (1)$$

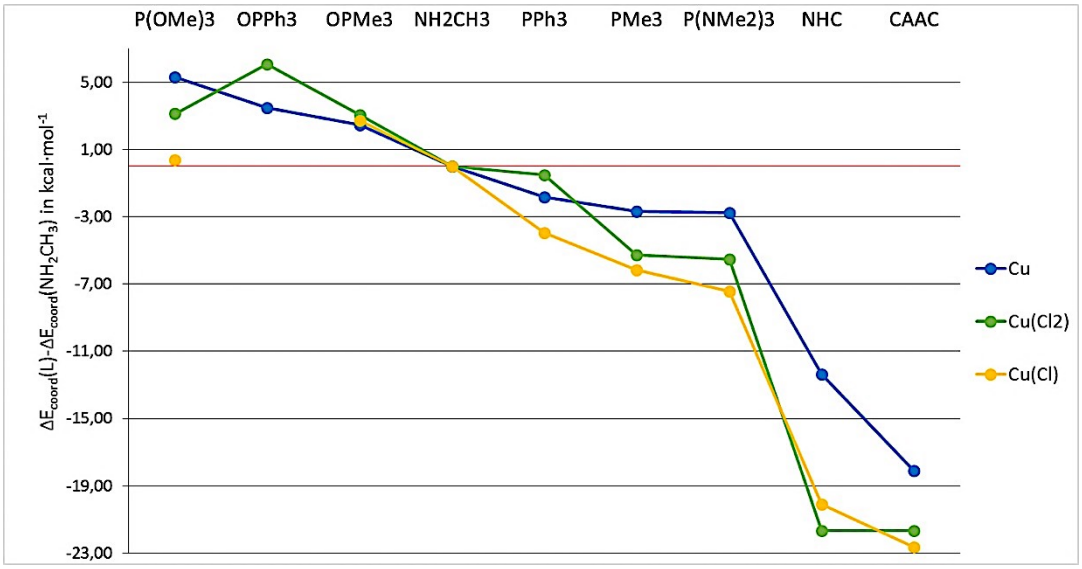

Figure III-10. *Comparison of coordination energy between the ligands (L: PR_3, NHC or CAAC) and CuX_n (n = 0, I, II; X = Cl, Br).*

In our work, the more nucleophile and electrophile cyclic (alkyl)(amino)carbenes (CAACs) ligands were chose for producing CuNPs. Unlike the investigation of S. Carenco,[39] the CuNPs were prepared in our work through a simple "one-pot" disproportionation reaction of CAACs-CuCl complexes in an organic solvent without adding reducers. All of the as-synthetized CAACs-CuCl complexes were prepared by J. L. Peltier, R. Jazzar and G. Bertrand's group from University of California (cooperative work).[6f,40,41]

The CAACs have been mostly synthetized by the "hydroiminiumation" route which was described by G. Bertrand's group.[42] The earlier route in 2005[12] (Figure III-11, top) shows the deprotonation of aldimine A with lithium diisopropylamide (LDA) leads to the aza-allyl anion which ring opens 1,2-epoxy-2-methylpro-pane, following subsequent treatment with triflic anhydride (TfOTf) and the cyclic aldiminium salts C are obtained. Lastly, the deprotonation of C with LDA gives the CAACs as a white solid. The method developed in 2007[42b] (Figure III-11, bottom) implies that the aza-allyl anions are formed by deprotonation of aldimines A and the reaction with 3-halogeno-2-methylpropene leads to the corresponding alkenyl aldimines B. Next, an excess of HCl is added and the reaction mixture is heated to form the cyclic aldiminium salts C. The final desired CAACs are achieved by the deprotonation of iminium salts C with a high yield.

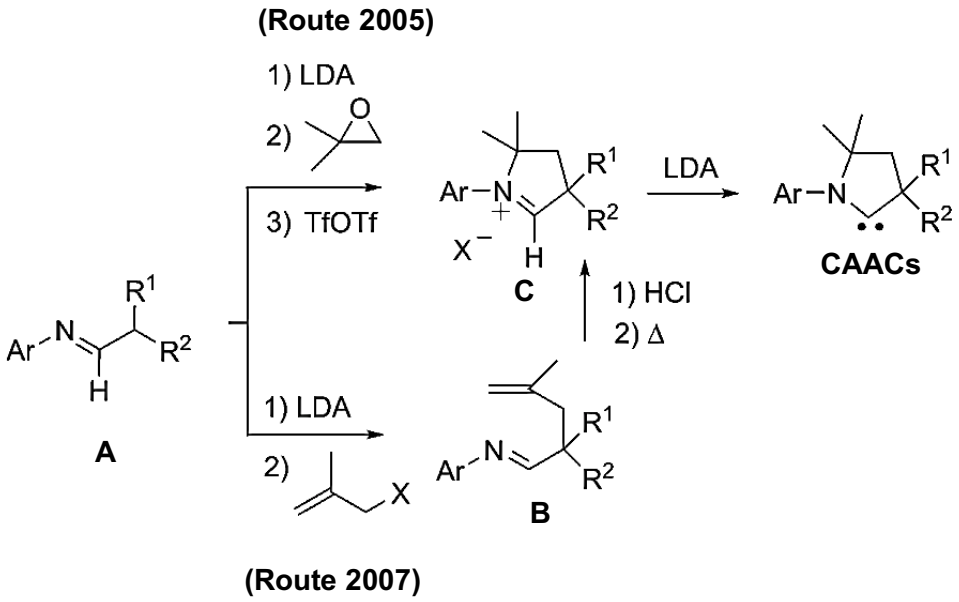

Figure III-11. *Two synthetic routes for obtaining CAACs which proposed by G. Bertrand's group. (Copyright from Ref.[6f])*

III. 3 Attempts of synthesis of copper nanoparticles from cyclic (alkyl)(amino)carbenes (CAACs)-CuCl complexes.

Controlling the size and shape of NPs is still the major challenge in the preparation of NHC-stabilized metal NPs.[16] To the best of our knowledge, the spherical shape is the most common morphology for NHC-coated metal NPs.[16,39] In this chapter, our goal is to synthetize CAACs-stabilized CuNPs with controlled size and shape by using a series of CAACs ligands (Figure III-12). Herein, CuNPs were prepared by a simple solution-phase method via the disproportionation of CAACs-CuCl complexes in alkylamine solvent. The general procedure is schematically illustrated in Scheme III-2. In this work, the synthesis parameters such as the steric effect of CAACs ligands, the concentration of precursor and the nature of amine solvent were investigated to deeper understand the formation process of CAACs-protected CuNPs.

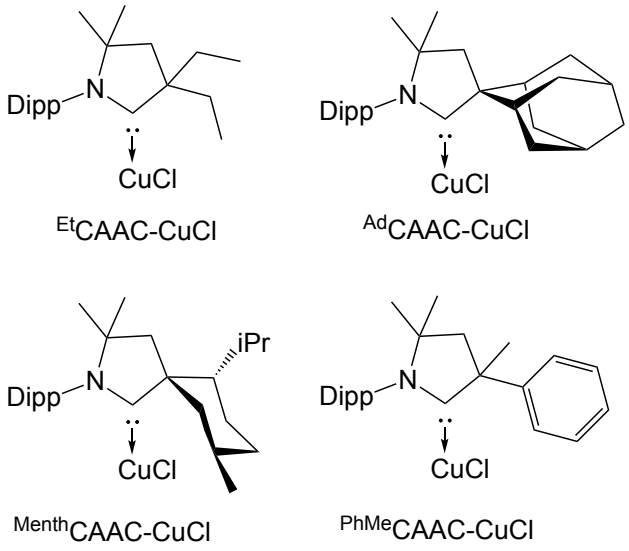

***Figure III-12**. Organometallic CAACs-CuCl complexes synthetized by G. Bertrand's group and used for the synthesis of CAACs-stabilized CuNPs in our work.*

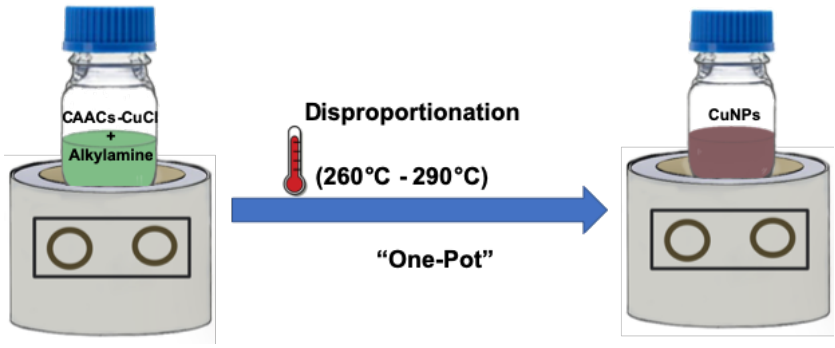

***Scheme III-2.** Schematic description of CuNPs synthesis from CAACs-CuCl.*

III. 3.1 Synthesis of CuNPs from ^{Et}CAAC-CuCl complex

For the first part of our work, the ^{Et}CAAC-CuCl complex with diethyl group as N-substituents, who have the smallest steric hindrance among the chosen CAACs ligands, was used for preparing the CuNPs.

III. 3.1.1 Effect of the amount of ^{Et}CAAC-CuCl complex and oleylamine

^{Et}CAAC-CuNPs were synthetized by a simple "one-pot" procedure in presence of only two reactants: ^{Et}CAACs-CuCl and oleylamine (Figure III-13, see Chapter V experimental section 3.2.A).

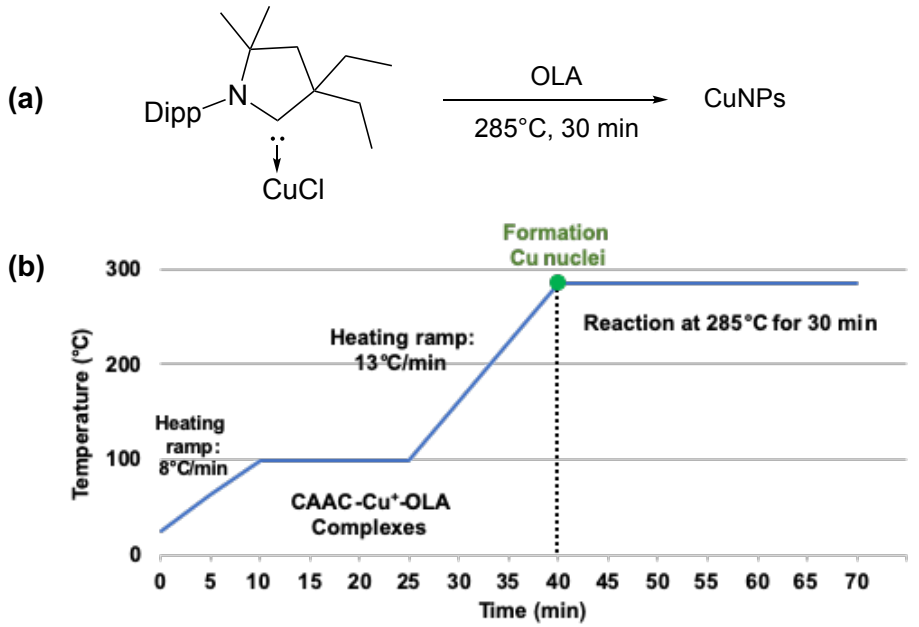

Figure III-13. *(a) Synthesis of CuNPs from ^{Et}CAAC-CuCl in oleylamine and (b) the corresponding graphic description of synthesis process.*

In a typical synthesis, n mmol (n = 0.15, 0.3, 0.6) of ^{Et}CAAC-CuCl is mixed in 4 mL of OLA in 25 mL vial capped with a septum pierced and connected to a schlenk line under nitrogen. The solution was stirred and heated to 100 °C in the sand bath, the temperature was maintained at 100 °C for 15 min (to dissolve all the salts) and a greenish solution was obtained. We proposed that the dissolution of salts during the heating for 15 min may be due to the formation of CAAC-Cu(I)-oleylamine complexes. To investigate this greenish solution, we compared the IR spectra of pure oleylamine (OLA) and of the mixture of ^{Et}CAAC-CuCl (30 mg) in OLA (1 mL) heated at 100 °C for 15 min (see Figure III-14). The N-H stretching vibration can be detected around 3338 cm^{-1} (blue), which is the characteristic peak of OLA. Two new peaks appear at 3289 and 3368 cm^{-1} which may due to the formation of Cu(I)-OLA through the

coordination of Cu(I) with the amine group of oleylamine.[43-45] In addition, a blue shift of the NH_2 bending (1619 cm^{-1}) was shown in the complex of Cu(I)-OLA compared to that in pure oleylamine (1574 cm^{-1}).[45,46] These results may indicated the formation of ^{Et}CAAC-Cu(I)-OLA complexes.

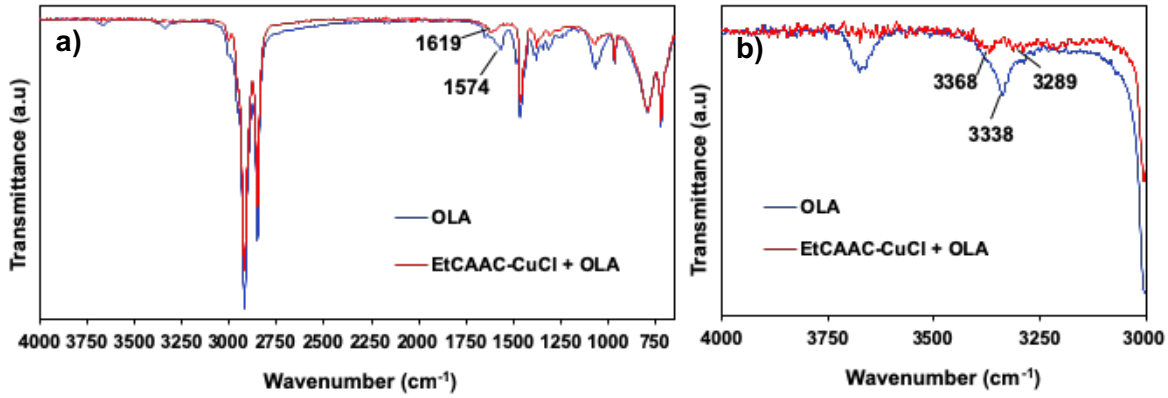

***Figure III-14**. IR spectra of Oleylamine and ^{Et}CAAC-Cu(I)-Oleylamine complex at frequency range (a) 4000-650 cm^{-1} and (b) 4000-3000 cm^{-1}.*

Subsequently, the temperature was quickly increased to 285 °C with a ramp of 13 °C/min. When the colorless solution slowly turned to gray, the reaction was maintained at 285 °C for 30 min, completing the synthesis NPs and giving a red-purple solution of copper NPs (Figure III-15). Then, the reaction solution was quickly put in a glove box under nitrogen atmosphere and naturedly cooled to room temperature. The NPs were precipitated with the addition of an excess of acetone and ethanol by centrifuging at 2500 rpm for 10 min to remove by-products. The obtained precipitate was then re-dispersed in hexane and centrifuged at 4000 rpm for 5 min. After two washing cycles, the precipitated NPs as a red solid were dried inside the glove box and kept for further analysis. As expected, the blue color of the supernatant observed after the washing procedure suggested the presence of Cu(II) in the solution, and thus that a disproportionation reaction took place.

Figure III-15a shows the typical TEM image of CuNPs prepared from 0.15 mmol of ^{Et}CAAC-CuCl. A mixture of triangular and ill-defined quasi-spherical NPs were observed. When the amount of ^{Et}CAAC-CuCl was increased from 0.15 to 0.3 mmol, the CuNPs change from triangular shape (mean perpendicular height equal to 146 ± 30 nm in) to a mixture of smaller cubic shape (mean edge length equal to 79 ± 12 nm) and few nanospheres (the ratio of cube/sphere is around 7/3 by counting about 300 particles) (Figure III-15b). Interestingly, once the amount of CAAC-CuCl complexes was increased to 0.6 mmol, well-defined nanowires with a mean size of 48.5 ± 16.3 nm in diameter and a few cubes were observed (Figure III-15c).

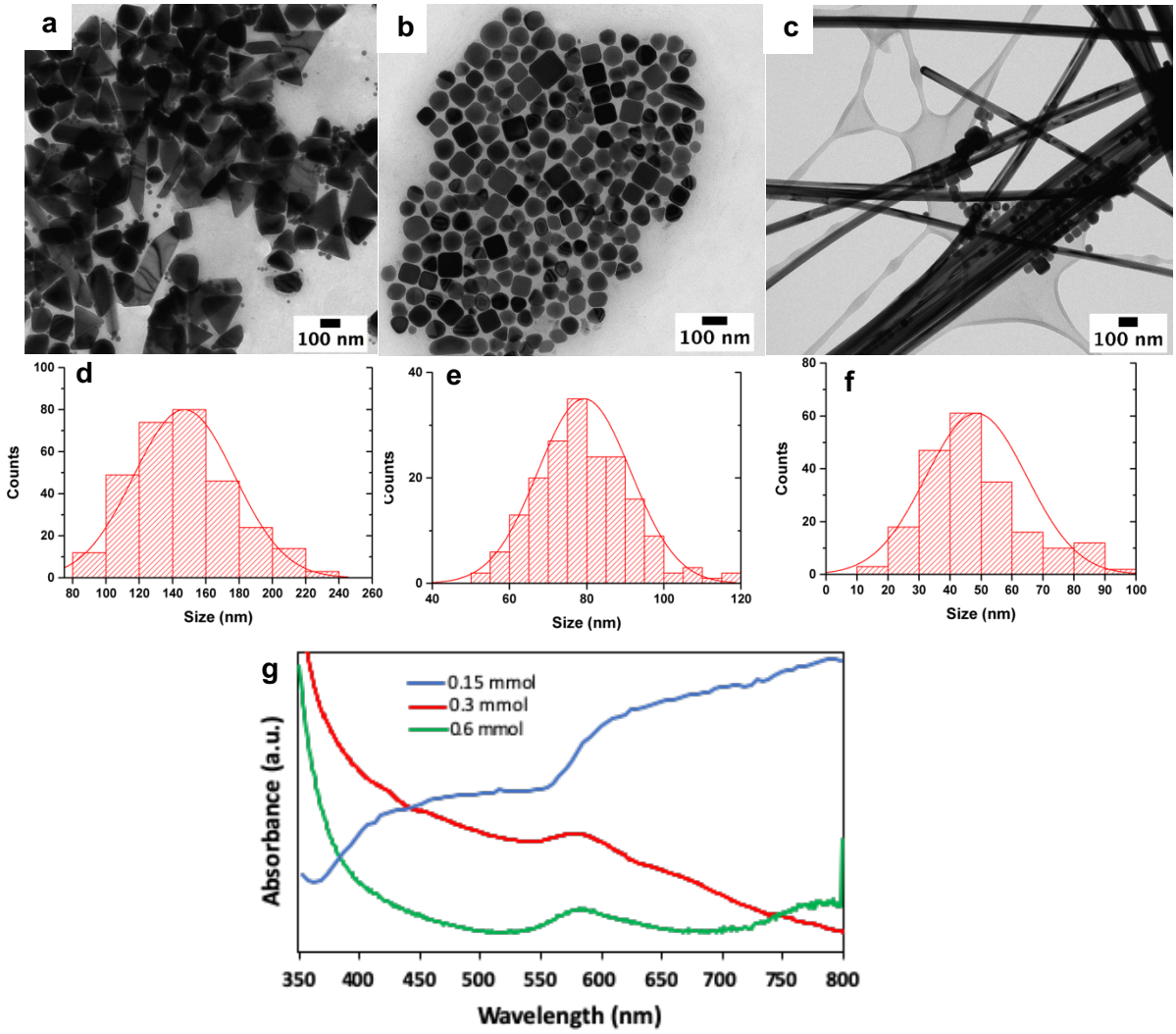

***Figure III-15**. Typical TEM images of CuNPs synthetized from different amounts of ^{Et}CAAC-CuCl of (a) 0.15 (b) 0,3 (c) 0.6 mmol in 4 mL of OLA and (d, e, f) the corresponding size histograms and (g) the corresponding UV-vis spectra.*

Figure III-15g shows the UV-vis absorption recorded from ^{Et}CAAC-CuNPs dispersed in OLA as solvent and synthesized from different amount of ^{Et}CAAC-CuCl. Among group 11 metallic nanospheres, Cu displays the longest wavelength of interband transition appearance in the absorption spectrum (about 600 nm), resulting in the lowest LSPR intensity due to their location in the interband. We observed a shape-dependent optical characteristic of copper NPs. Triangular NPs showed two large SPR peak at around 445 nm and 615 nm (blue spectrum). The widening of the peaks can be attributed to the large size distribution. Nevertheless, these peaks can be assigned to the out of plane quadrupole and in-plane dipole plasmon resonance.[48] For cubic shape NPs, we observed a unique SPR peak at 580 nm overlapping with the background absorption due to by the interband transition. According to the literature,

there is a single LSPR peak in the absorption spectra because of their isotropic shape.[45,49] In the case of Cu nanowires, two SPR peaks were observed at 586 nm and around 800 nm. According to the literature,[50] the peak positions depend on the nanowire diameter and length.

In conclusion, the concentration of ^{Et}CAAC-copper precursor has a significant impact on the final morphology and sizes of the Cu NPs. According to the LaMer theory,[51] the concentration of nuclei is a very important factor in the synthesis of NPs, as a high concentration of nuclei favors the small size of nanoparticle and vice versa (see Chapter I). In the case of 0.15 mmol of copper precursor dissolved in 4 mL of OLA with the maintained reaction conditions, the relatively low concentration of nuclei yields large NPs. On the contrary, when the concentration of ^{Et}CAAC-CuCl complexes was increased to 0.3 mmol smaller particles were formed. However, the influence of the CAAC ligand on the final shape of the CuNPs is still unclear.

After studying the influence of the quantity of ^{Et}CAAC-CuCl in the formation of CuNPs, the volume effect of oleylamine was also investigated in the case of 0.3 mmol copper precursor. Its volume was thus modified from 4 mL to 8 mL to deeper understand its role in the CuNPs size and shape control. In this work, OLA appears to have a strong effect on the final NP size and shape. Figure III-16a shows the typical TEM image of CuNPs obtained from 8 mL oleylamine in the presence of 0.3 mmol of ^{Et}CAAC-CuCl precursor by maintaining other reaction conditions constant. The NP size decreased with an average size of 43 ± 3.9 nm and a polydispersity of 9%, the NP shape become more spherical with the disappearance of cubic shapes (as seen in Figure III-15b). The corresponding UV-visible spectra is shown in Figure III-16c. An extremely broad LSPR peak with a maximum around 713 nm was observed which may be due to the superposition of different absorption peaks from broad size distribution or the aggregation of NPs (a few precipitates was observed in the colloidal solution). Interestingly, after comparing the results obtained from the same concentration of copper precursor: 0.15 mmol Cu(I)/4 mL OLA (Figure III-15a) vs 0.3 mmol Cu(I)/8 mL OLA (Figure III-16a), the different final shapes of CuNPs synthetized in both conditions were also observed. We hypothesized that the different total reaction volume may lead to the different temperature ramps of reaction solution, and thus would influence the nucleation and growth of NPs as the case of TOP discussed above (see Chapter II 4.1.1, page 50).

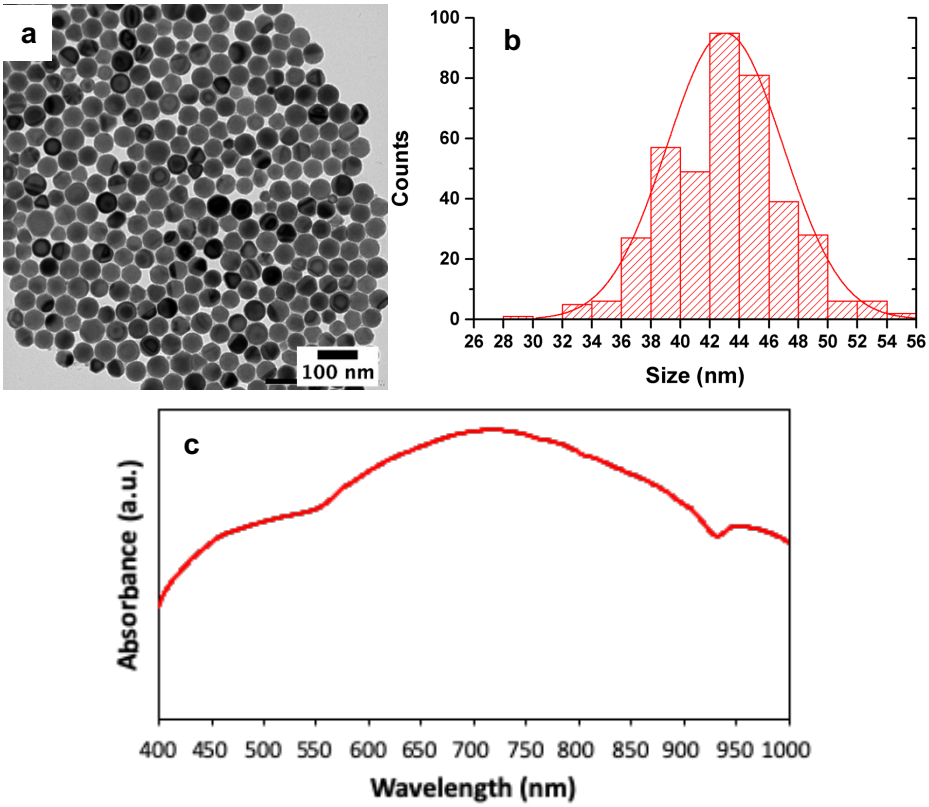

Figure III-16. *(a) Typical TEM image of CuNPs obtained from 0.3 mmol ^{Et}CAAC-CuCl in 8 mL of OLA (b) the corresponding size histogram and (c) UV-vis spectrum.*

XPS analysis

Due to the extreme sensitivity of Copper NPs to oxygen, we were unable to characterized their surfaces by IR analysis. Thus, we used X-ray photoelectron spectroscopy (XPS) to characterize the surface without exposing the sample to air.

XPS characterization of the NHC-stabilized metal NPs has been reported in the literature, such as Au,[54] Pd,[32] Pt[55] and Cu.[39] The coordination between the NHC ligands and NPs could be indicated by the C_{1s} and N_{1s} peaks and the position of latter.[54] In order to better understand the morphological evolution between the CuNPs synthetized in 4 mL and 8 mL oleylamine. The chemical state of surface and compositions of individual elements on these two NPs prepared were carried out by XPS measurements. All XPS results are collected in Table III-1, Figures III-17,18.

For the CuNPs obtained in 8 mL of oleylamine, the survey spectrum shows that this sample is composed of Cu, N, C, Cl and O (Figure III-17a). Firstly, the presence of copper was detected from Cu_{LM2} Auger spectra as shown in Figure III-18. In order to further identify the chemical metallic state copper, the Cu_{2p} peak was studied.[36] Two peaks at 932.43 eV and 952.18 eV were detected which corresponding to $Cu_{2P3/2}$ and $Cu_{2P1/2,}$ respectively. This could confirm that metallic copper was obtained in this NPs synthesis. Fitting the C_{1s} photopeak of CuNPs requires 3 contributions, each contribution is characteristic of a carbon chemical environment. The two peaks at 284.74 eV and 285.91 eV are the aliphatic carbons C-C and C-N, respectively. The 288.35 eV located the carbon, may be attributed to the satellite peak which come from the photoelectron excitation of the heterocycle ring.[53] The N_{1s} peak at 399.59 eV (At% = 2.3%) demonstrates the presence of N which may come from the NH_2 group of the oleylamine or also the N from heterocyclic ring of CAAC. Thus, these results do not allow to determine the percentage of CAAC ligand and oleylamine. Additionally, the presence of Cl^- ions on the CuNPs surface is shown by the Cl_{2p} photopeak at 198.05 eV (At% = 1.25%) which mostly come from the copper precursor ^{Et}CAAC-CuCl. The presence of oxygen may come from the washing step when the washing tube containing the NPs solution was moved out from the glove box. Oxygen contamination could also occur when the sample was introduced in the microscope.

For the CuNPs obtained in 4 mL of oleylamine (Figure III-17b, Figure III-18b), as was the case for NPs prepared from 8 mL, the N, C, Cl and O were detected. However, a large satellite peaks of Cu_{2p} at range of 938-948 eV was observed, which corresponds to a Cu-O bond and may be due to the oxidation of the sample during its transportation to Paris. After comparing the ratio of nitrogen (N) to copper deduced from the N_{1s} and Cu_{2p} peaks between these two CuNPs prepared in 8 and 4 mL of oleylamine, we found

that the N/Cu ratio of CuNPs (8mL) is lower (0.23) than that of CuNPs (4 mL) (0.39). The reason is still unclear.

Nevertheless, it is not fully possible to state on the presence of CAACs on the surface of the CuNPs from the XPS results.

***Table III-1**. XPS data for ^{Et}CAAC-CuNPs obtained from 8 mL and 4 mL of OLA.*

Sample	Elements	Peak BE	FWHM eV	Area (P) CPS.eV	Atomic %
$CuNPs_{(8\ mL)}$	Cu2p	932.43	1.28	258892.58	10
	Cu LM2	569.98	4.2	212829.67	0
	C1s	284.74	1.22	85475.01	49.28
	C1s A	285.91	1.75	10899.78	6.29
	C1s B	288.35	1.83	3440.54	1.99
	Cl2p	198.05	1.2	6267.74	1.25
	N1s	399.59	1.4	6202.84	2.3
	O1s	532.04	2.18	121091.95	28,89
$CuNPs_{(4\ mL)}$	Cu2p	934.68	2.99	150941.08	1.59
	C1s	285.06	0.98	125026.19	26.49
	C1s A	286.20	1.40	27028.06	5.73
	C1s B	288.42	1.85	15111.15	3.20
	N1s	400.03	1.83	5115.70	0.62
	O1s	532.25	2.14	96884.48	7.43

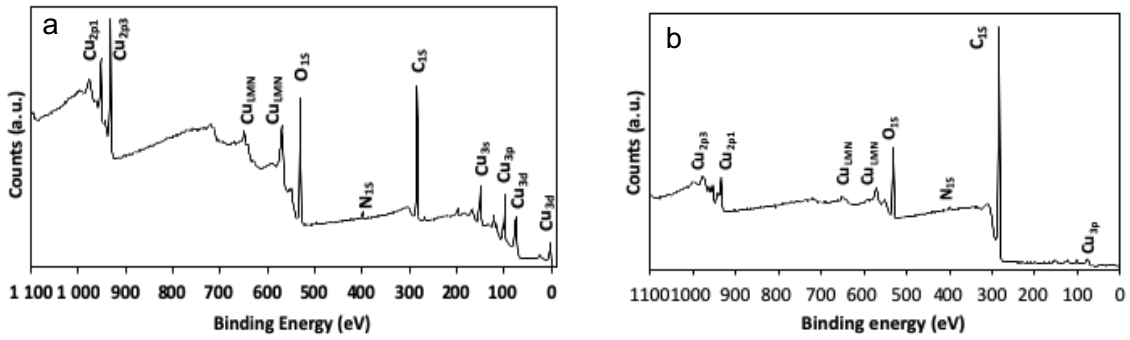

***Figure III-17**. XPS survey spectra of ^{Et}CAAC-CuNPs prepared from ^{Et}CAAC-CuCl as precursor in different volumes of oleylamine (a) 8 mL (b) 4 mL.*

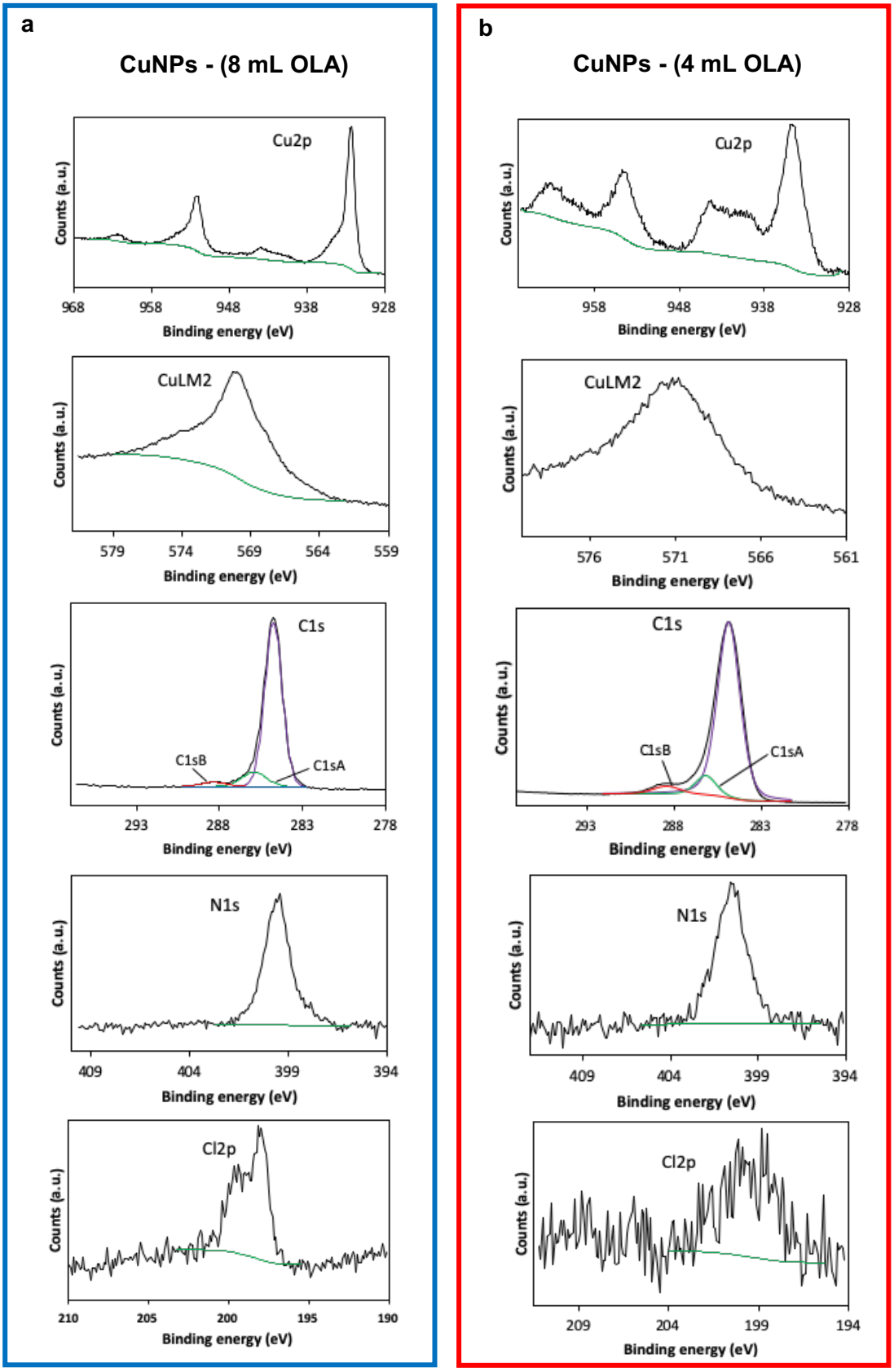

Figure III-18. *High resolution XPS spectra of Cu_{2p}, Cu_{LM2}, C_{1s}, N_{1s}, and Cl_{2p} of CuNPs prepared from ^{Et}CAAC-CuCl as precursor in different volumes of oleylamine (a) 8 mL (b) 4 mL.*

III. 3.1.2 Effect of the nature of the amine used as solvent.

In the current preparation of CuNPs, we evidenced that the solvent oleylamine plays an important role for obtaining the controlled size and shape of NPs, through the added volume. We have studied the effect of different primary amines on the shape-controlled synthesis of CuNPs in Chapter II. It is well known that the boiling point of the solvent is able to directly influence the size of particles.[57,60] The high boiling point (Bp) of the solvent increases the reactivity of the chemical compounds which lead to increase in the diameter of particle, and vice versa.[56] In the next investigations, we have chosen the dodecylamine (DDA) and also the binary solvent contains oleylamine (Bp: 364 °C) and dodecylamine (Bp: 259 °C) as solvent in our typical method synthesis (Figure III-19, see Chapter V experimental section 3.2.B and 3.2.C).

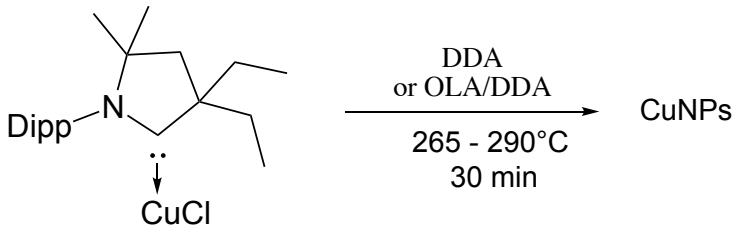

Figure III-19. *Synthesis of CuNPs from ^{Et}CAAC-CuCl in dodecylamine or a binary solvent (OLA/DDA).*

Figures III-20a, b show the typical TEM image of CuNPs obtained with an average size of 16.2 ± 2.3 nm (σ% = 14%) when oleylamine was replaced by dodecylamine (for a total volume of 4 mL) under a lower temperature 265 °C for 30 min. The size and morphology of NPs appear significantly modified with a decrease of the size and more anisotropic shapes. During the synthesis, a yellow solution was observed after heating at 100 °C during 15 min, which may indicate the CAAC-Cu(I)-DDA complex formation.[58] This complex formation was characterized by IR spectroscopy. The dodecylamine was shown to bond to copper ions by N-H functional groups.

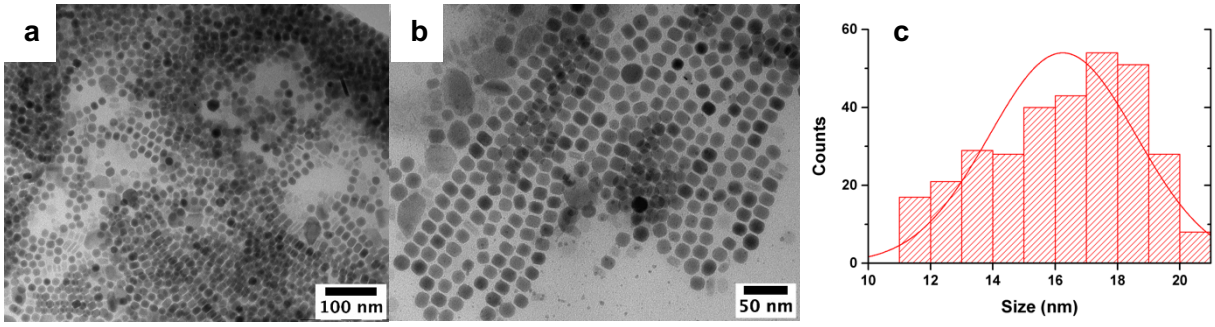

***Figure III-20**. (a-b) Typical TEM images of CuNPs synthetized when dodecylamine (DDA) was used as solvent and (c) the corresponding size histogram.*

Indeed, IR analysis was carried out on the mixture of ^{Et}CAAC-CuCl (30 mg) in DDA (1 mL) was heated at 100 °C for 15 min and compared to IR spectra of DDA, as shown in Figure III-21. The amine (N-H) stretching peaks of dodecylamine, appearing at 3168, 3255 and 3330 cm^{-1} correspond to values reported in the literature (blue).[59] The absence of (N-H) stretching band at 3330-3168 cm^{-1} of dodecylamine and two new peaks observed around 3372 and 3282 cm^{-1} are mostly attributed to the Cu(I)-DDA and the coordination of Cu(I) to the amine group of DDA (red). A similar phenomenon is reported by X. Zhou *et al*.[59] They show indeed that the Ag-DDA complex leads to the disappear of the amine (N-H) stretching peaks of dodecylamine at 3159, 3141 and 3323 cm^{-1}.

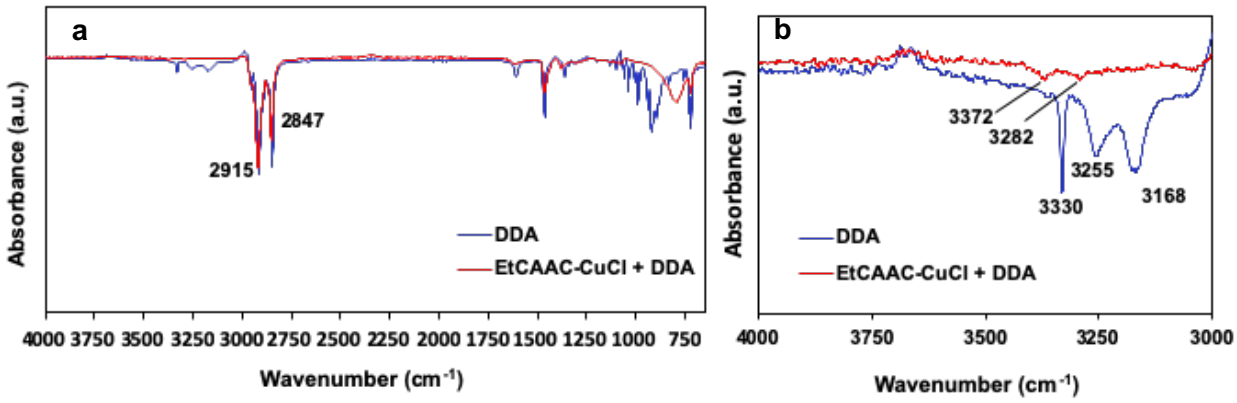

***Figure III-21**. IR spectra of Dodecylamine (DDA) and ^{Et}CAAC-Cu(I)-Dodecylamine complex at frequency range (a) 4000-650 cm^{-1} (b) 4000-3000 cm^{-1}.*

Subsequently, we used a binary solvent composed of OLA and DDA with different volume ratios of 1:1 and 3:1 for a total volume of 4 mL to synthetize ^{Et}CAAC-CuNPs. All experiments were performed by using the synthesis protocol described above (Figure III-14) at 290 °C for 30 min. Figure III-22 shows the TEM images of ^{Et}CAAC-CuNPs prepared from

the binary solvent of OLA/DDA with a volume ratio of 1:1 or 3:1, respectively. Polydisperse NPs (179 ± 31 nm) of mixed morphologies (cubic and quasi-spherical) were obtained with a volume ratio of 1:1 (OLA : DDA) (Figure III-22a). Interestingly, when this ratio was increased to 3:1, the NP mean size decreased to 96.6 ± 14.9 nm and well-defined pyramidal shaped NPs were formed, as shown in Figures III-22c, b. The advantage of these morphologies, compared to more classical spheres, is that they allow a better control of the optical properties (plasmon, color, local field) as a function of their dimensions. These shapes may also be of interest in catalysis for optical imaging or for detection in biological system. Single pyramidal NPs are also observed. The colloidal solution was analyzed by UV-visible spectroscopy (Figure III-22f). The spectrum displays two broad LSPR peaks at around 450 nm and 715 nm. Indeed, anisotropic particles should exhibit two or three peaks, depending on their shape.[61] The broadening of the peak could be due to large size distribution.

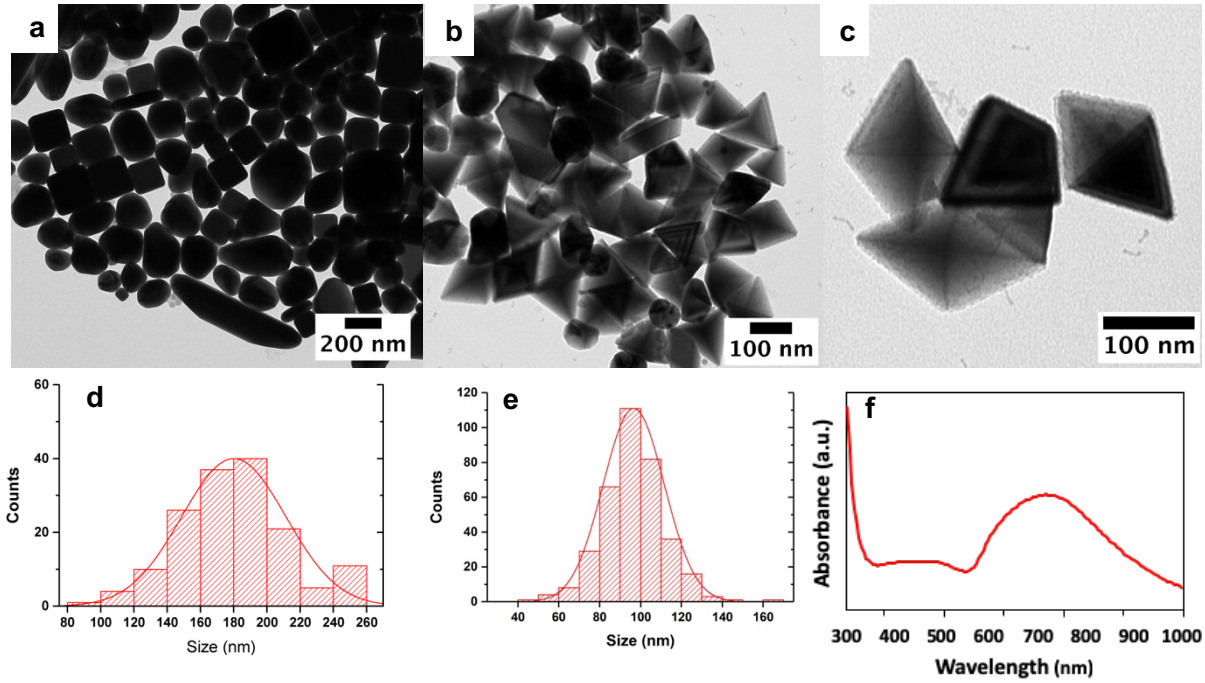

Figure III-22. *Typical TEM images of CuNPs synthetized in a binary solvent of OLA/DDA with different volume ratios of (a) 1:1 (b, c) 3:1 (d, e) the corresponding size histograms (f) UV-vis spectrum of nanopyramids obtained from the volume ratio of 3:1.*

For the further characterization of these copper pyramids, high-resolution transmission electron (HRTEM) and X-ray diffraction analysis were performed. Figure III-23a shows a HRTEM image of an individual pyramidal NPs. A lattice distance of 0.2 nm was deduced which correspond to space between (111) planes ($d_{(111)}$=0.21 nm) in *fcc* Cu (a= 0.3615 nm). Figure III-23b shows the

selected area electron diffraction (SAED) pattern performed on a set of pyramidal NPs and demonstrate that the nanopyramids correspond to metallic copper.[63]

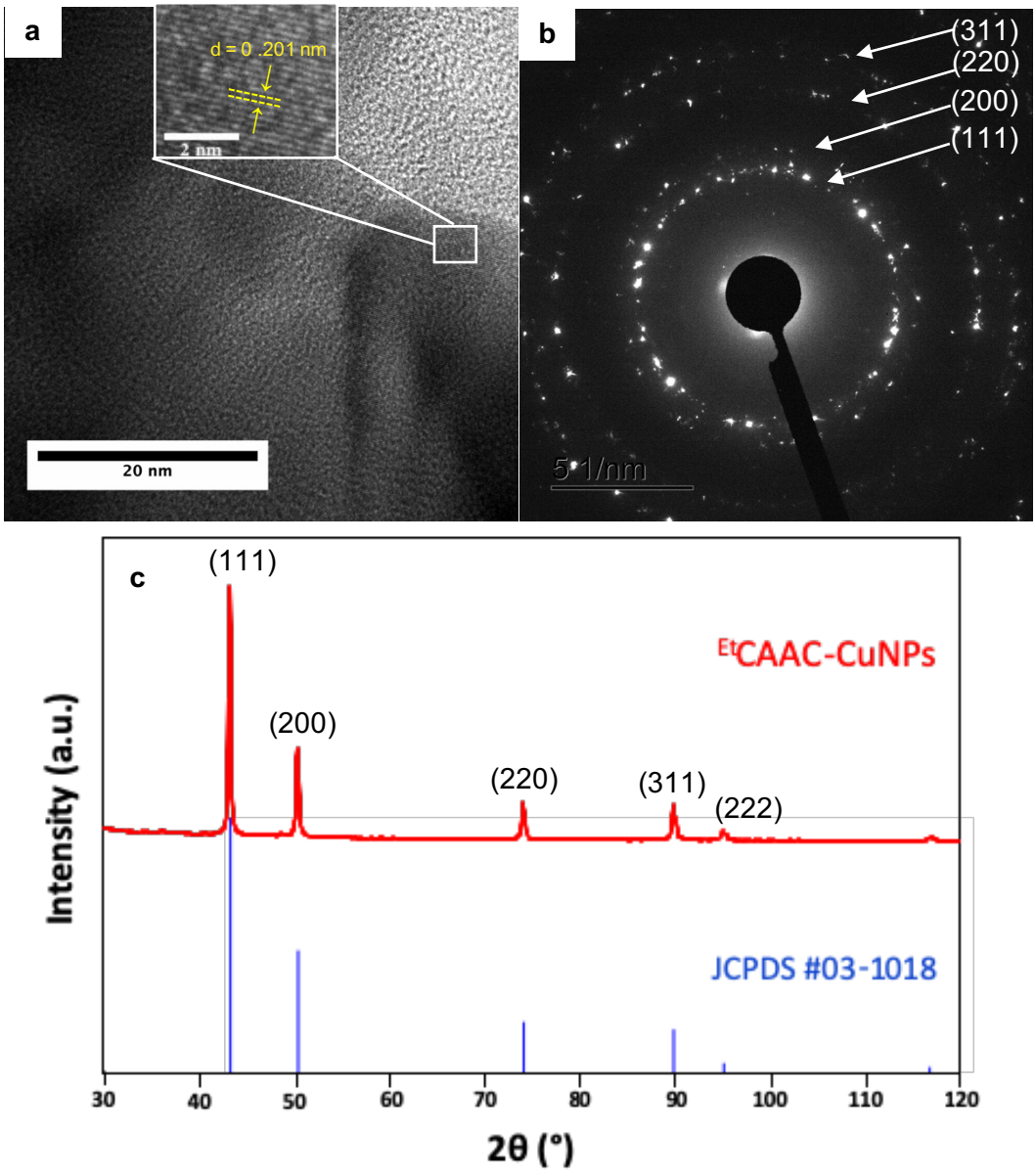

Figure III-23. *HRTEM images of (a) fcc single crystal (b) the corresponding SAED pattern and (d) powder XRD pattern (red: experimental, blue: theoretical) of CuNPs prepared from the mixture of OLA and DDA with a volume ratio of 3:1.*

The crystal structure of these pyramid-shaped CuNPs was also studied by Powder X-ray diffraction (XRD), as shown in Figure III-23c. The diffraction peaks located at 43.2°, 50.4°, 74.0°, 89.9° and 95.1° can be indexed to the (111), (200), (220), (311) and (222) crystal planes of *fcc* Cu, which in good agreement with reference JCPDS#03-1018. This confirms that the synthetic method developed here allows to form high crystal phase purity CuNPs.

To get insight into the elements present on the surface of the copper nanopyramids, energy-dispersive X-ray (EDX) was performed and mapping of the elements are presented of are shown in Figures III-24b. We observed that copper (Cu), nitrogen (N) and chloride (Cl) elements are uniformly distributed on the each of nanoparticle. N and C atoms may belong to the ^{Et}CAAC ligands or to the amine solvent. The element Cl on the particle surface must be from the precursor ^{Et}CAAC-CuCl. Figure III-24c shows the typical SEM image of the supposed CuNPs, confirming their pyramidal morphology.

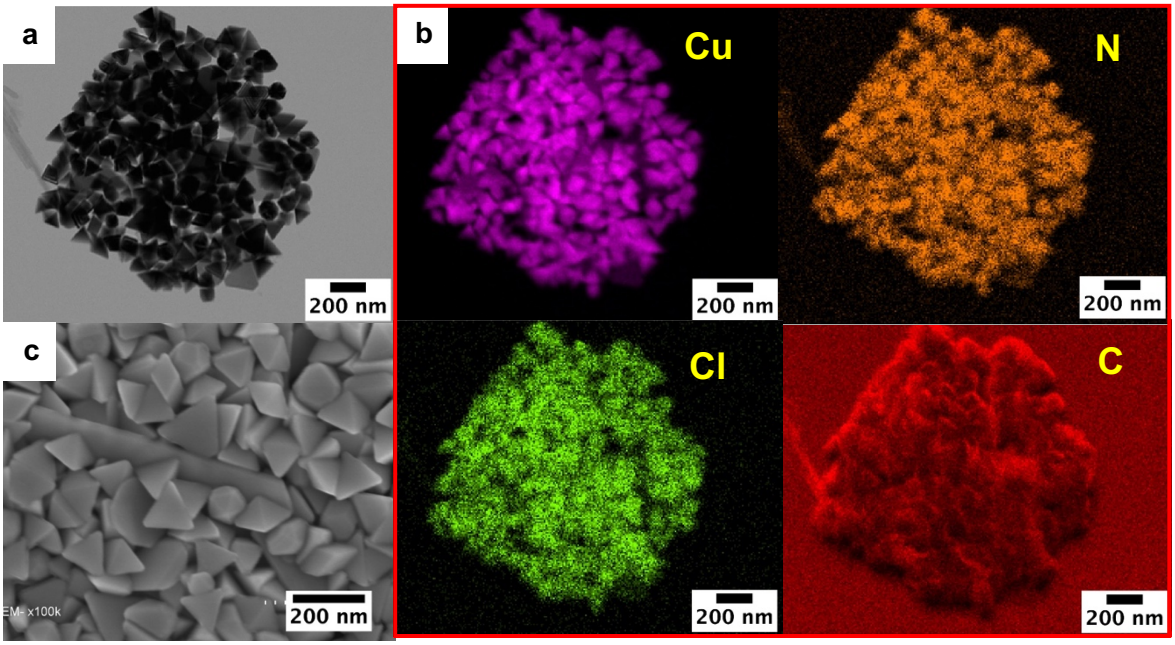

Figure III-24. *(a) Representative STEM image of Cu nanopyramids obtained from ^{Et}CAAC-CuCl in a binary solvent (OLA/DDA, 3/1) (b) corresponding elemental mapping of elements Cu, N, Cl, C and (c) corresponding typical SEM image.*

XPS analysis

XPS was carried out on the obtained pyramidal CuNPs obtained from the 3:1 of OLA:DDA ratio, to study the nature of the capping ligands on the particle surfaces. Results are reported in Table III-2 and Figure III-25, 26. As was the case for the CuNPs synthetized in pure oleylamine (see in section 3.1.1), C, N, Cl and O were detected and the copper spectrum is characteristic of metallic Cu(0). It is important to note that the signal of Cl_{2p} (At% = 1.5%) detected from the Cu nanopyramids (solvent OLA : DDA = 3 : 1) is remarkable. The capping agent role of Cl^- in the CuNPs shape control has been widely studied.[45,58] The C_{1s} spectrum showed 3 contributions, each contribution is characteristic of a carbon chemical environment. The two peaks at 284.77 eV and 285.86 eV may attribute to the aliphatic carbons C-C and C-N, respectively. The 288.39 eV located the carbon, may be attributed to the satellite peak which come from the photoelectron excitation of the heterocycle ring.[53]

***Table III-2**. XPS data for pyramid-shaped ^{Et}CAAC-CuNPs*

Element	Peak BE	FWHM eV	Area (P) CPS.eV	Atomic %
C1s	284.77	1.22	80662.37	48.94
C1s A	285.86	1.81	10922.87	6.63
C1s B	288.39	1.77	2815.59	1.71
Cl2p	198.1	1.13	7149.49	1.5
Cu LM2	570.3	4.41	152074.93	0
Cu2p	932.63	1.36	211887.63	8.62
N1s	399.6	1.25	5431.78	2.12
O1s	532.34	1.92	121367.29	30.48

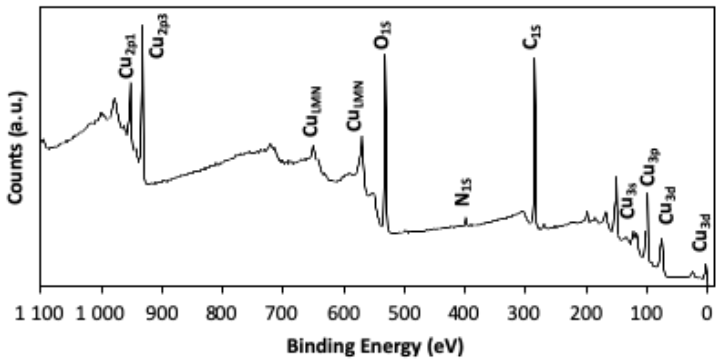

***Figure III-25.** XPS survey spectra of pyramidal CuNPs in a binary solvent OLA/DDA (3:1).*

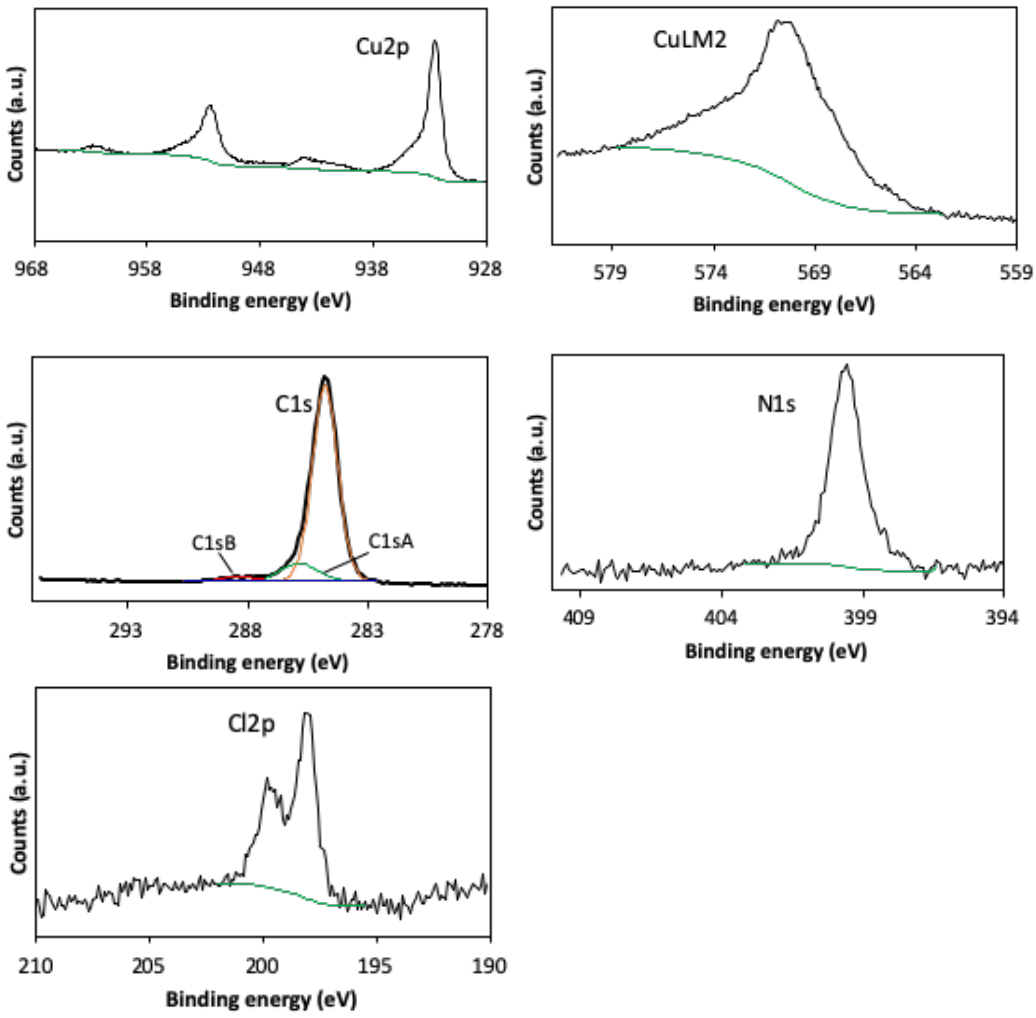

Figure III-26. *High resolution XPS spectra of Cu_{2p}, Cu_{LM2}, C_{1s}, N_{1s}, and Cl_{2p} of pyramidal CuNPs in a binary solvent OLA/DDA (3:1).*

***Table III-3**. Experimental conditions used for preparing CuNPs when ^{Et}CAAC-CuCl was used as the precursor with the corresponding size distributions.*

** For a total volume of 4 mL.*

Precursor			**Solvent**					**NPs Shape**	**NPs Size** (nm)	$\sigma^{\#}$ (%)
^{Et}CAAC-CuCl (mmol)			OLA (mL)		DDA (mL)	OLA/DDA*				
0.15	0.3	0.6	4	8	4	1:1	3:1			
✓			✓					Triangles (major)	146 ± 30	21
	✓		✓					Cubes, spheres	79 ± 12	15
	✓			✓				spheres	43 ± 3.9	9
	✓				✓			Quasi-spheres	16.2 ± 2.3	14
	✓					✓		Cubes, Quasi-spheres	179 ± 31	17
	✓						✓	Pyramids	96.6 ± 14.9	15
		✓	✓					Wires	48.5 ± 16.3	34

** For a total volume of 4 mL.*
$^{\#}$: Polydispersity

All results summarized in Table III-3 shown that the solvent nature and the concentration of copper precursor are critically important for controlling the shape and size of CuNPs prepared from ^{Et}CAAC-CuCl complex. As a result, increasing of ^{Et}CAAC-CuCl precursor concentration leads to the decrease of the mean particle size and also the shape was changed. It is worth noting that the small high-uniform spherical NPs can be produced when dodecylamine (DDA) is used as solvent instead of oleylamine. The use of binary mixture of DDA and OLA lead to more anisotropic shape such as pyramid or bipyramids depending on the volume ratio.

III. 3.2 Synthesis of CuNPs from ^{Ad}CAAC-CuCl complex

In this paragraph, CuNPs were prepared by replacing the ^{Et}CAAC-CuCl with ^{Ad}CAAC-CuCl as copper precursor, which brings more important steric hindrance on the N-substituent (Adamantyl). In this part, the influence of the amount of ^{Ad}CAAC-CuCl and the nature of amine solvent in nanoparticle synthesis was also studied.

III. 3.2.1 Effect of the amount of ^{Ad}CAAC-CuCl and oleylamine

The effect of different initial amounts of ^{Ad}CAAC-CuCl on the size and shape of CuNPs was investigated. All experiences were performed as the method described above (Figure III-13), the synthetic procedure see in Chapter V experimental section 3.2.D (Figure III-27).

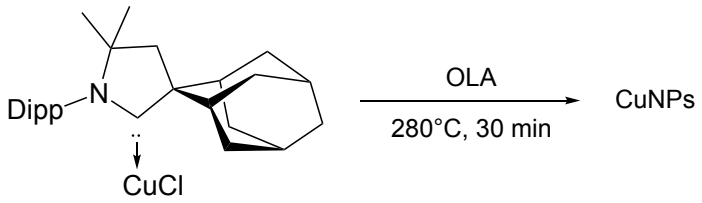

Figure III-27. *Synthesis of CuNPs from ^{Ad}CAAC-CuCl in oleylamine.*

In the typical synthesis, the solution of n mmol of ^{Ad}CAAC-CuCl (n = 0.15, 0.3 or 0.6) is mixed in 4 mL of oleylamine (OLA) in 25 mL vial capped with a septum and connected to a schlenk line under nitrogen. The solution was stirred and heated to 100°C in the sand bath, the temperature was maintained at 100 °C for 15 min (to dissolve all the salts) and a greenish-yellower solution was obtained. Similarly, the investigation of this greenish-yellower solution was performed by comparing the IR spectra of pure oleylamine (OLA) and of the mixture of ^{Ad}CAAC-CuCl (35 mg) in oleylamine (1 mL) previously heated at 100 °C for 15 min, (see Figure III-28). The N-H stretching vibration can be detected at about 3338 cm^{-1} (blue), which is a characteristic peak of oleylamine. We observed the N-H banding vibration shifts to 3213 cm^{-1} and a new peak located at 3126 cm^{-1} which is mostly due to the coordination of Cu(I) with amine group of oleylamine.[43-45] In addition, a blue shift of the NH_2 bending (1601 cm^{-1}) was shown in the complex of Cu(I)-OLA compared to that in oleylamine (1574 cm^{-1}).[45,46]

Subsequently, the temperature of the solution was quickly increased to 280 °C and kept at this temperature for 30 min. After cooling, a mixed solution of ethanol/acetone (1:1) was added to the NPs solution and the NPs were precipitated by centrifuging at 2500 rpm for 10 min, the obtained precipitated was re-dispersed in hexane and centrifugated at 4000 rpm for 5 min. After two washing cycles, the CuNPs were dried and kept for further analysis. Also, the blue color of the supernatant was also observed after the standard washing procedure

which suggesting the presence of Cu(II) in the solution, and thus showed that a disproportionation reaction underwent in this reaction condition.

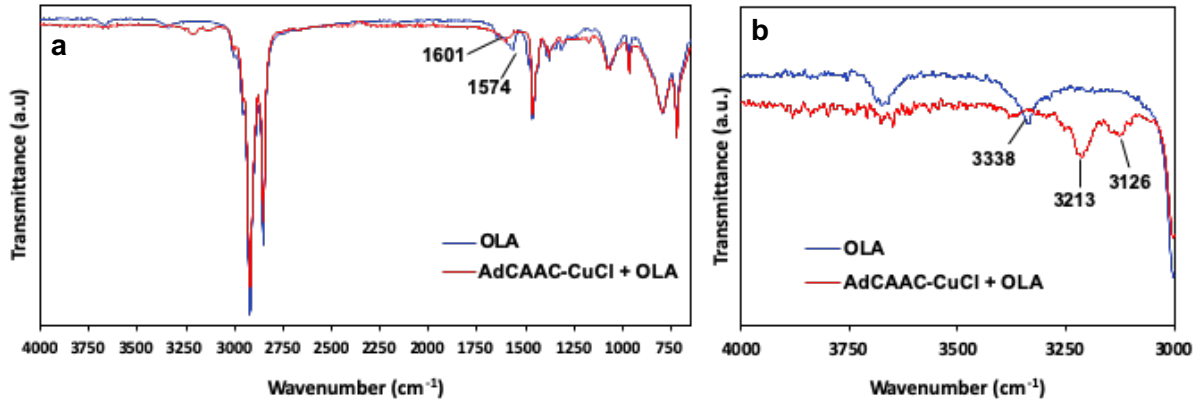

***Figure III-28**. IR spectra of OLA and ^{Ad}CAAC-Cu(I)-Oleylamine complex at frequency range (a) 4000-650 cm^{-1} (b) 4000-3000 cm^{-1}.*

The results of TEM analysis of synthetized copper NPs from different amounts of ^{Ad}CAAC-CuCl from 0.15 to 0.3 and 0.6 mmol and the corresponding size distribution histograms are shown in Figure III-29. As the amount of copper precursor increases, the shape of NPs evolves from monodisperse nanotriangles to high-uniform nanospheres and nanowires. In the case of 0.15 mmol of ^{Ad}CAAC-CuCl, the copper nanotriangles with an average size 29 ± 2.9 nm in perpendicular height and a low polydispersity (σ% = 10%) were observed (Figure III-29a). By increasing the concentration of ^{Ad}CAAC-CuCl, the NPs change from triangles to smaller spherical shape NPs (20 ± 1.4 nm, with a narrow size distribution (σ% = 7%) (Figure III-29b). For 0.6 mmol of copper precursor in 4 mL of OLA, nanowire with an average size of 44.3 ± 12.2 nm in diameter and a very few large triangles were observed (Figure III-29c).

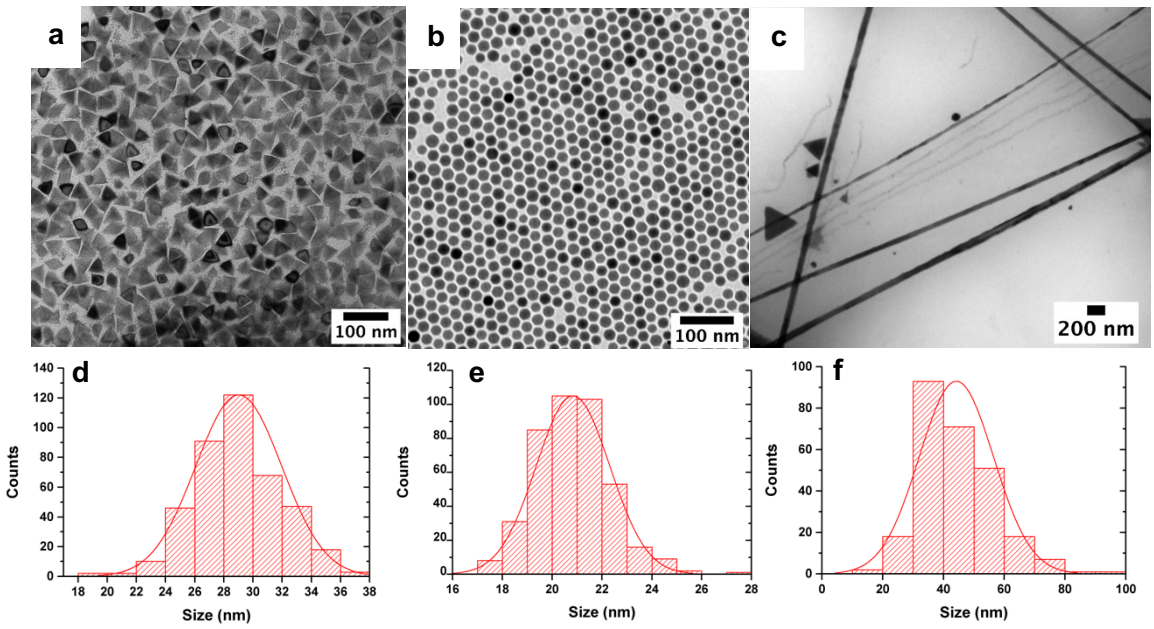

Figure III-29. *Typical TEM images of CuNPs synthetized from different amounts of ^{Ad}CAAC-CuCl of (a) 0.15 (b) 0.3 (c) 0.6 mmol and (d, e, f) the corresponding size histograms.*

In the previous section, we observed that the volume of oleylamine used had a dramatic effect on the final size and shape of the copper NPs. In the same way, herein, the volume of oleylamine was increased to 8 mL using 0.3 or 0.6 mmol of ^{Ad}CAAC-CuCl. As we can see in Figure III-30, the TEM analysis pictures show that different shapes of CuNPs were synthetized by increasing the oleylamine volume. The condition of 0.3 mmol ^{Ad}CAAC-CuCl/8 mL oleylamine promotes the synthesis of spherical NPs with an average size of 37 ± 7 nm (Figure III-30a). The shape of NPs changed from small sphere to large triangle (73.3 ± 15.7 nm in perpendicular height) when 0.6 mmol of copper precursor was used (8 mL of OLA) (Figure III-30b). In here, increasing the copper precursor concentration lead to the formation of larger NPs, as expected.

It is important to note that the morphology of NPs can be modified when the total reaction volume changes although the ratio of precursor/solvent is maintained. As shown in Figure III-29b, the uniform nanospheres were obtained from 0.3 mmol ^{Ad}CAAC-CuCl /4 mL of OLA. Nevertheless, the formation of nanotriangles was only observed from reaction condition of 0.6 mmol ^{Ad}CAAC-CuCl/8 mL of OLA (Figure III-30b). Although the ratios of Copper-to-OLA in both conditions equal to 0.075:1, however, the shapes of CuNPs obtained were completely different. This may due to different nucleation and growth of NPs with different reaction kinetics from the different solution volume (4 mL and 8 mL).

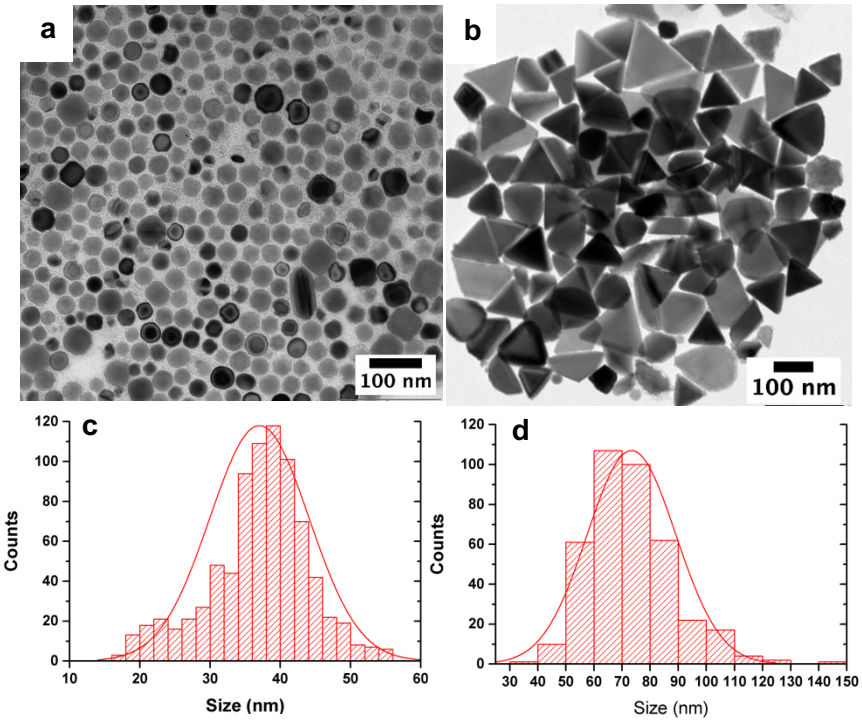

Figure III-30. *Typical TEM images of CuNPs synthetized from different amounts of ^{Ad}CAAC-CuCl of (a) 0.3 (b) 0.6 mmol for a total volume of oleylamine at 8 mL and (c, d) the corresponding size histograms.*

XPS analysis

These CuNPs prepared from the conditions of 0.3 mmol ^{Ad}CAAC-CuCl/4 mL of OLA and 0.6 mmol ^{Ad}CAAC-CuCl/8 mL of OLA, were characterized by XPS (Table III-4 and Figure III-31-32). The survey spectra of both CuNPs show the presence of C, N, O and Cl.

In both cases of CuNPs, the high-resolution of C_{1s} and N_{1s} peaks demonstrated the presence of CAAC on the nanoparticle surface. As shown in Figure III-32a-C_{1s}, there are three components to the carbon peaks at 284.92, 286.12 and 288.58 eV which may correspond to the aliphatic carbons C-C, C-N and the satellite peak which may come from the photoelectron excitation of the heterocycle ring. In addition, the N_{1s} peak presents two components (Figure III-32b-N_{1s}). The major peak at 400.16 eV may correspond to the amine from oleylamine. The second, at 402.2 eV with a position in the higher binding energies suggests the presence of heterocycle (CAAC).

Interestingly, we observed that the obtained ratio between the Cl (Cl_{2p}) and copper (Cu_{2p}) of the CuNPs prepared from 0.6 mmol copper precursor in 8 mL OLA (0.96) is much higher than the one of CuNPs obtained from 0.3 mmol copper precursor/4mL OLA (0.13). This

may be due to the morphological difference between the two shapes (triangle and sphere) of the CuNPs obtained.

***Table III-4**. XPS data for CuNPs prepared from ^{Ad}CAAC-CuCl with different Copper-to-Oleylamine ratios.*

Sample	Name	Peak BE	FWHM eV	Area (P) CPS.eV	Atomic %
CuNPs (0.3 mmol/4mL)	Cu2p	934.57	2.59	278163.74	4.06
	C1s	286.12	1.52	20952.58	6.16
	N1s	400.18	1.84	3394.04	0.57
	O1s	532.03	1.84	127198.77	13.53
	C1sA	284.92	1.35	241016.79	70.81
	C1sB	288.58	1.34	16605.89	4.88
CuNPs (0.6 mmol/8mL)	Cu2p	932.89	1.97	75838.09	0.78
	C1s	284.86	1.68	293119.96	60.93
	N1s	400.16	1.91	5624.02	0.67
	O1s	532.59	2.56	76779.94	5.78
	C1sA	284.57	1.02	112817.96	23.45
	C1sB	288.90	2.11	7838.27	1.63

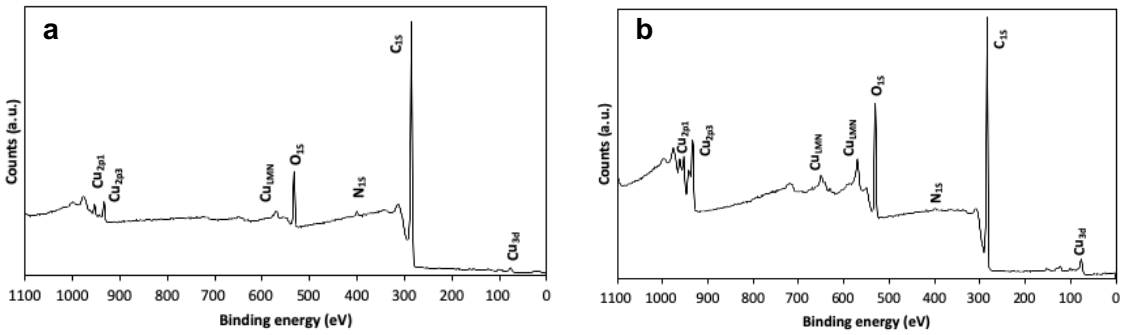

***Figure III-31.** XPS survey spectra of CuNPs obtained from different conditions: (a) 0.3 mmol ^{Ad}CAAC-CuCl/4 mL oleylamine and (b) 0.6 mmol ^{Ad}CAAC-CuCl/8 mL oleylamine.*

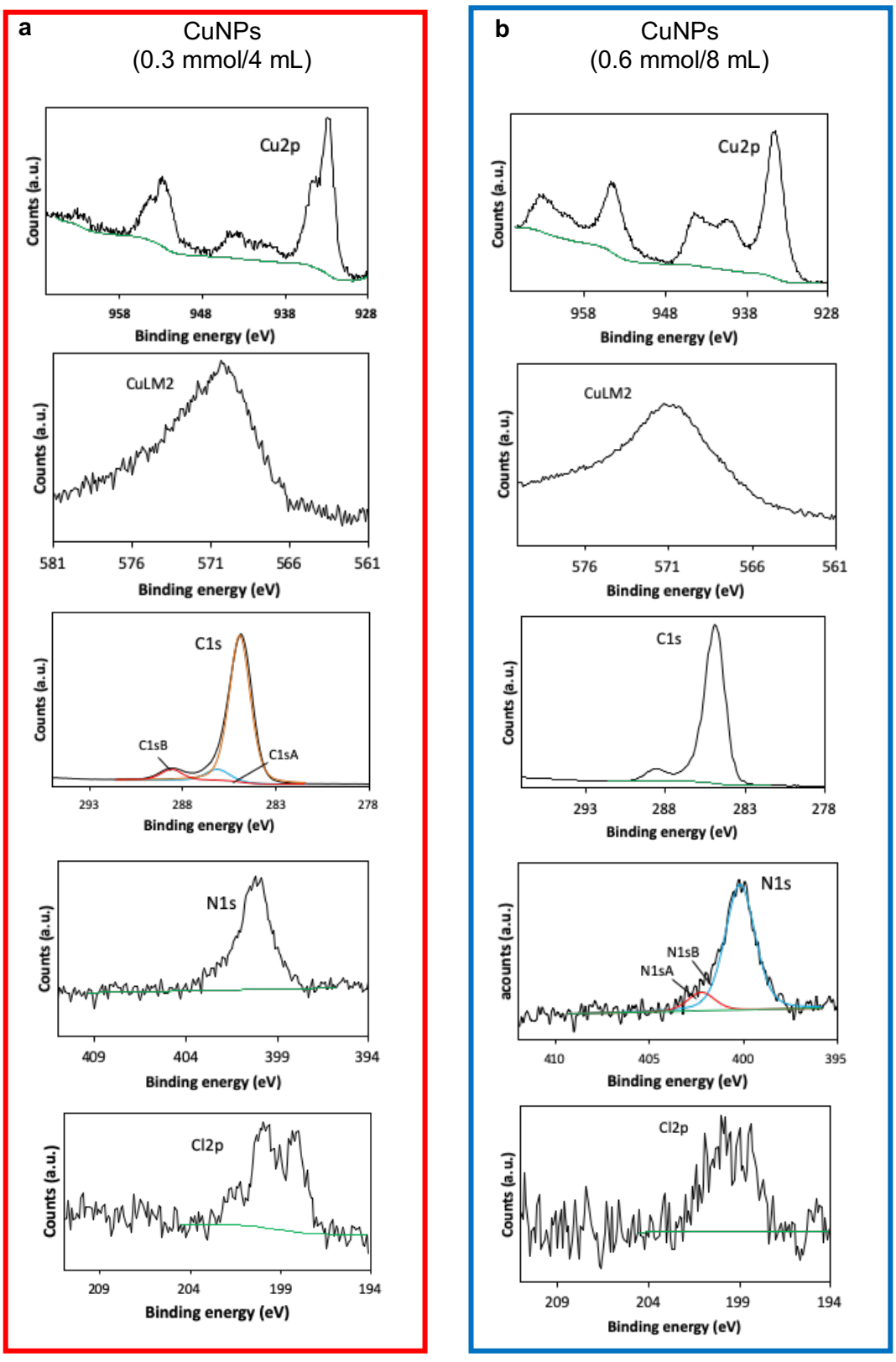

Figure III-32. *High resolution XPS spectra of Cu_{2p}, Cu_{LM2}, C_{1s}, N_{1s}, and Cl_{2p} of CuNPs obtained from different conditions: (a) 0.3 mmol ^{Ad}CAAC-CuCl/4 mL oleylamine and (b) 0.6 mmol ^{Ad}CAAC-CuCl/8 mL oleylamine.*

III. 3.2.1 Effect of the nature of amine

Since we observed that the shape and size of CuNPs obtained from ^{Et}CAAC-CuCl complex which were strongly dependent on the nature of the amine solvent, we also studied here the effect of the nature of the solvent on the preparation of CuNPs from ^{Ad}CAAC-CuCl. The synthesis of CuNPs was first investigated using only dodecylamine (4 mL) as a solvent, however, no formation of NPs was observed. Once 4 mL of a 3:1 volume ratio of OLA and DDA) was used, with a reaction temperature of 290°C and for a duration of 30 min (Figure III-33, Chapter V experimental section 3.2.F), NPs were observed by TEM (Figure III-34).

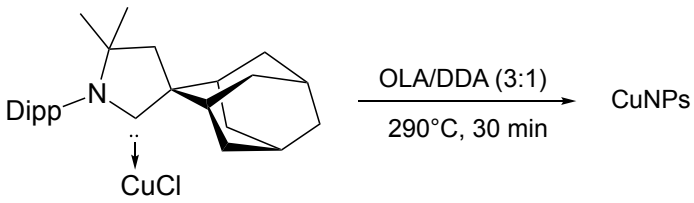

Figure III-33. *Synthesis of CuNPs from ^{Ad}CAAC-CuCl in a binary solvent of OLA/DDA (3:1) for a total volume of 4 mL.*

The TEM images show copper NPs with spherical morphology, an average size of 23.8 ± 0.5 nm and a very low polydispersity of 2%.

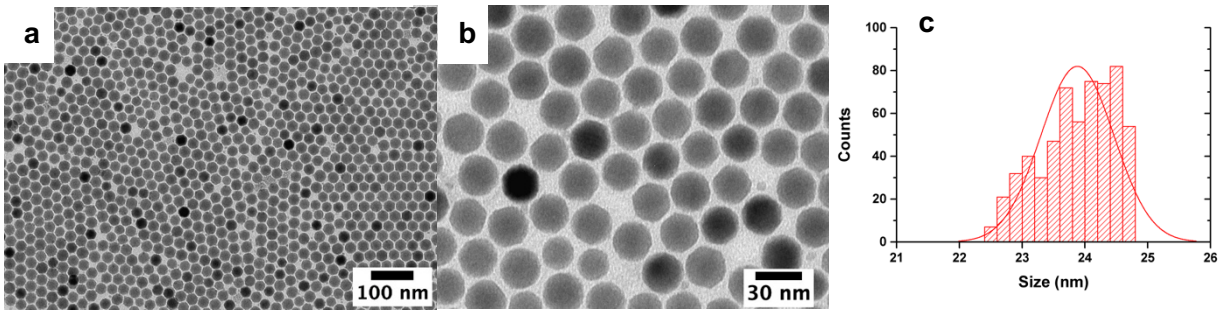

Figure III-34. *(a, b) Typical TEM images of CuNPs synthetized from the reaction condition of 0.3 mmol of ^{Ad}CAAC-CuCl in the mixed solvent of OLA/DDA (volume ratio: 3:1) for a total volume of 4 mL and (c) the corresponding size histogram.*

After comparison with the NPs obtained in oleylamine alone (Figure III-29b), it was observed that the binary mixture of solvents leads to the formation of larger spherical NPs (23 nm instead of 20 nm) but no obvious influence was observed on their shape by modifying the nature of the ^{Ad}CAAC-CuCl precursor. Nevertheless, when the oleylamine was replaced with

dodecylamine only, we did not observe neither the formation of NPs nor a precipitate (bulk). It is unclear why.

***Table III-4**. Experimental conditions used for preparing CuNPs when ^{Ad}CAAC-CuCl was used as the precursor with the corresponding size distributions.*

Precursor			**Solvent**				**NPs Shape**	**NPs Size** (nm)	**σ$^{\#}$ (%)**
^{Ad}CAAC-CuCl (mmol)			OLA (mL)		DDA (mL)	OLA:DDA* (3:1)			
0.15	0.3	0.6	4	8	4				
✓			✓				Triangles	29 ± 2.9	10
	✓		✓				Spheres	20 ± 1.4	7
	✓				✓		-	-	-
	✓					✓	Spheres	23.8 ± 0.5	2
	✓			✓			Quasi-spheres	37 ± 7	18
		✓	✓				Wires	44.3 ± 12.2	27
		✓		✓			Triangles	73.3 ± 15.7	21

** For a total volume of 4 mL.*
#: Polydispersity

All results summarized in Table III-4 shown that the size and shape of CuNPs using ^{Ad}CAAC-CuCl as precursor strongly depend on its amounts in the reaction medium. The shapes of the NPs evolve from triangle to sphere and wire with various sizes by modifying only the amount of precursor for a total reaction volume of 4 mL.

III. 3.3 Synthesis of CuNPs from ^{Menth}CAAC-CuCl complex

Here, we replaced the ^{Et}CAAC-CuCl by ^{Menth}CAAC-CuCl as copper precursor by using a similar synthetic procedure than the one described in section 3.2 (Figure III-13), with an increase of the temperature to 290 °C and a further stirring of 30 min. (See the general procedure used for these syntheses in Chapter V experimental section 3.2.G, Figure III-35).

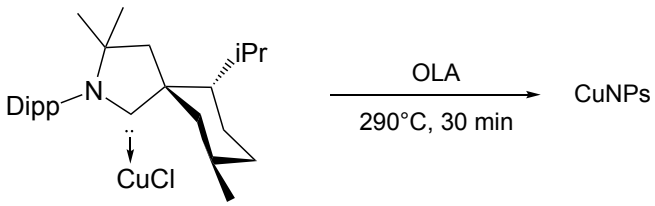

Figure III-35. *Synthesis of CuNPs from ^{Menth}CAAC-CuCl in oleylamine.*

As in previous cases, a yellower solution was observed when the reaction was heated at 100 °C and maintained for 15 min which can be attributed to the formation of ^{Menth}CAAC-Cu(I)-oleylamine according to the IR measurement. Figure III-36 shows the IR spectra of OLA and the mixture of ^{Menth}CAAC-CuCl and oleylamine after 15 min of heating at 100 °C. The N-H stretching vibration can be detected at about 3338 cm^{-1} (blue), which is the characteristic peak of oleylamine. In the spectra of mixture solution (red), two new peaks located at 3359 and 3126 cm^{-1} show the coordination of Cu(I) with the amine group of oleylamine. We also observed a blue shift of the NH_2 bending (1620 cm^{-1}) for the Cu(I)-OLA mixture compared to that of oleylamine (1574 cm^{-1}).[43-46]

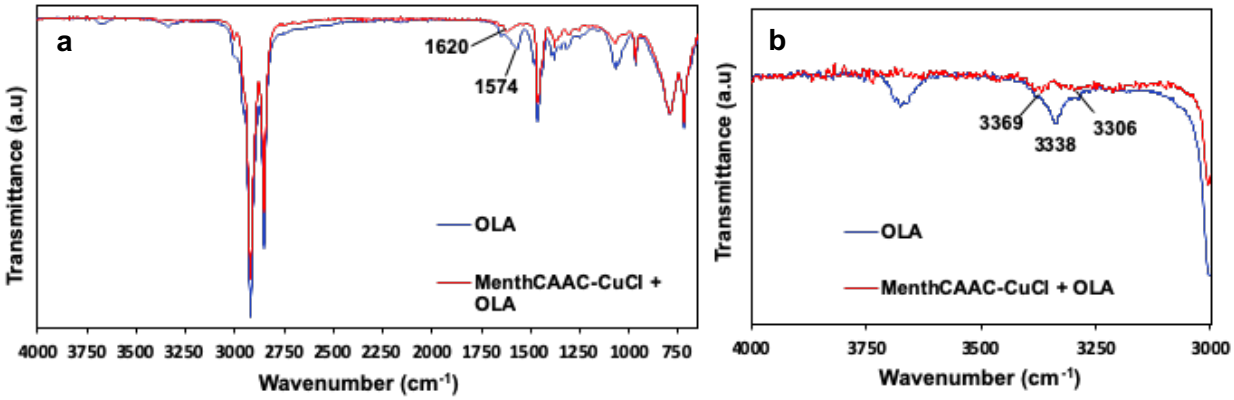

Figure III-36*. IR spectra of Oleylamine (OLA) and ^{Menth}CAAC-Cu(I)-Oleylamine complex at frequency range of (a) 4000-650 cm^{-1} (b) 4000-3000 cm^{-1}.*

In addition, a blue supernatant was also observed after the washing procedure in the subsequent reactions which indicate that Cu(II) was formed from a disproportionation reaction.

As previously, we have studied the effect of the Cu precursor amount and of the amount and the nature of the amine solvent on the shape and size of the Cu NPs.

III. 3.3.1 Effect of the amount of ^{Menth}CAAC-CuCl and oleylamine

The size and shape of the NPs are significantly influenced by the initial concentration of the copper precursor as observed in the last two sections. In the previous work, the influence of the amount of ^{Menth}CAAC-CuCl in the synthesis medium on the formation of NPs was also studied.

The typical TEM images of the NPs synthetized using a remaining total reaction volume of 4 mL (oleylamine) are shown in Figure III-37. As we can see in Figures III-34a and b, the use of an amount of 0.15 and 0.3 mmol ^{Menth}CAAC-CuCl complexes lead in both cases to the formation of triangle-shaped NPs, with sizes of 85.2 ± 19.2 nm and 82.8 ± 20 nm (in perpendicular height), respectively. It is worth noting that the copper nanotriangles obtained with 0.3 mmol have more well-defined morphology and smaller size. Besides, increasing the amount of ^{Menth}CAAC-CuCl to 0.6 mmol leads to the formation of wire-shaped NPs with an average size of 89.5 ± 52.7 nm in diameter. A similar phenomenon was also observed in sections 3.1 and 3.2 when the ratio of copper precursor to OLA was increased to 0.6 mmol/4 mL. It is unclear why the nanowires were formed in this case.

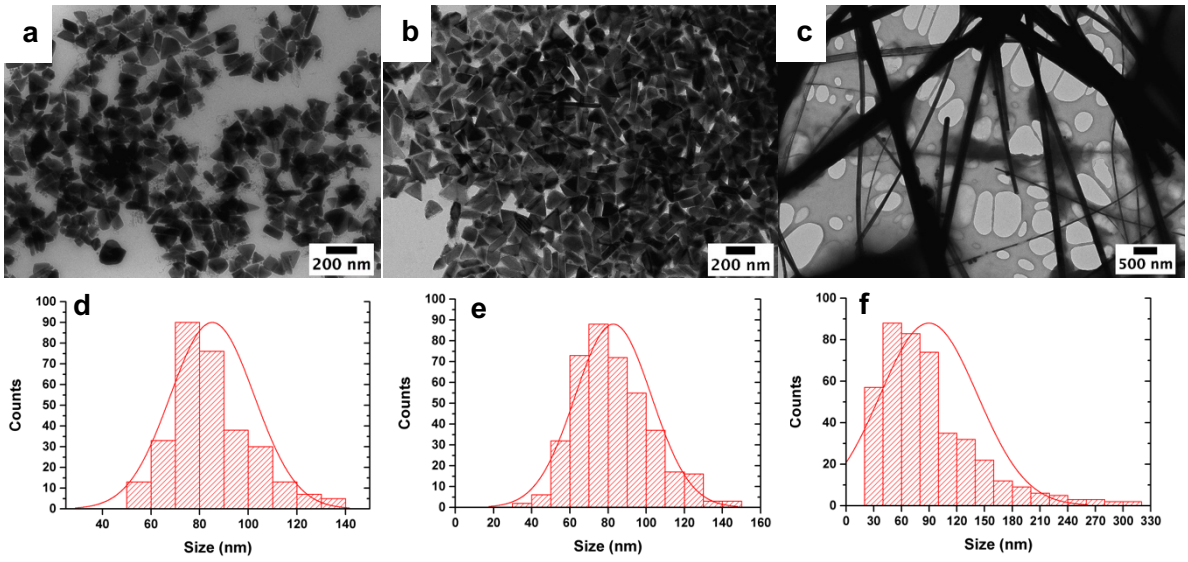

Figure III-37. *Typical TEM images of CuNPs synthetized from different amounts of ^{Menth}CAAC-CuCl of (a) 0.15 (b) 0.3 (c) 0.6 mmol in 4 mL of OLA and (d, e, f) the corresponding size histograms.*

After studying the influence of the amount of initial copper precursor, the influence of the volume of oleylamine was also investigated. Therefore, the experiments were carried out in an increased oleylamine volume of 8 mL in the presence of 0.3 or 0.6 mmol of ^{Menth}CAAC-CuCl. TEM images in Figure III-38 show that the size and morphology of NPs can be tuned by changing the concentration of ^{Menth}CAAC-CuCl precursor. Figure III-38a shows ill-defined triangle-shaped NPs with an average size of 122.3 ± 21.9 nm, along with few smaller spherical particles that were obtained for the use of 0.3 mmol of ^{Menth}CAAC-CuCl in 8 mL of oleylamine. Increasing the amount of copper precursor to 0.6 mmol, leads smaller triangular NPs with an average size of 89.4 ± 23.1 nm, along with some very small spherical particles. This result confirms that a high concentration of copper precursor induces a decrease of nanoparticle size, and also significantly influences their final shape.

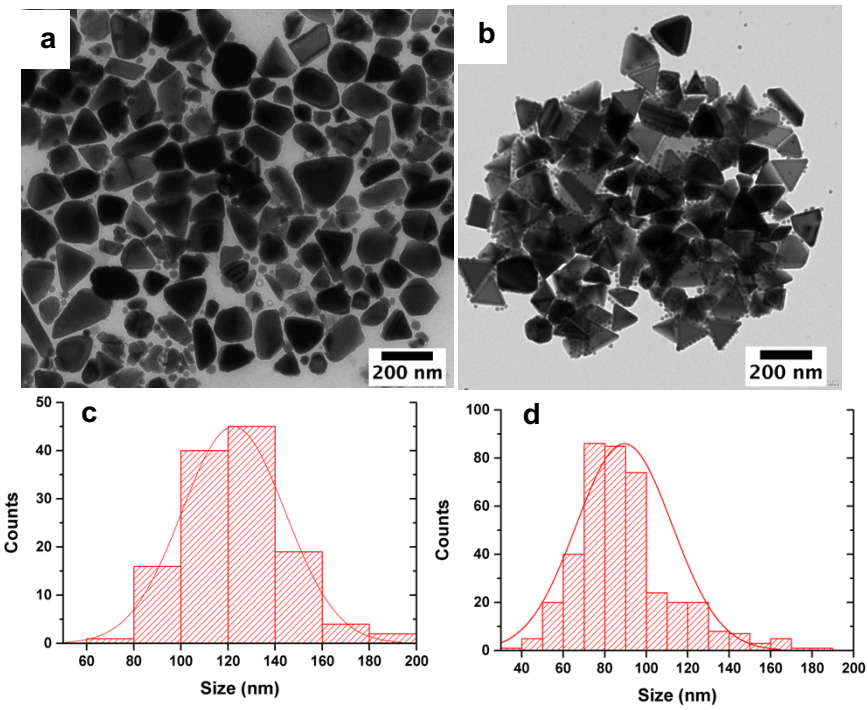

Figure III-38. *Typical TEM images of CuNPs synthetized in a volume of 8 mL of oleylamine, using different amounts of ^{Menth}CAAC-CuCl: (a) 0.3 mmol (b) 0.6 mmol and (c, d) the corresponding size histograms.*

XPS analysis

The Cu nanotriangles prepared from 0.3 mmol of ^{Menth}CAAC-CuCl in 4 mL of OLA were characterized by XPS (Table III-5 and Figure III-39). The survey spectra of both CuNPs show the presence of carbon, nitrogen, oxygen and chloride. The presence of metallic copper (932.90 eV) as a signal component and the high-resolution spectra confirm the formation of

metallic copper NPs, however, the presence of Cu-O band is also shown which may due to oxidation of NPs surface during the sample transportation. The N_{1s} photopeak detected at 400.10 eV (At% = 0.95%) is in agreement with the ligand compositions (oleylamine and CAAC) binding on the surface of NPs. The presence of Cl^- ions come from the initial copper precursor is also demonstrated by the peak detected at 200.06 eV (At% = 0.27%). As it was the case in the previous section, the presence of CAAC could be suggested by the high-resolution spectrum of C_{1s} (Figure III-32). Fitting the C_{1s} peak requires 3 contributions, each contribution is characteristic of a chemical environment: at 284.91 and 286.33 eV are located the aliphatic carbons C-C, C-N, at 288.11 eV may be indicated the satellite peak which come from the photoelectron excitation of the heterocycle ring.

***Table III-5**. XPS data for CuNPs obtained from ^{Menth}CAAC-CuCl.*

Element	Peak BE	FWHM eV	Area (P) CPS.eV	Atomic %
Cu2p	932.90	1.58	103466.01	1.41
Cl2p	200.06	1.62	2305.63	0.27
C1s	284.91	1.52	276096.23	72.64
C1sA	286.33	1.47	32173.52	10.62
C1sB	288.11	2.21	17255.62	5.31
N1s	400.10	1.97	6032.39	0.95
O1s	532.67	2.17	88239.37	8.80

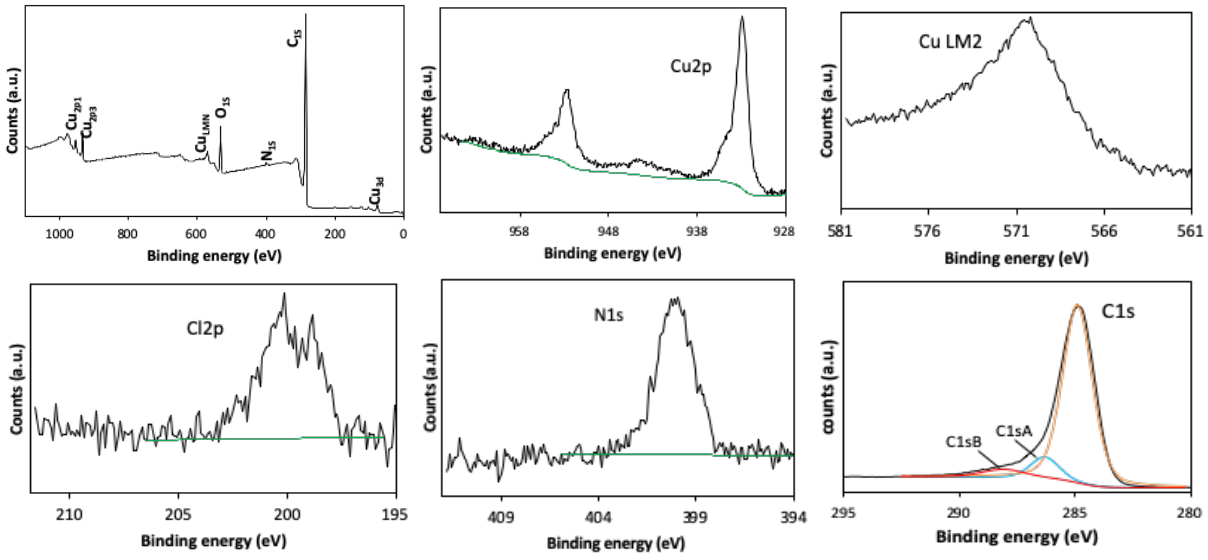

***Figure III-39.** XPS survey spectra and high resolution XPS spectra of Cu_{2p}, Cu_{LM2}, C_{1s}, N_{1s}, and Cl_{2p} of CuNPs obtained from 0.3 mmol ^{Menth}CAAC-CuCl/4 mL oleylamine.*

III. 3.3.2 Effect of the nature of the amine solvent

In this section, we also investigated the effect of the use of a mixture of oleylamine and dodecylamine as a solvent on the synthesis of CuNPs. The reaction was carried out in the binary mixture OLA/DDA with a volume ratio of 3:1 for a total volume of 4 mL in the presence of 0.3 mmol of copper precursor, according to the synthesis procedure described in Section 3.2 (Figure III-13) (see in Chapter V experimental section 3.2.H).

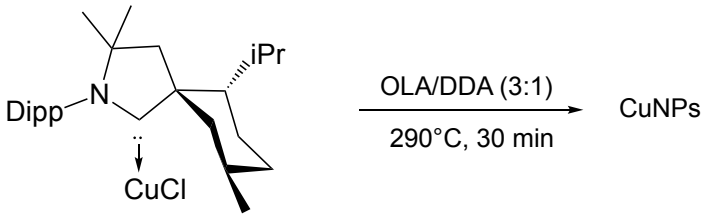

Figure III-40. *Synthesis of CuNPs from ^{Menth}CAAC-CuCl in a binary solvent of OLA/DDA (3:1) for a total volume of 4 mL.*

Figure III-41a shows the typical TEM image of CuNPs synthetized from ^{Menth}CAAC-CuCl. Ill-defined and highly polydisperse triangular NPs with an average size of 84.8 ± 16.2 nm in perpendicular height were formed. However, we did not obtain NPs when DDA was used as solvent in the synthesis instead of OLA.

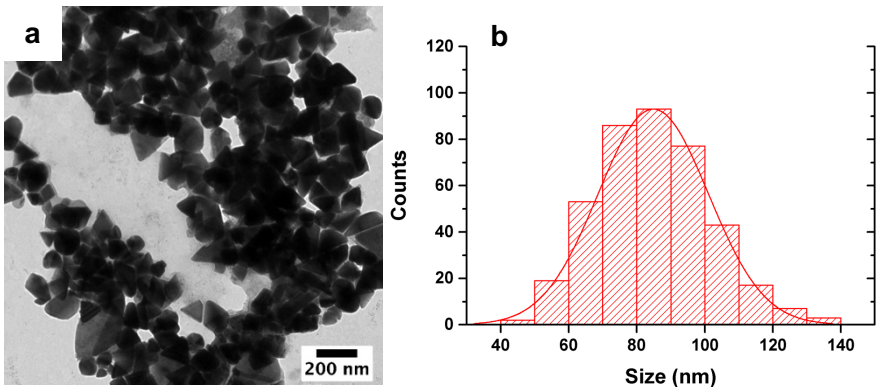

Figure III-41. (a) *Typical TEM images of CuNPs synthetized in a 1:1 (volume ratio) mixture of OLA/DDA for a total volume of 4 mL when ^{Menth}CAAC-CuCl (0.3 mmol) was used as precursor (b) the corresponding size histogram.*

***Table III-6**. Experimental conditions used for preparing CuNPs when ^{Menth}CAAC-CuCl was used as the precursor with the corresponding size distributions*.

Precursor			**Solvent**				**NPs shape**	**NPs Size** (nm)	$\sigma^{\#}$ (%)
^{Menth}CAAC-CuCl (mmol)			OLA (mL)		DDA (mL)	OLA:DDA* (3:1)			
0.15	0.3	0.6	4	8	4				
✓			✓				Triangles	85.1 ± 19.2	23
	✓		✓				Triangles	82.8 ± 20	24
	✓				✓		-	-	-
	✓					✓	Round triangles	84.8 ± 16.2	19
	✓			✓			Triangles	122.3 ± 21.9	18
		✓	✓				Wires	89.5 ± 52.7	-
		✓		✓			Triangles	89.4 ± 23.1	23

** For a total volume of 4 mL.*
$^{\#}$: Polydispersity

All results summarized in Table III-6 show that the shape of CuNPs using strongly depend on the amounts of the ^{Menth}CAAC-CuCl as precursor in the reaction medium. The higher concentration of initial copper precursor favors well-defined triangular shape of NPs. The morphological evolution from triangle to wire was also observed in only one case, by increasing the amount of precursor to 0.6 mmol for a total reaction volume of 4 mL.

III. 3.4 Synthesis of CuNPs from ^{PhMe}CAAC-CuCl complex

After testing other three CAACs ligands which have different steric hindrances of N-substituent including diethyl, menthyl and adamanthyl, we also tested the ^{PhMe}CAAC-CuCl complex which possess aromatic N-substituent on the CAAC as precursor in our CuNPs synthesis.

III. 3.4.1 Effect of the amount of ^{PhMe}CAAC-CuCl and oleylamine

In this work, the experiments were first performed with various amounts of ^{PhMe}CAAC-CuCl from 0.15 to 0.3 and 0.6 mmol in oleylamine (4 mL), heated to 290 °C, using the synthetic method reported in section 3.2 (Figure III-13). The synthetic procedure is shown in Chapter V experimental section 3.2.I. It is important to note that a blue supernatant was also observed after the washing procedure in these experiences. The presence of Cu(II) in the solution may demonstrate that the disproportionation reaction took place.

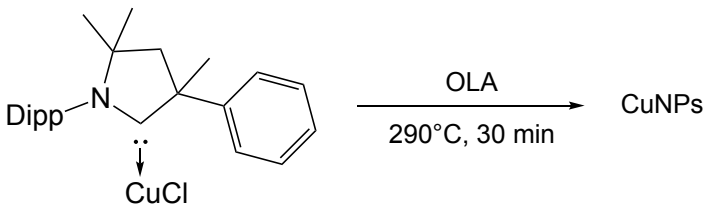

Figure III-42. *Synthesis of CuNPs from ^{PhMe}CAAC-CuCl.*

In the case of ^{PhMe}CAAC-CuCl complex, we did not obtain CuNPs for the use of an amount of 0.15 or 0.3 mmol of copper precursor. However, when increasing the precursor amount to 0.6 mmol, cubic NPs with an average size of 107.2 ± 24.8 nm and some quasi-nanospheres, were obtained, as shown in Figure III-43a. When the volume of OLA was increased from 4 mL to 8 mL, we observed larger nanocubes with an average size of 136 ± 40 nm, along with nanowires (Figure III-43b). The size of the CuNPs increased with a low concentration of precursor, which is in good accordance with LaMer theory.[51]

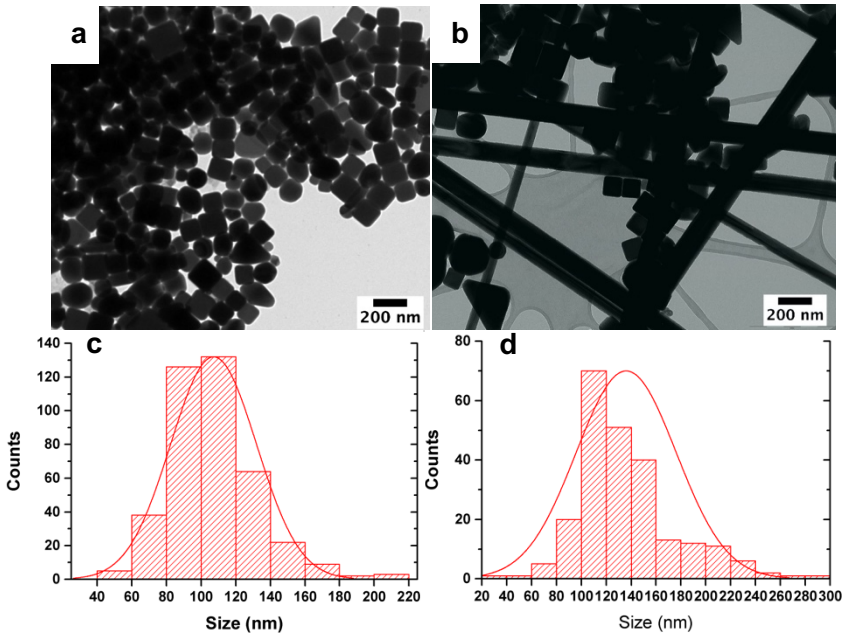

Figure III-43. *Typical TEM images of copper NPs synthetized in different volumes of OLA: (a) 4 mL (b) 8mL when 0.6 mmol of* ^{PhMe}*CAAC-CuCl was used as precursor and (c, d) the corresponding size histograms.*

III. 3.4.2 Effect of the nature of solvent.

As previously, we also investigated the effect of the use of dodecylamine as solvent. Firstly, the synthesis was performed in dodecylamine (DDA) alone (see in Chapter V experimental section 3.2.J). The typical TEM image (Figure III-45a) shows spherical NPs with a narrow size distribution of 16.6 ± 1.8 nm that were prepared from the reaction condition of 0.3 mmol ^{PhMe}CAAC-CuCl complex in 4 mL DDA during 30 min heating at 290 °C. As mentioned in Section 3.4.1, no formation of NPs was observed in oleylamine (4 mL) under identical reaction conditions. The reason for this difference in behavior is not clear yet.

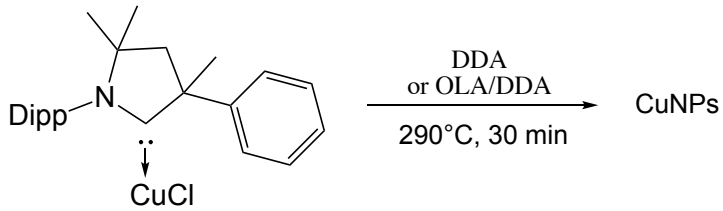

Figure III-44. *Synthesis of CuNPs from* ^{PhMe}*CAAC-CuCl in DDA only or a binary solvent of OLA/DDA (3:1) for a total volume of 4 mL.*

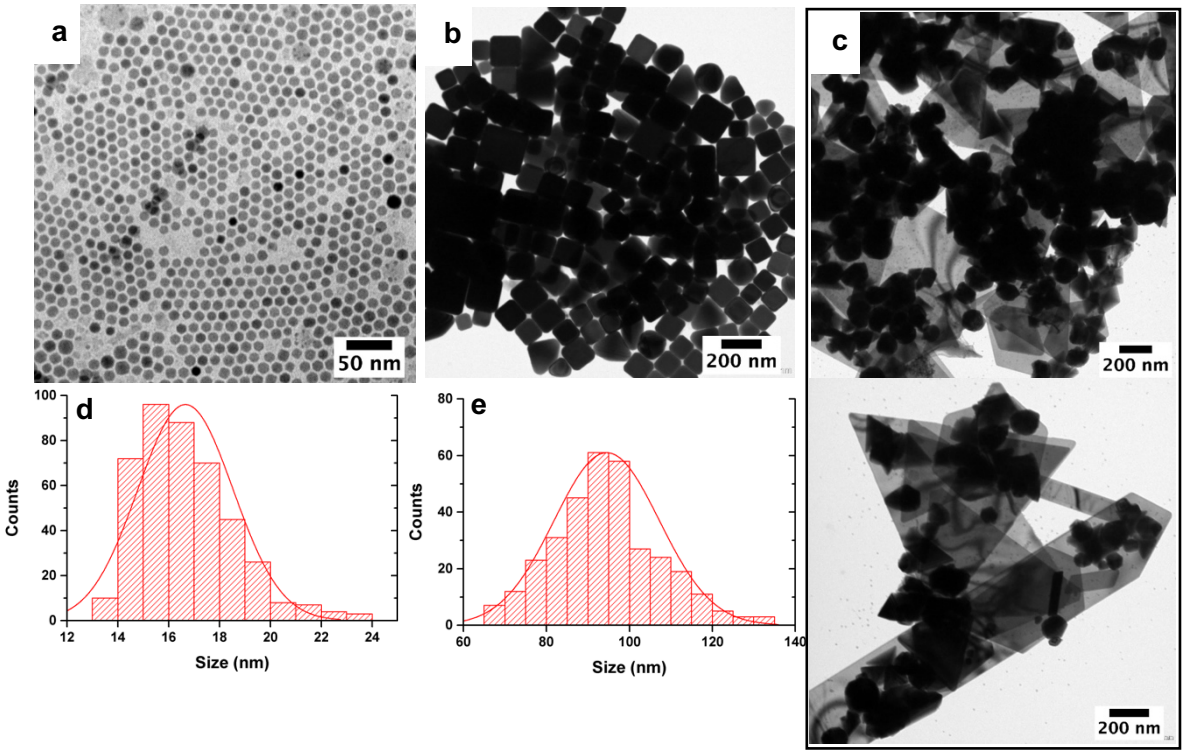

***Figure III-45**. Typical TEM images of CuNPs synthetized (a) in only DDA and in binary solvent OLA/DDA with volume ratio of (b) 3:1 (c)1:1 for a total volume of 4 mL and (d, e) the corresponding size histograms of (a) and (b).*

Subsequently, the investigation of the binary solvent contains OLA and DDA in different volume ratios of 3:1 and 1:1 for a total volume of 4 mL was carried out to synthetize copper NPs from 0.3 mmol of ^{PhMe}CAAC-CuCl (see in Chapter V experimental section 3.2.K). Typical TEM image (Figure III-45b) shows cube-shaped CuNPs with an average size of 94.5 ± 12.7 nm for a 3:1 volume ratio of OLA/DDA. Nevertheless, when the ratio between both solvents changed to 1:1, different NP morphologies including ill-defined quasi-nanosphere, nanotriangle, pyramid and few triangle bulks are observed (Figure III-45c). The same phenomenon was already observed in section 3.1 that the volume ratio of 1:1 (OLA/DDA) promoted larger, polydisperse, ill-defined nanoparticle compared to the volume ratio of 3:1. Oleylamine appears to play a relatively more important role as an organic ligand and/or solvent than dodecylamine on the shape and size control of NPs when the binary solvent was used.

***Table III-7**. Experimental conditions used for preparing copper NPs when ^{PhMe}CAAC-CuCl was used as the precursor with the corresponding size distributions*

Precursor			**Solvent**					**NPs shape**	**NPs Size** (nm)	$\sigma^{\#}$ (%)
^{PhMe}CAAC-CuCl (mmol)			OLA (mL)		DDA (mL)	OLA:DDA*				
0.15	0.3	0.6	4	8	4	3:1	1:1			
✓			✓					-	-	-
	✓		✓					-	-	-
	✓				✓			Spheres	16.6 ± 1.8	11
	✓					✓		Cubes	94.5 ± 12.7	13
	✓						✓	Large Anisotropic	-	-
		✓	✓					Cubes	107.2 ± 24,8	23
		✓		✓				Cubes, Wires	136 ± 40	29

** For a total volume of 4 mL.*
$^{\#}$: Polydispersity

All results summarized in Table III-7 show thus that the size and shape of CuNPs synthetized from ^{PhMe}CAAC-CuCl is also strongly affected by the nature of solvent. The monodisperse spherical NPs were produced by using 4 mL of DDA as solvent, however, no formation of NPs was observed in the reaction with OLA.

III. 4 Conclusion

In this chapter, we aimed to prepare CuNPs through a simple “one-pot” disproportionation reaction using only two reactants: CAACs-Cu(I) precursor and primary amine as solvent. CuNPs with various shapes were formed by tuning the nature of CAACs ligands, of the solvent, and the concentration of precursor. We have been able to synthetize CuNPs from CAACs-CuCl complexes for the first time. XPS measurements seem to indicate that the NPs are stabilized by the CAACs ligands. In order to confirm the presence of CAACs on the nanoparticle surface, further analysis based on MAS NMR have to be done in a next future. Important parameters enabling to control the morphology of CuNPs include the nature of the CAAC (^{Et}CAAC, ^{Ad}CAAC, ^{Menth}CAAC and ^{PhMe}CAAC), of the concentration of CAACs-CuCl precursors, or of the solvent (OLA, DDA or OLA/DDA mixture). Especially, in the cases of ^{Et}CAAC-CuCl and ^{PhMe}CAAC-CuCl, the use of DDA as the solvent was found to be crucial to obtain small monodisperse NPs.

In particular, pyramid-shaped CuNPs were synthetized from ^{Et}CAAC-CuCl in a binary solvent (OLA/DDA). They have great potential in optical or catalytic fields due to their unique shape.

In this work, various shapes of CuNPs were prepared with the use of CAACs-CuCl complexes but their theoretical yield is typically limited to 50% due to the synthetic disproportionation approach. In next chapter, we developed a fast, practical and scalable synthetic method through thermal decomposition of organocopper precursors to obtaining high yield and tunable size of spherical CuNPs.

III. 5 References

(1) M. Opkinson, C. Richter, M. Schedler, F. Glorius, *Nature*, **2014***, 510*, 485-496.

(2) a) A. Igau, H. Grgtzmacher, A. Baceiredo, G. Bertrand, J. Am. Chem. Soc. **1988**, *110*, 6463-6466; b) A. Igau, A. Baceiredo, G. Trinquier, G. Bertrand, *Angew. Chem. Int. Ed. Engl.*, **1989**, *28*, 621-622; *Angew. Chem.,* **1989**, *101*, 617-618; c) D. Bourissou, O. Guerret, F. Gabba, G. Bertrand, *Chem. Rev.*, **2000**, *100*, 39-91.

(3) A-J. Arduengo, R-L. Harlow, M-A. Kline, *J. Am. Chem. Soc.,* **1991**, *113*, 361-363.

(4) P. de Frémont, N. Marion, S. P. Nolan, *Coord. Chem. Rev.*, **2009**, *253*, 862-892.

(5) a) S. P. Nolan, *N-Heterocyclic Carbenes in Synthesis, John Wiley & Sons: Hoboken, NJ,* **2006;** b) F. Z. Dörwald, *Metal Carbenes in Organic Synthesis; John Wiley & Sons: Hoboken, NJ,* **2008**.

(6) a) M. N. Hopkinson, C. Richter, M. Schedler, F. Glorius, *Nature*, **2014**, *510*, 485-496; b) L. Mercs, M. Albrecht, *Chem. Soc. Rev.,* **2010**, *39*, 1903-1912; c) R. Visbal, C. Gimeno, *Chem. Soc. Rev.,* **2014**, *43*, 3551-3574; d) K. M. Hindi, M. J. Panzner, C. A. Tessier, C. L. Cannon, W. J. Youngs*, Chem. Rev.,* **2009**, *109,* 3859-3884; e) A. V. Zhukhovitskiy, M. J. MacLeod, J. A. Johnson, *Chem. Rev.,* **2015**, *115*, 11503-11532; f) M. Melaimi, R. Jazzar, M. Soleilhavoup, G. Bertrand, *Angew. Chem. Int. Ed.,* **2017**, *56*, 10046-10068.

(7) D. J. Nelson, S. P. Nolan, *Chem. Soc. Rev.,* **2013**, *42*, 6723-6753.

(8) a) F. E. Hahn, M. C. Jahnke, *Angew. Chem. Int. Ed.,* **2008**, *47*, 3122-3172; b) N. Kuhn and A. Al-Sheikh, *Coord. Chem. Rev.,* **2005**, *249*, 829-857; c) D. P. Curran, A. Solovyev, M. M. Brahmi, L. Fensterbank, M. Malacria, E. Lacôte, *Angew. Chem., Int. Ed.,* **2011**, *50*, 10294-10317.

(9) R-S. Thomas, C. Angela, *J. Organometallics Chem.,* **2021**, *938*, 121743.

(10) C. Cerezo-Navarrete, P. Lara, L-M. Martinez-Prieto, *Catalysis*, **2020**, *10*, 1144.

(11) X. Ling, N. Schaeffer, S. Roland, M. Pileni, *Langmuir,* **2015**, *31*, 12873-12882.

(12) V. Lavallo, Y. Canac, C. Präsang, B. Donnadieu, G. Betrand, *Angew. Chem. Int. Ed.*, **2005**, *44*, 5705-5709.

(13) M. Soleilhavoup, G. Bertrand, *Acc. Chem. Res*. **2015**, *48*, 256-266.

(14) A. V. Zhukhovitskiy, M. J. MacLeod, J. A. Johnson, *Chem. Rev.*, **2015,***115*, 11503-11532.

(15) L. S. Ott, M. L. Cline, M. Deetlefs, K. R. Seddon, R. G. Finke, *J. AM. Chem. Soc.*, **2005**, *127*, 5758-5759.

(16) a) C. J. Serpell, J. Cookson, A. L. Thompson, C. M. Brown, P. D. Beer, *Dalton Trans,* **2013**, *42* (5), 1385-1393; b) J. Vignolle, T. D. Tilley, *Chem. Commun.,* **2009**, *46*, 7230-7232; c) E. C. Hurst, K. Wilson, I. J. S. Fairlamb, V. Chechik, *New J. Chem.,* **2009**, *33* (9), 1837-1840; d) S. Roland, X. Ling, M-P. Pileni. *Langmuir*, **2016**, *32,* 7683-7696.

(17) C. K. Lee, C. S. Vasam, T. W. Huang, H. M. J. Wang, R. Y. Yang, C. S. Lee, I. J. B. Lin, *Organometallics,* **2006**, *25* (15), 3768-3775.

(18) P. Lara, O. Rivada-Wheelaghan, S. Conejero, R. Poteau, K. Philippot, B. Chaudret. *Angew. Chem. Int. Ed.,* **2011**, *50* (50), 12080-12084.

(19) E. A. Baquero, S. Tricard, J. C. Flores, E. de Jesús, B. Chaudret, *Angew. Chem. Int. Ed.,* **2014**, *53 (48*), 13220-13224.

(20) J. M Asensio, S. Tricard, Y. Coppel, R. Andrés, B. Chaudret, E. de Jesús, *Chem. Eur. J.,* **2017**, *23 (54),* 13435-13444.

(21) a) J. Vignolle, T. D. Tilley, *Chem. Commun.,* **2009**, 7230-7232; b) X. Ling, N. Schaeffer, S. Roland, M. Pileni, *Langmuir*, **2013**, *29*, 12647-12656; c) E. A. Baquero, S. Tricard, J.

C. Flores, E. de Jesus, B. Chaudret, *Angew. Chem. Int. Ed*., **2014**, *53*, 13220-13224; *Angew. Chem.,* **2014**, *126*, 13436-13440.

(22) a) P. Lara, O. Rivada-Wheelaghan, S. Conejero, R. Poteau, K. Philippot, B. Chaudret, *Angew. Chem. Int. Ed.,* **2011**, *50*, 12080-12084; *Angew. Chem.,* **2011**, *123*, 12286-12290; b) M. D. de los Bernardos, S. Pérez-Rodrguez, A. Gual, C. Claver, C. Godard, *Chem. Commun.,* **2017***, 53*, 7894-7897.

(23) a) R. W. Y. Man, C. H. Li, M. W. A. MacLean, O. V. Zenkina, M. T. Zamora, L. N. Saunders, A. Rousina-Webb, M. Nambo, C. M. Crudden, *J. Am. Chem. Soc*., **2018**, *140*, 1576-1579; b) E. C. Hurst, K. Wilson, I. J. S. Fairlamb, V. Chechik, *New J. Chem.,* **2009**, *33*, 1837-1840; c) C. Richter, K. Schaepe, F. Glorius, B. J. Ravoo, *Chem. Commun*., **2014**, *50*, 3204-3207.

(24) R. Ye, A. V. Zhukhovitskiy, R. V. Kazantsev, S. C. Fakra, B. B. Wickemeyer, F. D. Toste, G. A. Somorjai, *J. Am. Chem. Soc*., **2018**, *140*, 4144-4149.

(25) J. Vignolle, T. D. Tilley, *Chem. Commun.,* **2009**, *46*, 7230-7232.

(26) a) M. J. MacLeod, A. J. Goodman, H-Z. Ye, H-V-T. Nguyen, T. Van Voorhis, J. A. Johnson, *Nat. Chem.*, **2019**, *11*, 57-63; b) H, Lu, Z. Zhou, O. V. Prezhdo, R. L. Brutchey, *J. Am. Chem. Soc*., **2016**, *138,* 14844-14847.

(27) E. A. Baquero, S. Tricard, J. C. Flores, E. de Jesus, B. Chaudret, *Angew. Chem. Int. Ed.,* **2014**, *53,* 13220-13224.

(28) J. M. Asensio, S. Tricard, Y. Coppel, R. AndrØs, B. Chaudret, E. de Jesùs, *Chem. A. Euro. J.,* **2017**, *54*, 13435-13444.

(29) L. M. Martínez-Prieto, A. Ferry, L. Rakers, C. Richter, P. Lecante, K. Philippot, B. Chaudret, F. Glorius. *Acc. Chem. Res.*, **2018**, *51*, 376-384.

(30) L. M. Martínez-Prieto, L. Rakers, A. M. López-Vinasco, I. Cano, Y. Coppel, K. Philippot, F. Glorius, B. Chaudret, P. W. N. M. Van Leeuwen, *Chem. A. Eur. J.,* **2017**, *23*, 12779-12786.

(31) C. Amiens, B. Chaudret, D. Ciuculescu-Pradines, V. Collière, K. Fajerwerg, P. Fau, M. Kahn, A. Maisonnat, K. Soulantica, K. Philippot, *New J. Chem*., **2013**, *37*, 3374-3401.

(32) A. Rühling, K. Schaepe, L. Rakers, B. Vonhören, P. Tegeder, B. J. Ravoo, F. Glorius, *Angew. Chem. Int. Ed*., **2016**, *55*, 5856-5860.

(33) E.C. Hurst, K. Wilson, I. J. S. Fairlamb, V. Chechik, *New J. Chem*., **2009**, *33*, 1837-1840.

(34) C. Richter, K. Schaepe, F. Glorius, B. J. Ravoo, *Chem. Commun.,* **2014***, 50,* 3204.

(35) S. Engel, E. Fritz, B. J. Ravoo, *Chem. Soc. Rev*., **2017**, *46*, 2057-2075.

(36) M. B. Gawande, A. Goswami, F. X. Felpin, T. Asefa, X. Huang, R. Silva, X. Zou, R. Zboril, R. S. Varma, *Chem. Rev*., **2016**, *116*, 3722-3811.

(37) C. R. Larrea, C. J. Baddeley, M. R. Narouz, N. J. Mosey, J. H. Horton, C. M. Crudden, *Chem. Phys. Chem.*, **2017**, *18*, 3536.

(38) Ursula. S. D. Paul, Udo. Radius, *What Wanzlick Did Not Dare To Dream: Cyclic (Alkyl)(amino)carbenes (CAACs) as New Key Players in Transition-Metal Chemistry.*

(39) X. Frogneux, L. Hippolyte, D. Mercier, D. Portehault, C. Chanéac, C. Sanchez, P. Marcus, F. Ribot, L. Fensterbank, S. Carenco. *Chem. Eur. J.,* **2019**, *25*, 11481-11485.

(40) B. Rao, H. R. Tang, X. M. Zeng, L. Liu, M. Melaimi, G. Bertrand, *Angewandte*, **2015**, *54*, 14915-14919.

(41) R. Jazzar, M. Soleilhavoup, G. Bertrand. *Chem. Rev.,* **2020**, *120 (9)*, 4141-4168.

(42) a) R. Jazzar, R. D. Dewhurst, J. B. Bourg, B. Donnadieu, Y. Canac, G. Bertrand, Angew. *Chem. Int. Ed*., **2007**, *46*, 2899-2902; *Angew. Chem*. **2007**, *119*, 2957-2960; b) R. Jazzar, J. B. Bourg, R. D. Dewhurst, B. Donnadieu, G. Bertrand, *J. Org. Chem*., **2007**, *72*, 3492-

3499; c) X. Zeng, G. D. Frey, R. Kinjo, B. Donnadieu, G. Bertrand, *J. Am. Chem. Soc*., **2009**, *131*, 8690-8696.
(43) J. Luo, L. Han, N. N. Kariuki, L. Wang, D. Mott, C-J. Zhong, T. He, *Chem. Mater*., **2005,** *17***,** 5258-5290.
(44) J. K. Cooper, A. M. Franco, S. Gul, C. Corrado, J. Z. Zhang, *Langmuir*, **2011**, *27*, 8486-8493.
(45) H. Guo, Y. Chen, M. B. Cortie, X. Liu, Q. Xie, X. Wang, D-L. Peng, *J. Phys. Chem. C*., **2014**, *118*, 9801-9808.
(46) J. K. Cooper, A. M. Franco, S. Gul, C. Corrado, J. Z. Zhang, *Langmuir,* **2011**, *27(13),* 8486-8493.
(47) H-J. Yang, S-Y, He, H-L. Chen, H-Y. Tuan, *Chem. Mater*., **2014**, *26*, 1785-1793.
(48) H. Jia, W. Xu, J. An, D. Li, B. Zhao*, Spectrochimica Acta Part A,* **2006***, 64,* 956-960*.*
(49) Y. Wang, Y. Zheng, C. Huang, Y. Xia, J*. Am. Chem. Soc.,* **2013**, *135*, 5, 1941-1951.
(50) K. Locharoenrat, H. Sano, G. Mizutani, Sci. Technol. Adv. Mater., **2007**, *8* (4), 277-281.
(51) K. LaMer, H. Dinegar, Theory, *J. Am. Chem. Soc.,* **1950**, *72* (11), 4847-4854.
(52) Y. Liu, C. Wang, Y. Wei, L. Zhu, D. Li, J. S. Jiang, N. M. Markovic, V. R. Stamenkovic, S. Sun, *Nano. Lett*., **2011**, *11*, 1614.
(53) E. Frederick, T. W. Shaw, Matthew G. Frith, S. L. Bernasek, *Mater. Chem. Front.,* **2019**, *3*, 636.
(54) a). M. R. Narouz, C-H. Li, A. Nazemi, C. M. Crudden, *Langmuir* 2017, *33* (50), 14211-14219; b) K. Salorinne, R. W. Y. Man, C-H. Li, M. Taki, M. Nambo, C. M. Crudden, *Angew. Chem.,* **2017**, *129* (22), 6294-6298.
(55) L. M. Martínez-Prieto, I. Cano, A. Márquez, E. A. Baquero, S. Tricard, L. Cusinato, I. del, Rosal, R. Poteau, Y. Coppel, K. Philippot, B. Chaudret, J. Cámpora, P. W. N. M. van. Leeuwen, *Chem. Sci.,* **2017**, *8* (4), 2931-2941.
(56) S. Sun, H. Zeng, D. B. Robinson, S. Raoux, P. M. Rice, S.X. Wang, G. Li, J*. Am. Chem. Soc.,* **2004**, *126*, 273-279.
(57) M. Devaraj, R. Saravanan, R. Deivasigamani, V. K. Gupta, F. Gracia, S. Jayadevan, *J. Mol. Liq.*, **2016**, *221*, 930-941.
(58) L. Xu, J. Yang, *Phys. Sci. Rev.*, **2018**, pp. 20170080.
(59) L. Mo, D. Liu, W. Li, L. Wang, X. Zhou, *Appl. Surf. Sci.*, **2011**, *3021, 257* (13*),* 5746-5753.
(60) G. Mei, *Ann. Phys.*, **1908**, *25*, 377-445.
(61) A. K Pearce, T. R. Wilks, M. C. Arno, *R. O'Reilly, Nat. Rev. Chem.,* **2021**, *5*, 21-45.
(62) M. A. B. Aissa, B. Tremblay, A. Adrieux-Ledier, E. Maisonhaute, N. Raouafi, A. Courty, *Nanoscale*, **2015**, *7*, 3189-3195.

Chapter IV. Synthesis of CuNPs with well-defined size and shape via the thermal decomposition of organocopper compounds.

IV. 1 Introduction

In the last two chapters, we have discussed the shape control of CuNPs synthesis via a disproportionation pathway in an organic alkylamine solvent under high temperature. Although the disproportionation route is well-developed and leads to various CuNPs with controlled shapes and large range size, this method yields a small number of nanoparticles (NPs) since the maximum theoretical yield is limited to 50% and it is difficult to scale up the synthesis.[1] Additionally, this route is highly sensitive to heating rate and injection rate of the phosphorus or carbene ligand which makes the scale-up of such syntheses quite difficult to achieve readily.[2] Finally, an excess of alkylamine of high molecular weight is required for the CuNPs synthesis and the high amines coverage on the particle surface may limit some surface-depended applications of these NPs.

The objective of this chapter is to discover a rapid, greener and high-yielding chemical reduction method to prepare well-defined CuNPs. This new route is based on the thermolysis of organocopper precursors in the presence of a phosphorus ligand and the further addition of dodecanethiol to obtain homogeneous CuNPs in high-quantity.

This chapter starts with a concise presentation of organocopper reagents (section IV-2). Next first conditions enabling the preparation of well-defined CuNPs from organocopper reagents are presented and further optimized by tuning the organic ligand-to-copper ratio and the reaction temperature (IV-3). These CuNPs were well characterized by a series of analyses (e.g., TEM, HRTEM, XRD, EDX, XPS and UV-visible) to demonstrate their different sizes, shapes, crystalline structures, distinct surface compositions and plasmonic properties. Based on the optimized conditions, we then studied the influence of:

- the thiol stabilizer which is often used to prevent the coalescence of the NPs into bulk (e.g., addition time, amount, IV-4 and IV-5 respectively))

- the nature of phosphorous ligands (IV-6)

- the organometallic reagent-to-copper ratio and of the nature of organometallic reagent on the CuNPs synthesis (IV-7).

IV. 2 Thermolysis of organocopper compounds

In this paragraph, organocopper reagents are presented and some of their main properties are discussed.

The first organocopper reagent (PhCu) was isolated by R. Reich in 1923.[3] Since then, synthesis and structural studies of the organocopper compounds have received a continuous attention in the field of copper catalytic reaction.[4] Organocopper (RCu, R = alkyl or aryl and R-to-Cu ratio = 1) and organocuprate (R_2Cu, R = alkyl or aryl and R-to-Cu ratio = 2) compounds are highly used in organic synthesis (Scheme IV-1, equations 1 and 2 respectively). They are routinely obtained through organic transmetalations from organo-magnesium compounds (Grignard reagents), organo-lithium compounds or organo-zinc precursor by a Cu(I) salt at low temperature (see in Scheme IV-1, equations 1 and 2).[5] Those species are known to be thermally unstable and to decompose at low temperatures, generally between -90 °C and 0 °C depending on the nature of the organic moiety.

$$RM + CuX \xrightarrow[\text{low temperature}]{\text{THF or } Et_2O} \underset{\text{Organocopper}}{RCu} + MX \qquad (1)$$

R = Alkyl, Aryl; M = MgX, Li, ZnX; X = Cl,Br, I

$$2RM + CuX \xrightarrow[\text{low temperature}]{\text{THF or } Et_2O} \underset{\text{Organocuprate}}{R_2CuM} + MX \qquad (2)$$

$$RMgBr + CuCl \xrightarrow[\text{-50°C to 50°C}]{\text{n-}Bu_2O} \text{‘red metallic copper colloidal solution’} + \text{‘Black solid’} \qquad (3)$$

R = Ethyl, Phenyl

(C. R. Noller, 1936)

Scheme IV-1. *Synthesis and thermolysis studies of organocopper compounds.*[5,6]

In 1936, Noller *et al.*[6] first studied the decomposition reaction of ethylcopper reagents obtained from the mixture of CuCl (or CuBr) with an excess of ethylmagnesium bromide in ethereal solvents (Scheme IV-1, equation 3). The formation of a black solid and a red supernatant was observed. The authors assumed that the supernatants corresponded to a metallic copper colloidal solution. Later on, Kochi[7] and Whitesides[8]

independently investigated the decomposition reactions of organocopper species, followed by others.[9] In addition, Kochi's group[7] showed that the decomposition rate was increased by the addition of small amounts of solution containing colloidal copper, thus unveiling the existence of an autocatalytic process (Scheme IV-2, equation 4, red side). They reported one possible putative reaction pathway (as seen in Scheme IV-2, equation 5) show the influence of catalytic Cu(0) on the rate of the copper hydride elimination process, which lies within the framework of the results obtained by Whitesides's *et al.*[8] (Scheme IV-2, equation 6).

However, despite the interest of these seminal results, those works were not continued and the exact chemical nature of the red colloidal solution has not been studied.

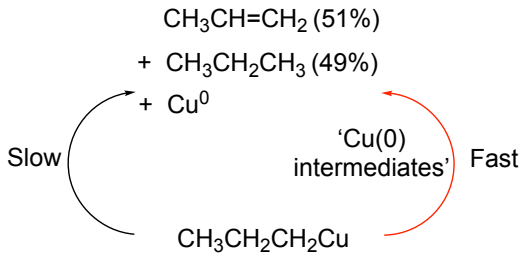

(4)

(J. Kochi et al. 1970)

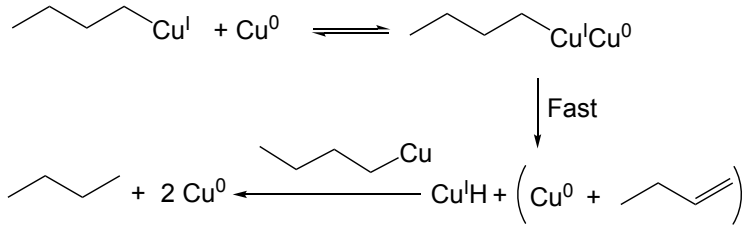

(5)

(J. Kochi et al. 1970)

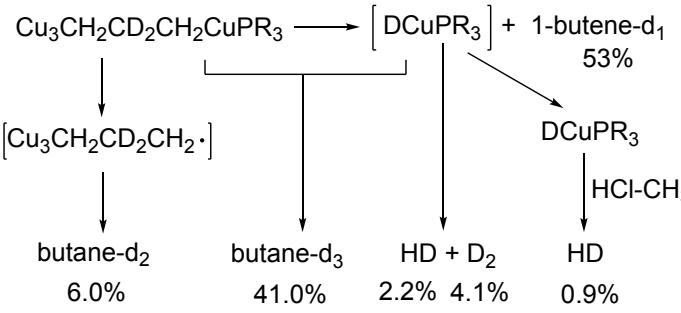

(6)

(G. Whitesides et al. 1970)

Scheme IV-2. *Autocatalytic decomposition of organocopper compounds (equation 4) and the putative reaction pathway in the presence of metallic Cu(0) during the decomposition of alkylcopper (equation 5)[7] and isotopic (deuterium) labelling study of the thermal decomposition of alkylcopper (equation 6).[8]*

When starting our work, the first objective was to determine the exact nature of the Cu(0) stemming from the thermal decomposition of RCu. Indeed, if this reaction produces NPs instead of copper bulk, then it may be an original and simple access route to CuNPs. This study starts with the thermolysis of copper chloride in the presence of triphenylphosphine (PPh_3) with subsequent addition of dodecanethiol (DDT) according to the general procedure represented in Figure IV-1.

The influence of several reaction parameters on the synthesis of well-defined CuNPs was next studied. They include: the amount of phosphine ligand, the temperature, the injection time and amount of DDT, the nature of the phosphorous ligand, the nature and amount of the Grignard reagent. Some experiments were also achieved to better understand the processes involved in the birth and growth of CuNPs by this route. In the optimized conditions, a scale-up of the synthesis was realized.

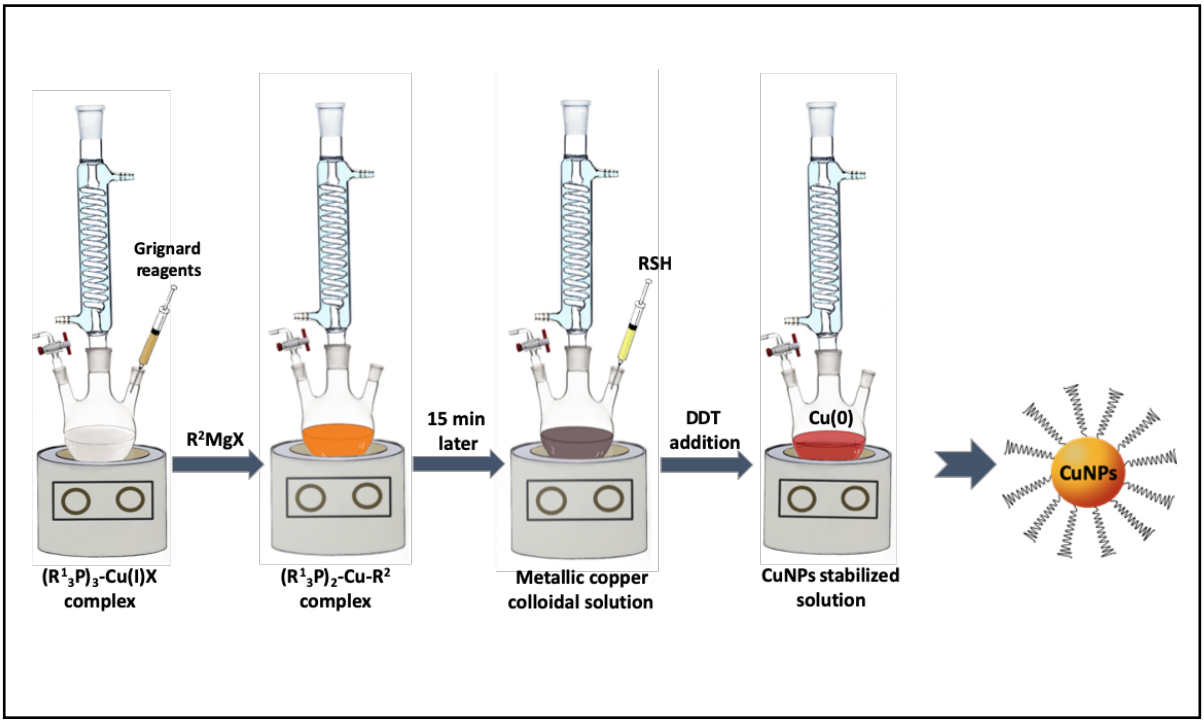

Figure IV-1. *General procedure of CuNPs synthesis via organometallic thermal decomposition.*

IV. 3 First conditions for the synthesis of well-defined CuNPs from CuCl, PPh_3, n-BuMgCl and dodecanethiol and further optimization of the phosphine-to-copper ratio and of the temperature

IV. 3.1 First conditions enabling the synthesis of well-defined CuNPs from CuCl, PPh_3, *n*-BuMgCl

At first, the preparation of CuNPs was realized by the thermal decomposition of organocopper in the presence of triphenylphosphine (PPh_3) at room temperature (rt). In the previous work (Chapter I), the preparation of CuNPs with narrow size (3.5-11 nm) by the reduction of $CuCl(PPh_3)_3$ complexes in the presence of alkylamine was reported by A. Courty's group.[10] For our first CuNPs synthesis attempts we decided to use 3 equiv. of PPh_3 to complex with CuCl (1 equiv.) in order to form the same $CuCl(PPh_3)_3$ complex that has a good solubility in THF.

In the typical synthesis (see in Chapter V experimental section 3.3.A), 1 mmol of copper chloride (CuCl) and 3 mmol of triphenylphosphine (PPh_3) have been stirred in dry THF (10 mL) at room temperature under an inert atmosphere to generate a colorless homogeneous solution corresponding to $(R_3P)_3$-Cu(I) complex. 1 mmol of butylmagnesium chloride (*n*-BuMgCl, Grignard reagent) was then rapidly injected and the solution began to darken immediately from colorless to brown and then dark-brown, which might indicate the beginning of the Cu(I) to Cu(0) reduction process and/or the beginning of the nucleation process . After a few seconds, the solution appeared black completely. After 15 min, 4 mmol of dodecanethiol (DDT) were added into the dark solution in order to prevent the precipitation of bulk copper. It is known that thiols are common surfactants and can be used as excellent capping agents, the application of thiols as capping agents for CdTe QDs synthesis was firstly reported by A. J. Nozik and co-workers.[11] Thiol ligands have also often been used as capping ligands to synthesize monodisperse and well-defined copper sulfide ($Cu_{2-x}S$) nanocrystals.[12] In our case, the DDT addition induced an instant color change from black to red. The role of DDT will be discussed in details in next sections. The solution was stirred one more hour at room temperature (Figure IV-2).

Afterwards, a standard work-up of washing/centrifugation sequences was realized to remove the by-products formed from the formation of organocopper and maybe also organic ligands in excess in the reaction solution. The NPs solution was centrifuged at 2500 rpm for 10 min, the supernatant was removed and the precipitate re-dissolved in chloroform and centrifugated at 4000 rpm for 5 min. After two dissolution-precipitation cycles, the NPs were dried and stored in the glove box for further analyses.

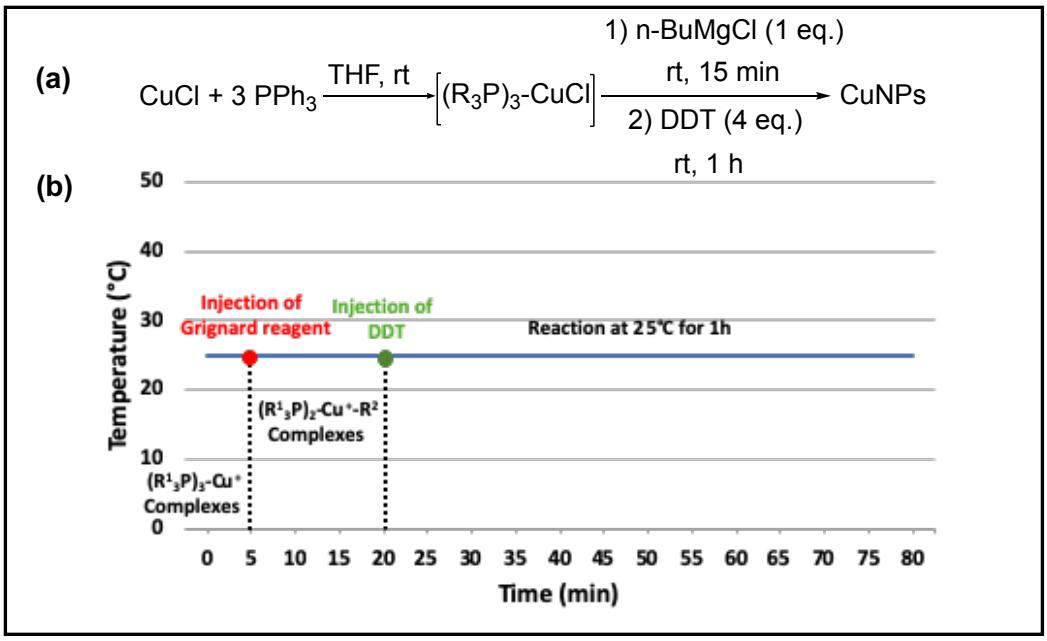

Figure IV-2. *(a) First attempt of CuNPs synthesis through the thermal decomposition of the organocopper compound at room temperature and (b) the corresponding graphic description of synthesis process.*

A deep purple powder was obtained whose TEM images show spherical NPs with an average size of 5.4 ± 0.5 nm (σ% = 9%) (Figure IV-3a, b). UV-vis absorbance spectrum of these nanospheres (Figure IV-3c), exhibits a LSPR peak around 580 nm which is in agreement with the values reported of pure copper NPs.[10,13]

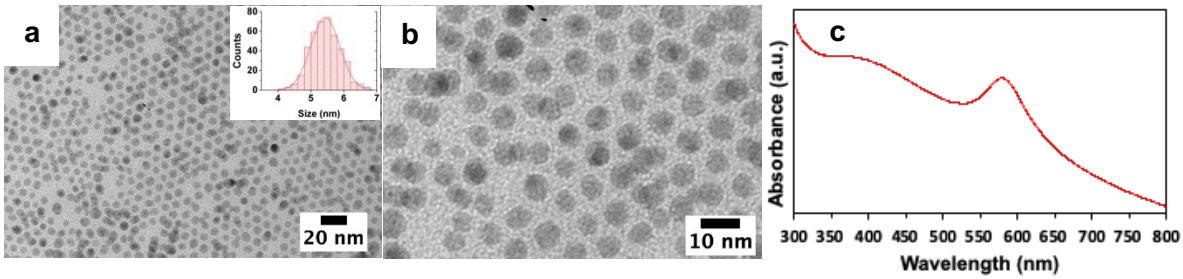

Figure IV-3. *(a-b) Typical TEM images of the CuNPs from reaction conditions of CuCl/3 equiv. PPh_3/n-BuMgCl/rt and (c) the corresponding UV-vis spectrum (580 nm). The spectra are required from the CuNPs dispersed in chloroform.*

IV. 3.2 Optimization of the PPh_3-to-copper ratio and of the temperature

In the first two chapters of this thesis, it was emphasized that the amount of phosphorus ligands and the reaction temperature can both affect the final size of CuNPs. Firstly, to better understand the effect of PPh_3 quantity on the CuNPs synthesis, the above-described procedure (see in Figure IV-2) was repeated in the presence of 1 or 5 equivalents of PPh_3 instead of 3 as compared to copper. It is noteworthy that with 5 equivalents of PPh_3, the formation of a white gel was observed and prevented the isolation of CuNPs. When 1 mmol of PPh_3 was present in solution, CuNPs with an average size of 5.5 ± 0.7 nm were synthetized, as shown in Figure IV-4a. No obvious size change has thus been observed (compared to 5.4 ± 0.5 nm, $\sigma\%$ = 9% for 3 equivalents), however, the CuNPs obtained from 1 equiv. of PPh_3 are more polydisperse ($\sigma\%$ = 13%).

Next, the influence of the reaction temperature was explored and the synthesis of CuNPs with Phosphine-to-Cu ratio of 1:1 or 3:1 were performed at 65 °C (refluxing THF), (see Chapter V experimental section 3.3.B). Figure IV-4b shows typical TEM images of CuNPs obtained from the Phosphine-to-Cu ratio of 1:1, with an average size of 5.5 ± 0.6 nm ($\sigma\%$ = 11%). An increase of the reaction temperature from rt to 65 °C had no effect upon the CuNPs size. With a 3:1 ratio at 65 °C, quite monodisperse NPs were also obtained with a very slight size increase from 5.4 ± 0.5 nm at rt (Figure IV-3) to 5.6 ± 0.6 nm *($\sigma\%$* = 10%*)* (Figure IV-4c). UV-vis absorbance spectrum of these CuNPs synthetized is shown in Figure IV-5b, green curve, a plasmon absorbance at around 582 nm is observed. Here, in the case of these two ratios (1:1 or 3:1), an increase of the temperature from rt to 65 °C had thus not significant influence on the size of NPs.

It is worthy to note that in refluxing THF, partial aggregation of particles could be observed from TEM results. To avoid the assembly behavior of NPs and improve their polydispersity, the amount of PPh_3 was increased to 5 equivalents (Figure IV-4d). In refluxing THF, no gel formation was observed as was the case at rt. Figure IV-4d shows the typical TEM image of well-defined spherical CuNPs with an average size of 8.5 ± 0.4 nm and their histograms of size distribution show an improved polydispersity of 4% as compared to the one obtained with a Phosphine-to-Cu ratio of 1:1 or 3:1. A LSPR peak slightly undergoes a redshift to 585 nm as expected (Figure IV-5c, red curve).[26] All samples show an absorption profile around 580-585 nm. The CuNPs prepared with our method thus absorb in the UV-vis region and such optical properties offer promising opportunities for applications in the field of photovoltaics for example.[14]

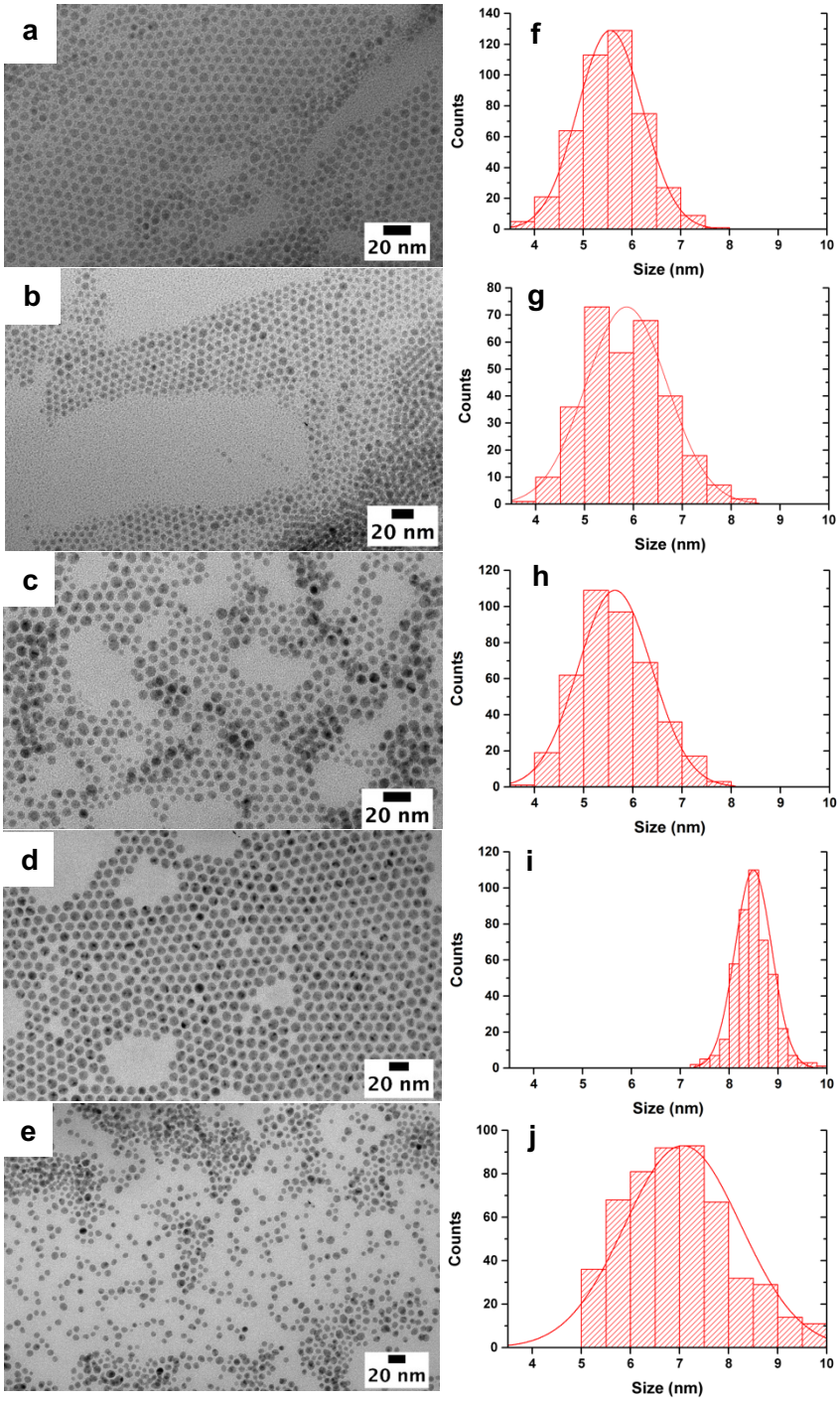

Figure IV-4. *Typical TEM images of the copper NPs from different reaction conditions: (a) CuCl/1 equiv. PPh_3/n-BuMgCl/rt (b) CuCl/1 equiv. PPh_3/n-BuMgCl/65 °C (c) CuCl/3 equiv. PPh_3/n-BuMgCl/65 °C (d) CuCl/5 equiv. PPh_3/n-BuMgCl/65 °C (e) CuCl/5 equiv. PPh_3/n-BuMgCl/-30 °C to 65 °C and (f, g, h, I, j) the corresponding size histograms.*

In order to get clear observation of temperature effect on the CuNPs synthesis in the thermal decomposition of alkylcopper, the reaction temperature was modified to - 30 °C - 65 °C with a P-to-Cu ratio of 5:1 (see in Chapter V experimental section 3.3.J). As seen above, the

CuNPs obtained (7.1 nm, *σ*% = 15%) (Figure IV-4e) from 1 equiv. of *n*-BuCu formed at low temperature (-30 °C) before the heating of the reaction mixture (65 °C) were smaller but more polydisperse than the ones synthetized (8.5 nm, *σ*% = 4%) from optimized conditions (addition of 1 equiv. of *n*-BuMgCl on the Cu(I)-phosphine complex at 65 °C). The higher polydispersity observed may be rationalized by the lower thermal decomposition rate of the organocopper reagent.

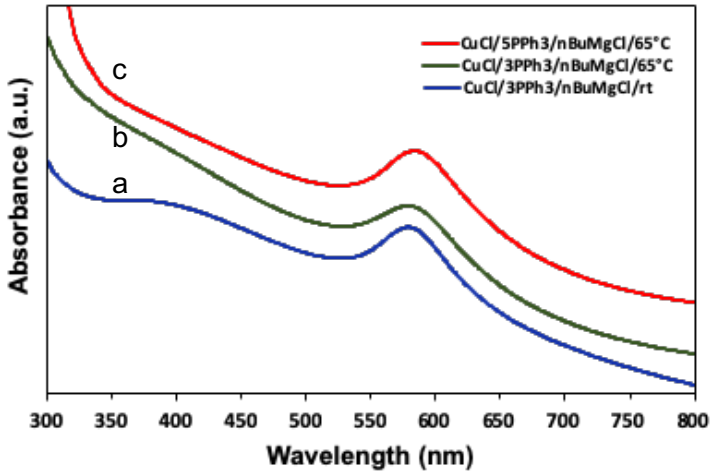

***Figure IV-5**. UV-vis spectroscopy of CuNPs obtained from (a) CuCl/3 equiv. PPh_3/n-BuMgCl/rt (580 nm) (b) CuCl/3 equiv. PPh_3/n-BuMgCl/65 °C (582 nm) (c) CuCl/5 equiv. PPh_3/n-BuMgCl/65 °C (585 nm).*

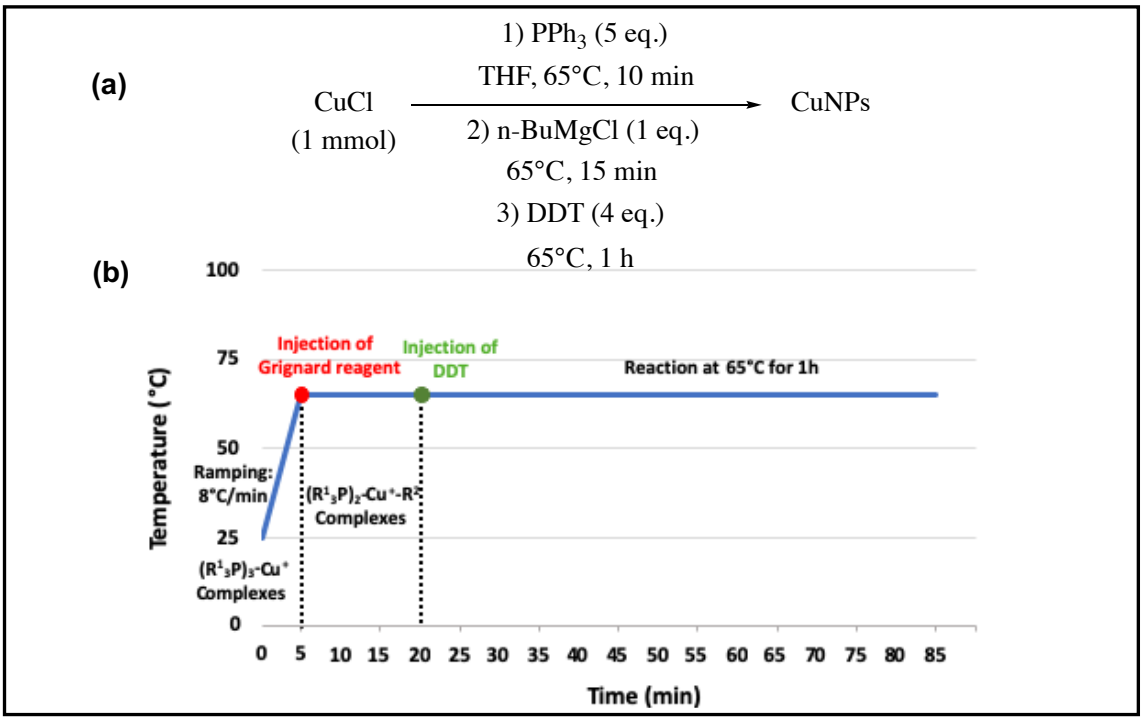

***Figure IV-6**. (a) Optimized synthetic condition (5 equiv. of PPh_3, 65 °C) for the CuNPs synthesis and (b) the corresponding graphic description of the synthesis process.*

IV. 3.3 Complete characterization of the CuNPs obtained from CuCl, PPh_3, *n*-BuMgCl and DDT with optimized PPh_3-to-phosphine ratio (5:1) and optimized temperature (65 °C)

High-resolution transmission electron microscopy (HRTEM) was next carried out to investigate the crystallographic structure of CuNPs obtained from the optimized conditions (PPh_3-to-Cu ratio of 5:1 et 65 °C). The HRTEM images reveal that the NPs are well crystallized and correspond to a mixture of face-centered cubic (*fcc*) single crystals (Figure IV-7a) and multiply twinned (MTP) particles (Figure IV-7b). A lattice distance of 0.201 nm was deduced from the selected area electron diffraction (SAED) pattern (Figure IV-7c) which corresponds to the (111) planes of the *fcc* Cu structure.

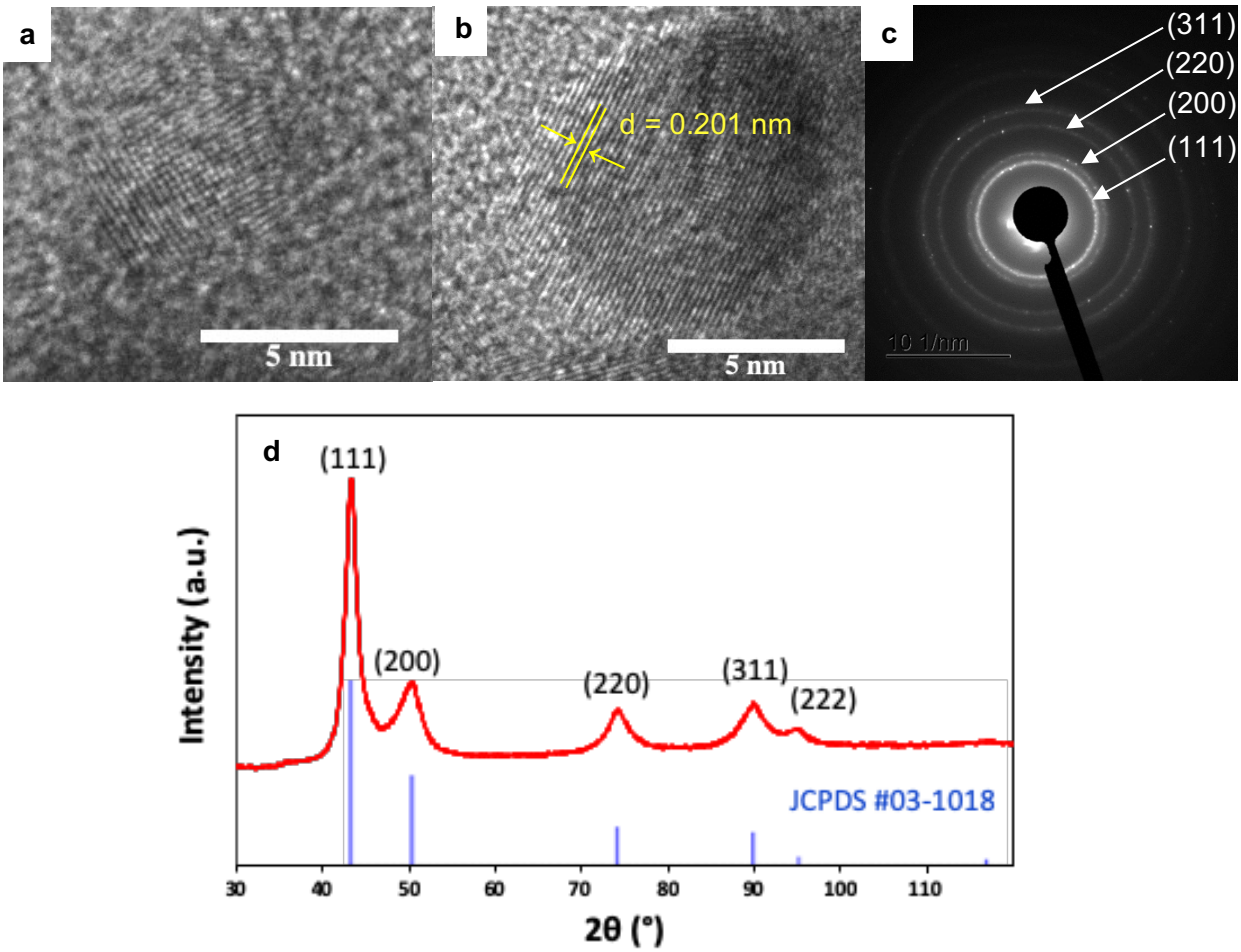

Figure IV-7. *HRTEM images of (a) MTP's particle (b) fcc single crystal (c) the corresponding SAED pattern and (d) powder XRD pattern (red: experimental, blue: theoretical) of CuNPs prepared in the optimized condition from CuCl/PPh_3 (1:5)/n-BuMgCl in refluxing THF (65 °C) and stabilized by DDT (4 equiv.).*

Powder X-ray diffraction (XRD) analysis in Figure IV-7d was next implemented in order to confirm the crystallinity and the structure of the CuNPs. Indeed, the XRD pattern shows that all the detected diffractions can be indexed to the crystal structure of metallic Cu(0). The diffraction peaks located at 43.3°, 50.4°, 74.1°, 89.9° and 95.1° can be indexed to the (111), (200), (220), (311) and (222) crystal planes of face-centered-cubic (*fcc*) structure of Cu (with conference to JCPDS #03-1018), respectively. The pattern is very clean, no diffraction peaks characteristic of Cu_2O and/or CuO were observed, which confirms the formation of pure CuNPs.

To get insight into the elements present in the NPs, energy-dispersive X-ray (EDX) was achieved and mapping of the elements also provided (Figure IV-8), respectively. EDX analysis shows the presence of elements Cu, S, P, O, Mg, Cl, C and Ni. In addition to the major signal assigned to element Cu, the spectra also highlighted a significant amount of S (Figure IV-8a). The mapping shows that copper and sulfur atoms are distributed uniformly in each of NPs (Figure IV-8b). Mg and P atoms respectively likely coming from the salt formed during the transmetalation and the PPh_3 ligand were also observed, but to a lesser extent. Cl atoms likely coming from the CuCl precursor and/or Grignard reagent (*n*-BuMgCl) can also be found. The C and Ni peaks arise from the lacey carbon-coated nickel TEM, and the element C can also be assigned to the alkyl group present of the DDT. Surface O atoms may come from the washing step when the washing tube containing the NPs solution was moved out from the glove box. Oxygen contamination could also occur when the sample was introduced in the microscope.

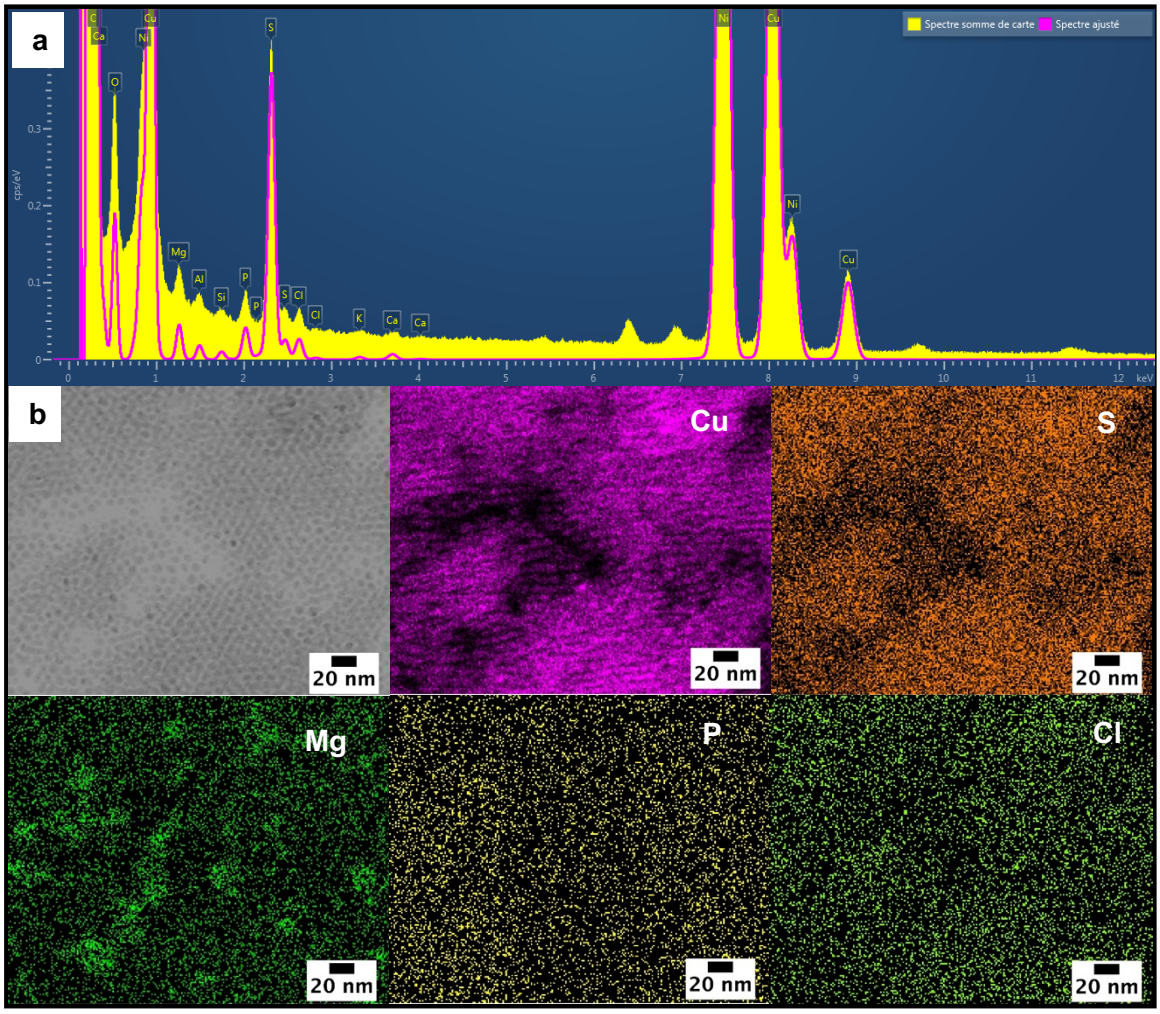

***Figure IV-8**. (a) EDX spectra of CuNPs obtained from the optimized condition CuCl/PPh_3 (5equiv.)/n-BuMgCl in refluxing THF and stabilized by DDT (4 equiv.) and (b) STEM image of CuNPs and the corresponding elemental mapping of elements Cu, S, Mg, P, Cl.*

The nature of the ligands absorbed on the surface of NPs was further characterized by X-ray photoelectron spectroscopy (XPS) analysis. All results were collected in Table IV-1 and Figure IV-9, 10.

***Table IV-1**: XPS data (binding energy: BE, assignment and composition) for CuNPs.*

Elements		Peak BE (eV)	FWHM eV	Area (P) CPS.eV	Atomic %
C1s		285.00	1.56	127089	67
Cl2p		199.59	0.29	2835	0.5
Cu2p		932.80	3.39	591049	21
Cu(I or 0)	$2p_{1/2}$	932.4	1.83	163295	10.1
	$2p_{3/2}$	951.9	1.83	85616	
Cu(II)	$2p_{1/2}$	934.1	2.53	184036	9.9
	$2p_{3/2}$	953.8	2.53	96221	
O1s		530.69	3.37	31870	7
P2p		131.00	0.42	821	<0.1
S2p1/2		163.00	3.27	16703	4.34
$(S2p_{1/2})_A$		162.27	1.63	3712.22	-
$(S2p_{3/2})_A$		163.44	1.64	1854.60	-
$(S2p_{1/2})_B$		163.97	1.86	1993.72	-
$(S2p_{3/2})_B$		165.14	1.86	997.21	-

The survey spectrum shows peaks attributed to C_{1s}, Cu_{2p}, O_{1s}, S_{2p}, P_{2p} and small signals corresponding to Cl_{2p}, and Si_{2p} (see Table IV-1 and Figure IV-9). Theoretically, S_{2p} XPS peak is composed of two contributions, namely $S_{2p1/2}/S_{2p3/2}$, each of them characterised by a full width at half maximum (FWMH) less than 2 eV. $S_{2p1/2}/S_{2p3/2}$ contributions have commonly a relative peak intensity of ½ and a binding energy (BE) difference of 1.1 eV. Here, the S_{2p} XPS signal contains more than one $S_{2p1/2}/S_{2p3/2}$ system according to the peak shape (see Figure IV-10a). The main $S_{2p1/2}/S_{2p3/2}$ doublet at 162.5/163.4 eV corresponds to the Cu-S bond[15] whereas the other one at 163.9/165.1 eV can be attributed to unbonded thiols.[16] Fitting the S_{2p} peak using four components is not accurate enough to obtain a quantitative interpretation of the spectra. However, the relative contribution of the two systems to the sulfur XPS signal can be estimated from peak areas and leads to a ratio of Cu-S/free SH between 2 and 3 depending on the fixed fitting parameters. Consequently, the relative content of sulfur in the overall sample, i.e., the atomic percentage (At%) of thiol bonded to CuNPs, is

estimated to be between 2% and 3%. P_{2p} trace (%At < 0.1%) can be also observed at 131 eV (At% < 0.1%) (Figure IV-10b),[17] a position that matches the theoretical one for a phosphine function. According to the ratio between the atomic percentage of P and S_{162eV}, the content of DDT is at least 1 order of magnitude higher than that of triphenylphosphine in the NP vicinity. Figure IV-10c presents the XPS spectra in the 930-970 eV range. The two main peaks observed contributions correspond to the $Cu_{2p1/2}$ (532 eV) and the $Cu_{2p3/2}$ (950 eV) BE. Cu(I) and Cu(0) have almost the same XPS spectra, to distinguish the two oxidation degrees, the L3MM Auger band was acquired (see Figure IV-10d). Unfortunately, the spectrum shows a single broad peak (maximum at 917.4 eV), which makes it impossible to clearly discriminate between Cu(I) and Cu(0). Therefore, we deconvoluted the Cu_{2p} XPS signal using two different contributions: the first one at 932.4 eV (Cu(0) or Cu(I)) and the second one at 934.1 eV (for Cu(II)) (see Figure IV-10c and Table IV-1). From integration, At% of ca. 10% and 11% for respectively Cu(II) and Cu(0 or I) are obtained. The At% of oxygen (7.1%) is close to the value of Cu(II), which may indicate that CuO is the main oxidized form of Cu. This hypothesis is also supported by the fact that NPs are subjected to well-known air-driven oxidation processes, responsible for the formation of Cu(II). In summary, Cu NPs are likely composed of an equal amount of Cu(II) and Cu(0).

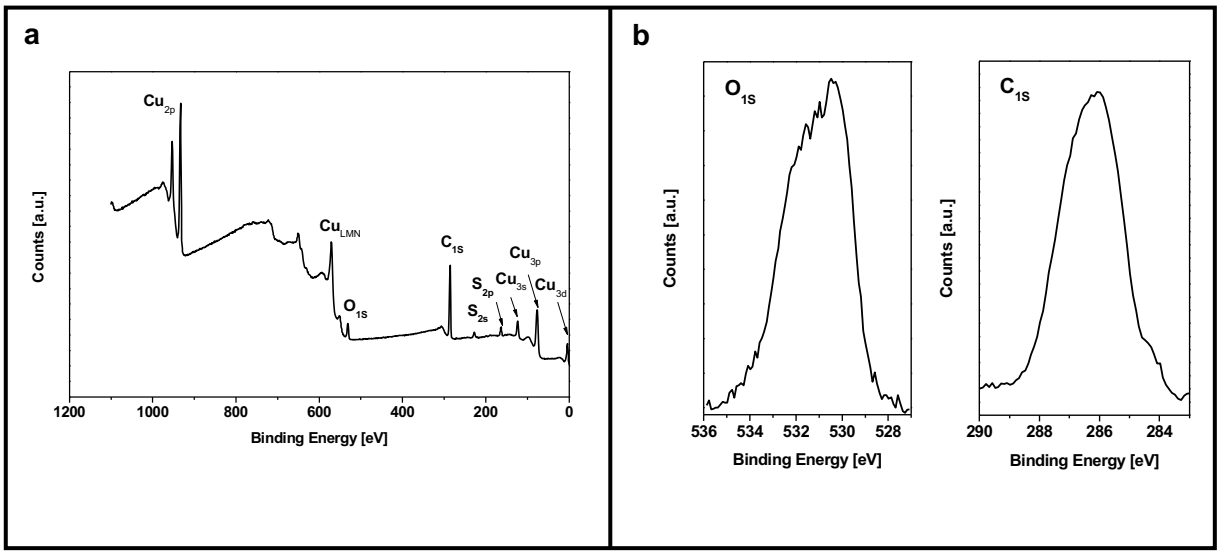

***Figure IV-9**. (a) XPS survey spectra (b) High-resolution XPS spectra of C_{1s} and O_{1s}*

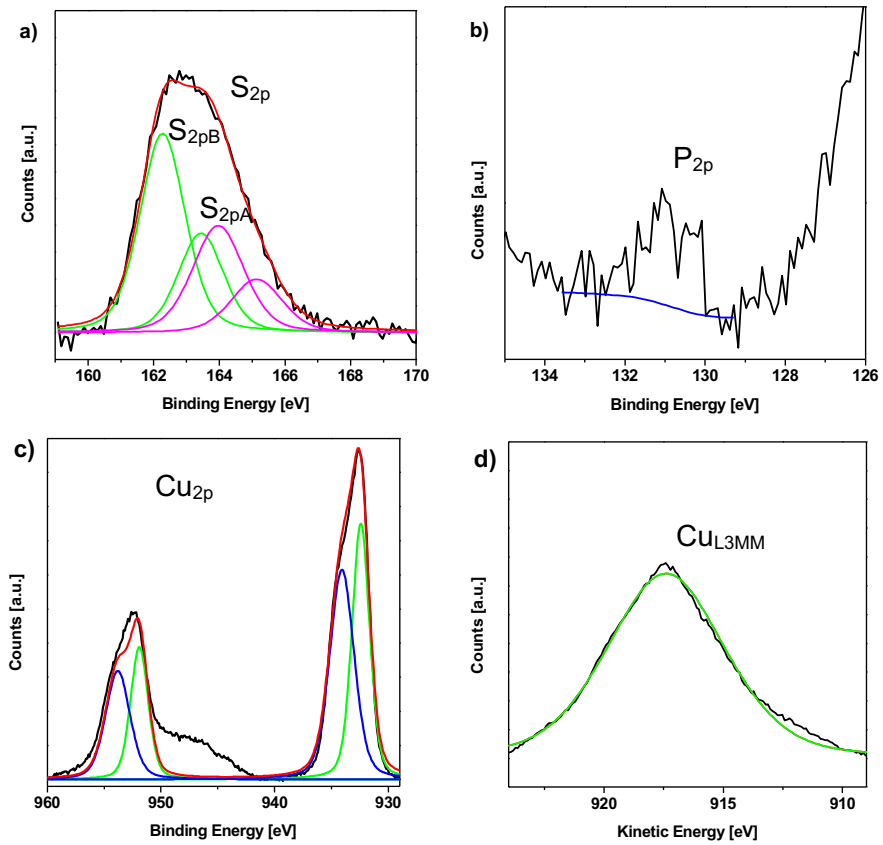

Figure IV-10. *High resolution XPS spectra of (a) S_{2p} showing (red curve) simulated spectra from the fitting with (green and magenta curves) two doublets; (b) P_{2P}, due to the low P content, P_{2P} is presented before (blue curve) baseline correction; (c) Cu_{2p} (black curve) High resolution XPS spectra of Cu_{2p}, (red curve) simulated spectra from the fitting with (green and blue curves) two doublets; (d) Cu_{L3MM}.*

A novel method to produce CuNPs has thus been discovered and the optimized conditions at this stage include the use of 5 equiv. of PPh_3 in refluxing THF. The other factors that may also influence the formation and/or morphologies of the CuNPs include the injection time and amount of sulfur ligand (DDT), the nature and amount of phosphorus ligand, the Grignard reagent-to-Copper ratio and the nature of Grignard reagent. In the three following paragraphs, the effect of these parameters on the outcome of the reaction is studied and presented.

IV. 4 Influence of the injection time of DDT on the morphology of CuNPs

We investigated the effect of the time between the addition of the Grignard reagent and the introduction of DDT for a total reaction time of 1 h 15 while the other reaction parameters were kept constant. Using the same procedure described above (see general procedure Figure IV-6), the DDT was added after 0.5, 5 or 30 min instead of the 15 min used in the optimized conditions (see in Chapter V experimental section 3.3.C). The typical TEM images (Figure IV-11a-c) obtained confirm the formation of spherical CuNPs with a mean size 6.7 ± 0.8 nm (σ% = 12%), 7.7 ± 0.5 nm (σ% = 6%), or 8.3 ± 0.5 nm (σ% = 6%), prepared from these three different injection times (0.5 min, 5 min and 30 min).

The addition of DDT after 0.5 or 5 minutes resulted in a slight but significant decrease of the particles size: from 8.5 nm (after 15 min) to 7.7 nm (after 5 min) and 6.7 nm (after 0.5 min). In the last case (Figure IV-11a), besides the NPs size was decreased, a relative higher polydispersity was also obtained (σ% = 12%) compared to others (< 6%). Additionally, the less spherical shape of NPs (0.5 min) was observed from TEM analysis. As a result, prolonging the DDT injection time from 0.5 to 15 min enables to improve the polydispersity of the CuNPs. Contrarily, delaying the addition to 30 min did not affect the morphology nor the particles size. We find out that the addition of DDT at 15 min after Grignard reagent is sufficient to produce CuNPs with well-defined shape and size. Interestingly, for the addition of DDT at 15 minutes after the Grignard reagent, an increase of the total reaction time to 3 h 15 also did not affect the final size and shape of CuNPs, as shown in Figure IV-11d.

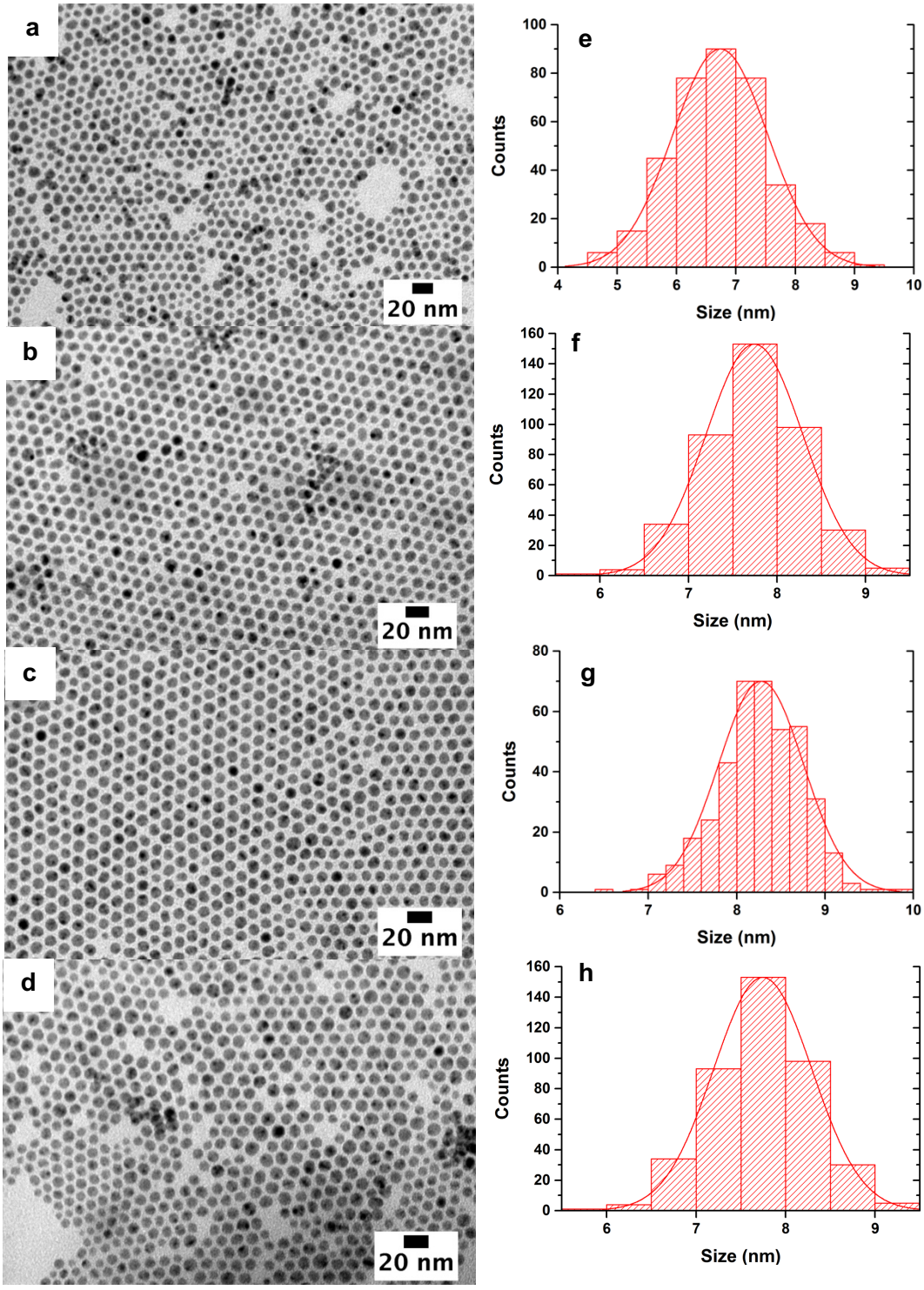

***Figure IV-11**. Representative TEM images of CuNPs obtained with different injection times of DDT after Grignard reagent addition (a) 0.5 min (b) 5 min (c) 30 min and (d) 15 min with an increase of the total reaction time to 3 h 15 and (e, f, g, h) the corresponding size histograms.*

The fact that the size of the NPs increased with increasing the injection time of DDT after the Grignard reagent (Figure IV-11a-c) prompted us to explore the morphology of the copper particles before the addition of the DDT. Hence, and in order to better understand the mechanism involved in the genesis of NPs, a next set of experiments were carried out which aimed at assessing the nature of the intermediate copper species formed before the introduction of DDT. The reaction solution was taken out after the Grignard reagent was added at different reaction times 5, 10, 15 and 30 min, in the absence of DDT and while others reaction conditions ($CuCl/5PPh_3/1$*n*-BuMgCl) were maintained (see in Chapter V experimental section 3.3.D). To collect these intermediate compounds, the solution was directly precipitated with an excess of ethanol by centrifugation at 4000 rpm at 10 min after different reaction times. A dark precipitate was obtained after two washing cycles.

The evolution of CuNPs synthesized from the reactions in the absence of DDT at different times after the injection of Grignard reagent has been characterized by TEM and HRTEM analysis. TEM images (Figure IV-12a-d) clearly show a bulk phase likely composed of agglomerated quite polydisperse spheroids. As the reaction time increased, the size of spheroids increased from 11 ± 2 nm (at 5 min) to 13 ± 2 nm (at 10 min) to 19 ± 4.9 nm (at 15 min) and 19 ± 4 nm (at 30 min). It could also be observed that the final size of spheroids was not modified if the reaction time was increased from 15 min to 30 min. This is in good agreement with our previous observations since there was no significant size change when the DDT was added after 15 min or 30 min.

The copper nanospheroids obtained after 10 min were further characterized by HRTEM and EDX to investigate their crystalline structure and the chemical element present on the particle surface. Figures IV-13a,b show the typical HRTEM images of spheroid NPs which are well crystallized, a mixture of face-centered cubic (*fcc*) single crystals and multiply twinned (MTP) particles were also observed here. Additionally, the pattern of selected electron diffraction (SAED) is shown in Figure IV-13c and confirmed that metallic Cu(0) was produced. The SAED pattern clearly shows the four diffraction rings (111), (200), (220) and (311) facet corresponding to interplanar distances of face-centered cubic (*fcc*) copper (JCPDS #03-1018), a lattice distance of 0.201 nm was deduced which corresponds to the (111) planes of the *fcc* Cu structure.

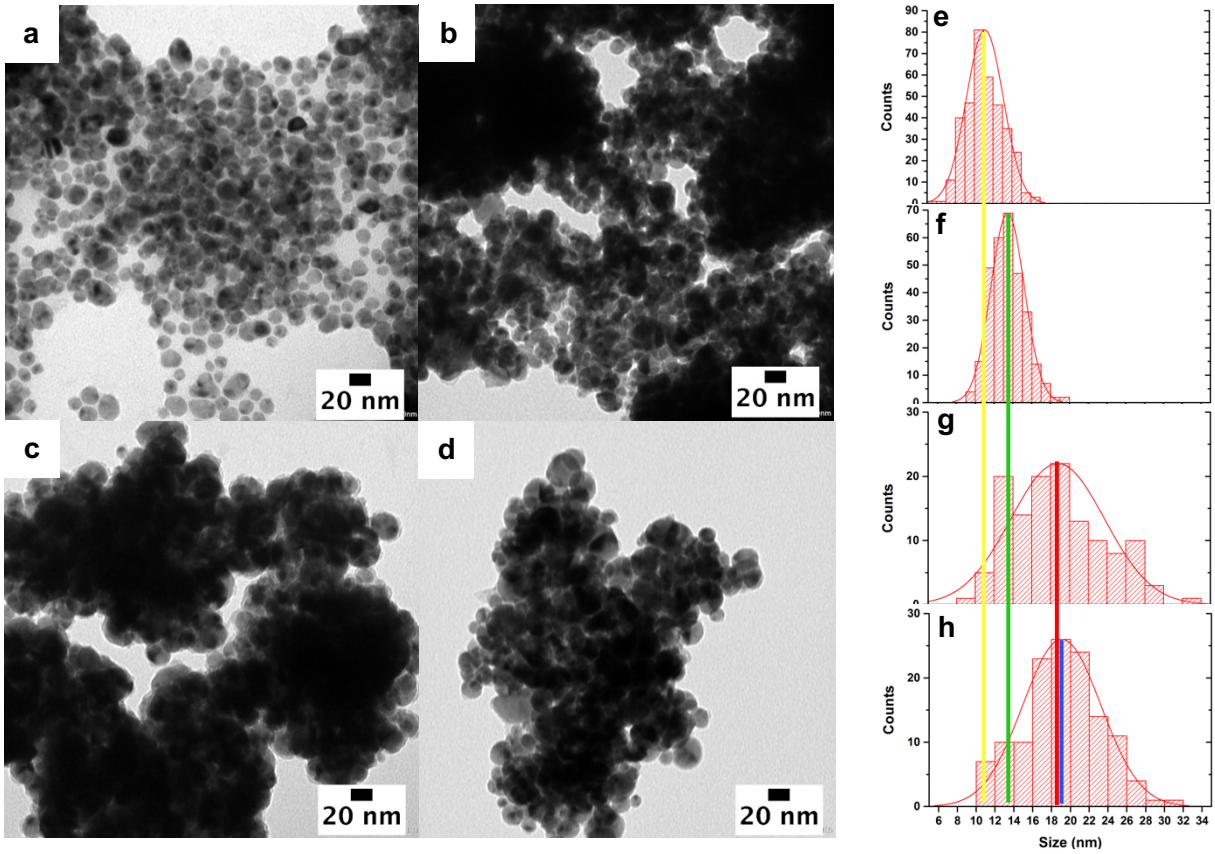

***Figure IV-12**. Representative TEM images of CuNPs obtained with different reaction times without addition of DDT at (a) 5 min (b) 10 min (c) 15 min and (d) 30 min and (e, f, g, h) the corresponding size histograms.*

The EDX spectra (Figure IV-13d) and mapping (Figure IV-13e) of the Cu spheroids NPs synthesized show the uniform presence of elements Cu, Cl, P, and Mg on the NPs surface. From the EDX spectra, in addition to the major signal of elemental Cu present, significant signals corresponding to Cl were also observed.

As mentioned in Chapter I, the steric effect of ligands not only influence the growth rate, the shape and the final size of particles, but they also prevent the uncontrolled growth and agglomeration of the NPs.[19,20] Despite its moderate steric hindrance as compared to long-chain ligands usually employed in the preparation of CuNPs (Trioctylphosphine oxide (TOPO), Trioctylphosphine (TOP) and Oleylamine (OLA))[1], triphenylphosphine (PPh_3) seems to prevent the NPs coalescence in the absence of DDT. The coordination of PPh_3 to CuNPs was already evidenced in previous reports.[10,13]

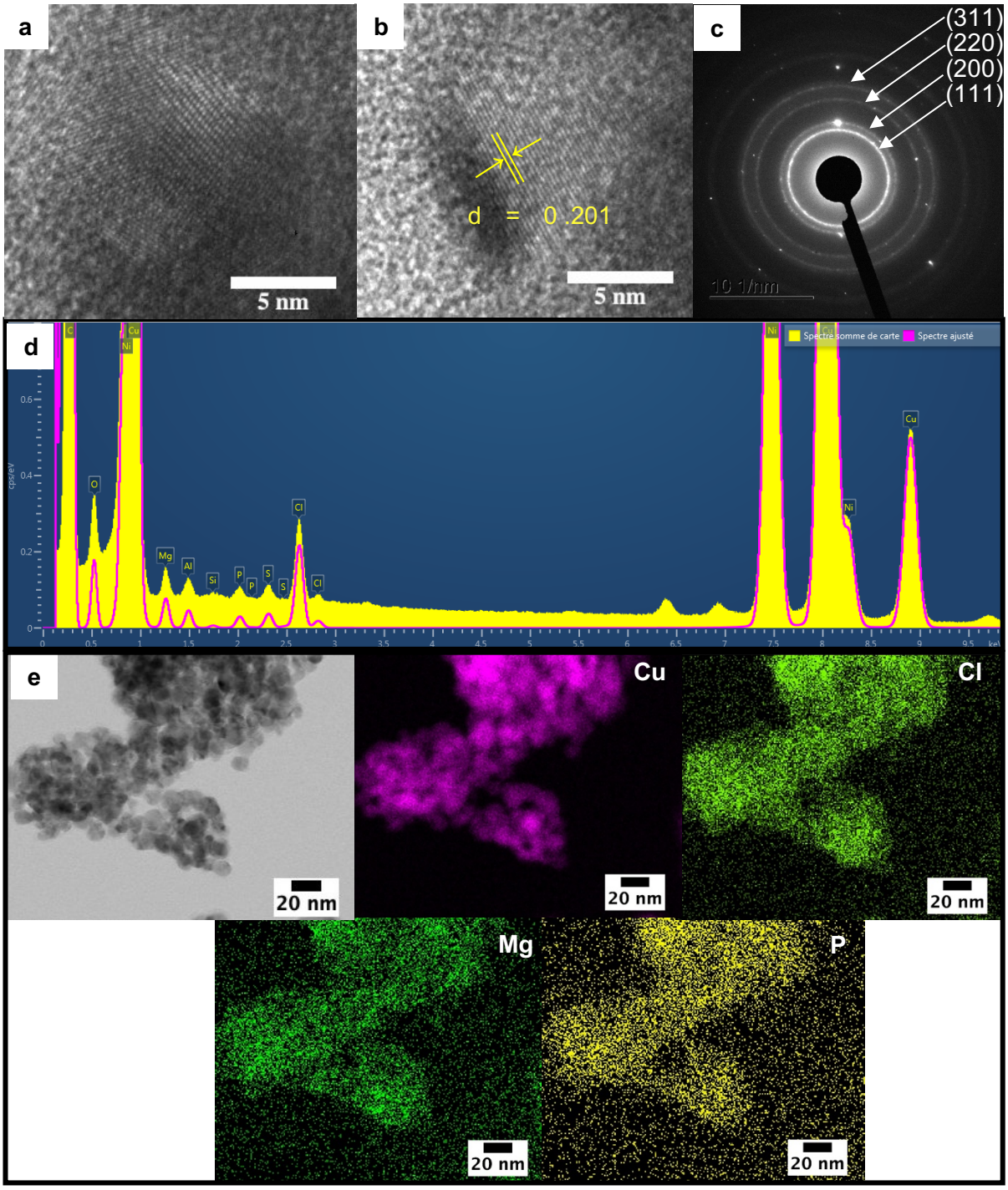

***Figure IV-13**. HRTEM images of (a) MTP's particle (b) a fcc single crystal (c) the corresponding SAED pattern of Cu spheroid NPs obtained from the condition CuCl/5PPh$_3$/n-BuMgCl in refluxing THF without the addition of DDT at 10 min (d) the corresponding EDX spectra and (e) STEM images of the CuNPs and corresponding elemental mapping of elements Cu, Cl, Mg and P.*

Interestingly, the presence of Mg derived from Grignard reagent was also clearly demonstrated by EDX analysis. However, the role of Mg, if any, is still unclear. Its presence may be due to insufficient washing of the CuNPs. The minor presence of sulfur is likely due to a contamination from the previous sample analyzed in the microscope and corresponding to DDT-stabilized CuNPs (Figure IV-4d).

In our work, a large size (19 nm) of polydisperse copper nanospheroids was detected at 15 min after the addition of Grignard reagent in the absence of DDT. Surprisingly, the large NPs agglomerates gave rise to smaller and well-defined monodisperse spherical NPs (8 nm) with a narrow size attribution (σ% = 4%) after the introduction of DDT. This phenomenon might be due to ligand-exchange carried out among the dodecanethiol (DDT), PPh_3 and halide ions (as shown in Figure IV-14). The previous results obtained from XPS and EDX analyses gave a general tendency of the different ratios of elements composing the surface ligands before and after the injection of DDT. We found that the coverage of P and Cl elements on NPs surface is significantly decreased after injection of DDT, whereas the presence of S was indicated by a strong signal.

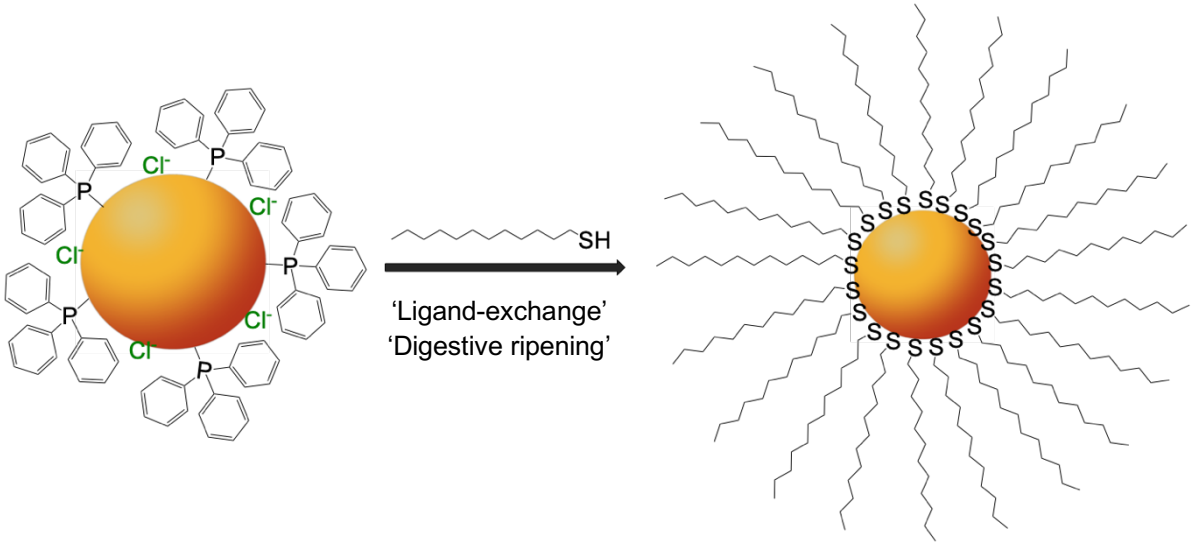

Figure IV-14. *Schematic illustration of possible ligands exchange reaction after injection of DDT.*

It is well known that during a ligand exchange, the ligands bound to the particle surface in the first step can be replaced by others that have higher affinity and stronger binding to NPs. For example, Woehrle *et al*. (2005)[21] reported the PPh_3-thiols exchange on gold NPs (AuNPs). They demonstrated that PPh_3-stabilized AuNPs (1.5 nm) undergo ligand exchange with added thiols to form thiol-stabilized AuNPs. In this case, the size of Au cores remained intact but the stability against heat, aggregation and decomposition of NPs was increased. S. Förster and co-workers (2019)[22] studied the digestive-ripening growth mechanism to describe in details the

formation of small AuNPs with low-polydispersity from larger ones during the PPh_3-DDT exchange. They demonstrated that the bigger PPh_3-stabilized AuNPs obtained at the beginning of reaction in the absence of DDT, were not very stable due to their higher surface defects than small ones. After adding DDT into the reaction, the large PPh_3-stabilized NPs (12 nm, σ% = 32%) were selectively broken down into smaller ones (1 nm, σ% = 4%), the DDT-stabilized small NPs as new nuclei grow gradually from 1 to 5 nm (after 2 h). Meanwhile, the PPh_3 on the initial small NPs were partially replaced by added DDT ligands. Additionally, the digestive-ripening process has also been applied in the preparation of CuNPs. For example, J. Chakraborty's group[23] reported the synthesis of monodispersed CuNPs (5 nm) from a reduction of $CuCl_2$•$2H_2O$ by $NaBH_4$ in the presence of tetra-octylammonium bromide (TOAB) and DDT in toluene through a two-step synthetic methodology using digestive ripening process (see in the Chapter I, section I.4). Such a digestive-ripening process could rationalize our observations in the case of DDT-coated CuNPs formation.

Along these lines, it appeared interesting to compare the amount of copper initially introduced in the reaction and the amount of copper contained in the final CuNPs. This was estimated as follows: given that the surface coverage of NPs by thiols is estimated to 75%,[23b] that dodecanethiol surface area is around 16 $Å^2$ and that the density of Cu is 8.9 $g.cm^{-3}$, it can be calculated that in the final NPs obtained from the optimized reaction conditions (8 nm in diameter), the thiol ligands represent around 13% of their weight. This calculation of mass excess due to dodecanethiol ligands was validated by low frequency Raman spectroscopy measurements performed on silver NPs.[23c] Roughly 87% of their weight thus corresponds to copper which means that the yield is almost quantitative, more than 90% of introduced copper being incorporated in CuNPs. It is worthy to note that the insoluble residue decanted away represents a very small amount as compared to the mass of salt introduced from the beginning.

IV. 5 Influence of the amount of DDT added

Another parameter that may affect the final size of the CuNPs is the amount of dodecanethiol (DDT). The next investigation on the size evolution of CuNPs was performed by tuning the amount of DDT from 4 to 2 and 8 equivalents (see in Chapter V experimental section 3.3.E). Figures IV-15a, b show the typical TEM images of CuNPs synthesized with different amounts of DDT (2 equiv. or 8 equiv.). The results show that increasing of the DDT amount produced smaller particles from 14 ± 4 nm (2 equiv., σ% = 28%) to 8.5 ± 0.4 nm (4 equiv., σ% = 4%) and 6.2 ± 0.5 nm (8 equiv., σ% = 8%). We suggest that the amount of DDT correlates with the decomposition rate of larger nanospheroids and therefore limit the aggregation of "nuclei" (or small NPs),

which leads to control the particle size. Our experimental observations are in accordance with the crucial role played by the DDT for modeling the final spherical CuNPs issued from their spheroid parent agglomerates, which is consistent with a possible “top-down” process enabling the preparation of CuNPs from the pre-organized “bulk”.

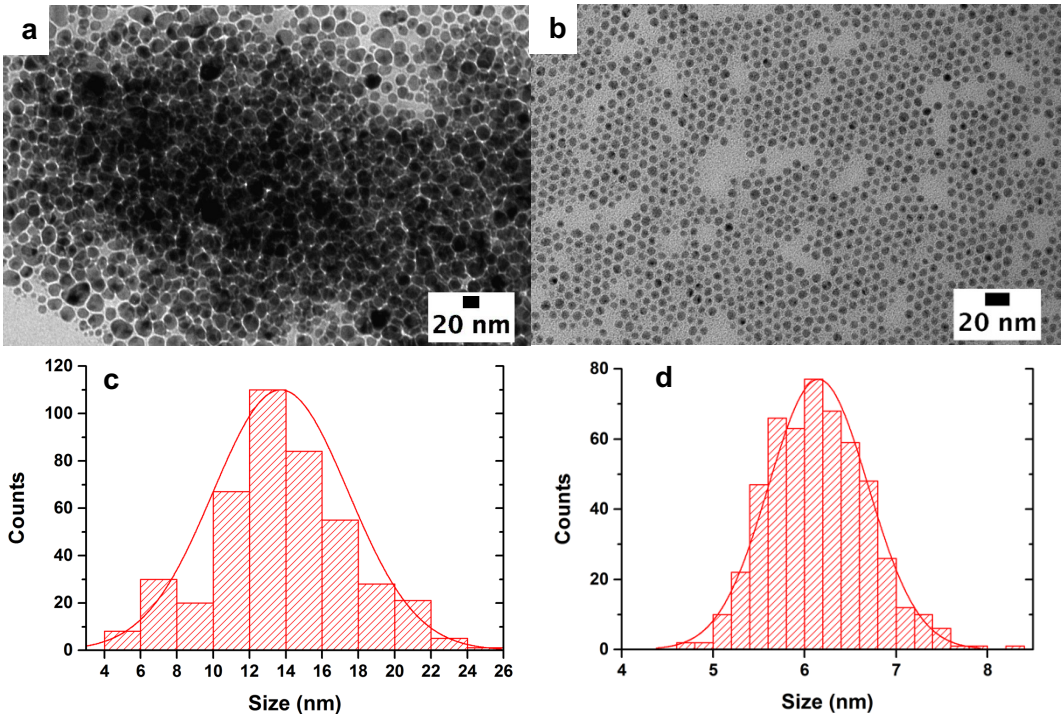

Figure IV-15. *Representative TEM images of CuNPs obtained with different amounts of DDT (a) 2 equiv. (b) 8 equiv. (c, d) the corresponding size histograms.*

The different synthetic conditions of CuNPs were overall described in Table IV-2.

***Table IV-2**. Experimental conditions were used for preparing CuNPs in the presence of PPh_3 with evolved reaction conditions by maintaining the same total reaction time for 1h15 and the corresponding size distributions.*

Precursor	**PPh_3 (equiv.)**			**T (°C)**			**DDT (equiv.)**			**t* (min)**				**NPs Size (nm)**	**σ# (%)**
	1	**3**	**5**	**25**	**65**	**-30 to 65**	**2**	**4**	**8**	**0.5**	**5**	**15**	**30**		
CuCl (1mmol)	✓			✓				✓				✓		5.5 ± 0.7	13
		✓		✓				✓				✓		5.4 ± 0.5	9
		✓			✓			✓				✓		5.6 ± 0.6	10
			✓		✓			✓				✓		8.5 ± 0.4	4
			✓		✓			✓		✓				6.7 ± 0.8	12
			✓		✓			✓			✓			7.7 ± 0.5	7
			✓		✓			✓					✓	8.3 ± 0.5	6
			✓		✓		✓					✓		14 ± 4.0	28
			✓		✓				✓			✓		6.2 ± 0.5	8
			✓			✓						✓		7.1 ± 1.1	15

**: injection time of DDT after Grignard reagent*
#: Polydispersity

IV. 6 Influence of the nature of the phosphine ligand

Previous studies showed that the nature of phosphorus ligands is a key factor to control the shape of as-synthetized CuNPs (see in Chapters II). In this work, the PPh_3 is thought to play a role as a capping ligand at the beginning of the reaction during the reduction and nucleation steps. In order to better understand the phosphorus ligands effect on the CuNPs synthesis by thermal decomposition, we have chosen certain phosphorus ligands studied in Chapter II, such as trioctylphosphite (TOPT), trimethylphosphite ($P(OMe)_3$), trioctylphosphine (TOP) and tris(dimethylamino)phosphine ($P(NMe_2)_3$) to produce CuNPs in this synthetic system. Next the thermal decomposition of organocopper reagent was realized in presence of various PR_3 ligands in the optimized reaction condition: 1 mmol of CuCl, 5 equiv. of PR_3, 1 equiv. of *n*-BuMgCl at 65 °C (Figure IV-6, Figure IV-16). At the exception of the phosphorus

ligands, all other reaction parameters were maintained (see in Chapter V experimental section 3.3.F-I).

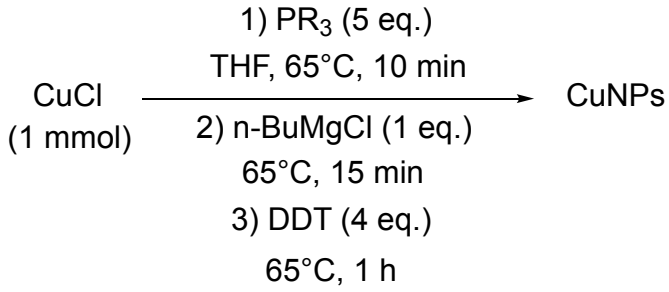

Figure IV-16. *Synthesis of CuNPs in the presence various PR_3 ligands.*

The different synthetic conditions of CuNPs were overall described in Table IV-4. Figure IV-17 displays the TEM images and size histograms of CuNPs obtained from the reaction of CuCl in presence of different phosphorus ligands: TOPT, $P(OMe)_3$, TOP and $P(NMe_2)_3$. In the case of TOPT (Figure IV-17a), polydisperse spherical NPs with an average size of 6.4 ± 1.3 nm *(σ*% = 20%*)* were obtained. As shown in Figure IV-14b, the use of $P(OMe)_3$ yielded monodisperse quasi-spherical NPs with an average size of 8.8 ± 0.9 nm *(σ*% = 10%*).* Importantly, in the presence of TOP (Figure IV-14e), we observed different morphologies mainly including quasi-spherical and, to a lesser extent, triangle- and hexagonal shaped NPs (18 ± 2.7 nm). This was the first time that we have observed triangular and hexagonal shape for NPs synthesized from an organocopper reagent. Interestingly, well-defined nanoflower-shaped NPs (Figure IV-17f) with a mean size of 28.3 ± 4.7 nm were synthesized for the use of $P(NMe_2)_3$. Such anisotropic shapes can be of interest for applications including SERS as shown in the case of related gold, silver nanoflowers.[24]

To confirm the crystalline structure of nanoflower-like NPs obtained from $P(NMe_2)_3$, powder X-ray diffraction (XRD) was performed and the diffraction patterns (Figure IV-18) of the nanoflowers shows the face-centered cubic copper phase. The diffraction peaks located at 43.28°, 50.41°, 74.09°, 89.87°, and 95.03° can be attributed to the (111), (200), (220), (311) and (222) planes of copper, which are good agreement with the conference JCPDS No. 03-1018, respectively.

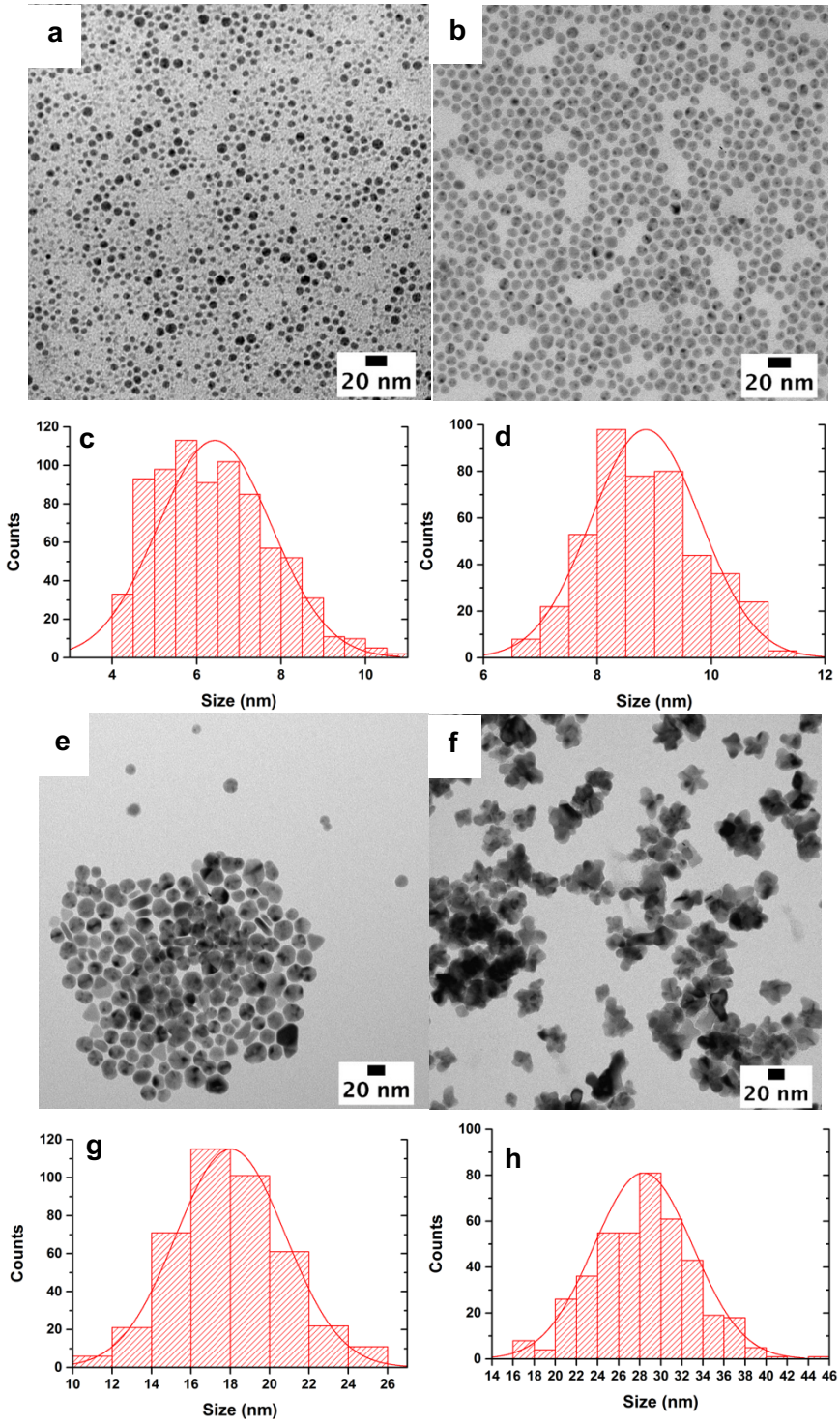

***Figure IV-17**. Typical TEM images of CuNPs obtained with different phosphorus ligands (a) TOPT (b) $P(OMe)_3$ (e) TOP (f) $P(NMe_2)_3$ and (c, d, g, h) the corresponding size histograms.*

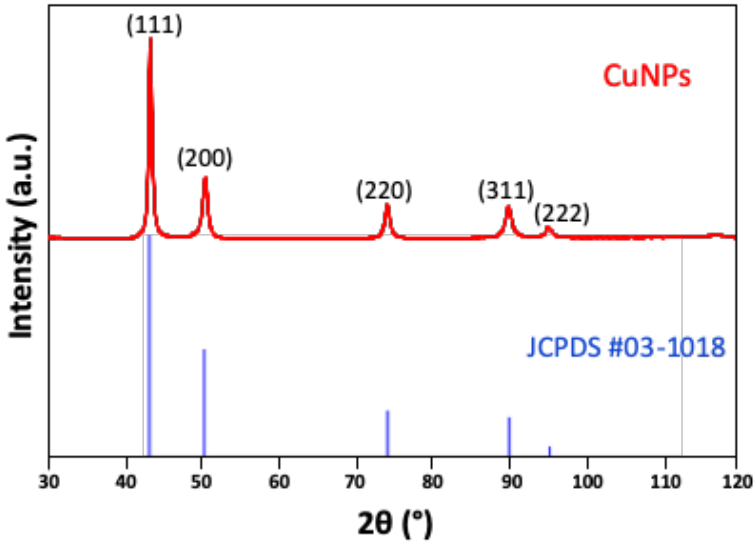

Figure IV-18. *Powder X-ray diffraction (XRD) pattern of flower-like NPs prepared using $P(NMe_2)_3$ as phosphorus ligand (with conference of JCPDS No. 03-1018).*

Table IV-3*. Experimental conditions used for preparing CuNPs by tuning phosphorus ligands and the corresponding size distributions.*

Precursor	**PR_3 Ligands (5 equiv.)**				**NPs Shape**	**NPs Size** (nm)	**σ*** (%)
	TOPT	$P(OMe)_3$	TOP	$P(NMe_2)_3$			
CuCl (1 mmol)	✓				Spherical	6.4 ± 1.3	20
		✓			Quasi-spherical	8.8 ± 0.9	10
			✓		Mixture: spherical, triangular, hexagonal	18 ± 2.7	15
				✓	Flower-like	28.3 ± 4.7	17

**: Polydispersity*

These results show that the type of phosphorus ligands is critically important for controlling the morphology of NPs synthesized by the organocopper thermolysis reaction. It is well known that NPs formation could be controlled by kinetic and thermodynamic growth factors, such as the reaction temperature, the capping agent and the precursor.[21] In the previous work, the effect of the temperature and the capping ligands on the size and shape of CuNPs synthesis have been investigated. In the next sections, our investigations will focus on the nature of the Grignard reagent and the Grignard reagent-to-copper ratio. The stability of the resulting organocopper/organocuprate compounds will depend on both of these

parameters. Therefore, both of these parameters may influence the kinetics of the thermolysis and therefore, the further formation and morphologies of CuNPs.

IV. 7 Influence of the Grignard reagent-to-copper ratio and the nature of the Grignard reagent

In the previous works, the synthesis of CuNPs have been largely investigated by tuning various reaction parameters, such as the amount of phosphine ligand, the temperature, the injection time and amount of DDT and the nature of the phosphorous ligand, through the thermal decomposition of organocopper reagent. In this section, we next investigated the influence of Grignard reagent-to-Copper ratio and the nature of Grignard reagent on the size and shape of CuNPs synthesis. In the previous investigations, the addition of 1 equiv. of *n*-BuMgCl was required to form the organocopper reagent (RCu) in the first stage of reaction. Here, we first investigated the Grignard reagent-to-Copper ratio on the CuNPs, the amount of Grignard reagent was increased from 1 to 2 (or 4, or 8) equivalents, in order to form corresponding organocuprate reagents (R_2Cu) and possible heteroleptic complexes ($R_2CuMgX•(RMgX)_2$ and $R_2CuMgX•(RMgX)_6$). As mentioned in section IV.2, when the added amount of Grignard reagent more than 1 equiv., the formation of organocuprate will be favored. Therefore, before starting the investigation of Grignard reagent amount on the CuNPs preparation, the formation pathway of organocuprate was firstly presented.

IV. 7.1 Organocuprates and the putative decomposition pathway of organocopper

Organocuprates with the general formula R_2CuLi, also called Gilman cuprate, was first described by H. Gilman et co-workers in 1952.[25] A large number of investigations were conducted to prepare new types of organocuprates and their synthetic application in organic chemistry, such as Normant cuprate ($R_2Cu•MgX$)[26] and Lipshutz cuprate ($LiCuR_2•LiCN$).[27-31] The general preparation of organocuprate reagents is shown in Figure IV-19.

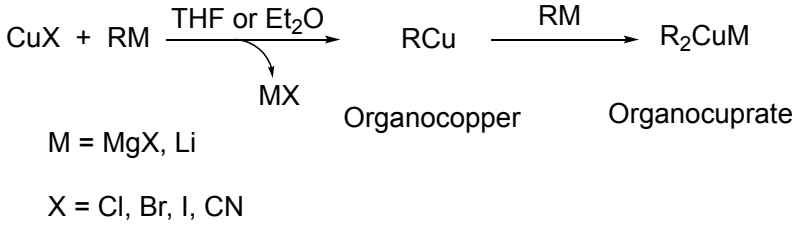

Figure IV-19. *General preparation of organocuprates reagents.*

In our study, the Normant organocuprate ($R_2Cu•MgX$) was used for synthesizing CuNPs. Compared to the neutral organocopper reagents, the organocuprate reagents are more reactive as nucleophiles since they are charged compounds. In general, the preparation of organocuprate is performed at low temperature (usually ranging from -80 °C to -20 °C) to prevent their thermic decomposition. Therefore, in our next investigations, all experiences were performed at a low temperature (-30 °C) during the preparation of organocuprate.

Based on the studies reported by Kochi's[7] and Whitesides's[8] groups (section IV-2), we proposed a possible thermolysis pathway of organocopper reagents leading to metallic Cu(0) together with the *n*-butane and *n*-butene (Figure IV-20). As a three-step process: i) a β-elimination step yielding *n*-butene and an unstable copper hydride species (Cu-H); ii) a metathesis of the latter with the second equivalent of *n*-butylcopper(I) to form *n*-butane and a dicopper species; iii) the subsequent homolytic cleavage of the Cu-Cu bond to produce the metallic Cu(0).

However, the thermal decomposition pathway of organocuprate reagents is still unclear.

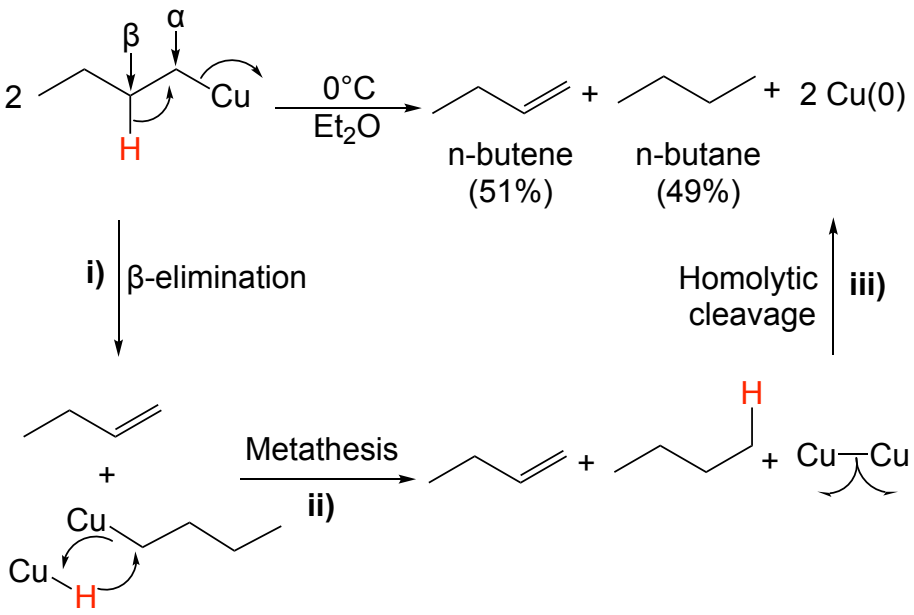

Figure IV-20. *The putative mechanism of thermal decomposition of organocopper reagent to form the metallic copper atoms.*

IV. 7.2 Effect of the amount of n-BuMgCl by using PPh_3 as the ligand

The organocuprates being more stable that the corresponding organocopper reagents, it is expected that the Cu(I) to Cu(0) reduction rate and subsequent nucleation may be impacted by the amounts of Grignard reagent used. Playing with the Grignard reagent-to-Copper ratio may thus give access to different morphology and/or size of CuNPs.

The protocol used for CuNPs preparation from organocuprate (Grignard reagent-to-Copper ratio > 1) is similar as the one for organocopper, except that the initial temperature was -30 °C instead of 25 °C to enable the formation of the organocuprate (see in Chapter V experimental section 3.3.J).

The effect of this lower initial temperature on the size and shape of NPs was also evaluated in the optimized conditions described previously in the case of the organocopper reagent (Grignard reagent-to-Copper ratio = 1, see below).

Therefore, in the typical synthesis, 1 mmol of CuCl and 5 mmol of PPh_3 were dissolved in 10 mL of dry THF at rt and stirred for 5 min under a nitrogen flow. After all solid was dissolved and a colorless homogeneous solution was obtained, the reaction was continuously stirred at -30 °C in in a thermostatic aqueous ethylalcohol bath. After 5 min, 2 mmol (or 4 mmol, or 8 mmol) of *n*-BuMgCl was quickly added into the colorless solution. The colorless solution slowly turned to orange, the reaction was continuously stirred at -30 °C for 1 h. Next, the orange solution was heated to 65 °C, gradually darkened and finally turned dark. After 15 min, 4 equiv. of DDT were added into the dark solution and the resulting red solution instantaneously formed was stirred at 65 °C for 1 h (Figure IV-21). The hot solution was cooled to rt and then the cooled NPs solution were precipitated after the addition of absolute ethanol in excess by centrifugation at 2500 rpm for 10 min. The precipitate obtained was redissolved in $CDCl_3$ and centrifugated at 4000 rpm for 5 min. After two dissolution/precipitate washing cycles, the CuNPs were stored as a red powder in the glove box for further analysis.

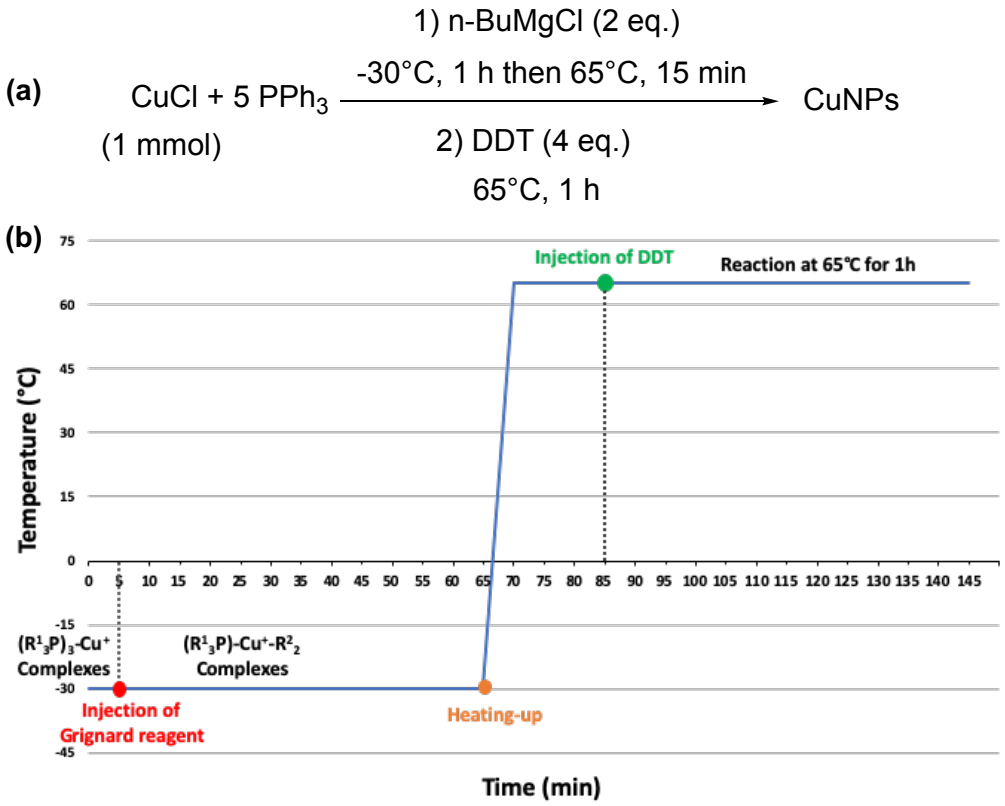

***Figure IV-21**. (a) Typical synthesis of CuNPs via thermal decomposition of organocuprate procedure (2 equiv. of n-BuMgCl, -30 °C to 65 °C) and (b) the corresponding graphic description of synthesis process.*

Figure IV-22 shows the typical TEM images of the CuNPs synthetized with different amounts of *n*-BuMgCl (2, 4 or 8 equiv.) (i.e., organocuprate reagents (R_2Cu) and possible heteroleptic complexes (*n*-$Bu_2CuMgCl$•(*n*-$BuMgCl)_2$ and *n*-$Bu_2CuMgCl$•(*n*-$BuMgCl)_6$)). As the Grignard reagent-to-Copper ratio increases, the size of CuNPs slightly increases from 7.6 ± 1.1 nm and 7.7 ± 1.2 nm and 8.9 ± 1.1 nm, and the polydispersity remains low (< 15%).

Once the amount of *n*-BuMgCl was 2 equiv., the CuNPs obtained with an average size of 7.6 ± 1.1 nm (σ% = 14%), as shown in Figure IV-22a. No significant size increasing was observed when the amount of *n*-BuMgCl was increased from 2 equiv. to 4 equiv. (from 7.6 ± 1.7 nm to 7.7 ± 1.2 nm, σ% = 16%), as shown in Figure IV-22b. However, once the 8 equiv. of *n*-BuMgCl was added, a significant increase of the size of the CuNPs was observed (8.9 ± 1.1 nm, σ% = 12%), as seen in Figure IV-22c.

From these results, we observed that the amount of Grignard reagent is able to influence the final size and polydispersity of CuNPs.

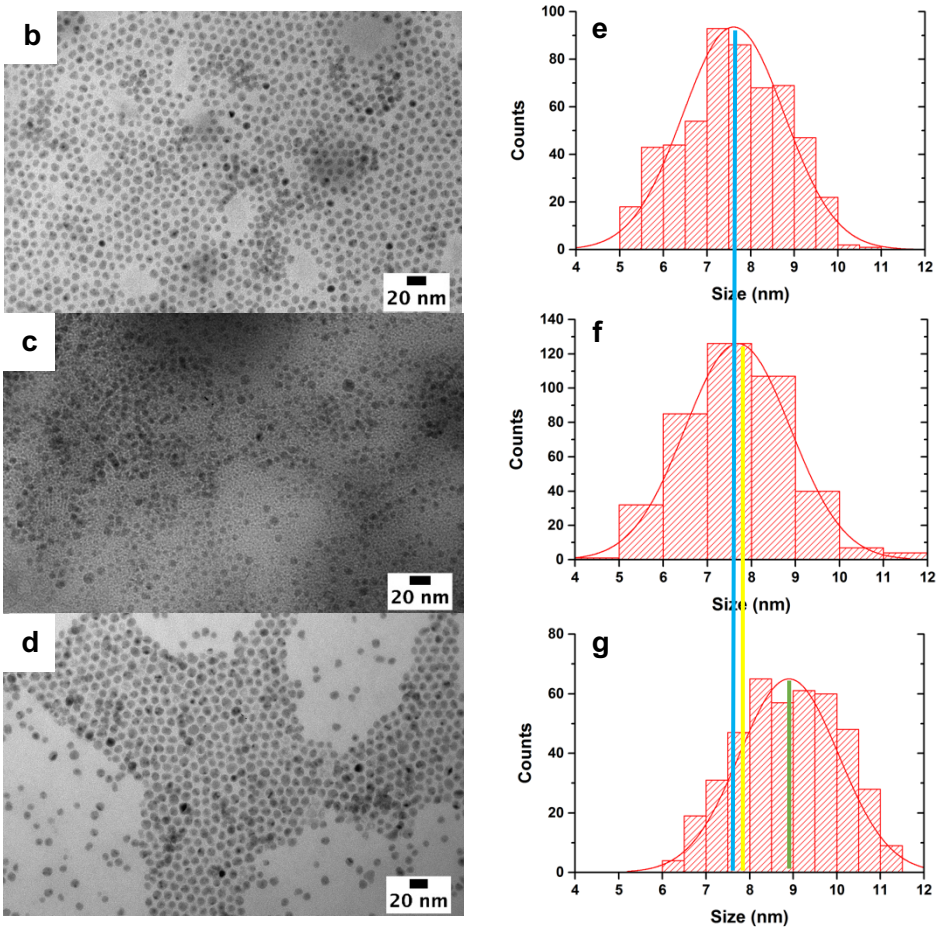

***Figure IV-22**. Typical TEM images of CuNPs obtained from the reaction of organocuprate reagent by addition of n-BuMgCl with different amounts: (a) 2 equiv. (b) 4 equiv. (c) 8 equiv. and (e, f, g) the corresponding size histograms.*

IV. 7.3 Effect of the amount of *n*-BuMgCl with TOP as the ligand

In the section IV.3.4, a very few triangle-shaped CuNPs have been observed in the thermal decomposition of organocopper (RCu) reaction in the presence of TOP ligands. In order to get clear observation of the effect of phosphine ligand on the morphology of NPs, we decided to replace the PPh_3 with TOP in the thermal decomposition of organocuprates (R_2Cu) with different Grignard reagent-to-Copper ratios.

The CuNPs syntheses were performed from CuCl with different amounts of *n*-BuMgCl (2 equiv. or 4 equiv.) in the presence of 5 equiv. of TOP, from -30 °C to 65 °C, using the evolved synthetic procedure (see in Chapter V experimental section 3.3.K). Figure IV-23a shows the typical TEM image of high uniform spherical NPs with an average size of 7.2 ± 0.6 nm (σ% =

8%) that were obtained from 2 equiv. of *n*-BuMgCl in the presence of TOP. Surprisingly, when the amount of *n*-BuMgCl was increased from 2 equiv. to 4 equiv., a significant size increase of the quasi-spherical CuNPs (12.5 ± 1.6 nm (σ% = 13%), Figure IV-23b) was observed which was not the case when PPh_3 was used as the ligand (around the same size for 2 or 4 equivalents of Grignard reagent). Moreover, the TEM image also highlighted the formation of few triangles (∽12 nm in perpendicular height) that were formed in addition to spheres. Figure IV-23e shows the UV-vis absorbance spectra of CuNPs obtained from 2 and 4 equiv. of *n*-BuMgCl and TOP as phosphine ligand. Two absorption bands located at 565 nm and 605 nm, in agreement with values reported, were assigned to CuNPs.[32] As we have discussed before, the size or shape of NPs can strongly influence the position and shape of plasmon absorption of NPs.[33] There was a red shift from 565 to 605 nm according to the particles size increase from 7 nm to 12 nm, the 40 nm of redshift may be also due to the presence of triangle shapes.

The TOP is often used to control the shape of final CuNPs due to the good affinity of the phosphorous atom for the surface of the particles and for the presence of the long chains which better prevent the NPs to coalese.[34] In our previous work (Chapter II), the electronic and steric properties of TOP and PPh_3 ligands have been studied and compared. The TOP has stronger affinity for NPs as compared to PPh_3 and also displays selective absorption on the different crystallographic faces of NPs.[34] This may be at the origin of the formation of triangular morphologies never observed with PPh_3 and this morphological evolution (from spheres to triangles) is favored for the use of a mixture of Grignard reagent and organocuprate reagents (1 equiv. CuCl for 4 equiv. *n*-BuMgCl). At this stage, the reason for this is still unclear.

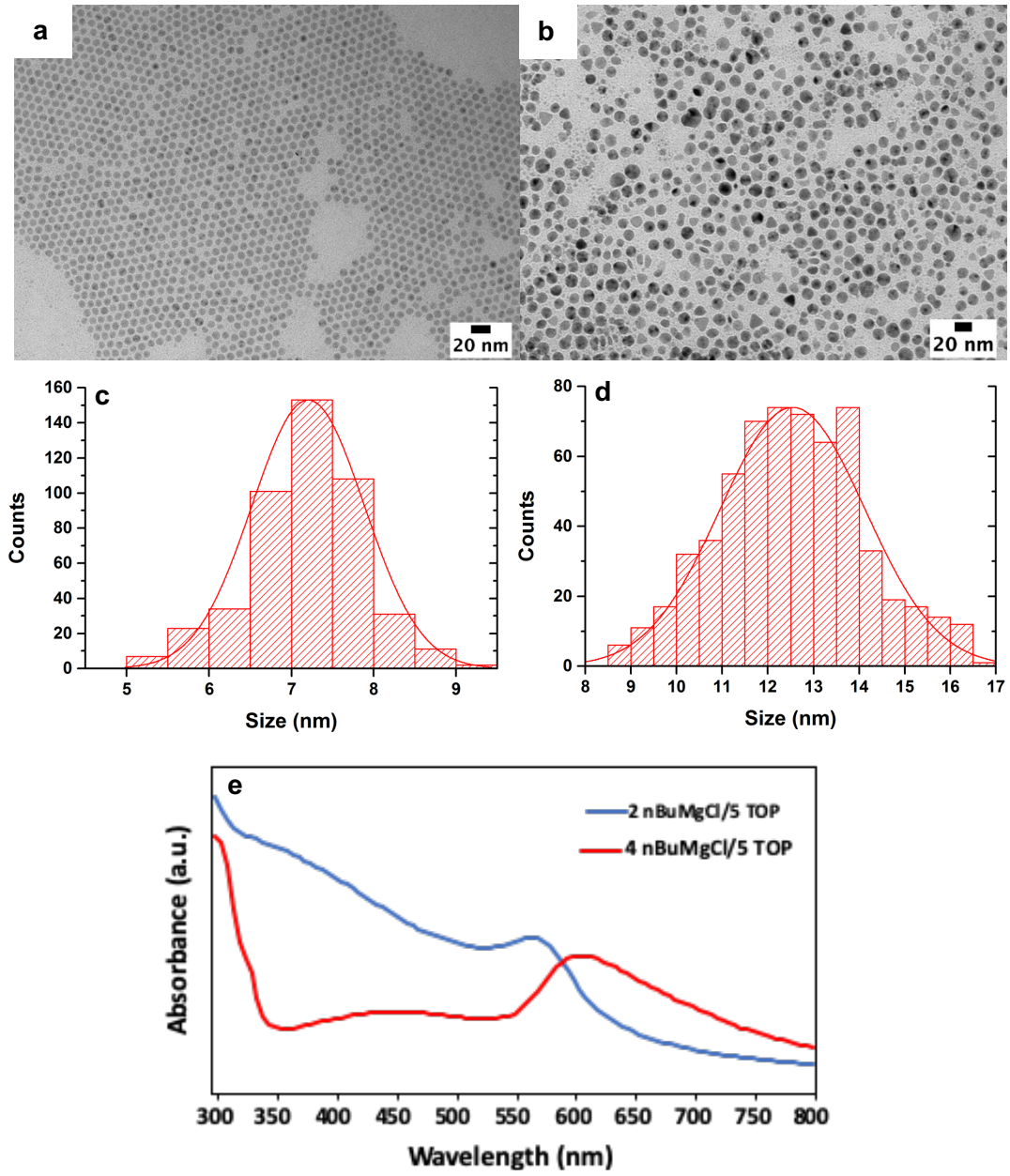

***Figure IV-23**. Typical TEM images of CuNPs obtained in the presence of TOP (5 equiv.) with different amounts of n-BuMgCl (a) 2 equiv. (b) 4 equiv. (c, d) the corresponding size histograms and (e) the corresponding UV-Vis spectrums (bleu: 565 nm, red: 605 nm).*

IV. 7.4 Effect of the nature of the Grignard reagent with PPh_3 as the ligand

The nature of Grignard reagent was next investigated to study the correlation between their chemical structure and the formation of NPs.

In the previous section, we have proposed a putative mechanism for the thermal decomposition of organocopper (or organocuprate) compounds based on Whitesides's mechanism study (Schema IV-17). In these processes, the elimination of an hydrogen atom on the *β*-carbon is the key step for achieving the decomposition of organocopper and to thus generate the unstable copper hydride species at the origin of the release of Cu(0). In order to get insight into the chemical process occurring during the thermolysis, several Grignard reagents were tested as precursors to obtain reactive organocopper species. Some of them possess hydrogen atom on the *β*-carbon and can undergo *β*-elimination (Table IV-4, entries 1-3) while others do not (entries 4-6). In the next sections, the syntheses of CuNPs were investigated under conditions with or without possibility of *β*-elimination.

Table IV-4.* *Structural formula of the Grignard reagents and their number of β-hydrogen.*

Entry	R_2MgX compounds	Structural formula	Number of *β*-hydrogen	*β*-elimination (Yes or No)
1	*n*-BuMgCl*	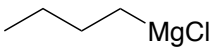	2	Yes
2	EtMgBr		3	Yes
3	*t*-BuMgCl	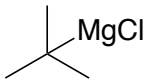	9	Yes
4	isopropenylMgBr	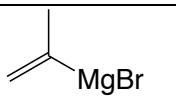	3	No (?)
5	PhMgCl	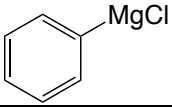	2	No
6	MeMgCl		0	No

**: the results were collected in the section IV.7.2*

In the first part of this section, the synthesis of CuNPs via thermolysis of alkyl organocopper reagent was studied, namely *n*-BuCu, *n*-Bu_2Cu•MgCl (see in section IV.7.2), EtCu, Et_2Cu•MgX (X = Cl, Br), *t*-BuCu, *t*-Bu_2Cu•MgCl.

It is described that thermal stability of alkylcopper reagents are in following order: primary alkylcopper > secondary alkylcopper > tertiary alkylcopper. For example, the thermal stability of *t*-BuCu is few seconds at -90 °C in THF.[35]

This thermal stability order may be explained by the stability order of the corresponding double bond yielded by the *β*-elimination reaction that occurred during the thermolysis.

IV. 7.4.1 Alkyl Grignard reagent with β-elimination possible (EtMgBr, t-BuMgCl)

All experiments were performed using the procedure described above (Figure IV-21) with the amount of Grignard reagent ranging from 1 to 2 equivalents (see in Chapter V experimental section 3.3 L-M, Figure IV-24).

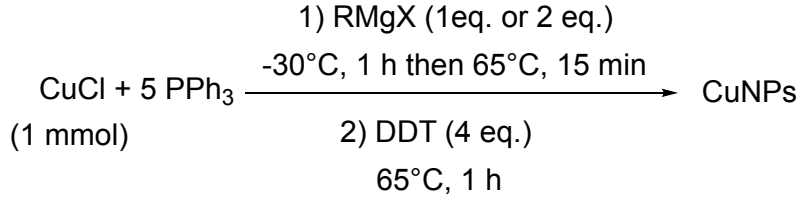

Figure IV-24. *Synthesis of CuNPs from different Grignard reagents (RMgX) in the presence of 5 equiv. of PPh_3.*

We first investigated the preparation of NPs using CuCl and different amounts of EtMgBr (1 or 2 equiv.). The typical TEM images of obtained NPs and the corresponding size distribution histograms are shown in Figure IV-25. Monodisperse spherical NPs with an average size of 9.9 ± 0.9 nm (σ% = 9%) were obtained from the thermolysis of EtCu (Figure IV-25a). The NPs synthetized from Et_2Cu•MgX reagent (X = Cl, Br) were slightly bigger than those stemming from EtCu. Their average size is 10.4 ± 1.4 nm (σ% = 13%) and they have a less spherical morphology than the one obtained from EtCu (Figure IV-25b). As a result, the use of a Normant organocopper reagent lead to the slight increasing of the particle size, but do not have a significant effect on the particle shape. By comparison with the CuNPs synthetized from *n*-BuCu (7.1 ± 1.1 nm, σ% = 15%) and *n*-Bu_2Cu•MgCl (7.6 ± 1.1 nm, σ% = 14%), these NPs obtained from EtCu and Et_2Cu•MgX (X = Cl, Br) are larger with almost the same polydispersity. It is worth noting that the solution color changed

slower from colorless to orange when the EtMgBr was added, as compared to *n*-BuMgCl, which is in good accordance with the known higher thermal stability of the EtCu compared to *n*-BuCu reagent.

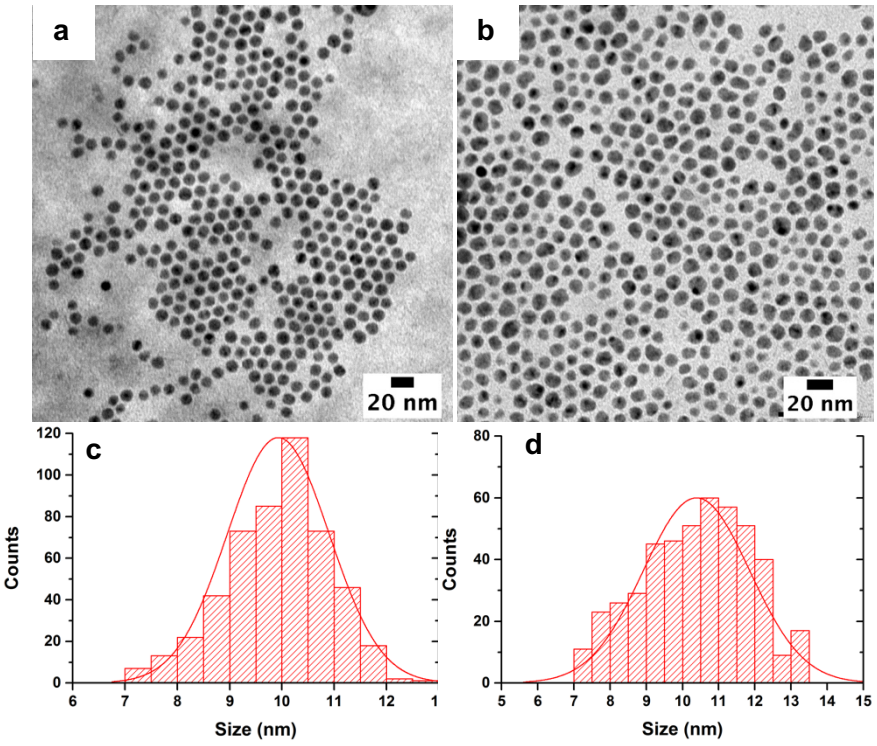

***Figure IV-25**. Typical TEM images of CuNPs synthesized in the presence of EtMgBr with different amounts (a) 1 equiv. (b) 2 equiv. under reaction temperatures at -30°C to 65 °C and (c, d) the corresponding size histograms.*

Subsequently, experiments were carried out with 1 equiv. or 2 equiv. of *t*-BuMgCl per CuCl. Figure IV-26a shows the typical TEM image of quasi-spherical CuNPs obtained from *t*-BuCu with an average size of 10.1 ± 1.7 nm (σ% = 17%) and a few nanorods-like of ∽24 nm in length and ∽11 nm in width. Larger NPs were also observed by increasing the amount of *t*-BuMgCl to 2 equiv. per CuCl in order to yield the Normant cuprate *t*-Bu_2Cu•MgCl. Its thermolysis gave NPs of similar morphologies with an increased mean size of 14.9 ± 2.5 nm (σ% = 17%), as shown in Figure 26b. As discussed above, the thermal decomposition of the organocuprate is slower than the organocopper analogue, which leaded to a slower nucleation rate thus resulted the larger NPs is in good accordance with LaMer's theory. Similarly, we observed that the NPs size was greatly increased from 7 nm to 15 nm and the obtained NPs are anisotropic when the organocuprate *t*-Bu_2Cu•MgCl was used instead of *n*-Bu_2Cu•MgCl.

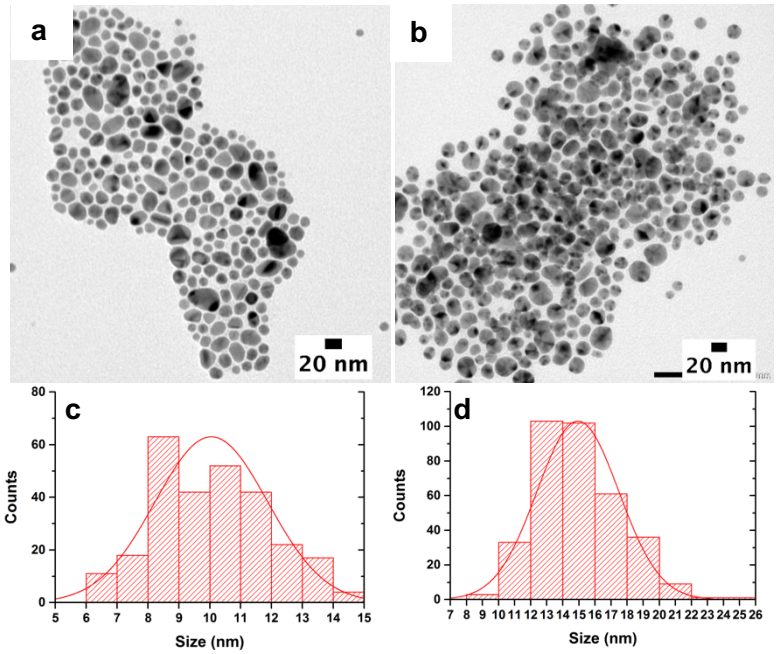

***Figure IV-26**. Representative TEM images of CuNPs synthesized from different amounts of t-BuMgCl: (a) 1 equiv. (b) 2 equiv. and (c, d) the corresponding size histograms.*

According to LaMer's theory,[36] the high concentration of monomer promotes the formation of small homogeneous NPs than lower one. As we discussed in Chapter I, the concentration of monomer highly depends on serval parameters, and the reduction rate of the metallic precursor is one of them. The fast reduction rate of the precursor leads to a high concentration of monomer, thus to result a burst nucleation and consequently produce small NPs with high uniformity. However, these results are in contrast to the LaMer's theory, because the thermal decomposition rate of *t*-Bu_2Cu•MgCl is faster than *n*-Bu_2Cu•MgX (X = Cl, Br).

And also, the morphology of CuNPs could be affected by the nature of Grignard reagent such as the case of *t*-BuMgCl, although it is not greatly.

Therefore, the size of CuNPs could be affected by serval parameters instead of the only decomposition rate of alkylcopper. However, the exact reason for the increase in nanoparticle size by using these three Grignard reagents is still unclear.

IV. 7.4.2 Organocopper reagents bearing no eliminable hydrogen in β-position to copper (isopropenylMgBr, PhMgCl, MeMgBr)

In order to get more insights on the effect of chemical structure of Grignard reagent in the CuNPs synthesis, we also used several organocopper reagents unable to undergo *β*-elimination of CuH, stemming from isopropenylMgBr, PhMgCl and MeMgBr (Table IV-5). Interestingly, we have still observed the formation of NPs with some of them.

Figure IV-27a shows the typical TEM image of CuNPs synthesized from isopropenylCu, with an average size of 3.5 ± 0.5 nm (σ% = 14%). The thermolysis of (isopropenyl)$_2$Cu•MgX (X = Cl, Br) gave CuNPs with a mean size of 3.3 ± 0.4 nm (σ% = 12%), as shown in Figure IV-27b. No significant difference in size was thus observed between the CuNPs obtained from the organocopper or the organocuprate reagent. However, the use of as the Normant reagent gave CuNPs with a lower polydispersity (from 14% to 12%). It is important to note that the solution color change was also much slower than in the case of *n*-BuCu and *n*-Bu$_2$Cu•MgCl. These NPs has much smaller size than the ones obtained from *n*-BuCu (7 nm). This result is unexpected and it also do not fit to LaMer's theory.[36]

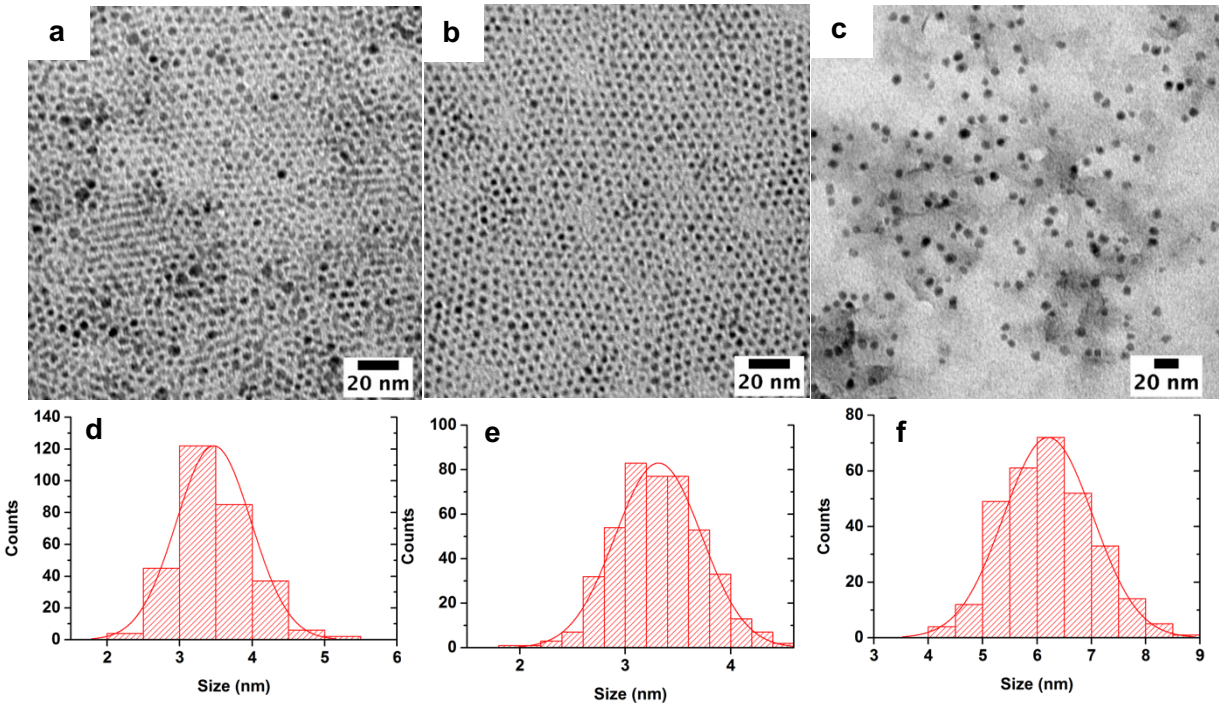

Figure IV-27. *Typical TEM images of CuNPs synthesized in the presence of CuCl and (a) 1 equiv. (b) 2 equiv. of isopropenylMgBr and (c) 2 equiv. of PhMgCl under reaction temperatures at -30 °C to 65 °C and (d, e, f) the corresponding size histograms.*

The thermolysis of PhCu did not lead to the formation of NPs, whereas Ph_2Cu•MgCl gave spherical CuNPs with an average size of 6.2 ± 0.8 nm (σ% = 13%) (as seen in Figure IV-27c). It is worthy to note that no CuNPs could be synthetized from MeCu or Me_2Cu•MgCl due to the formation of a gel in both cases.

In the literature, in addition to the reductive *β*-elimination, others thermal decomposition pathways of metal alkyl have been reported,[37,38] such as homolytic scission, bimolecular C-C bond formation, etc (Figure IV-28). When *β*-elimination is impossible, the direct homolytic cleavage of Cu-C often occurs.[39,40,41] For example, the thermal decomposition of MeCu via the homolytic scission was reported by S. Pasynkiewicz *et al.*[42] (Figure IV-29). But, the exact decomposition pathways of isopropenylcopper and phenylcopper which were formed by using isopropenylMgBr and PhMgCl are still unclear.

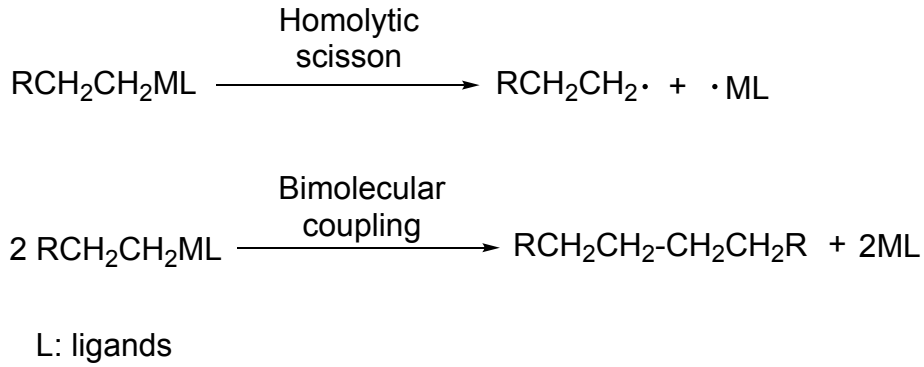

Figure IV-28. *Possible pathways for the thermal decomposition of metal alkyl complexes.*

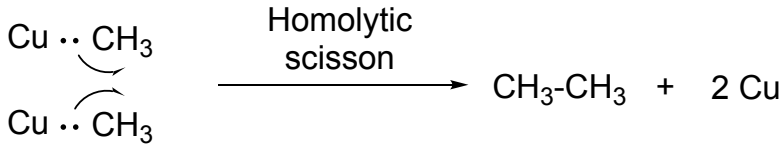

Figure IV-29. *The thermal decomposition of methylcopper (MeCu) via homolytic scission.*[36]

Table IV-5. *Experimental organocuprate conditions used for preparing CuNPs using different Grignard reagents and the corresponding size distributions.*

Grignard reagent					**PPh_3 (5 eq.)**	**TOP (5 eq.)**	**NPs shape**	**NPs size** (nm)	**σ*** (%)
eq.	**1**	**2**	**4**	**8**					
n-BuMgCl	✓				✓		Quasi-spherical	7.1 ± 1.1	15
		✓			✓		Spheres	7.6 ± 1.7	22
			✓		✓		Spheres	7.7 ± 1.3	17
				✓	✓		Spheres	8.9 ± 1.1	12
		✓				✓	Spheres	7.2 ± 0.6	8
			✓			✓	Quasi-spherical, Triangle	12.5 ± 1.6	12
EtMgBr	✓				✓		Spheres	9.9 ± 0.9	9
		✓			✓		Quasi-spherical	10.4 ± 1.4	13
t-BuMgCl	✓				✓		Spheres	10.1 ± 1.8	17
		✓			✓		Quasi-spherical	14.9 ± 2.5	16
Isopropenyl-MgBr	✓				✓		Spheres	3.5 ± 0.5	14
		✓			✓		Spheres	3.3 ± 0.4	12
PhMgCl	✓				✓		-	-	-
		✓			✓		Spheres	6.2 ± 0.8	13
MeMgCl	✓				✓		-	-	-
		✓			✓		-	-	-

** : Polydispersity.*

All results summarized in Table IV-6 shown that the nature of Grignard reagent is critically important for controlling the size of CuNPs, but slightly affect their shape controlling. From the results obtained in the case of MeCu and Me_2Cu•MgCl, there was no observation of CuNPs synthetized. And for the CuNPs obtained from isopenylCu, $(isopenyl)_2Cu$•MgX (X = Cl, Br), PhCu and Ph_2Cu•MgCl, due to their different radical decomposition mechanism from the

reductive *β*-elimination, however, there was formation of NPs but of lower quality than the ones obtained from *n*-BuCu. The reason is still unclear. In addition, the RCu resulted in higher-quality of NPs than their R_2Cu•MgX (X = Cl, Br) analogues.

IV. 8 Photolysis of organocopper compounds

In addition to the thermolysis of organocopper reagents approach, there is another reported route for the decomposition of organocopper reagent that is the photolysis at low temperature.[41] We have also tested this method to prepared the CuNPs with different reaction conditions A (CuCl/5 equiv. PPh_3/*n*-BuMgCl/*hυ*/-30 °C) and B (CuCl/5 equiv. PPh_3/*n*-BuMgCl/4 equiv. DDT/*hυ*/-30 °C). The protocols used for the photolysis of organocopper compounds as seen in Chapter V experimental section 3.3.Q-R. For the reaction condition A (without addition of DDT), there was a formation of gray gel after reaction completed. In the case of reaction B (with addition of DDT), when the reaction was stopped after 24 h stirring at -30 °C, a greenish-orange solution was observed instead of a reddish solution. However, during the washing step, the supernatant turned to red. The NPs isolated were analyzed by TEM (Figure IV-30) after a standard washing step, the spherical CuNPs were obtained with an average size of 5.73 ± 0.67 nm (*σ*% = 12%). But, the occurrence of the CuNPs formation is still unclear at which stage, photolysis at -30 °C step or washing step at rt.

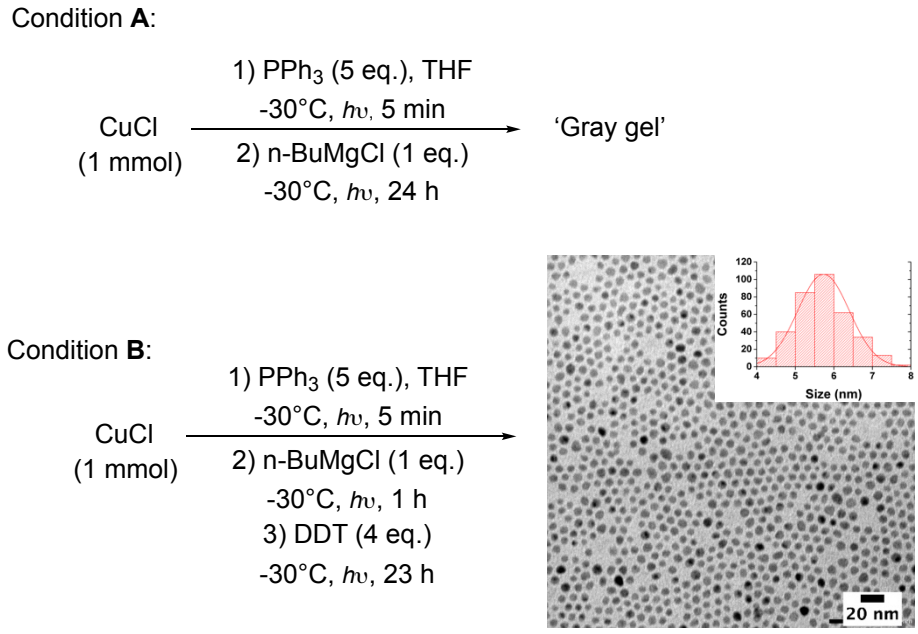

Figure IV-30. *Synthesis of CuNPs via photolysis of organocopper reagents.*

IV. 9 Scale-up of the CuNPs synthesis

Through a careful optimization of reaction conditions, such as the reaction temperature, the amount and injection time of DDT and the amount and nature of Grignard reagent, high uniformity of CuNPs size was obtained through a reproducible and practical procedure of thermal decomposition of butyl copper reagent. To the best of our knowledge, the large scalable synthesis of monodisperse high-quantity copper NPs is not easily achieved.

Therefore, the NPs synthesis was increased to a 5 mmol scale with the optimized conditions (see in Chapter V experimental section 3.3.R), starting from 5 mmol (495 mg) of CuCl and 25 mmol of PPh_3 (5 equiv.) in 50 mL of dry THF at 65 °C. Following the addition of the Grignard reagent (5 equiv.) and the DDT (4 equiv.), the red dark solution mixture was stirred at 65 °C for 1 h. A standard work up of washing/centrifugation sequences yielded a first principal batch of 270 mg of size-selected CuNPs with an average size of 8.4 ± 0.6 nm and an obtained low polydispersity (8%), as shown in Figure IV-31a. It is similar to the results obtained at the 1 mmol scale of CuNPs synthesis presented above (Figure IV-4e). It is worthy to note that the second batch of 100 mg of smaller CuNPs could be selected from the supernatant with an average size of 7.1 ± 1.3 nm (σ% = 18%) (Figure IV-31b).

These results show the potential of the discovered synthetic route for the large-scale synthesis of CuNPs without changing the monodispersity and shape of particles. We do believe that such possible scale-up is a strong asset of the methodology both from a fundamental and industrial viewpoint.

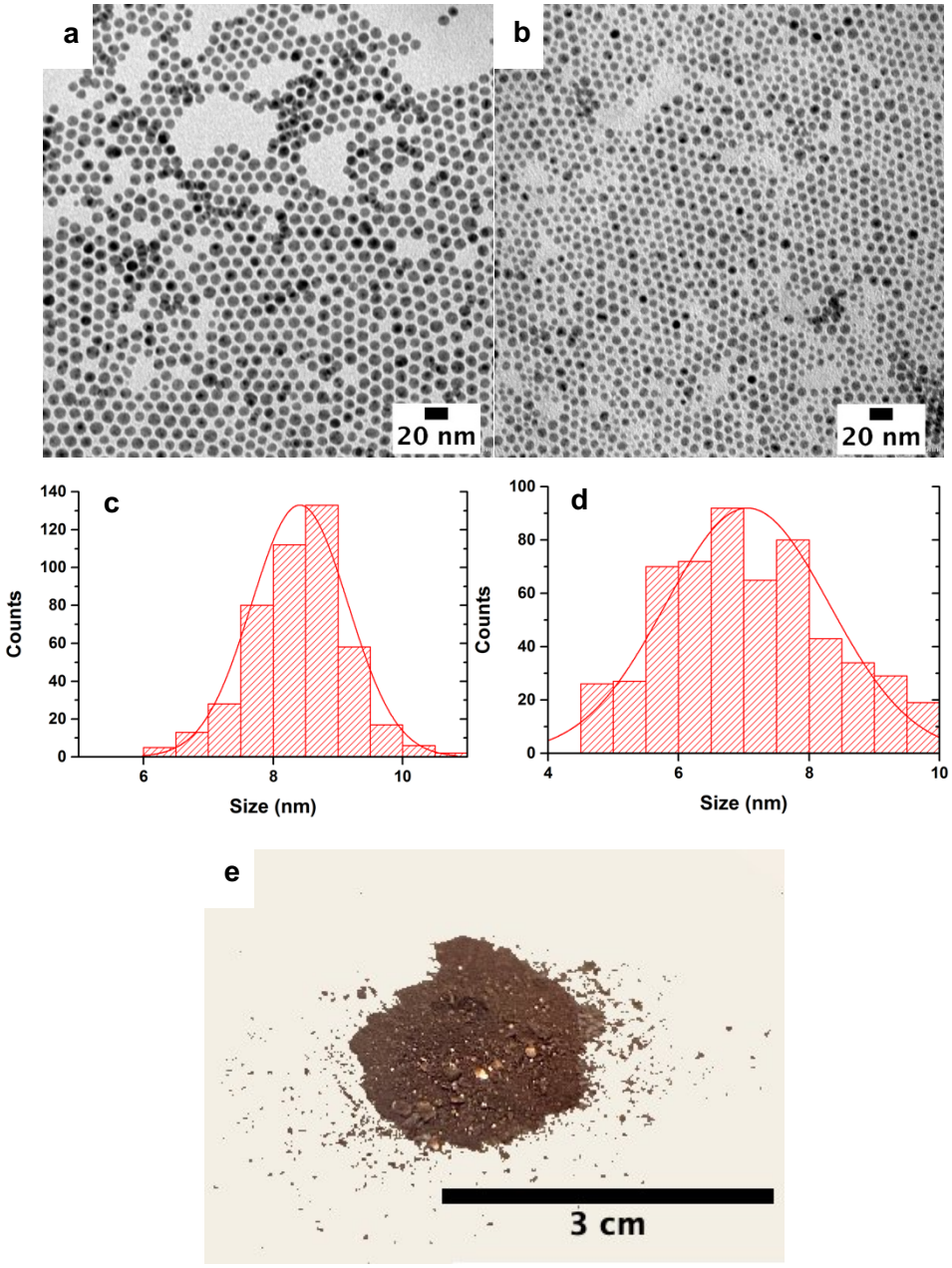

***Figure IV-31**. Typical TEM images of the CuNPs obtained through a large-scale synthesis (a) the main batch (270 mg, 8.4 ± 0.6 nm) (b) the smaller batch (100 mg, 7.1 ± 1.3 nm) (c, d) the corresponding size histograms and (e) the corresponding picture of the main batch of NPs.*

IV. 10 Conclusion

In conclusion, we reported here a simple, innovative and robust thermolysis approach for the synthesis of well-defined CuNPs with narrow size distribution, without employing an excess of long chain alkylamine, often used as the solvent. Using this more atom-economic method, CuNPs were synthetized with tunable size ranging from 3 to 20 nm by modifying several reaction parameters (e.g. the amount of phosphine ligand, the temperature, the injection time and amount of DDT, the nature of the phosphorous ligand, the nature and amount of the Grignard reagent).

This method involves organocopper (RCu) and organocuprate (R_2Cu•MgX) compounds, both prepared in situ from commercially available copper halides and Grignard reagents. Both organocopper or organocuprate reagents were shown to undergo thermal decomposition under mild conditions (65 °C maximum) to synthetize CuNPs.

Syntheses of CuNPs with tunable sizes

In the case of organocopper (RCu), the optimal reaction conditions in terms of PPh_3 to-copper ratio and temperature were first investigated. High-uniformity spherical CuNPs with a mean size of 8 nm (σ% = 4%) were obtained at 65 °C using a PPh_3-to-CuCl ratio of 5, 1 equiv. of *n*-BuMgCl and of 4 equiv. of DDT (as compared to CuCl). These CuNPs were confirmed to be metallic Cu(0) with face centered cubic (*fcc*) structure through HRTEM, SAED and XRD analyses. From these initial conditions, the effect of other parameters was studied and it could be found that spherical CuNPs were obtained in most of the cases. Interestingly, their size could be controlled by:

- tuning the time between the addition of the Grignard reagent and the DDT (from 0.5 to 30 minutes): obtention of spherical NPs with sizes ranging from 6.7 nm (σ% = 12%) to 8.5 nm (σ% = *4*%).

- tuning the amount of DDT: obtention of spherical NPs with sizes ranging from 6.2 nm (σ% = 8%) with 8 equivalents to 14 nm (σ% = 28%) with 2 equivalents of DDT.

- changing the nature of the organocopper reagents prepared from various Grignard reagent: obtention of quasi-spherical CuNPs with sizes of 3.5 nm (σ% = 14% with isopropenylCu), 9.9 nm (σ% = 9% with EtCu), 10.1 nm (σ% = 17% with *t*-BuCu). The nature of the copper substituent thus appears as a key factor to control the NPs size. A decomposition pathway of alkylcopper compounds that is well-described in the literature involve a β-elimination process. Interestingly, CuNPs could also be obtained from copper reagents that cannot undergo β-elimination such as isopropenyl-copper.

The use of organocuprate or a mixture of organocuprate and Grignard reagent (for the use of 4, 6, 8 equiv. of RMgCl with 1 equiv. CuCl) did generally not change the final shape of

the CuNPs. However, it was found that starting from organocuprates yielded to a significant size increase of the CuNPs in the case of *n*-Bu_2Cu•MgCl and *t*-Bu_2Cu•MgCl which was not the case when using Et_2Cu•MgX or (isopropenyl)$_2$Cu•MgX.

- from 7.1 nm (σ% = 15%) with *n*-BuCu to 8.9 nm (σ% = 15%) with *n*-Bu_2Cu•MgCl/6 *n*-BuMgCl.

- from 10.1 nm (σ% = 17%) with *t*-BuCu to 14.9 nm (σ% = 16%) with *t*-$BuCu_2$•MgCl.

- from 9.9 nm (σ% = 9%) with EtCu to 10.4 nm (σ% = 13%) with Et_2Cu•MgX (X = Cl, Br).

- from 3.5 nm (σ% = 14%) with isopropenylCu to 3.3 nm (σ% = 12%) with (isopropenyl)$_2$Cu•MgX (X = Cl, Br).

Concerning the shape control

Interestingly, changing the nature of the phosphorous ligands could both affect the shape and the sizes of CuNPs. For examples, triangles or hexagons could be observed when using trioctylphosphite (TOPT) as the phosphorous ligand but they were obtained as mixtures with quasi-spherical NPs. The use of $P(NMe_2)_3$ resulted in the formation of flower-like NPs. Such anisotropic shapes can be of interest for applications including SERS.

This study enabled to highlight useful tools to prepare spherical (or quasi-spherical) CuNPs of tunable size. To a lesser extent, it was also possible to modify the shape.

Study of the process involved in the formation of CuNPs

In the optimized conditions (PPh_3-to-CuCl ratio = 5, 1 equiv. of *n*-BuMgCl, 4 equiv. of DDT), the copper species formed before the addition de DDT were studied by HRTEM, EDX and TEM in order to better understand the processes involved in the synthesis of CuNPs. These results showed the presence of chloride and PPh_3 on the surface of the large copper spheroids intermediates that were formed before the addition of DDT. They have crystalline Cu(0) with *fcc* structure, and their size increased with time from 11 nm (5 minutes reaction time) to 19 nm (after 15 or 30 minutes). After the addition of DDT, CuNPs isolated displayed a size of 8 nm. Such size change (from 19 nm to 8 nm) may be due to a digestive-ripening process.

IV. 11 References

(1) a) M. Strach, V. Mantella, J. R. Pankhurst, P. Iyengar, A. Loiudice, S. Das, C. Corminboeuf, W. van Beek, R. Buonsanti, *J. Am. Chem. Soc.*, **2019**, *141*, 16312-16322; b) H. J. Yang, S. Y. He, H. L. Chen, H. Y. Tuan, *Chem. Mater.*, **2014**, *26*, 1785-1793; c) H. Guo, Y. Chen, M. B. Cortie, X. Liu, Q. Xie, X. Wang, D. L. Peng, *J. Phys. Chem.* C., **2014**, *118*, 9801-9808; d) H. Guo, X. Liu, Q. Xie, L. Wang, D. L. Peng, P. S. Branco, M. B. Gawande, RSC Adv., **2013**, *3*, 19812-19815; e) E. Ye, S. Y. Zhang, S. Liu, M. Y. Han, *Chem. Eur. J.,* **2011**, *17*, 3074-3077.

(2) M. Strach, V. Mantella, J. R. Pankhurst, P. Iyengar, A. Loiudice, S. Das, C. Corminboeuf, W. van Beek, R. Buonsanti**,** *J. Am. Chem. Soc.,* **2019**, *141* (41), 16312-16322.

(3) R. Reich, C.R. Acad, *Sci. Paris*, **1923**, *177*, 322.

(4) a) E. Erdik, F. Eroglu, *Main Group Met. Chem.,* **1997**, *22* (7), 463-467; b) Sh. O. Badanyan, M. G. Voskanyan, Zh. A. Chobanyan, *Russ. Chem. Rev.,* **1981**, *50*, (11), 1074-1086.

(5) a) Z. Rappoport, I. Marek, The Chemistry of Organocopper Compounds, Wiley, London, **2009**; b) N Krause (Ed), Modern Organocopper Chemistry, Wiley-VCH, Mörlenbach, **2002**; c) H. Gilman, R. G. Jones and L.A. Woods, *J. Org. Chem.,* **1952**, *17* (12), 1630-1634.

(6) C. B. Linn, C. R. Noller, *J. Am. Chem. Soc.*, 1**936**, *58*, 816-819.

(7) K. Wada, M. Tamura, J. Kochi, *J. Am. Chem. Soc.*, **1970**, *92*, 6656-6658.

(8) G. M. Whitesides, E. R. Stedronsky, C. P. Casey, J. San Filippo Jr, J. Am. Chem. Soc., **1970**, *92*, 1426-1427.

(9) a) D. M. Knotted, D. M. Grove, W. J. J. Smeets, A. L. Spek, G. van Koten, *J. Am. Chem. Soc.*, **1992**, *114*, 3400-3410; b) C. Ullenius, B. Christenson, *Pure Appl. Chem.*, **1988**, *60*, 57; c) G. van Koten, J. G. Noltes, *COMC-III*, **1982**,*14*, 709.

(10) M. Ali Ben Aissa, B. Tremblay, A. Andrieux-Ledier, E. Maisonhaute, N. Raouafi, Alexa Courty, *Nanoscale*, **2015**, *7*, 3189.

(11) T. Rajh, O. I. Mićić, A. J. Nozik, *J. Phys. Chem.*, **1993**, *97*, 11999.

(12) a) M. J. Turo, J. E. Macdonald, *ACS. Nano,* **2014**, 8, 10205-10213; b) L. Chen, G. Li, *ACS. Appl. Nano Mater.*, **2018**, *1*, 4587-4593.

(13) X. Frogneux, L. Hippolyte, D. Mercier, D. Portehault, C. Chanéac, C. Sanchez, P. Marcus, F. Ribot, L. Fensterbank, S. Carenco, *Chem. Eur. J.*, **2019**, *25*, 11481-11485.

(14) C. L. Huang, G. Kumar, G. D. Sharma, F. C. Chen, *Appl. Phys. Lett.*, **2020**,*116*, 253302.

(15) P. E. Laibinis, G. M. Whitesides, *J. Am. Chem. Soc.,* **1992**, *114*, 9022-9028.

(16) D. G. Castner, K. Hinds, D. W. Grainger, *Langmuir,* **1996**, *12*, 5083-5086.

(17) S. M. Chang, Y. Y. Hsu, T. S. Chan, *J. Phys. Chem. C.,* **2011**, *115*, 2005-2013.

(18) Tahir, D.; Tougaard, S. *J. Phys.: Condens. Matter.,* **2012**, *24*, 175002.

(19) C. B. Murray, D. C. Norris, M. G. Bawendi, *J. Am. Chem. Soc.*, **1993**, *115*, 8706.

(20) S. Sun, C. B. Murray, *J. Appl. Phys.*, **1999**, *85*, 4325.

(21) a) G. H. Woehrle, L. O. Brown, J. E. Hutchinson, *J. Am. Chem. Soc.*, **2005**, *127*, 2172-2183; b) G. H. Woehrle, J. E. Hutchinson, *Inorg. Chem.*, **2005**, *44*, 6149-6158.

(22) X. Chen, M. Wei, S. Jiang, S. Förster, *Langmuir*, **2019**, *35*, 12130-12138.

(23) A. H. Shaik, J. Chakraborty, *RSC Adv.,* **2015**, *5*, 85974-85977.

(24) a) A. S. Patel, S. Juneja, P. K. Kanaujia, V. Maurya, G. V. Prakash, A. Chakraborti, J. Bhattacharya, *Nano-Struct. & Nano-Objects*, **2018**, *16*, 329-336; b) M. Sajitha, B. Abraham, R. B. Nelliyil, K. Yoosaf, *ACS Appl. Nano Mater.,* **2021**, *4* (10), 10038-10046.

(25) H. Gilman, R. G. Jones, L. A. Woods, *J. Org. Chem.,* **1952,** *17,* 1630-1634.
(26) J. F. Normant, *Pure Appl. Chem.*, **1978,** *50,* 709-715.
(27) B. H. Lipshutz, M. Koerner, D. A. Parker, *Tetrahedron Lett.*, **1987**, *28 (9),* 945-948.
(28) J-P. Gorlier, L. Hamon, J. Levisalles, J. Wagnon, *J. Chem. Soc., Chem. Commun*., **1973**, 88.
(29) W. H. Mandeville, G. M. Whitesides, *J. Org. Chem*., **1974**, *39*, 400-405.
(30) K. Koosha, J. Berlan, M. L. Capmau, W. Chodkiewicz, *Bull. Soc. Chim. France*, **1975**, 1284-1290.
(31) a) R-D. Acker, *Tetrahedron Lett*., **1977**, *18*, 3407-3410; b) P. Four, H. Riviere, P. W. Tang, *Tetrahedron Lett*., **1977**, *18*, 3879-3882.
(32) a) R. Sierra-Ávila, M. Pérez-Alvarez, G. Cadenas-Pliego, V-C. Padilla, C. Ávila-Orta, O-P. Camacho, E. Jiménez-Regalado, E. Hernández-Hernández, and R-M Jiménez-Barrera**,** *J. Nanomater.*, **2015**, Article ID: 367341; b) T. M. D. Dang, T. T. T. Le, E. Fribourg-Blanc, M. C. Dang, *Adv. Nat. Sci.: Nanosci. Nanotechnol.*, **2011**, *2(2),* Article ID: 025004.
(33) a) G. Mie, *Ann. Phys.*, **1908**, *25*, 377-445; b) P. Mulvaney, *Langmuir*, *12(3),* 788-800, **1996**; c) U. Kreibig, M. Vollmer, *Optical Properties of Metal Clusters*, Springer, Berlin, Germany, **1995**.
(34) H. Guo, Y. Chen, M. B. Cortie, X. Liu, Q. Xie, X. Wang, D. Peng, *J. Phys. Chem. C.,* **2014**, *118*, 9801-9808.
(35) a) G. M. Whitesides, W. F. Fischer, Jr. J. S. San Filippo, R. W. Basche, H. O. House, *J. Am. Chem. Soc.,* **1969**, *91*, 4871-4882; b) G. H. Posner, C. E. Whitten, J. J. Sterling, *J. Am. Chem. Soc.,* **1973**, *95*, 7788-7800.
(36) K. LaMer, H. Dinegar, *J. Am. Chem. Soc.,* **1950**, *72* (11), 4847-4854.
(37) P. S. Braterman, R. J. Cross, *Chem. Soc. Rev*., 1**973**, *2*, 271.
(38) M. C. Baird, J. *Organornetal. Chern*., **1974**, *64*, 289.
(39) G.M. Whitesides, E.J. Panek, E.R. Stredonsky, *J. Am. Chem. Soc.*, **1972**, *94*, 232.
(40) M.F. Lappert, R. Pearce, *J. Chem. Soc. Chem. Com*., **1973**, *24*.
(41) A. Miyashita, A. Yamamoto, *Bull. Chem. Soc. Japan.*, **1977**, *50*, 1102.
(42) a) S. Pasynkiewicz, J. Poplawska, *J. Organometallic Chem.*, **1985**, *282*, 427; b) S. Pasynkiewicz, S. Pikul, J. Poplawska, *J. Organometallic Chem.*, **1985**, *293*, 125-130.

Conclusion and Perspective

The synthesis of copper nanoparticles (CuNPs) with controlled shape and size have received increasing interest for a few years. The ability to control the shape and size of CuNPs have found enormous potential for altering their plasmonic, catalytic and optoelectronic properties. During these 3 years of thesis study, we successfully synthetized CuNPs with tunable size and shape through several chemical methods.

The **first chapter** of this work presented a brief overview of the most recent reports showing how metals nucleate and grow in solution-phase synthesis. We thus focused on the reaction factors that are able to influence the final size and shape of the NPs, and also the specific optical property of CuNPs (LSPR). We also presented a few examples of methods reported in the literature for synthetizing CuNPs through chemical reduction routes.

The **Chapter II** focused on the synthesis of CuNPs via the disproportionation route performed in the presence of various phosphorus ligands (i.e., TOP, TOPO, PPh_3, $P(PhMe_3)_3$, $P(OMe)_3$, $P(OC_8H_{17})_3$, $P(NMe_2)_3$, $P(O)((NMe_2)_3)$. From the use of these phosphorus ligands, we were able to prepare CuNPs with various shapes: cubes, spheres, octahedra, tetrahedra, rectangles, hexagons or wires (see some examples in Table 1). Furthermore and in order to rationalize, we attempted to find a correlation between the properties of phosphorus ligands (sterics, electronics, calculated coordination energy to copper, disproportionation energy of the corresponding PR_3-Cu complex) on the one hand, and the different morphologies of CuNPs synthetized on the other hand. Even if we did not find a simple effective model to predict the effect of phosphorous ligands, some tendencies could be highlighted. For example, our experimental results indicate that within a same family of phosphorous ligand, the steric hindrance enables to tune the final morphology of the CuNPs synthetized (i.e., PPh_3 versus $P(PhMe_3)_3$, $P(OMe)_3$ versus $P(OC_8H_{17})_3$). Among the morphologies obtained, the formation of unprecedented Cu nanotetrahedra in the presence of $P(OMe)_3$ can be highlighted. The original shape of these NPs may bring unexpected properties and enable their application in various fields.

In addition, among the ligands studied, $P(NMe_2)_3$ lead to very original hexagonal NPs. This ligand was not only responsible for the morphology of the resulting NPs but it was also shown to promote the formation of Cu_3P nanocrystals instead of Cu(0) NPs usually obtained through the disproportionation route. We were able to manage the selective formation of Cu_3P or Cu(0) nanoobjects by changing the primary amine solvent (DDA vs OLA) which was not described earlier to our knowledge. Besides, a mixture of OLA and DDA lead to the formation of unprecedented Cu nanorectangles and once again, such morphologies may be of interest in terms of applications. More studies are needed to understand the role played by DDA and

to exploit the potential of this binary amine solvent in order to obtain various CuNPs morphologies.

In addition, some experimental conditions such as the nature of the hotplate or of the reactor used for synthesis were found to play a crucial role. This was rationalized by the fact that such parameters have a direct influence on the heating ramp. The latter was shown to have important effect on the NPs shape, sometimes as important as the ligand itself. The injection mode of the ligand (hot-injection or heating-up procedures) and the reaction time were also key factors for morphology control.

For a given ligand, it was also checked through several examples that the ligand-to-copper ratio as well as the halide initially present in the copper salt both had a significant effect on the size of the resulting NPs while generally maintaining the shape.

Table 1. *Selected TEM images of CuNPs obtained by using various phosphorus ligands*

TOP			TOPO	
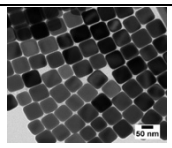	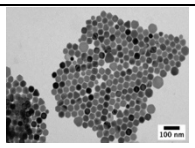	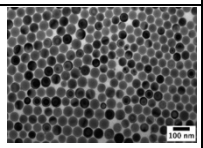	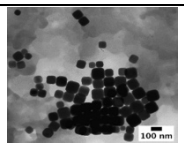	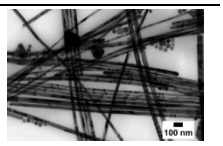
PPh_3		$P(PhMe_3)_3$	$P(OMe)_3$	$P(OC_8H_{17})_3$
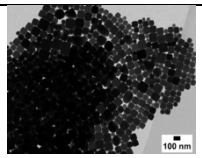	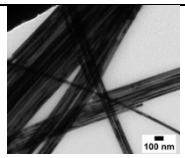	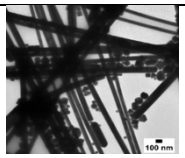	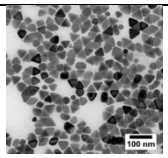	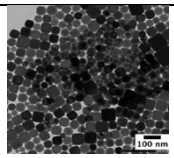
$P(NMe_2)_3$				
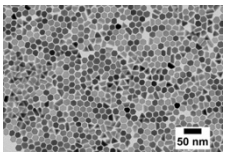	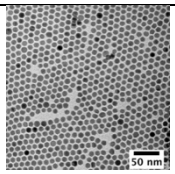		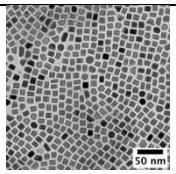	

In **Chapter III**, we investigated the preparation of CuNPs with various morphologies (cubes, spheres, wires, triangles and pyramids) (see some examples in Table 2) through a simple “one-pot” disproportionation reaction using only two reactants: CAACs-Cu(I) complexes and a primary amine as the solvent. The synthesis of CuNPs was realized by tuning the nature of CAACs ligands or solvent, and the amount of precursor or solvent. The stabilization of NPs by CAACs was illustrated by XPS analysis through different N_{1s} peak positions. The steric hindrance of the C-substituent of the heterocycle (^{Et}CAAC, ^{Ad}CAAC, ^{Menth}CAAC and ^{PhMe}CAAC) and the Cu-to-OLA ratio were found to have a critical effect on the morphology of CuNPs. In addition, the nature of primary amine used as solvent was found to control the final shape and

size of NPs. In the cases of ^{Et}CAAC-CuCl and ^{PhMe}CAAC-CuCl, the use of DDA as the solvent was found to be crucial to obtain small monodisperse CuNPs.

One of the more striking result in this part concerns the formation of nanopyramids-shaped CuNPs synthetized from ^{Et}CAAC-CuCl in a binary solvent (OLA/DDA). Due to their unique morphology, we do believe that these CuNPs have great potential for example in optics or catalysis.

Lastly, we are the first to demonstrate that the extremely stable CAACs-Cu complexes can be used as precursors for CuNPs synthesis and that the CAACs are able to stabilize the CuNPs while significantly control their final size and shape.

This work has thus opened the door in the chemistry of metal nanoparticles by using the CAACs-CuCl as the copper precursor. Considering the future work, there are still several axes to explore: the synthesis of CuNPs with fine control of size and shape by playing for example with key reaction parameters highlighted in the case of phosphines in Chapter II (nature of the solvent, use of the binary system OLA/DDA…), the understanding of the NPs formation pathway, or the synthesis of other metals nanoparticles (e. g. Ag, Au).

Table 2. *TEM images of CuNPs obtained by using various CAACs-CuCl complexes.*

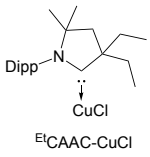 ^{Et}CAAC-CuCl	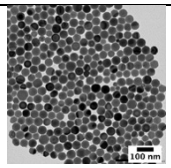	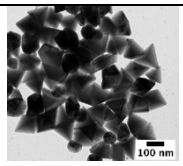
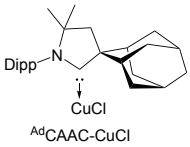 ^{Ad}CAAC-CuCl	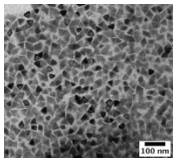	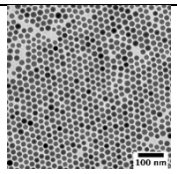
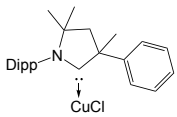 ^{PhMe}CAAC-CuCl	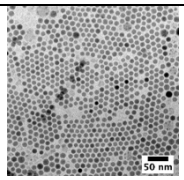	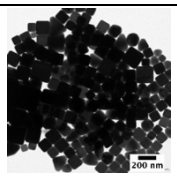

In **Chapter IV**, we reported a simple, innovative and robust thermal decomposition of organocopper reagents issued from organomagnesium compounds, for the synthesis of well-defined CuNPs with narrow size distribution. Using this more atom-economic method, CuNPs were synthetized with tunable size ranging from 3 to 20 nm by modifying several reaction parameters (e.g. the amount of phosphine ligand, the temperature, the injection time and amount of DDT, the nature of the phosphorous ligand, the nature and amount of the Grignard reagent). The most monodisperse NPs were obtained when the reaction conditions of 5 equiv. of PPh_3, 4 equiv. of DDT and 1 equiv. *n*-BuMgCl to CuCl at 65 °C were used (Table 3). The

successful scale-up of the synthesis enabled to obtain decigrams of CuNPs. This thermolysis approach involves organocopper (RCu) and organocuprate (R_2Cu•MgX) compounds, both organocopper or organocuprate reagents were shown to undergo thermal decomposition under mild conditions to synthetize CuNPs.

To try to rationalize the results obtained and in order to better understand the processes involved in the synthesis of CuNPs by this new route, we have investigated the copper species formed before the addition of DDT by HRTEM, EDX and TEM analyses. The formation of large copper spheroids intermediates (19 nm) shown to contain chloride and PPh_3 was highlighted. After the addition of DDT, CuNPs isolated displayed a size of 8 nm under identical reaction conditions. We assumed that such size change (from 19 nm to 8 nm) may be due to a digestive-ripening process.

So far, the NPs synthetized by the thermal decomposition of organocopper/organocuprates are mainly spherical. The further development of a more versatile route enabling to get CuNPs with different shapes is needed to get more possibilities in terms of applications. For reaching this objective, an optimization of several key reaction parameters has to be achieved. Along these lines, some very encouraging results have been obtained by changing the PPh_3 ligand by TOP or $P(NMe_2)_3$. Indeed, in these cases, preliminary results show that more anisotropic morphologies can be obtained.

Lastly, the study of the stability CuNPs with exposition time under air has to be achieved.

Table 3. *TEM image of CuNPs synthetized from the optimized reaction condition (left) and the corresponding picture of CuNPs in solid state (right).*

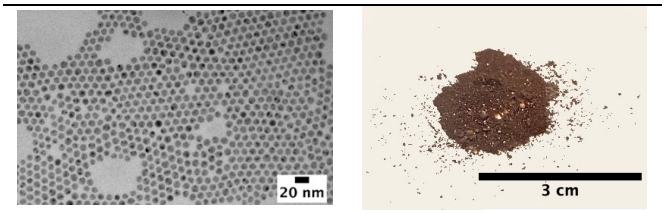

During the third year of this thesis work, the catalytic properties of some of CuNPs synthetized in our work were evaluated in the hydrogenation of CO_2. These studies were achieved by a Master 2 intern T. Mujong during six months (financial support from SATT). The last results obtained are really promising and show that certain CuNPs synthetized in our work have a bright future in the field of catalysis.

Résumé en français

Le sujet de cette thèse concerne la synthèse de nanoparticules de cuivre (CuNPs) de morphologie et de taille contrôlées *via* des réactions de dismutation de complexes de Cu(I) ou de décomposition thermique d'organocuivres ainsi que l'étude de leurs propriétés physico-chimiques.

Ce manuscrit est composé de quatre principaux chapitres et d'une partie expérimentale :

Le premier chapitre est une introduction bibliographique décrivant les méthodes et stratégies de synthèse des nanoparticules métalliques. Parmi ces méthodes, les voies de synthèse chimiques sont plus particulièrement discutées, que ce soit du point de vue des théories permettant de rationaliser les mécanismes de nucléation et de croissance de ces nanoparticules, ou des différents facteurs influençant leurs formes et leurs tailles de ces nanoparticules. Un état de l'art de la littérature concernant la réduction de sels de cuivre par des réactifs moléculaires (boranes, amines, hydrazine, hydrogène…) est effectué, et les avantages et inconvénients de ces différentes méthodes sont discutées.

Le deuxième chapitre décrit les résultats que nous avons obtenu lors de l'étude de la synthèse de nanoparticules de cuivre par réaction de dismutation de complexes cuivre/amines/phosphine. Il commence par une introduction où sont présentés et commentés les résultats de la littérature concernant les réactions de dismutation des sels de cuivre. Cette première sous partie se termine par la description des objectifs que nous nous étions fixés au commencement de ce travail, à savoir mesurer les effets des différents paramètres de cette réaction (la concentration, la température de réaction, l'ordre d'introduction des réactifs, le nombre d'équivalents et la nature des phosphines employées comme ligands…) sur la morphologie des nanoparticules pour tenter d'établir un modèle prédictif.

Le chapitre est ensuite subdivisé en 4 sous-parties où nos résultats sont regroupés par famille de ligands phosphorés utilisés : i) les alkyls phosphines et les oxydes d'alkyl phosphine,

ii) les aryls phosphines, iii) les alkyls phosphites et iv) les phosphoramides et les phosphoramidites. Pour chacune de ces sous-parties sont décrites les procédures expérimentales employées, les caractérisations des nanoparticules obtenues (UV, TEM, HRTEM, XPS, XRD, ICP, RMN…).

Les conclusions tirées de l'ensemble de cette étude sont qu'il n'est pas possible de trouver une corrélation générale entre les caractéristiques physico-chimiques des ligands phosphorés étudiés (pKa, encombrement stérique, énergies d'affinité avec le sel de cuivre (I) utilisé) et la morphologie des nanoparticules de cuivre obtenues. Il s'est en effet avéré que des facteurs cruciaux comme la structure des complexes de cuivre en solution et leurs cinétiques de transformation devaient impérativement être pris en compte pour l'élaboration du modèle initialement recherché.

Ces travaux ont néanmoins permis d'obtenir un ensemble de connaissances intéressantes sur les facteurs influençant la croissance des nanoparticules de cuivre comme la vitesse de chauffage des milieux réactionnels, les températures de réaction et l'ordre d'introduction des différents réactifs, la nature du sel de cuivre employé, et notamment de l'halogène contre-ion du Cu(I) de départ. De manière intéressante, il a été possible d'observer certaines tendances concernant les effets de la nature des substituants du phosphore sur la forme des nanoparticules obtenues pour une famille de ligand phosphorés donnée. Nous avons aussi pu obtenir une collection de nanoparticules de cuivre métallique parfaitement cristallisées et possédant des formes originales qui pourraient être de bons candidats pour diverses réactions catalysées, aussi bien par voies chimiques qu'électrochimiques.

Durant cette étude nous avons aussi découvert de manière accidentelle une nouvelle voie d'accès à des nanoparticules appartenant à la famille des phosphures métalliques, les Cu_3P. Elle consiste en un chauffage de complexes de cuivre (I) ou (II) et de HMPT dans l'oleylamine. Les différents paramètres de cette réaction ont été étudiées, et la méthodologie que nous avons développée permet un accès simple, rapide et hautement reproductible à ces nanoparticules particulièrement prisées comme semi-conducteurs. Elle permet aussi de pouvoir moduler leurs tailles tout en conservant un haut degré de qualité. De manière

intéressante nous avons découvert qu'un choix judicieux de l'amine primaire utilisée comme solvant permet d'orienter à volonté la réaction vers la formation de nanoparticules de Cu(0) ou de Cu_3P, ainsi que de contrôler la forme de ces dernières (hexagonales ou rectangulaires).

Le troisième chapitre décrit les résultats que nous avons obtenu dans les réactions de dismutation de complexes de Cuivre ligands par des carbènes de la famille des CAACs. Ce type de carbènes n'avait jamais été employé auparavant comme ligand pour des réactions de dismutation. Nous avons dans un premier temps démontré que l'utilisation de ces partenaires permettait l'obtention de nanoparticules de cuivre (0), nous les avons caractérisés par UV, TEM, pour les plus intéressants, par HRTEM et MEB, et nous avons ensuite étudiés l'influence de différents paramètres comme l'encombrement stérique des CAACs employés, le ratio complexe Cu(I)-CAAC/oleylamine et la nature de l'amine primaire utilisée comme solvant sur la forme et la taille des nanoparticules obtenues. De nombreuses nanoparticules de cuivre (0) de formes originales ont été obtenues de manière simple et reproductible. Parmi elles, des particules de forme parfaitement pyramidales sont particulièrement intéressantes pour de potentielles applications en optique ou en catalyse chimique.

Dans le dernier chapitre de cette thèse nous avons mis au point une nouvelle voie d'accès aux nanoparticules de cuivre (0) qui n'utilise pas d'amines à longues chaines comme solvant et qui se fait dans des conditions réactionnelles beaucoup plus douces que celles décrites pour les réactions de dismutation. Elle repose sur l'exploitation de la réaction de décomposition thermique de dérivés organocuivreux ou organocuprates. Il est connu depuis les années 1930 que les alkyls cuivres en solution dans des solvants éthérés se décomposent spontanément à une température inférieure à 0 °C pour donner un mélange équimolaire d'alcanes et d'alcènes ainsi que du cuivre métallique selon un mécanisme impliquant une première étape de béta-élimination de CuH. Cependant, cette réaction contre-productive pour la synthèse organique n'a été que très peu étudiée et la nature exacte du cuivre produit n'avait jamais été déterminée. Nous avons donc décidé d'étudier cette réaction pour en déterminer le potentiel synthétique dans le cadre de la production de nanoparticules de cuivre. Nous avons tout d'abord mis au point un premier protocole permettant l'obtention de particules qui ont été

entièrement caractérisées par l'ensemble des méthodes d'analyses disponibles, à savoir l'UV, le TEM, le HRTEM, le XRD et l'XPS. Ces analyses ont démontré que la réaction de thermolyse de complexes organocuivre-PPh_3 produisait des nanoparticules de cuivre (0) de forme sphérique et de taille contrôlée. Une étude plus approfondie de cette réaction a montré que l'ajout de dodécane thiol dans le milieu réactionnel après l'étape de thermolyse donnait lieu à un phénomène original de fracture des nanoparticules initialement formées et conduisait à l'obtention de nanoparticules parfaitement sphériques et monodisperses. Une étude des différents paramètres de cette réaction a permis de mettre au point une méthodes rapide, simple et robuste permettant un bon contrôle de la taille des nanoparticules synthétisées.

Encouragés par ces résultats nous avons entrepris une étude approfondie de cette réaction en faisant varier la nature des organocuivres de départ. Outre le *n*-BuCu, ont aussi été testés le dibutyl cuprate *n*-Bu_2•MgCl, l'éthyl cuivreux et le diéthyl cuprate EtCu et Et_2Cu•MgX, le methyl cuivreux et le dimethyl cuprate MeCu et Me_2Cu•Mgx, le *tert*-butyl cuivreux et le di-*tert*-butyl cuprate *t*-BuCu et *t*-Bu_2Cu•MgCl, l'isopropenyl cuivreux et le di-isopropenylcuprate, isopropenylCu et $(isopropenyl)_2$Cu•MgCl et enfin le phenyl cuivreux et le diphenyl cuprate PhCu et Ph_2Cu•MgCl.

La décomposition thermique d'organocuivreux ou d'organocuprates possédant un hydrogène en béta du cuivre ont conduit à la formation de nanoparticules de cuivre (0) sphériques d'une taille comprise entre 7 et 14 nm en fonction du précurseur utilisé. La vitesse de ces réactions dépend de la nature de l'organocuivre de départ, les cuprates se décomposant moins vite que les cuprates, et est proportionnelle à la stabilité de la double liaison issue de la première étape de *β*-élimination de CuH, le *t*-BuCu produisant du *gem*-diméthyl éthylène se décomposant beaucoup plus vite que son analogue EtCu qui fournit lui de l'ethylène. Ces différences de cinétique ne semblent néanmoins pas avoir d'influence significative sur la taille des nanoparticules formées.

De manière intéressante, les organocuivres ne possédant pas de chaine alkyl permettant la réaction de béta-élimination de CuH et connus pour se décomposer selon un mécanisme radicalaire donnent aussi lieu à la formation de nanoparticules sphériques de

cuivre (0), à l'exception des méthyl cuivreux et cuprates. Ces réactions sont néanmoins plus lentes et produisent des particules de plus petite taille (3,5 nm pour l'emploi de PhCu).

D'autres types de ligands phosphorés du cuivre ont été testés dans nos conditions standard de réaction, ce qui a permis de faire varier la forme des nanoparticules produites. Par exemple, l'emploi de trioctylphosphite à conduit à la formation d'un mélange de nanoparticules de cuivre (0) de forme triangulaire et hexagonale.

Enfin, il a été possible de faire un premier essai de montée en échelle de cette réaction en partant de 5 mmol de sel de cuivre. La décomposition du butylcuivreux obtenu par addition d'un équivalent de n-BuMgCl sur une solution du complexe $CuCl•(PPh_3)_n$ à 65 °C dans 25 mL de THF suivit de l'addition de 4 équivalents de DDT et d'un chauffage à reflux pendant une heure a permis d'obtenir 370 mg de nanoparticules de Cu(0) d'une qualité comparable à celles issues de réactions à plus petite échelle.

Chapter V. Experimental Section

Table of contents

V. 1. Chemicals

Commercial reagents were used without further purification, except stated otherwise, which stored in a glovebox in order to avoid any traces of moisture or air contamination. Cu(I) chloride (CuCl, 99.99%), Cu(I) bromide (CuBr, 99.99%), Cu(I) Iodine (CuI, 99.5%), Cu(II) chloride ($CuCl_2$, 99%), Cu(II) bromide ($CuBr_2$, 99%), Copper(I) tetra(acetonitrile) tetrafluoroborate ($Cu(CH_3CN)_4BF_4$, 97%), Cu (II) acetate ($Cu(COOCH_3)_2$, 98%), Cu (I) acetate ($CuCOOCH_3$, 97%), tris(dimethylamino)phosphine (HMPT, 97%), hexamethylphosphoric acid triamide (HMPA, 99%), trimethyl phosphite ($P(OMe)_3$, 97%), triphenyphosphine (PPh_3, 99%), butylmagnesium chloride solution (*n*-BuMgCl, 2.0 M solution in THF), ethylmagnesium chloride solution (EtMgCl, 2.0 M solution in THF), phenylmagnesium chloride solution (PhMgCl, 1.0 M solution in THF), *tert*-butylmagnesium chloride solution (*t*-BuMgCl, 1.0 M solution in THF), isopropenylmagnesium bromide solution (isopropenylMgBr, 0.5 M solution in THF), dodecylamine (DDA, 98%), 1-dodecanethiol (≥ 98 %) were purchased from Sigma-Aldrich. Oleylamine (OLA, 80-90%), and methylmagnesium bromide solution (MeMgBr, 1 M solution in THF) were purchased from Acros. Trioctylphosphite (TOPT, > 85%) was purchased from TCI Deutschland GmbH. Copper(I) cyanide (CuCN, 98%), trioctylphosphine (TOP, 90%), trioctylphosphine oxide (TOPO, 90%) were purchased from Alfa Aesar. Absolute ethanol, hexane and chloroform were purchased from SIGMA, VWR and CARLO ERBA and used without further purification. THF was distilled over sodium/benzophenone and handled under an atmosphere of nitrogen.

V. 2. General characterization techniques

2.1 Transmission electron microscopy (TEM).

TEM images of copper nanoparticles (CuNPs) were obtained using a JOEL 1200 EX microscope with an accelerating voltage of 120 kV. All CuNPs samples were prepared by dropping the nanoparticles suspensions in hexane or chloroform onto a carbon-coated nickel grid, then dried on the surface of the grid under inert gas. For each sample, TEM images were taken from different parts of the grid and used to estimate the size distribution of copper nanoparticles. High-resolution TEM (HRTEM) images, selected area electron diffraction (SAED) patterns and energy dispersive X-ray (EDX) were collected on a JOEL 2200FS TEM at 200 kV. Image J software was used for measuring the size of nanoparticles around 300-500 NPs and the size distribution was determined using the Origin-Pro 9.1.

2.2 Scanning Electron Microscopy

Scanning Electron Microscopy **(SEM)** was carried out on Hitachi S-4800 Scanning Electron Microscope by a team of Scanning Electron and photonic Microscopies of Institut Européen des Membranes (IEM). The samples were prepared by depositing serval drops of colloidal solution on a nickel grid.

2.3 Ultraviolet-visible (UV-Vis) Spectroscopy

UV-vis spectroscopy is used to study the optical properties, surface plasmon resonance in nanoparticles. The shift of UV-Vis peaks can be used to learn the size and morphology of nanoparticles. For example, the shift of UV-Vis peaks of copper nanoparticles with cubic shape towards longer wavelength compared to the spherical copper nanoparticles. The UV-Vis spectroscopy was performed on a V-770 UV-Visible/NIR spectrophotometer at room temperature with the wavelength range of 300 to 2000 nm. Before each run, background subtraction was performed with the solvent system of choice. The measurements were performed in a quartz cell with 1 cm optical path length.

2.4 X-ray photoelectron spectroscopy (XPS)

XPS was conducted with a K-Alpha+ system (ThermoFisher Scientific, East-Grinsted, UK) fitted with a micro-focused and monochromatic Al Kα X-ray source (spot size of 400 µm, 1486.6 eV). Spectrometer pass energy was 150 eV for the survey and 40 eV for the narrow high-resolution regions. The samples were prepared by depositing several drops of the solution on a silicon wafer. TEM images were recorded prior to XPS analysis to ensure that individual nanoclusters are actually present. The XPS measurement was performed by Pr. Vincent Noël in ITODYS of the University of Paris.

2.5 Powder X-ray diffraction (XRD).

Powder XRD patterns were collected with Ni-filtered Cu $K_{\alpha 1/\alpha 2}$ (λ = 1.5418 Å) radiation in a reflection geometry on a Pananalytical X'Pert Pro-MPD diffractometer, operating at a working voltage and current of 45 kV and 20 mA. In preparing the sample, the powder sample was formed by precipitating of nanoparticles with ethanol and centrifuging at 4000 rpm for 10 min before drying at room temperature in an N_2-filled glovebox. The dry precipitate was pulverized and the resulting powder was used to fill a glass plate. The XRD measurement was operated by Mrs. Dominique Granier in the platform RRXG at the University of Montpellier.

2.6 Nuclear magnetic resonance spectroscopy (NMR)

^{31}P NMR (162 MHz) spectra were recorded at room temperature on a Bruker Ultra Shield 400 Plus and all samples were prepared in the stated deuterated solvent ($CDCl_3$, ^{1}H: d 7.26 ppm, ^{13}C: d 77.16 ppm; DMSO, ^{1}H: d 2.50 ppm, ^{13}C: d 39.52 ppm). Where air sensitive, the samples was prepared in the nitrogen filled glovebox. Multiplicities are reported using the following abbreviations: s (singlet), d (doublet), t (triplet), q (quartet), quint (quintet), sept (septuplet), m (multiplet), br (broad), Ar (aromatic) or a suitable combination.

2.7 Fourier-transform infrared spectroscopy (FT-IR)

FT-IR spectra were recorded with Perkin-Elmer Spectrum 1000 and the absorptions are given in wavenumbers (cm^{-1}). The infrared spectroscopy allows investigating the formation of the copper-amine complex during the formation of NPs. In our work, the concentration of copper-oleylamine and copper-dodecylamine complexes samples was prepared same as the reaction solution of synthetic protocol.

2.8 Inductively coupled plasma mass spectrometry (ICP-MS)

Inductively coupled plasma mass spectrometry (ICP-MS) was performed on ICP-MS Agilent 7900 by Mr. Mickaël Bigot of ChV group at University of Montpellier. ICP-MS analysis was used to detect metal copper thus confirming the quantitative yield of copper nanoparticles.

V. 3. Copper nanoparticles synthesis

3.1 Chapter II

3.1.A. Synthesis from CuX (X = Cl, Br, I) and TOP (1.6, or 3.2, or 4, or 5 eq.) by hot-injection

In a typical process, CuCl (60 mg, 0.6 mmol, 1 eq.) [or CuBr (86 mg, 0.6 mmol, 1 eq.), or CuI (114 mg, 0.6 mmol, 1 eq.)] was weighted in an N_2-filled glovebox and was mixed in oleylamine (7 mL, 21 mmol, 35 eq.) in a 25 mL glass vial capped with a septum pierced and connected to a schlenk line under nitrogen. The mixture was stirred by strong magnetic stirring and heated to 100 °C under inert gas (N_2) for 15 min and a greenish solution was obtained. Then TOP (1 mmol, 446 µL, 1.6 eq.) [or (1.9 mmol, 836 µL, 3.2 eq.), or (2.5 mmol, 1.12 mL, 4 eq.), or (3 mmol, 2.23 mL, 5 eq.)] was quickly added into the greenish solution and the mixture was continuously stirred at 100 °C for 5 minutes. Then the temperature rapidly raised to 285 °C with a heating ramp of 13 °C/min and maintained for 1 hour (or 2 hours). The formation of CuNPs is evidenced by a slow color change of the solution from colorless to orange and finally to red-purple. After the reaction stopped, the nanoparticles dispersed in the organic layer which were purified by adding an excess of absolute ethanol and using centrifugation at 2500 rpm for 10 min to remove all organic compounds that rest in the solution. The supernatant was discarded and the precipitate is dispersed in hexane followed by a centrifuging at 4000 rpm for 5 min. After one more redispersion/precipitation cycle with chloroform and centrifugated. The copper nanoparticles were naturedly dried in the glove box in a red powder for storage and further analysis.

3.1.B. Synthesis from $[Cu(CH_3CN)_4]PF_6$, CuCN, $Cu(CH_3COO)$ and $Cu(CH_3COO)_2$ and TOP (1.6 eq.) by hot-injection

In a typical process, $[Cu(CH_3CN)_4]PF_6$ (223.63 mg, 0.6 mmol, 1 eq.) [or CuCN (53,74 mg, 0.6 mmol, 1 eq.), $Cu(CH_3COO)$ (73.5 mg, 0.6 mmol, 1 eq.), or $Cu(CH_3COO)_2$ (108.9 mg, 0.6 mmol, 1 eq.)] was weighted in an N_2-filled glovebox and was mixed in oleylamine (7 mL, 21 mmol, 35 eq.) in a 25 mL glass vial capped with a septum pierced and connected to a schlenk line under nitrogen. The mixture was stirred by strong magnetic stirring and heated to 100 °C under inert gas (N_2) for 15 min and a greenish solution was obtained. Then TOP (1 mmol, 446 µL, 1.6 eq.) was quickly added into the greenish solution and the mixture was continuously stirred at 100 °C for 5 minutes. Then the temperature rapidly raised to 285 °C (or 240-265 °C) with a heating ramp of 13 °C/min and maintained for 1 hour (or 2 hours). The formation of CuNPs is evidenced by a slow color change of the solution from colorless to

orange and finally to red-purple. After the reaction stopped, the nanoparticles dispersed in the organic layer which were purified by adding an excess of absolute ethanol and using centrifugation at 2500 rpm for 10 min to remove all organic compounds that rest in the solution. The supernatant was discarded and the precipitate is dispersed in hexane followed by a centrifuging at 4000 rpm for 5 min. After one more redispersion/precipitation cycle with chloroform and centrifugated. The copper nanoparticles were naturedly dried in the glove box in a red powder for storage and further analysis.

3.1.C. Synthesis from CuX (X = Cl, Br) and TOPO (1.6, or 3 eq.) by hot-injection

In a typical process, CuCl (60 mg, 0.6 mmol, 1 eq.) [or CuBr (86 mg, 0.6 mmol, 1 eq.)] was weighted in an N_2-filled glovebox and is mixed in oleylamine (7 mL, 21 mmol, 35 eq.) in 25 mL glass vial capped with a septum pierced and connected to a schlenk line under nitrogen. The mixture was stirred by strong magnetic stirring and heated to 100 °C under inert gas (N_2) for 15 min and a greenish solution was obtained. Then TOPO (386 mg, 1 mmol, 1.6 eq.) (or 733 mg, 1.9 mmol, 3 eq.) was quickly added into the solution and the mixture immediately turned to colorless. The mixture was continuously stirred at 100 °C for 5 minutes. Then the temperature rapidly raised to 285 °C with a heating ramp of 13 °C/min and maintained for 1 hour. The formation of CuNPs is evidenced by a slow color change of the solution from colorless to orange and finally to red-purple. Precipitation and centrifugation of nanoparticles was carried out as for the previous synthesis **3.1.A**.

3.1.D. Synthesis from CuX (X = Cl, Br) and TOPO (1.6 eq.) by heating-up

In a typical process, CuCl (60 mg, 0.6 mmol, 1 eq.) [or CuBr (86 mg, 0.6 mmol, 1 eq.)] and TOPO **(**386 mg, 1 mmol, 1.6 eq.) were weighted into a Pyrex 25 mL glass vial along with oleylamine (7 mL, 21 mmol, 35 eq.) under inert atmosphere, the mixture was stirred by strong magnetic stirring and heated to 100 °C under inert gas (N_2) for 15 min and a greenish-yellower solution was obtained. Then the temperature rapidly raised to 280 °C with a heating ramp of 13 °C/min and maintained for 1 hour. The formation of CuNPs is evidenced by a slow color change of the solution from colorless to orange and finally to red-purple. Precipitation and centrifugation of nanoparticles was carried out as for the previous synthesis **3.1.A**.

3.1.E. Synthesis from CuX (X = Cl, Br) and PPh_3 (1.6 eq.) by hot-injection

In a typical process, CuCl (60 mg, 0.6 mmol, 1 eq.) [or CuBr (86 mg, 0.6 mmol, 1 eq.)] was weighted in an N_2-filled glovebox and is mixed in oleylamine (7 mL, 21 mmol, 35 eq.) in 25 mL glass vial capped with a septum pierced and connected to a schlenk line under nitrogen. The mixture was stirred by strong magnetic stirring and heated to 100 °C under inert gas (N_2) for 15 min and a greenish solution was obtained. Then PPh_3 (262 mg, 1 mmol, 1.6 eq.) was

quickly added into the solution and the mixture turned to colorless immediately. The mixture was continuously stirred at 100 °C for 5 minutes. Then the temperature rapidly raised to 270 °C with a heating ramp of 13 °C/min and maintained for 1 hour (or 2 hours). The formation of CuNPs is evidenced by a slow color change of the solution from colorless to orange and finally to red-purple. Precipitation and centrifugation of nanoparticles was carried out as for the previous synthesis **3.1.A**.

3.1.F. Synthesis from CuX (X = Cl, Br) and $P(PhMe_3)_3$ (1.6 eq.) by hot-injection

In a typical process, CuCl (0.6 mmol, 60 mg, 1 eq.) [or CuBr (86 mg, 0.6 mmol, 1 eq.)] was weighted in an N_2-filled glovebox and is mixed in oleylamine (7 mL, 21 mmol, 35 eq.) in 25 mL glass vial capped with a septum pierced and connected to a schlenk line under nitrogen. The mixture was stirred by strong magnetic stirring and heated to 100 °C under inert gas (N_2) for 15 min and a greenish solution was obtained. Then $P(PhMe_3)_3$ (1 mmol, 389 mg, 1.6 eq.) was quickly added into the solution and the mixture slowly turned to colorless. The mixture was continuously stirred at 100 °C for 5 minutes. Then the temperature rapidly raised to 270 °C with a heating ramp of 13 °C/min and maintained for 1 hour (or 2 hours). The formation of CuNPs is evidenced by a slow color change of the solution from colorless to orange and finally to red-purple. Precipitation and centrifugation of nanoparticles was carried out as for the previous synthesis **3.1.A**.

3.1.G. Synthesis from CuX (X = Cl, Br) and $P(OMe)_3$ (1.6 eq.) by hot-injection

In a typical process, CuCl (60 mg, 0.6 mmol, 1 eq.) [or CuBr (86 mg, 0.6 mmol, 1 eq.)] was weighted in an N_2-filled glovebox and is mixed in oleylamine (7 mL, 21 mmol, 35 eq.) in 25 mL glass vial capped with a septum pierced and connected to a schlenk line under nitrogen. The mixture was stirred by strong magnetic stirring and heated to 100 °C under inert gas (N_2) for 15 min and a greenish solution was obtained. Then $P(OMe)_3$ (118 µL, 1 mmol, 1.6 eq.) (or 225 µL, 1.9 mmol, 3 eq.) was quickly added into the solution and the mixture slowly turned to colorless. The mixture was continuously stirred at 100 °C for 5 minutes. Then the temperature rapidly raised to 245 °C with a heating ramp of 13 °C/min and maintained for 1 hour. The formation of CuNPs is evidenced by a slow color change of the solution from colorless to gray and finally to dark-purple. Precipitation and centrifugation of nanoparticles was carried out as for the previous synthesis **3.1.A**.

3.1.H. Synthesis from CuX (X = Cl, Br) and $P(O\text{-octyl})_3$ (TOPT) (1.6 eq.) by hot-injection

In a typical process, CuCl (60 mg, 0.6 mmol, 1 eq.) [or CuBr (86 mg, 0.6 mmol, 1 eq.)] was weighted in an N_2-filled glovebox and is mixed in oleylamine (7 mL, 21 mmol, 35 eq.) in 25 mL glass vial (or a three-neck flask) capped with a septum pierced and connected to a

schlenk line under nitrogen. The mixture was stirred by strong magnetic stirring and heated to 100 °C under inert gas (N_2) for 15 min and a greenish solution was obtained. Then P(O-octyl)$_3$ (376 µL, 1 mmol, 1.6 eq.) was quickly added into the solution and the mixture quickly turned to colorless. The mixture was continuously stirred at 100 °C for 5 minutes. Then the temperature rapidly raised to 290 °C with a heating ramp of 13 °C/min and maintained for 1 hour. The formation of CuNPs is evidenced by a slow color change of the solution from colorless to orange and finally to red-purple. Precipitation and centrifugation of nanoparticles was carried out as for the previous synthesis **3.1.A**.

3.1.I. Synthesis from CuCl and PO(NMe$_2$)$_3$ (HMPA) (1.6 eq.) by hot-injection

In a typical process, CuCl (60 mg, 0.6 mmol, 1 eq.) was weighted in an N_2-filled glovebox and was mixed in oleylamine (7 mL, 21 mmol, 35 eq.) of in 25 mL vial capped with a septum pierced and connected to a schlenk line under nitrogen. The mixture was stirred by strong magnetic stirring and heated to 100 °C under inert gas (N_2) for 15 min and a green-yellower solution was obtained. Then P(O)(NMe$_2$)$_3$ (174 µL, 1 mmol, 1.6 eq.) was quickly added into the solution and the mixture quickly turned to yellower. The solution was continuously stirred at 100 °C for 5 minutes. Then the reaction solution was quickly heated up to 290 °C (13 °C/min) and maintained at the desired temperature for 1 hour. The formation of CuNPs is evidenced by a slow color change of the solution from yellower to orange and finally to gray-purple. Precipitation and centrifugation of nanoparticles was carried out as for the previous synthesis **3.1.A**.

3.1.J. Synthesis from CuX$_n$ (n = 1, 2; X = Cl, Br, I, CN) and P(NMe$_2$)$_3$ (HMPT) in OLA at 265 °C by hot-injection

In a typical process, CuCl (0.6 mmol, 60 mg, 1 eq.) [or CuBr (86 mg, 0.6 mmol, 1 eq.), or CuI (114 mg, 0.6 mmol, 1 eq.), or CuCN (54 mg, 0.6 mmol, 1 eq.), or $CuCl_2$ (81 mg, 0.6 mmol, 1 eq.), or $CuBr_2$ (134 mg, 0.6 mmol, 1 eq.)] was weighted in an N_2-filled glovebox and is mixed in oleylamine (7 mL, 21 mmol, 35 eq.) in 25 mL vial capped with a septum pierced and connected to a schlenk line under nitrogen. The mixture was stirred by strong magnetic stirring and heated to 100 °C under inert gas (N_2) for 15 min and a greenish solution was obtained. Then P(NMe$_2$)$_3$ (109 µL, 0.6 mmol, 1 eq.) was quickly added into the solution and the mixture quickly turned to yellower. The mixture was continuously stirred at 100 °C for 5 minutes. Then temperature quickly raised to 265 °C (13 °C/min) and maintained for 1 hour. The formation of CuNPs is evidenced by a slow color change of the solution from colorless to orange and finally to red-purple. Precipitation and centrifugation of nanoparticles was carried out as for the previous synthesis **3.1.A**.

3.1.K. Synthesis from CuCl and $P(NMe_2)_3$ in OLA at various temperatures by hot-injection

In a typical process, CuCl (60 mg, 0.6 mmol, 1 eq.) was weighted in an N_2-filled glovebox and is mixed in oleylamine (7 mL, 21 mmol, 35 eq.) in 25 mL vial capped with a septum pierced and connected to a schlenk line under nitrogen. The mixture was stirred by strong magnetic stirring and heated to 100 °C under inert gas (N_2) for 15 min and a greenish solution was obtained. Then $P(NMe_2)_3$ (109 µL, 0.6 mmol, 1 eq.) was quickly added into the solution and the mixture quickly turned to yellower. The mixture was continuously stirred at 100 °C for 5 minutes. Then temperature quickly raised (13 °C/min) to a desired temperature (245 °C, 265 °C or 290 °C) and maintained for 1 hour. The formation of CuNPs is evidenced by a slow color change of the solution from colorless to orange and finally to red-purple. Precipitation and centrifugation of nanoparticles was carried out as for the previous synthesis **3.1.A**.

3.1.L. Synthesis from CuCl and $P(NMe_2)_3$ with different P/Cu ratios (1, 1.6, 3, or 5) in OLA at 265 °C by hot-injection

In a typical process, CuCl (60 mg, 0.6 mmol, 1 eq.) was weighted in an N_2-filled glovebox and is mixed in oleylamine (7 mL, 21 mmol, 35 eq.) in 25 mL vial capped with a septum pierced and connected to a schlenk line under nitrogen. The mixture was stirred by strong magnetic stirring and heated to 100 °C under inert gas (N_2) for 15 min and a greenish solution was obtained. Then $P(NMe_2)_3$ (109 µL, 0.6 mmol, 1 eq.) [or (182 µL, 1 mmol, 1.6 eq.), or (346 µL, 1.9 mmol, 3 eq.), or (546 µL, 3 mmol, 5 eq.)] was quickly added into the solution and the mixture quickly turned to yellower. The mixture was continuously stirred at 100 °C for 5 minutes. Then temperature quickly raised to 265 °C (13 °C/min) and maintained for 1 hour. The formation of CuNPs is evidenced by a slow color change of the solution from colorless to orange and finally to red-purple. Precipitation and centrifugation of nanoparticles was carried out as for the previous synthesis **3.1.A**.

3.1.M. Synthesis from CuCl and $P(NMe_2)_3$ (HMPT) in DDA by hot-injection

In a typical process, CuCl (60 mg, 0.6 mmol, 1 eq.) was weighted in an N_2-filled glovebox and is mixed in 7 mL (30 mmol, 50 eq.) of dodecylamine (DDA) in 25 mL glass vial capped with a septum pierced and connected to a schlenk line under nitrogen. The mixture was stirred by strong magnetic stirring and heated to 100 °C under inert gas (N_2) for 15 min and a greenish solution was obtained. Then $P(NMe_2)_3$ (182 µL, 1 mmol, 1.6 eq.) was quickly added into the solution and the mixture quickly turned to yellower. The mixture was continuously stirred at 100 °C for 5 minutes. Then the temperature rapidly raised to 240 °C with a heating ramp of 13 °C/min and maintained for 1 hour. The formation of CuNPs is

evidenced by a slow color change of the solution from yellower to brown and finally to reddish-brown. After the reaction stopped, the nanoparticles dispersed in the organic layer which were purified by adding an excess of absolute ethanol/acetone (1:1) and using centrifugation at 2500 rpm for 10 min to remove all organic compounds that rest in the solution. The supernatant was discarded and the precipitate is dispersed in hexane followed by a centrifuging at 4000 rpm for 5 min. After one more redispersion/precipitation cycle with hexane and centrifugated. The copper nanoparticles were naturedly dried in the glove box in a red powder for storage and further analysis.

3.1.N. Synthesis from CuCl and $P(NMe_2)_3$ (HMPT) in a binary solvent of OLA/DDA by hot-injection

In a typical process, CuCl (60 mg, 0.6 mmol, 1 eq.) was weighted in an N_2-filled glovebox and mixed in a binary solvent of oleylamine (3.5 mL, 15 mmol, 25 eq.)/dodecylamine (3.5 mL, 11 mmol, 18 eq.) inside a 25 mL glass vial capped with a septum pierced and connected to a schlenk line under nitrogen. The mixture was stirred by strong magnetic stirring and heated to 100 °C under inert gas (N_2) for 15 min and a green-yellower solution was obtained. Then $P(NMe_2)_3$ (182 µL, 1 mmol, 1.6 eq.) of was quickly added into the solution and the mixture quickly turned to yellower. The mixture was continuously stirred at 100 °C for 5 minutes. Then the temperature rapidly raised to 260 °C with a heating ramp of 13 °C/min and maintained for 1 hour. The formation of CuNPs is evidenced by a slow color change of the solution from yellower to brown and finally to dark. Precipitation and centrifugation of nanoparticles was carried out as for the previous synthesis **3.1.I**.

3.2 Chapter III

3.2.A. Synthesis from ^{Et}CAAC-CuCl complex in OLA

In a typical process, ^{Et}CAAC-CuCl (62 mg, 0.15 mmol, 1 eq.) [or (123 mg, 0.3 mmol, 1 eq.), or (246 mg, 0.6 mmol, 1 eq.)] and oleylamine (4 mL, 12 mmol) (or 8 mL, 24 mmol) were introduced in a 25 mL glass vial capped with a septum pierced and connected to a schlenk line under nitrogen. The solution was stirred and heated to 100 °C in the sand bath, the temperature was maintained at 100 °C for 15 min and a greenish solution was obtained. The reaction temperature was quickly increased to 285 °C at a ramping of 13 °C/min. When the colorless solution slowly turned to gray, the reaction was continuously maintained at 285 °C for 30 min completed the synthesis nanoparticles and a red-purple solution containing copper nanoparticles was obtained. Then, the reaction solution was quickly removed into the glove box and naturedly cooled to room temperature. The nanoparticles were precipitated with the addition of an excess of acetone/ethanol (1:1) by centrifuging at 2500 rpm for 10 min to remove the by-products. The obtained precipitate was then re-dispersed in hexane and re-precipitated at 4000 rpm for 5 min. After two washing cycles, the nanoparticles in red-purple solid were dried inside of glove box and kept for further analysis.

3.2.B. Synthesis from ^{Et}CAAC-CuCl complex in DDA

In a typical process, ^{Et}CAAC-CuCl (123 mg, 0.3 mmol, 1 eq.) and dodecylamine (4 mL, 17 mmol, 57 eq.) were introduced in a 25 mL glass vial capped with a septum pierced and connected to a schlenk line under nitrogen. The solution was stirred and heated to 100 °C in the sand bath, the temperature was maintained at 100 °C for 15 min and a yellower solution was obtained. The reaction temperature was quickly increased to 265 °C at a ramping of 13 °C/min. When the colorless solution slowly turned to greenish-gray, the reaction was continuously maintained at 265 °C for 30 min completed the synthesis nanoparticles and a red-purple solution containing copper nanoparticles was obtained. Precipitation and centrifugation of nanoparticles was carried out as for the previous synthesis **3.2.A**.

3.2.C. Synthesis from ^{Et}CAAC-CuCl complex in a binary solvent of OLA/DDA

In a typical process, ^{Et}CAAC-CuCl (123 mg, 0.3 mmol, 1 eq.) is mixed in a binary solvent of oleylamine/dodecylamine with a volume ratio of 1:1 (2 mL/2 mL) [or 3:1 (3 mL/1 mL)] for a total volume of 4 mL in a 25 mL glass vial capped with a septum pierced and connected to a schlenk line under nitrogen. The solution was stirred and heated to 100 °C in the sand bath, the temperature was maintained at 100 °C for 15 min and a greenish-yellower solution was obtained. The reaction temperature was quickly increased to 290 °C at a ramping of 13 °C/min. When the colorless solution slowly turned to greenish-gray, the reaction was

continuously maintained at 290 °C for 30 min completed the synthesis nanoparticles and a red-purple solution containing copper nanoparticles was obtained. Precipitation and centrifugation of nanoparticles was carried out as for the previous synthesis **3.2.A**.

3.2.D. Synthesis from ^{Ad}CAAC-CuCl complex in OLA

In a typical process, ^{Ad}CAAC-CuCl (71 mg, 0.15 mmol, 1 eq.) [or (142 mg, 0.3 mmol, 1 eq.), or (284 mg, 0.6 mmol, 1 eq.)] and oleylamine (4 mL, 12 mmol) (or 8 mL, 24 mmol) were introduced in a 25 mL vial capped with a septum pierced and connected to a schlenk line under nitrogen. The solution was stirred and heated to 100 °C in the sand bath, the temperature was maintained at 100 °C for 15 min and a yellower solution was obtained. The reaction temperature was quickly increased to 280 °C at a ramping of 13 °C/min. When the colorless solution slowly turned to grayish, the reaction was continuously maintained at 280 °C for 30 min completed the synthesis nanoparticles and a red-purple solution containing copper nanoparticles was obtained. Precipitation and centrifugation of nanoparticles was carried out as for the previous synthesis **3.2.A**.

3.2.E. Synthesis from ^{Ad}CAAC-CuCl complex in DDA

The same protocol was applied as the previous synthesis **3.2.B**.

3.2.F. Synthesis from ^{Ad}CAAC-CuCl complex in a binary solvent of OLA/DDA

In a typical process, ^{Ad}CAAC-CuCl (0.3 mmol, 142 mg, 1 eq.) was mixed in a binary solvent of oleylamine (3 mL, 9 mmol, 30 eq.)/dodecylamine (1 mL, 4.3 mmol, 14 eq.) in a 25 mL glass vial capped with a septum pierced and connected to a schlenk line under nitrogen. The solution was stirred and heated to 100 °C in the sand bath, the temperature was maintained at 100 °C for 15 min and a greenish-yellower solution was obtained. The reaction temperature was quickly increased to 290 °C at a ramping of 13 °C/min. When the colorless solution slowly turned to grayish, the reaction was continuously maintained at 290 °C for 30 min completed the synthesis nanoparticles and a reddish-purple solution containing copper nanoparticles was obtained. Precipitation and centrifugation of nanoparticles was carried out as for the previous synthesis **3.2.A**.

3.2.G. Synthesis from ^{Menth}CAAC-CuCl complex in OLA

In a typical process, ^{Menth}CAAC-CuCl (72 mg, 0.15 mmol, 1 eq.) [or (144 mg, 0.3 mmol, 1 eq.), or (288 mg, 0.6 mmol, 1 eq.)] and oleylamine (4 mL, 12 mmol) (or 8 mL, 24 mmol) in a 25 mL vial capped with a septum pierced and connected to a schlenk line under nitrogen. The solution was stirred and heated to 100 °C in the sand bath, the temperature was maintained at 100 °C for 15 min and a greenish solution was obtained. The reaction temperature was

quickly increased to 290 °C at a ramping of 13 °C/min. When the colorless solution slowly turned to grayish, the reaction was continuously maintained at 290 °C for 30 min completed the synthesis nanoparticles and a red-purple solution containing copper nanoparticles was obtained. Precipitation and centrifugation of nanoparticles was carried out as for the previous synthesis **3.2.A**.

3.2.H. Synthesis from ^{Menth}CAAC-CuCl complex in a binary solvent of OLA/DDA

In a typical process, ^{Menth}CAAC-CuCl (144 mg, 0.3 mmol, 1 eq.) was mixed in a binary solvent of oleylamine (3 mL, 9 mmol, 30 eq.)/dodecylamine (1 mL, 4.3 mmol, 14 eq.) in a 25 mL vial capped with a septum pierced and connected to a schlenk line under nitrogen. The protocol as for synthesis **3.2.F** was applied.

3.2.I. Synthesis from ^{PhMe}CAAC-CuCl complex in OLA

In a typical process, ^{PhMe}CAAC-CuCl (67 mg, 0.15 mmol, 1 eq.) [or (135 mg, 0.3 mmol, 1 eq.), or (269 mg, 0.6 mmol, 1 eq.)] and oleylamine (4 mL, 12 mmol) (or 8 mL, 24 mmol) were introduced in a 25 mL glass vial capped with a septum pierced and connected to a schlenk line under nitrogen. The solution was stirred and heated to 100 °C in the sand bath, the temperature was maintained at 100 °C for 15 min and a greenish solution was obtained. The reaction temperature was quickly increased to 290 °C at a ramping of 13 °C/min. When the colorless solution slowly turned to yellower-grayish, the reaction was continuously maintained at 290 °C for 30 min completed the synthesis nanoparticles and a reddish-purple solution containing copper nanoparticles was obtained. Precipitation and centrifugation of nanoparticles was carried out as for the previous synthesis **3.2.A**.

3.2.J. Synthesis from ^{PhMe}CAAC-CuCl complex in DDA

In a typical process, ^{PhMe}CAAC-CuCl (135 mg, 0.3 mmol, 1 eq.) and dodecylamine (4 mL, 17 mmol, 58 eq.) were introduced in a 25 mL glass vial capped with a septum pierced and connected to a schlenk line under nitrogen. The solution was stirred and heated to 100 °C in a sand bath, the temperature was maintained at 100 °C for 15 min and a yellower solution was obtained. The reaction temperature was quickly increased to 290 °C at a ramping of 13 °C/min. When the colorless solution slowly turned to brownish-gray, the reaction was continuously maintained at 290 °C for 30 min completed the synthesis nanoparticles and a red-purple solution containing copper nanoparticles was obtained. Precipitation and centrifugation of nanoparticles was carried out as for the previous synthesis **3.2.A**.

3.2.K. Synthesis from ^{PhMe}CAAC-CuCl complex in a binary solvent of OLA/DDA

In a typical process, ^{PhMe}CAAC-CuCl (135 mg, 0.3 mmol, 1 eq.) was mixed in a binary solvent of oleylamine/dodecylamine with a volume ratio of 1:1 (2 mL/2 mL) [or 3:1 (3 mL/1 mL)] for a total volume of 4 mL in a glass 25 mL vial capped with a septum pierced and connected to a schlenk line under nitrogen. The solution was stirred and heated to 100 °C in the sand bath, the temperature was maintained at 100 °C for 15 min and a greenish-yellower solution was obtained. The reaction temperature was quickly increased to 290 °C at a ramping of 13 °C/min. When the colorless solution slowly turned to greenish-gray, the reaction was continuously maintained at 290 °C for 30 min completed the synthesis nanoparticles and a red-purple solution containing copper nanoparticles was obtained. Precipitation and centrifugation of nanoparticles was carried out as for the previous synthesis **3.2.A**.

3.3 Chapter IV

3.3.A. Synthesis from 1-5 equiv. of PPh_3 at 25 °C

In a typical process, CuCl (99 mg, 1 mmol, 1 eq.) and PPh_3 [1 eq. (262 mg, 1 mmol), or 3 eq. (787 mg, 3 mmol), or 5 eq. (1.31 g, 5 mmol)] were dissolved in 10 mL of dry THF in a Pyrex 25mL glass vial inside a nitrogen filled glovebox by strong magnetic stirring at room temperature (25 °C). After all the solids were dissolved and colorless solution obtained, *n*-BuMgCl (2.0 M solution in THF, 1 eq., 0.5 mL, 1 mmol) was quickly injected into the colorless solution. The color of the suspension gradually changed from colorless to yellow, bright orange and finally dark with varied intermediate stages. After 15 min, 1-dodecanethiol (1 mL, 4 mmol, 4 eq.) was added and the reaction medium consequently turned to dark-red. After 1 h of stirring at room temperature, the reaction was stopped. The copper nanoparticles were precipitated by centrifugation of the mix at 2500 rpm for 10 min. The supernatants were decanted away and chloroform was added to the precipitate, the nanoparticles with varied sizes were separated by centrifugation at 4000 rpm for 5 min. After two dissolution-precipitation cycles, the Cu nanospheres were dispersed in anhydrous hexane and dropped on TEM grid for further analysis.

Note: With 5 equiv. PPh_3, the formation of a gel was observed, preventing the stirring of the solution and thus the formation of well-defined CuNPs.

3.3.B. Synthesis from 1-5 equiv. of PPh_3 at 65 °C

In a typical process, CuCl (1 eq., 99 mg, 1 mmol) and PPh_3 [1 eq. (262 mg, 1 mmol), or 3 eq. (787 mg, 3 mmol), or 5 eq. (1.31 g, 5 mmol)] were dissolved in 10 mL of dry THF in a 25 mL three-neck flask connected to a Schlenk line was purged under nitrogen by strong magnetic stirring at 65 °C. After all the solids were dissolved and colorless solution obtained, *n*-BuMgCl (2.0 M solution in THF, 1 eq., 0.5 mL, 1 mmol) was quickly injected into the colorless solution with a syringe. The color of suspension gradually changed from colorless, bright-yellow and finally dark. After 15 min of heating at 65 °C, 1-dodecanethiol (4 eq., 1 mL, 4 mmol) was added into the mixture and a dark-red suspension was obtained. The reaction was stirred at 65 °C for 1 h before cooling to room temperature. The copper nanoparticle suspension was centrifuged directly at 2500 rpm for 10 min. Then the precipitate was decanted away and absolute ethanol was added to the red supernatant, Cu nanospheres were precipitated by centrifugation at 4000 rpm for 5 min. They were dispersed in anhydrous chloroform and collected by centrifugation at 4000 rpm for 5 min, the Cu nanospheres were dropped on a TEM grid for further analysis.

3.3.C. Synthesis from 5 equiv. of PPh_3 at 65 °C with different injection times of DDT (0.5, 5, 15 or 30 min)

In a typical process, CuCl (1 eq., 99 mg, 1 mmol) and PPh_3 (5 eq., 1.31 g, 5 mmol)) were dissolved in 10 mL of dry THF in a 25 mL three-neck flask connected to a Schlenk line was purged under nitrogen by strong magnetic stirring at 65 °C. After all the solids were dissolved and colorless solution obtained, *n*-BuMgCl (2.0 M solution in THF, 1 eq., 0.5 mL, 1 mmol) was quickly injected into the colorless solution with a syringe. The color of suspension gradually changed from colorless, bright-yellow and finally dark. After 30 s (or 5 min, or 15 min, or 30 min) of heating at 65 °C, 1-dodecanethiol (4 eq., 1 mL, 4 mmol.) was added into the mixture and a dark-red suspension was obtained. The reaction was stirred at 65 °C for a total reaction time of 1 h 15 before cooling to room temperature. The copper nanoparticle suspension was centrifuged directly at 2500 rpm for 10 min. Then the precipitate was decanted away and absolute ethanol was added to the red supernatant, Cu nanospheres were precipitated by centrifugation at 4000 rpm for 5 min. They were dispersed in anhydrous chloroform and collected by centrifugation at 4000 rpm for 5 min, the Cu nanospheres were dropped on a TEM grid for further analysis.

3.3.D. Synthesis from 5 equiv. of PPh_3 at 65 °C without addition of DDT.

CuCl (1 equiv., 99 mg, 1 mmol) and PPh_3 (5 equiv., 1,31 g, 5 mmol) were dissolved in 10 mL of dry THF in a 25 mL three-neck flask connected to a Schlenk line was purged under nitrogen by strong magnetic stirring at 65 °C. After all the solids were dissolved and colorless solution obtained, *n*-BuMgCl (2.0 M solution in THF, 1 equiv., 0.5 mL, 1 mmol) was quickly injected into the colorless solution of copper salt using a syringe. The color of the reaction medium gradually changed from colorless to bright-yellow and finally dark. After 5 min (or 10 min, or 15 min, or 30 min), the reaction solution was taken out and the copper nanoparticles were precipitated by centrifugation at 2500 rpm for 10 min. The supernatants were decanted away and the precipitate subsequently dissolved in chloroform followed by centrifugation at 4000 rpm for 5 min. After two dissolution-precipitation cycles, the Cu nanoparticles were dispersed in anhydrous hexane and dropped on TEM grid for further analysis.

3.3.E. Synthesis from 5 equiv. of PPh_3 at 65 °C with different amounts of DDT (2 or 8 equiv.)

In a typical process, CuCl (1 eq., 99 mg, 1 mmol) and PPh_3 (5 eq. 1.31 g, 5 mmol) were dissolved in 10 mL of dry THF in a 25 mL three-neck flask connected to a Schlenk line was purged under nitrogen by strong magnetic stirring at 65 °C. After all the solids were dissolved and colorless solution obtained, *n*-BuMgCl (2.0 M solution in THF, 1 eq., 0.5 mL, 1 mmol) was quickly injected into the colorless solution with a syringe. The color of suspension gradually

changed from colorless, bright-yellow and finally dark. After 15 min of heating at 65 °C, 1-dodecanethiol (2 eq. 0.5 mL, 2 mmol) [or (8 eq., 2 mL, 8 mmol)] was added into the mixture and a dark-red suspension was obtained. The reaction was stirred at 65 °C for 1 h before cooling to room temperature. The copper nanoparticle suspension was centrifuged directly at 2500 rpm for 10 min. Then the precipitate was decanted away and absolute ethanol was added to the red supernatant, Cu nanospheres were precipitated by centrifugation at 4000 rpm for 5 min. They were dispersed in anhydrous chloroform and collected by centrifugation at 4000 rpm for 5 min, the Cu nanospheres were dropped on a TEM grid for further analysis.

3.3.F. Synthesis from 5 equiv. of TOPT (P(O-octyl)$_3$) at 65 °C

CuCl (1 eq., 99 mg, 1 mmol) and TOPT (5 eq., 1.88 mL, 5 mmol) were dissolved in 10 mL of dry THF in a 25 mL three-neck flask connected to a Schlenk line was purged under nitrogen by strong magnetic stirring at 65 °C. After all the solids were dissolved and colorless solution obtained, *n*-BuMgCl (2.0 M solution in THF, 1 eq., 0.5 mL, 1 mmol) was quickly injected into the colorless solution with a syringe. The color of suspension gradually changed from colorless, bright-yellow and finally dark. After 15 min of heating at 65 °C, 1-dodecanethiol (4 eq., 1 mL, 4 mmol.) was added into the mixture and a dark-red suspension was obtained. The reaction was stirred at 65 °C for 1 h before cooling to room temperature. Precipitation of the CuNPs was carried out as for the previous synthesis **3.3.B**.

3.3.G. Synthesis from 5 equiv. of P(OMe)$_3$ at 65 °C

CuCl (1 eq., 99 mg, 1 mmol) and P(OMe)$_3$ (5 eq., 590 µL, 5 mmol) were dissolved in 10 mL of dry THF in a 25 mL three-neck flask connected to a Schlenk line was purged under nitrogen by strong magnetic stirring at 65 °C. The same protocol was applied as for the previous synthesis **3.3.E**.

3.3.H. Synthesis from 5 equiv. of TOP at 65 °C

CuCl (1 equiv., 99 mg, 1 mmol) and TOP (5 equiv., 2.23 mL, 5 mmol) were dissolved in 10 mL of dry THF in a 25 mL three-neck flask connected to a Schlenk line was purged under nitrogen by strong magnetic stirring at 65 °C. After all the solids were dissolved and a colorless solution obtained, *n*-BuMgCl (2.0 M solution in THF, 1 equiv., 0.5 mL, 1 mmol) was quickly injected into the colorless solution of copper salt using a syringe. The color of the reaction medium gradually changed from colorless to bright-yellow and finally dark. After 15 min of heating at 65 °C, 1-dodecanethiol (4 eq., 1 mL, 4 mmol.) was added into the mixture and a dark-reddish suspension was obtained. The reaction was stirred at 65 °C for 1 h before cooling

to room temperature. Precipitation of the CuNPs was carried out as for the previous synthesis **3.3.A.**

3.3.I. Synthesis from 5 equiv. of $P(NMe_2)_3$ at 65 °C

CuCl (1 eq., 99 mg, 1 mmol) and $P(NMe_2)_3$ (5 eq., 910 µL, 5 mmol) were dissolved in 10 mL of dry THF in a 25 mL three-neck flask connected to a Schlenk line was purged under nitrogen by strong magnetic stirring at 65°C. After all the solids were dissolved and a colorless solution obtained, *n*-BuMgCl (2.0 M solution in THF, 1 equiv., 0.5 mL, 1 mmol) was quickly injected into the colorless solution of copper salt using a syringe. The color of the reaction medium gradually changed from colorless to bright-yellow and finally dark. After 15 min of heating at 65 °C, 1-dodecanethiol (4 eq., 1 mL, 4 mmol.) was added into the mixture and a dark-brown suspension was obtained. The reaction was stirred at 65 °C for 1 h before cooling to room temperature. Precipitation of the CuNPs was carried out as for the previous synthesis **3.3.A**.

3.3.J. Synthesis from 5 equiv. of PPh_3 with different amount of *n*-BuMgCl (1, 2, 4 or 8 equiv.) at -30 °C to 65 °C

CuCl (1 eq., 99 mg, 1 mmol) and PPh_3 (5 eq., 1.31 g, 5 mmol) were dissolved in 10 mL of dry THF in a 25 mL three-neck flask connected to a Schlenk line was purged under nitrogen by strong magnetic stirring at room temperature. After all the solids were dissolved, the obtained colorless solution was transferred to a glace bath and strongly stirred at -30 °C for 5 min, the *n*-BuMgCl (2.0 M solution in THF, 1 equiv., 0.5 mL, 1 mmol) [or (2 equiv., 1mL, 2 mmol), or (4 equiv., 2 mL, 4 mmol), or (8 equiv., 4 mL, 8 mmol)] was quickly injected into the colorless solution of copper salt using a syringe. The color of the reaction medium gradually changed from colorless to bright-yellow and finally orange. After 1 hour of stirring at -30 °C, the orange solution was quickly removed to an oil bath for heating at 65 °C, the orange solution instantaneously turned dark. After 15 min of stirring at 65 °C, 1-dodecanethiol (4 eq., 1 mL, 4 mmol.) was added into the mixture and a red solution was obtained. The reaction was stirred at 65°C for 1 h before cooling to room temperature. The reaction solution was naturedly cooled to room temperature and then the cooled NPs solutions were precipitated after the addition of excess EtOH by centrifugation at 2500 rpm for 10 min. The precipitate obtained was re-dispersed in chloroform and centrifugated at 4000 rpm for 5 min. After two dissolution/precipitate cycles, the CuNPs were dried and conserved as a red powder in the glove box for further analysis.

3.3.K. Synthesis from 5 equiv. of TOP with different amount of *n*-BuMgCl (2 or 4 equiv.) at -30 °C- 65 °C

CuCl (1 eq., 99 mg, 1 mmol) and TOP (5 eq., 2.23 mL, 5 mmol) were dissolved in 10 mL of dry THF in a 25 mL three-neck flask connected to a Schlenk line was purged under nitrogen by strong magnetic stirring at room temperature. After all the solids were dissolved, the obtained colorless solution was transferred to a glace bath and strongly stirred at -30 °C for 5 min, the *n*-BuMgCl (2.0 M solution in THF, 2 equiv., 1 mL, 2 mmol) (or 4 equiv., 2 mL, 4 mmol) was quickly injected into the colorless solution of copper salt using a syringe. The color of the reaction medium gradually changed from colorless to bright-yellow and finally yellower-orange. After 1 hour of stirring at -30 °C, the orange solution was quickly removed to an oil bath for heating at 65 °C, the orange solution instantaneously turned dark. After 15 min of stirring at 65 °C, 1-dodecanethiol (4 eq., 1 mL, 4 mmol.) was added into the mixture and a red-dark solution was obtained. The reaction was stirred at 65 °C for 1 h before cooling to room temperature. Precipitation of the CuNPs was carried out as for the previous synthesis **3.3.J**.

3.3.L. Synthesis from 5 equiv. of PPh_3 and EtMgCl at -30 °C to 65 °C

CuCl (1 eq., 99 mg, 1 mmol) and PPh_3 (5 eq., 1.31 g, 5 mmol) were dissolved in 10 mL of dry THF in a 25 mL three-neck flask connected to a Schlenk line was purged under nitrogen by strong magnetic stirring at room temperature. After all the solids were dissolved, the obtained colorless solution was transferred to a glace bath and strongly stirred at -30 °C for 5 min, the EtMgCl (2.0 M solution in THF, 1 equiv., 0.5 mL, 1 mmol) (or 2 equiv., 1 mL, 2 mmol) was quickly injected into the colorless solution of copper salt using a syringe. The color of the reaction medium gradually changed from colorless to yellower and finally orange. After 1 hour of stirring at -30°C, the orange solution was quickly removed to an oil bath for heating at 65°C, the orange solution instantaneously turned dark. After 15 min of stirring at 65 °C, 1-dodecanethiol (4 eq., 1 mL, 4 mmol.) was added into the mixture and a red solution was obtained. The reaction was stirred at 65 °C for 1 h before cooling to room temperature. Precipitation of the CuNPs was carried out as for the previous synthesis **3.3.J**.

3.3.M. Synthesis from 5 equiv. of PPh_3 and *t*BuMgCl at -30 °C to 65 °C

CuCl (1 eq., 99 mg, 1 mmol) and PPh_3 (5 eq., 1.31 g, 5 mmol) were dissolved in 10 mL of dry THF in a 25 mL three-neck flask connected to a Schlenk line was purged under nitrogen by strong magnetic stirring at room temperature. After all the solids were dissolved, the obtained colorless solution was transferred to a glace bath and strongly stirred at -30 °C for 5 min, the *t*-BuMgCl (2.0 M solution in THF, 1 equiv., 0.5 mL, 1 mmol) (or 2 equiv., 1mL, 2 mmol) was quickly injected into the colorless solution of copper salt using a syringe. The color of the reaction medium gradually changed from colorless to bright-yellow and finally orange. After 1

hour of stirring at -30 °C, the orange solution was quickly removed to an oil bath for heating at 65 °C, the orange solution instantaneously turned dark. After 15 min of stirring at 65 °C, 1-dodecanethiol (4 eq., 1 mL, 4 mmol.) was added into the mixture and a red solution was obtained. The reaction was stirred at 65 °C for 1 h before cooling to room temperature. Precipitation of the CuNPs was carried out as for the previous synthesis **3.3.J**.

3.3.N. Synthesis from 5 equiv. of PPh_3 and isopropenylMgBr at -30 °C to 65 °C

CuCl (1 eq., 99 mg, 1 mmol) and PPh_3 (5 eq., 1.31 g, 5 mmol) were dissolved in 10 mL of dry THF in a 25 mL three-neck flask connected to a Schlenk line was purged under nitrogen by strong magnetic stirring at room temperature. After all the solids were dissolved, the obtained colorless solution was transferred to a glace bath and strongly stirred at -30 °C for 5 min, the isopropenylMgBr (0.5 M solution in THF, 1 equiv., 2 mL, 1 mmol) (or 2 equiv., 4 mL, 2 mmol) was quickly injected into the colorless solution of copper salt using a syringe. The color of the reaction medium very slowly changed from colorless to bright-yellow and finally yellow-orange. After 1 hour of stirring at -30 °C, the orange solution was quickly removed to an oil bath for heating at 65 °C, the orange solution instantaneously turned dark. After 15 min of stirring at 65 °C, 1-dodecanethiol (4 eq., 1 mL, 4 mmol.) was added into the mixture and a red solution was obtained. The reaction was stirred at 65 °C for 1 h before cooling to room temperature. Precipitation of the CuNPs was carried out as for the previous synthesis **3.3.J**.

3.3.O. Synthesis from 5 equiv. of PPh_3 and PhMgBr at -30 °C to 65 °C

CuCl (1 eq., 99 mg, 1 mmol) and PPh_3 (5 eq., 1.31 g, 5 mmol) were dissolved in 10 mL of dry THF in a 25 mL three-neck flask connected to a Schlenk line was purged under nitrogen by strong magnetic stirring at room temperature. After all the solids were dissolved, the obtained colorless solution was transferred to a glace bath and strongly stirred at -30 °C for 5 min, the PhMgCl (2.0 M solution in THF, 1 equiv., 0.5 mL, 1 mmol) (or 2 equiv., 1 mL, 2 mmol) was quickly injected into the colorless solution of copper salt using a syringe. The color of the reaction medium very slowly changed from colorless to yellower. After 1 hour of stirring at -30 °C, the orange solution was quickly removed to an oil bath for heating at 65 °C, the yellower solution slowly turned gray-brown. After 15 min of stirring at 65 °C, 1-dodecanethiol (4 eq., 1 mL, 4 mmol.) was added into the mixture and a reddish solution was obtained. The reaction was stirred at 65 °C for 1 h before cooling to room temperature. Precipitation of the CuNPs was carried out as for the previous synthesis **3.3.J.**

3.3.P. Synthesis from 5 equiv. of PPh_3 and MeMgBr at -30 °C to 65 °C

The same protocol was applied as for the previous synthesis **3.3.N**, except the addition of MeMgCl (1.0 M solution in THF, 1 eq., 1 mL, 1 mmol) (or 2 eq., 2 mL, 2 mmol).

3.3.Q. Synthesis of CuNPs from 5 equiv. of PPh_3 at -30 °C/$h\upsilon$ (condition A)

CuCl (1 eq., 99 mg, 1 mmol) and PPh_3 (5 eq., 1.31 g, 5 mmol) were dissolved in 10 mL of dry THF in a 25 mL three-neck flask connected to a Schlenk line was purged under nitrogen by strong magnetic stirring in a thermostatted aqueous ethylalcohol bath controlled to -30 °C. After 5 min (all the solids were dissolved), the *n*-BuMgCl (2.0 M solution in THF, 1 equiv., 0.5 mL, 1 mmol) was quickly injected into the colorless solution of copper salt using a syringe under a 100-Watt spiral lamp. The color of the reaction medium very slowly changed from colorless to yellower. After 24 h of stirring at -30 °C, the gray-white gel was observed in the solution.

3.3.R. Synthesis of CuNPs from 5 equiv. of PPh_3 with 4 equiv. of DDT at -30 °C/$h\upsilon$ (condition B)

CuCl (1 eq., 99 mg, 1 mmol) and PPh_3 (5 eq., 1.31 g, 5 mmol) were dissolved in 10 mL of dry THF in a 25 mL three-neck flask connected to a Schlenk line was purged under nitrogen by strong magnetic stirring in a thermostatted aqueous ethylalcohol bath controlled to -30 °C. After 5 min (all the solids were dissolved), the *n*-BuMgCl (2.0 M solution in THF, 1 equiv., 0.5 mL, 1 mmol) was quickly injected into the colorless solution of copper salt using a syringe under a 100-Watt spiral lamp. The color of the reaction medium very slowly changed from colorless to yellower. After 1 h, 1 mL of DDT is added into the orange-yellower solution. After 23 h of stirring at -30 °C, a greenish-orange solution was obtained. When the thermostatted aqueous ethylalcohol bath was removed, the temperature of reaction solution slowly raised to rt and the solution color slightly darken until be dark-greenish. The reaction solution was washed by were precipitated by centrifugation at 2500 rpm for 10 min. The supernatants were decanted away and the precipitate subsequently dissolved in chloroform followed by centrifugation at 4000 rpm for 5 min. After two dissolution-precipitation cycles, the Cu nanoparticles were dispersed in anhydrous hexane and dropped on TEM grid for further analysis. During the washing step, the solution slowly turned to reddish.

3.3.S. Synthesis from 5 equiv. of PPh_3 at 65 °C in a 5 mmol scale

In a typical process, CuCl (1 equiv., 495 mg, 5 mmol) and PPh_3 (5 equiv. 1.31 g, 25 mmol) were dissolved in 50 mL of dry THF in a 100 mL flask inside a nitrogen filled glovebox by strong magnetic stirring at 65 °C. After all the solids were dissolved and colorless solution obtained, *n*-BuMgCl (2.0 M solution in THF, 1 equiv., 2.5 mL, 5 mmol) was quickly injected into

the colorless solution. The color of the suspension gradually changed from colorless to yellow, bright orange and finally dark with varied intermediate stages. After 15 min, 1-dodecanethiol (4 equiv., 5 mL, 20 mmol) was added and the reaction medium consequently turned to dark-red. After 1 h of stirring at room temperature, the reaction was stopped. The copper nanoparticles were precipitated by centrifugation at 2500 rpm for 10 min. The obtained supernatants were precipitated by adding an excess of absolute ethanol and centrifugation at 2500 rpm for 10 min. The precipitate was re-dispersed in chloroform and centrifugated at 4000 rpm for 5 min. The first batch of precipitate was re-dispersed in chloroform and the size-selected nanoparticles were collected by centrifugation at 4000 rpm for 5 min. After two dissolution-precipitation cycles for each batch, a small amount of Cu nanospheres were dispersed in anhydrous hexane and dropped on TEM grid for further analysis and the main batch of CuNPs in red solid was dried and conserved inside of glove box.